II. SCIENTIFIC PAPERS SUBMITTED FROM SESSIONS

1. Physical Oceanography Sessions

A. Circulation and water mass structure of the Okhotsk Sea and Northwestern Pacific
B. Sea ice and its relation to circulation and climate
C. Waves and tides
D. Physical oceanography of the Japan Sea / East Sea

Seasonal Variability of the Pycnocline in La Perouse Strait and Aniva Gulf

Valentina D. BUDAEVA[1] and Vyacheslav G. MAKAROV[2]

[1] Far Eastern Regional Hydrometeorological Research Institute, Vladivostok, Russia
[2] Pacific Oceanological Institute, Russian Academy of Sciences, Vladivostok, Russia

The properties of the pycnocline reflect a number of processes (i.e., atmosphere-ocean heat exchange, vertical and horizontal motions, etc.) which influence the water structure (Vinogradov et al., 1984; Lebedev and Aizatulin, 1984; Ozmidov, 1986; Zyryanov, 1980; Trotsenko et al., 1992). Investigation of the temporal-spatial pycnocline variability plays an important role for fishery and ecology of the productive shelf regions within the Far Eastern Marginal Seas.

The most difficult problem in evaluating the pycnocline characteristics is to find the point of inflection based on discrete density estimations at the standard horizons assuming, in advance, continuous vertical assignment of the density function *r(z)*. Layer by layer calculations are unacceptable since such way permits one to define the layer of the maximal density change, but not the inflection point. In order to eliminate the uncertainty, as a rule, the spline approximation is used (Ahlberg et al., 1967). This approach allows restoration of the curve of vertical distribution *r(z)* in the preliminary searched layer of the maximum density change with the help of a polynomial of the third order and then to determine the position of the inflection.

An algorithm to define the pycnocline characteristics is given below. Firstly, the layer $[z_i, z_{i+1}]$ of the maximum density change *r(z)* was found from discrete experimental data. In the cases when the maximal change *r(z)* covered more that one layer their combination was considered as the layer $[z_i, z_{i+1}]$. Within this layer distribution of *r(z)* was approximated by the cubic spline:

$$\rho(z) = a_0 z^3 + a_1 z^2 + a_2 z + a_3 \qquad (1)$$

In order to find the coefficients a_i (i = 0-3) the following boundary condition have been applied:

$$\rho(z)\big|_{z=z_i} = \rho_i \; ; \quad \rho(z)\big|_{z=z_i+1} = \rho_{i+1} \; ;$$

$$\left.\frac{\partial\rho}{\partial z}\right|_{z=z_i} = \begin{cases} 0, & z_i = 0 \\ D_i = \left[\rho(z_i) - \rho(z_{i-1})\right]/(z_i - z_{i-1}), & z_i > 0 ; \end{cases}$$

$$\left.\frac{\partial\rho}{\partial z}\right|_{z=z_{i+1}} = \begin{cases} D_{i+1} = \left[\rho(z_{i+2}) - \rho(z_{i+1})\right]/(z_{i+2} - z_{i+1}), & z_{i+1} < H \; ; \\ 0, & z_{i+1} = H \end{cases}$$

As a result the system of four algebraic equations was obtained and solved using the standard approach.

By equating to zero the second derivative of the function *r(z)*:

$$d^2\rho/dz^2 = 6a_0 z_p + 2a_1 = 0, \qquad (2)$$

the point of $r(z)$ inflection z_p was computed:

$$z_p = -a_1 / 3a_0 .$$

The first derivative of the function $r(z)$ gives the density gradient. By substituting the equation (2) in (1), the expression for calculation of the pycnocline intensity at the depth z_p , i.e., the maximum vertical density gradient G_{max} in the fixed point was received.

$$G_{max} = \left.\frac{d\rho}{dz}\right|_{z=z_p} = a_2 - \frac{a_1^2}{3a_0} . \qquad (3)$$

The analytical equations to determine coefficients a_i have been obtained from the boundary conditions:

$$a_0 = -2\left[\frac{(\rho_i - \rho_{i+1})}{(z_i - z_{i+1})^3} - 0{,}5\frac{(D_i + D_{i+1})}{\left((z_i - z_{i+1})^2\right)}\right];$$

$$a_1 = \frac{(D_i - D_{i+1}) - 3a_0\left(z_i^2 - z_{i+1}^2\right)}{2(z_i - z_{i+1})};$$

$$a_2 = (1/2)\cdot\left[(D_i + D_{i+1}) - 3a_0\left(z_i^2 - z_{i+1}^2\right) - 2a_1(z_i + z_{i+1})\right]$$

Based on the given algorithm the charts of the maximum vertical density gradients (G_{max}) and the depths of their location (z_p) in spring, summer, and fall have been prepared and used to reveal the spatial pycnocline structure and its annual transformation in La Perouse Strait and Gulf of Aniva (Fig. 1). The multi-year means of the seasonal density fields, being restored in the nodes of regular net by the standard graphic packages, have been applied for our calculations.

The charts clearly demonstrate that the pycnocline shape is a result of the water dynamic in the region. Thus, the Soya Current meandering leads to the vorticity strengthening in the current field and as a consequence, to the rising or deepening of the pycnocline.. For example, the Soya Current cyclonic meander south-eastward off the Cape of Krilion is responsible for the pycnocline movement upward to a depth of 10 m (Fig. 1a) and an increase of the intensity up to 0.06-0.07 sda/m (specific density anomaly per meter) (Fig.1d). The Soya current anticyclonic meander in the La Perouse Strait, on the contrary, forms an intensive downwelling zone where the pycnocline deepens to a depth of 30-35 m (Fig. 1c).

The pycnocline properties are influenced by the intrusion of external water in the region. The Gulf of Aniva is characterized by the intense river runoff which in summer period causes the increased persistence of two-layer vertical water stratification and the high (more than 0.1 sda/m) pycnocline intensity in the upper layer (Fig. 1e). The sources of external water for the La Perouse Strait are the streams or mesoscale vortexes of the East-Sakhalin Current (Fig. 1b).

The spatial heterogeneity in the depth distribution of the pycnocline location is most vividly expressed in spring and fall (Fig. 1a-c). In addition to the dynamic reasons, the spatial heterogenity could be correspondingly explained by the radiation heating and the fall-winter convection in spring and fall,. During the transitional seasons, the horizontal field structure of z_p is represented by the

combination of closed isolines considered as the local dynamic formations. Within these formations the depth of the pycnocline location changes abruptly, and the sharp density variations are observed similar to those for other regions of the World Ocean, in particular, for the Sea of Scotia (Lebedev and Aizatulin, 1984) and the Gulf of Aden (Trotsenko et al., 1992).

In the summer period, within the Gulf of Aniva, the large area of sinking waters is formed due to the prevailing of anticyclonic current. As a result the pycnocline deepens and reaches the depth of 20 m (Fig. 1b). The pycnocline rises slightly northward and in the nearshore zone of upwelling it becomes thin and shows significant gradients (Fig. 1e).

Significant seasonal variations of the maximum vertical density gradients are revealed in the La Perouse Strait and Gulf of Aniva. The lowest G_{max} values of 0.02-0.05 sda/m are found in spring and fall (Fig. 1d, 1f) and the highest G_{max} values of 0.14-0.18 sda/m are displayed in summer (Fig. 1e). As a whole, summer is characterised by a more homogeneous distribution of z_p and by the general increase of G_{max} values, approximately by an order. During this season, a decrease of vertical density gradient location to 15-20 m is also observed everywhere. These essential differences in the vertical density stratification are related, mainly, to the annual insolation variation and seasonal transformation of the current fields.

Our results show that the pycnocline within the shelf zone in the La Perouse Strait and Gulf of Aniva is characterized by the strong seasonal variability with preserved mosaic G_{max}. distribution during all seasons. This is evidence that the area under study is a region with a complex climatic regime of dynamic and thermohaline water structure formation. In perspective the properties and interannual variability of the pycnocline in other regions within the Sakhalin Shelf have to be evaluated.

REFERENCES

Ahlberg, J.H., E.N. Nilson, and J.L. Walsh. 1967. Theory of splines and their applications. N.Y., Academic Press. 316 p.

Lebedev, V.L., and T.A. Aizatulin. 1984. The classification of the oceanological attributes of increased biological productivity of the marine waters. Voprosy Geografii No 125. Oceany i Gizn:160-172. (in Russian).

Ozmidov, R.S. 1986. The inter-layers of hydrophysical parameters and its role in formation of hydrochemical and hydrobiological fields in the ocean. Issledovaniya ekosistemy pelagiali Chernogo morya. M., Nauka. p. 9-18. (in Russian).

Trotsenko, B.G., S.P. Klimenko, V.V. Dronov, and G.P. Korshunova. 1992. The seasonal pycnocline variability of the Bay of Aden. Okeanologiya. 32(4):647-653. (in Russian).

Vinogradov, M.E., A.A. Elizarov, and P.A. Moiseev. 1984. The biological efficiency of dynamically active zones in the open ocean. Proc. III Congress of Soviet Oceanologists. M., Nauka. p.107-127. (in Russian).

Zyryanov, V.N. 1980. The water dynamics in the south-western Atlantic and features of pycnocline locations. Okeanograficheskie Issledovaniya Promyslovyh Raionov Mirovogo Okeana. M., Pishevaya promyshlennost. p. 50-64. (in Russian).

FIGURES

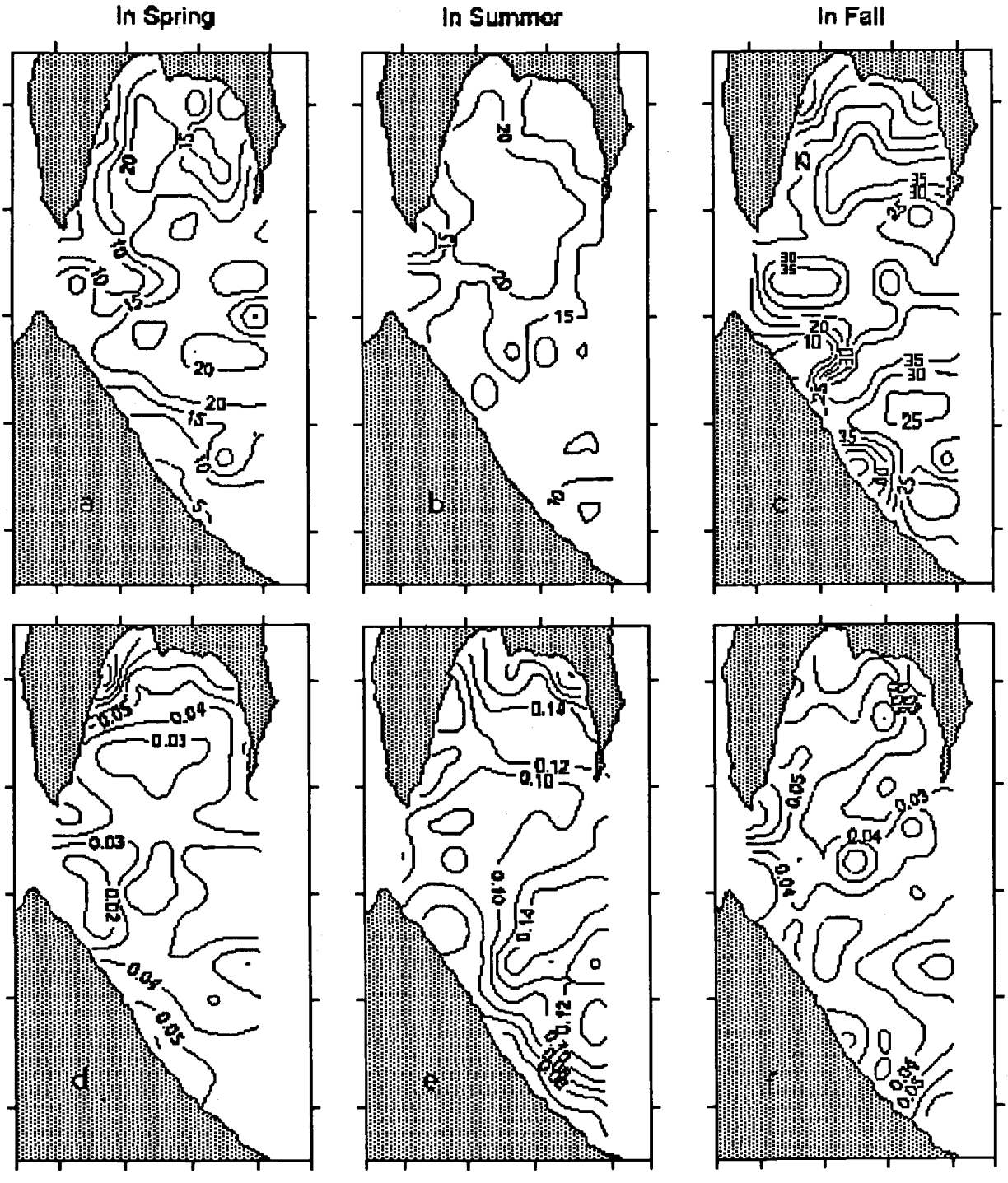

Fig. 1. Multi-year means of the maximum vertical density gradients and depths of their location in the Gulf of Aniva and La Perouse Strait in spring (a, d), summer (b, e) and fall (c, f).

Modeling of the Typical Water Circulations in the La Perouse Strait and Aniva Gulf Region

Valentina D. BUDAEVA[1] and Vyacheslav G. MAKAROV[2]

[1] Far Eastern Regional Hydrometeorological Research Institute, Vladivostok, Russia
[2] Pacific Oceanological Institute, Russian Academy of Sciences, Vladivostok, Russia

INTRODUCTION

The Aniva and La Perouse Region is characterized by a quite complex spatial water circulation structure. It was shown that the circulation patterns are determined by the sea level gradient of the northern Japan Sea and southwestern Okhotsk Sea parts (Aota, 1970; 1975; 1982; 1988), but there is not general agreement on the gradient's nature. In some works the supposition has been stated that the sea level gradient is due to a difference in the sea water density between the Japan and Okhotsk Seas, whereas other papers considered such factors as atmospheric circulation and tidal currents (Leonov, 1960; Shelegova, 1960).

The Japan Sea water discharge through the La Perouse Strait, under the influence of the sea level gradient, has essential fluctuations within the range of the interannual, seasonal and synoptic scales. Data on the diurnal mean transport through the La Perouse Strait are extremely limited. Regarding the seasonal variability of discharge, it is known (Aota, 1988) that in the warm period (July - October) the eastward (east or south-east) transport with velocities of about 50-80 cm/sec prevails. In the early winter, the resulting vector of the flow reverses and has a northwestward direction; at that time the current velocity, as a rule, does not exceed 10-15 cm/sec.

In the warm period, the diurnal currents are dominant in the Aniva and La Perouse Region, and the main axis directions for diurnal and semidiurnal currents correspond to the direction of the mean flow. In the early winter, the diurnal and semidiurnal currents become significantly weaker (Aota, 1988).

Due to the shallow waters (the maximal depth is about 130-140 m) and the funnel-shaped configuration of the shoreline in the Aniva and La Perouse areas, the water circulation in this region is under the great influence of the relatively strong monsoon type local winds. Under some baric conditions, these winds can transform the sea level gradient and the current structure on the southern Sakhalin shelf. Therefore, to understand the water circulation variability it is crucial to reveal atypical characteristics of the background currents resulting from these transformations.

The goal of this paper is to construct the typical water circulation schemes for the La Perouse and Aniva Region taking into account the different types of the regional baric field applying numerical modelling. Such an approach was successfully used previously for the Chukchi Sea (Kulakov, 1993).

MODEL DESCRIPTION

An improved version of the 3D diagnostic model (Budaeva et al., 1980) worked out for the coastal Sakhalin waters was applied to estimate water circulation in the La Perouse Strait and Aniva Gulf Region. Diagnostic calculations of water circulation and the three-dimensional field of the

currents have been performed for the different regional baric situations (Atlas, 1977; Atlas, 1979). The grid used approximated the area with the steps of 10'x12'. The number of grid nodes was 72 and the maximal calculated level was 125 m. The numerical modeling was conducted in the frames of linear equations for shallow waters under the condition of free flowing liquid boundaries and a discharge through the La Perouse Strait. In accordance with the our previous results (Budaeva et al., 1980) the sea water baroclinity was considered.

RESULTS

Figs. 1a and 1b present schemes of the integral circulation and surface currents corresponding to the type (I) of the regional baric situation. This type is characterized by the southward winds (southwestern and southern) that induce a significant sea level elevation in the eastern part of the Aniva Gulf and a sea level depression along the Okhotsk Sea coast of Hokkaido Island. Under the effect of the winds water circulation in the La Perouse Strait and Aniva Gulf region becomes anticyclonic and, as a rule, vertically homogeneous. As a consequence of circulation intensification, an increased inflow of the relatively warm Japan Sea waters is observed in the western and central parts of the Aniva Gulf and their transport along the Okhotsk Sea coast of Hokkaido. The anticyclonic mesoscale eddy generated in the offshore area of the La Perouse Strait is the major element of such a type of water circulation. It should be noted that the maximal development of the eddy is found under the influence of the southwestern winds and within the area of 45°30' and 46°00'N with a transport about 0.3 Sv. The highest surface current velocities (greater than 50 cm/sec) are revealed at the entrance to La Perouse Strait near the Capes of Krilion and Aniva and on the northern periphery of the mesoscale anticyclonic eddy.

A similar type of the water circulation, that could be generally considered as type (I), is observed when the western winds prevail (Fig. 1c). The only difference from the type (I) is found in the structure of the surface currents along the Okhotsk Sea coast of Hokkaido where a sea level depression is manifested less clearly and the scheme of currents is closer to the climatic circulation.

Figs. 1d and 1e demonstrate schemes of the integral water circulation and surface currents corresponding to the regional baric situation of the type (II). It is characterized by the northern and northwestern winds that generate low sea level in the northern shallow part of the Aniva Gulf and a sea level elevation along the Okhotsk Sea coast of Hokkaido. Changes in water circulation are observed, mainly, in the formation of the mesoscale cyclonic eddy-meander on the western periphery of the Soya current and in the water rising in the northern shallow part of the Aniva Gulf. The cyclonic current active, mainly, in the surface layer (up to 50 m) is observed from the western side of this meander, whereas a non-persistent anticyclonic current is noted eastward off the main flow. When this type of regime exists, an increase of compensative near bottom inflow of the transformed Japan Sea waters is revealed in the central and east part of the Aniva Gulf, from which point, being under the effect of the eastern and southeastern flows, it follows to the southwestern part of the Okhotsk Sea.

Figs. 1f - 1h illustrate the schemes of the integral circulation and the surface currents associated with the type (III) of the regional baric situation. This circulation is formed when the northeastern, eastern and southeastern winds occur and create a "counter current" in the La Perouse Strait for the eastward transport of the Japan Sea waters. Prevailing winds cause a sea level elevation in the northern (southeastern winds) or western (northeastern and eastern winds) parts of the La Perouse Strait and Aniva Gulf region. This decreases the sea level gradient between the Japan and Okhotsk Seas and can even change the sign of the gradient in the La Perouse Strait and favor the western flow in the Strait. In this case the currents has a vividly pronounced two-layer vertical structure. In the surface layer (above 15-20 m) the main current flows westward/southwestward and, as a result, the

Soya current is blocked along the Okhotsk Sea coast of the Hokkaido. According to our estimations the maximum velocities at the surface can reach 50-80 cm/sec in the La Perouse Strait, and 20-30 cm/sec in the Aniva Gulf. The current has the right rotation but at the depth of 25-30 m it reverses, and the velocities observed are 2-4 times lower as compared with the surface velocities. The water circulation, corresponding to the type (III) of the regional baric situation, has the most anomalous character and leads to non-regular intraseasonal disturbances of the hydrological water structure along the southwestern coast of Sakhalin Island (Shelegova, 1960).

The model calculations show that in the La Perouse Strait and Aniva Gulf region the current fields are essentially dynamic and demonstrate the strong dependence on the type of regional baric situation. In such cases the current structure has a number of peculiarities. Generally, during prevailing northeastern, northern or eastern, northwestern (southeastern) winds the two-layer vertical structure of currents is found and with southwestern, western (southern) winds it has, mostly, one direction. The major activity of the mesoscale cyclonic eddies is observed when the persistent types III (eastern,, northeastern and southeastern winds) and II (northern and northwestern winds) of the regional baric situation occur, and the anticyclonic eddy exists under the influence of the southern southwestern and western winds (the baric situation of type I).

The proposed method of standardization and dialogue computer program for the typical circulation calculations generated by the wind in the La Perouse Strait and Aniva Gulf region are useful for the diagnostic aims of the present climate and providing the navigation service with the available information.

REFERENCES

Aota, M. 1970. Study of the variation of oceanographic condition North-East of Hokkaido in the Sea of Okhotsk. Low Temp. Sci. Ser. A. 28:261-279.

Aota, M. 1975. Studies on the Soya warm current. Low Temp. Sci. Ser. A. 33:151-172.

Aota, M. 1982. On oceanic structure of a frontal region of Soya warm current. Low. Temp. Sci. Ser. A. 4:207-215.

Aota, M., M. Ishikawa, and T. Yamada. 1988. Dynamic of flow in the Soya Strait. Low Temp. Sci. Ser. A. 47:147-160.

Atlas of typical wind fields in the Okhotsk Sea. Yugno-Sakhalinsk. 1977. 110 p. (in Russian)

Atlas of typical fields of zone of continental shelf around Sakhalin. Yugno-Sakhalinsk. 1979. 113 p. (in Russian)

Budaeva, V.D., V.G. Makarov, and I. Yu Melnikova. 1980. The diagnostic calculations of stationary currents in the Aniva Gulf and La Perouse Strait. Trudy DVNIGMI. 87:66-78. (in Russian)

Kulakov, Yu.M. 1993. The simulation of typical circulation of waters of Chukchi Sea. Trudy AANII. 429:76-85. (in Russian)

Leonov, A.K. 1960. Okhotsk Sea. Regional oceanography.Part.1. L.: Gidrometeoizdat. p. 186-290. (in Russian)

Shelegova, E.K. 1960. The cases of sharp cooling of the waters in summer period at southwestern coast of Sakhalin. Izvestiya. TINRO. 46:249-251. (in Russian)

FIGURES

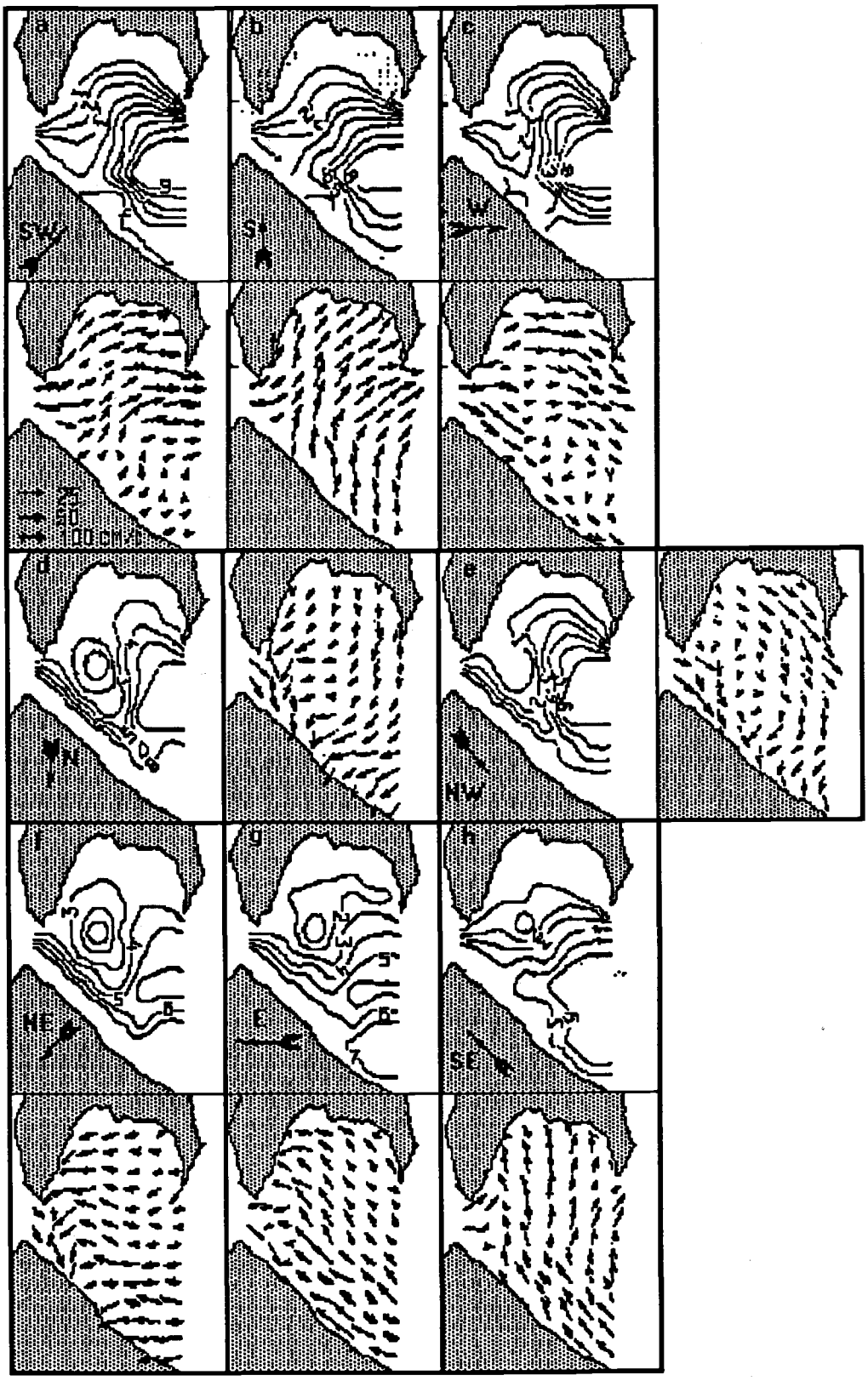

Fig. 1. Schemes of the integral circulation and surface currents in the La Perouse Strait and Aniva Gulf region for the different regional basic situations:
Type I - prevailing of SW (a), S (b) and W (c) winds;
Type II - prevailing of N (d) and NW (e) winds;
Type III -prevailing of NE (f), E (g) and SE (h) winds.

Anticyclogenesis over the Okhotsk Sea and its Influence on Weather

Nina A. DASHKO[1], Sergey M. VARLAMOV[2], Young-Ho HAN[3] and Young-Seup KIM[3]

[1] Far-Eastern State University, Vladivostok, Russia
[2] Far-Eastern Regional Hydrometeorological Research Institute, Vladivostok, Russia
[3] National Fisheries University of Pusan, Pusan, Republic of Korea

The anticyclonic activity over the Far Eastern Seas is one of the reasons for the weather anomalies over the adjacent territories. The anticyclogenesis over the Okhotsk Sea, most developed in May-July, contributes significantly to the synoptic processes in summer. In the years of active anticyclogenesis the air temperature over Primorye, Sakhalin and the Western Kamchatka coast is mostly below normal. Precipitations over Sakhalin and Kamchatka are also below normal, whereas over Primorye, on the contrary, they are above average.

At the beginning of summer, especially at the end of May and June, the intensification of the anticyclone occurs over the Okhotsk Ridge and moves towards the Japan Sea, across the periphery to the south of Primorye. The maritime air mass appearance is accompanied by the southern or south-eastern winds reaching sometimes about 15-20 m/sec, as well as by rain, drizzle or fogs. Such situations can continue for 5-7 days and lead to a decrease of the daily mean air temperature in Vladivostok up to 9-10°C, while the daily mean air temperatures in June from the multi-year observations is 12.8°C (Manual of the Short-term.., 1965; Dashko and Teslenko, 1991).

June in South Primorye is a transition period from spring to summer, and thus, a month of weather contrasts. It is a central month in the first half of the summer monsoon which provides the coast of Primorye with a continuous drizzle, thick fogs and strong, primarily, southern winds (Manual of the Long-term.., 1968; Dashko and Teslenko, 1991).

Fig. 1 demonstrates that the temperature regime in June in Vladivostok is distinctly different from the temperature regime of Nice and Rome located at the same latitude. The monthly mean air temperature in Vladivostok from April till July is the same as in Stockholm situated at 59°N (Fig. 1).

The duration of day light increases from 14 hours 32 minutes in May to 15 hours 12 minutes in June. The duration of sun radiance, on the contrary, decreases from 170 hours in May to 130 hours in June, on average. The ratio of the actual to the possible sun radiance duration is 41% in May and only 32 % in June.

The monthly mean temperature in June is 12-13°C. This is slightly lower than in September and can be compared with the mean air temperature in the first half of October. The air temperature shows significant variations during the month: the minimal temperature of 4.4°C and the maximal of 32°C were recorded (Soviet Union's Climatic Reference Book, 1966-1970). It should be noted that moving off the coast, the continental climatic features prevail and June becomes the typical warm summer month.

The comparison of the summer weather characteristics over the Primorye edge of Russia and Korean Peninsula, based on a 50 year data set from observations at meteorological stations, demonstrated that the air temperature field distribution depends, to a great extent, on the circulation peculiarities and thermal state of the Okhotsk Sea.

For more detailed analysis, the correlation matrices were constructed for the monthly mean air temperature at stations of Primorye and Korean Peninsula and the monthly mean meteorological parameters (pressure, air temperature, surface geopotential at 500 gPa), their derivatives ($\partial S / \partial x$, $\partial S / \partial y$, $\partial^2 S / \partial x \partial y$, $\partial^2 S / \partial x^2$, $\partial^2 S / \partial y^2$) and Laplacians ΔS at 30 points over the Okhotsk Sea and adjacent regions. The correlation coefficients of 0.7 were found between the monthly mean air temperature and air pressure over the Okhotsk Sea and the monthly mean air temperature at stations of Primorye and Korean Peninsula (Fig. 2). The significant correlation coefficients were also revealed between the monthly mean air temperature and the first $\partial S / \partial y$ and second $\partial^2 S / \partial y^2$ derivatives, and Laplacians for the air pressure field at sea level (P_o) and the geopotential at standard pressure level 500 mbar and their relative topography (Fig. 3).

The cold subsurface (dichothermal) layer of the Okhotsk Sea creates the favorable conditions for the intensification and stability of the anticyclonic atmospheric fields in the region. On climatic maps for the summer months (from the beginning of May and sometimes even from the end of April) the pressure fields over the Okhotsk Sea are revealed as the ridge of the North Pacific anticyclone.

The permanent North Pacific (Honolulu, Hawaii) anticyclone is an enormous high warm baric formation developed over the warm oceanic surface within the high pressure band of the Pacific subtropical and tropical zones (20-40°N) with a center located to the north of the Hawaiian Islands. The appearance of the North Pacific anticyclone results from dynamic factors and is supported by migration of Arctic and Asiatic continent anticyclones into the system.

The summer thermal conditions over the oceanic surface lead to the ridge propagation from the source towards the Far Eastern Seas, in particular, to the Okhotsk Sea. Under the favorable tropospheric thermodynamic conditions in the Maritime Polar Air Mass over the Okhotsk Sea the original anticyclone generates a cold baric formation with the relatively low height extension.

Generally, from May till July, in the period of the most intensive anticyclogenesis, the high pressure fields over the Okhotsk Sea were observed from 27 up to 60 days or, on average, in a half of all cases (47%) with an increase in June up to 55% (Table 1). The ridge was detected two times more often than the anticyclone centre. The essential variations in the yearly mean distribution of the high pressure fields over the Okhotsk Sea were revealed. For example, in June the ridge or anticyclone centre was fixed from 6 up to 24 days. The summary duration of the whereabouts over the Sea was 10-14 days for the anticyclone and 15-19 days for the ridge.

The lowest air temperatures were recorded in the period of the most intensive anticyclogenesis. A weakening of the anticyclone induced an enhancement of the air temperature in Vladivostok, Magadan and at other stations.

The same conclusions were made based on the analysis of the air temperature variations at the station of the Korean Peninsula (Pyongyang and Seoul) (Fig. 4).

Thus, the Okhotsk maritime anticyclogenesis is a result of the atmospheric processes not over the temperate zone but their interaction with the ocean and the processes over the Tropical and Arctic zones in the Northern Hemisphere. The role of the anticyclonic activity in the Far Eastern weather formation is not doubted and complex.

REFERENCES

Dashko, N.A., and E.I. Teslenko. 1991. Study of Thermal Regime in June over the South Primorye. Obninsk Informormation Centre of All Union Hydrometeorological Research Institute. WDC. 1090:gm-91. (in Russian).

Manual of the Long-term (3-10 days) Weather Forecast. 1968. L., Gidrometeoizdat. (in Russian).

Manual of the Short-term Weather Forecast. 1965. L., Gidrometeoizdat. (in Russian).

Soviet Union's Climatic Reference Book (Solar radiation, air temperature). 1966-1970. L., Gidrometeoizdat. (in Russian).

TABLES AND FIGURES

Table 1. Frequency (days, %) of anticyclonic and cyclonic baric fields over the Okhotsk Sea

Characteristics		Month			In all of the period
		May	June	July	
		Anticyclonic field			
Ridge of	min (days)	1	4	3	16
high pressure	max (days)	16	16	18	39
Average	(days)	7.5	9.8	10.4	27.4
	%	24.2	32.7	33.5	29.8
Centre of	min (days)	0	1	2	6
high pressure	max (days)	13	10	19	27
Average	(days)	4.5	5.8	5.4	15.8
	%	14.5	19.3	17.4	17.2
In all	min (days)	3	6	8	27
	max (days)	24	24	26	60
Average	(days)	12	15.6	15.7	43
	%	38.7	52	50.6	47
		Cyclonic field			
In all	min (days)	7	6	5	32
	max (days)	28	24	23	65
Average	(days)	19	14.4	15.3	49
	%	62.3	48	49.4	53

FIGURES

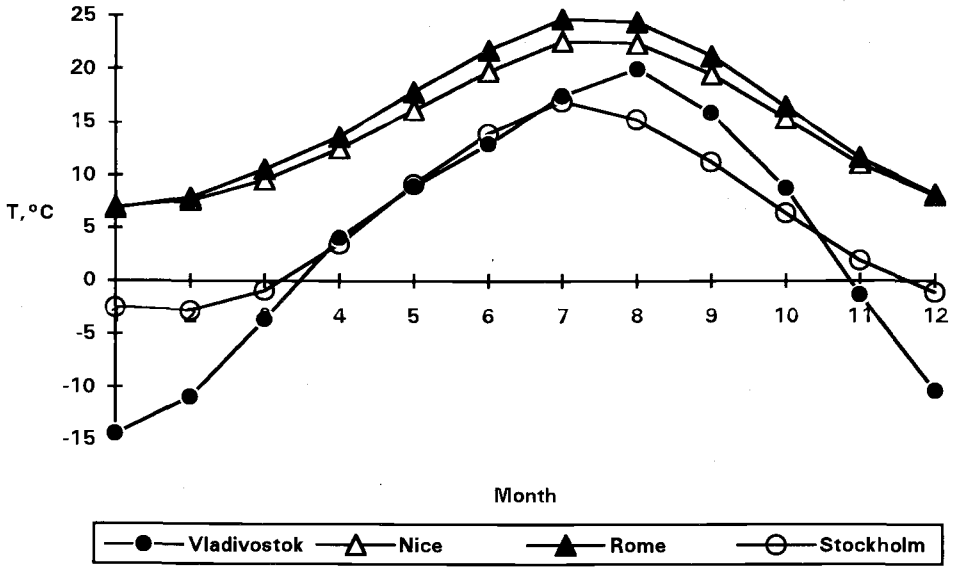

Fig. 1. The monthly (January - December) mean air temperature in Vladivostok, Nice, Rome and Stockholm.

a)

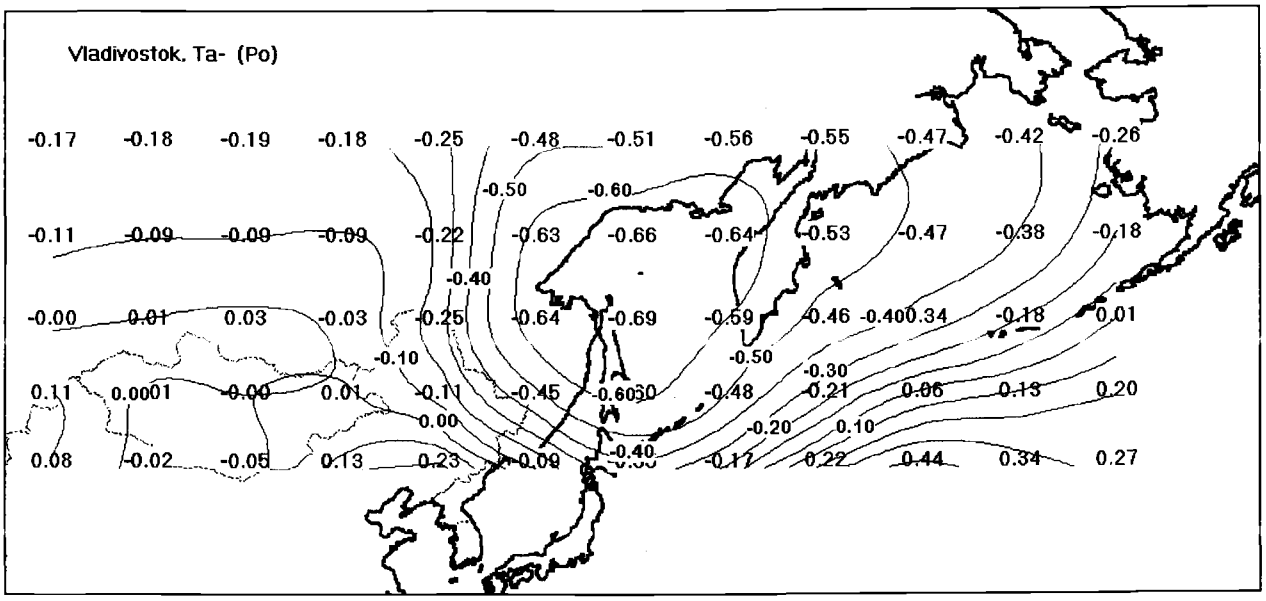

b)

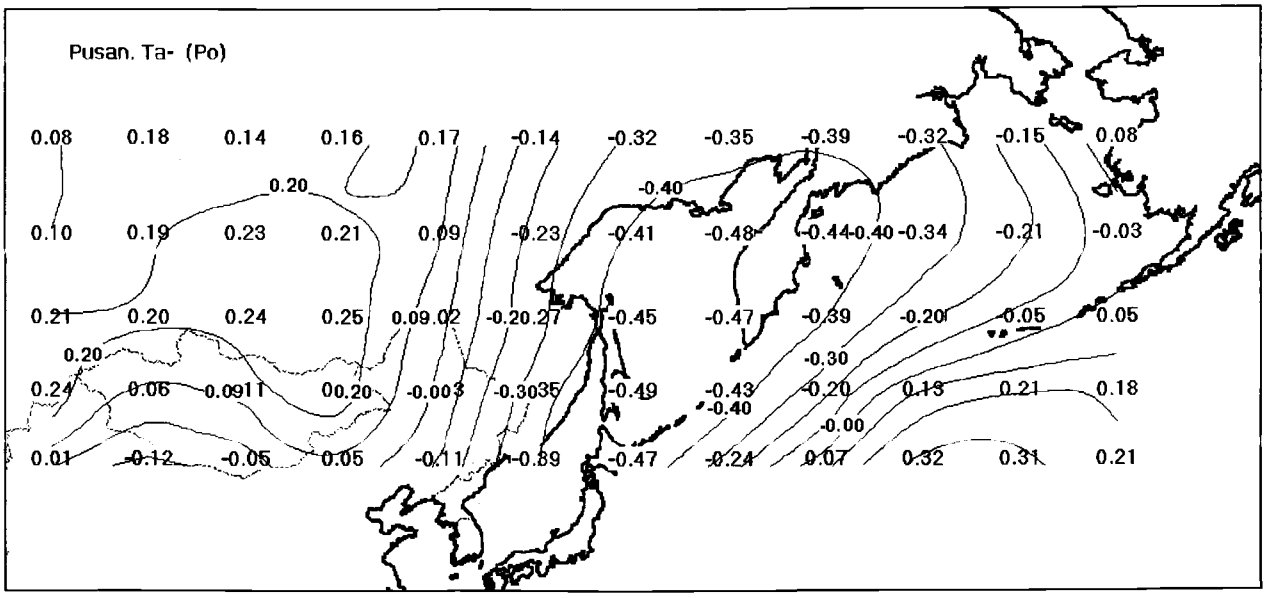

Fig. 2. Cross-correlation of the average monthly air temperature at stations Vladivostok (a) and Pusan (b) with air pressure over the Okhotsk Sea in June.

a)

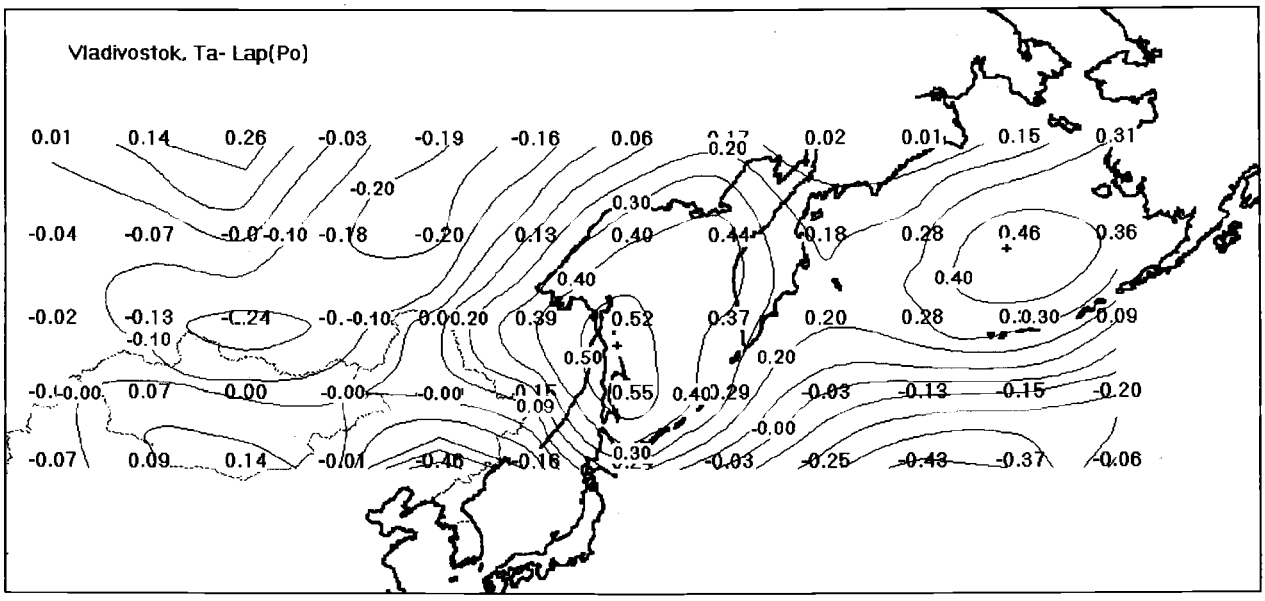

b)

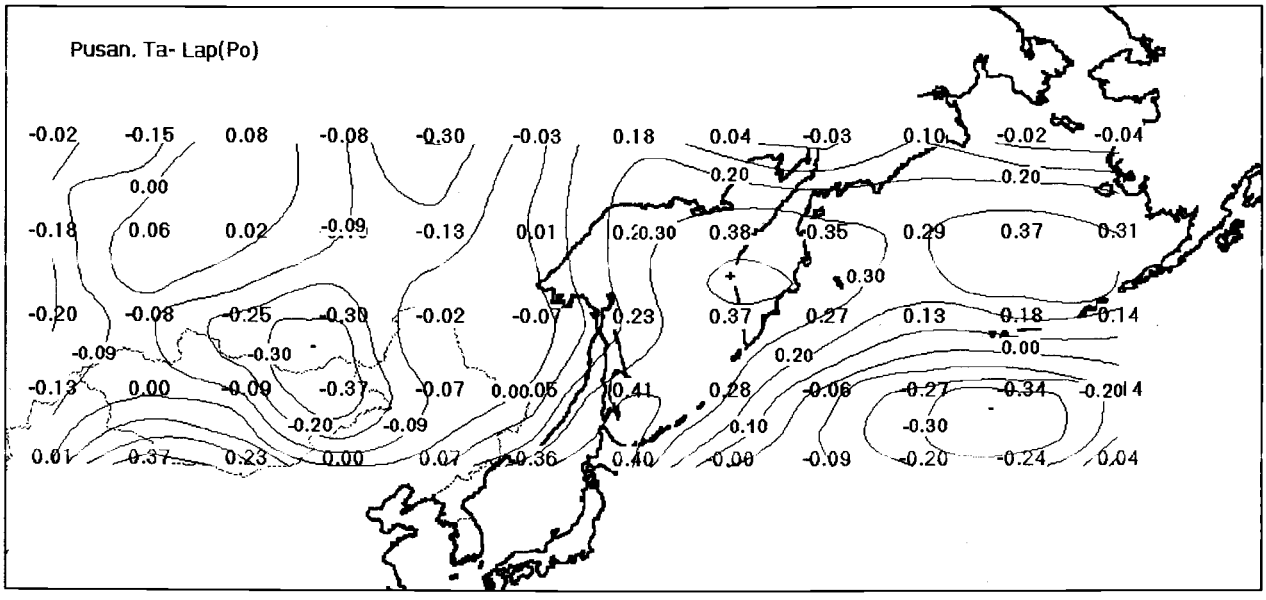

Fig. 3. Cross-correlation of the average monthly air temperature at stations Vladivostok (a) and Pusan (b) with the air pressure derivatives over the Okhotsk Sea in June.

a)

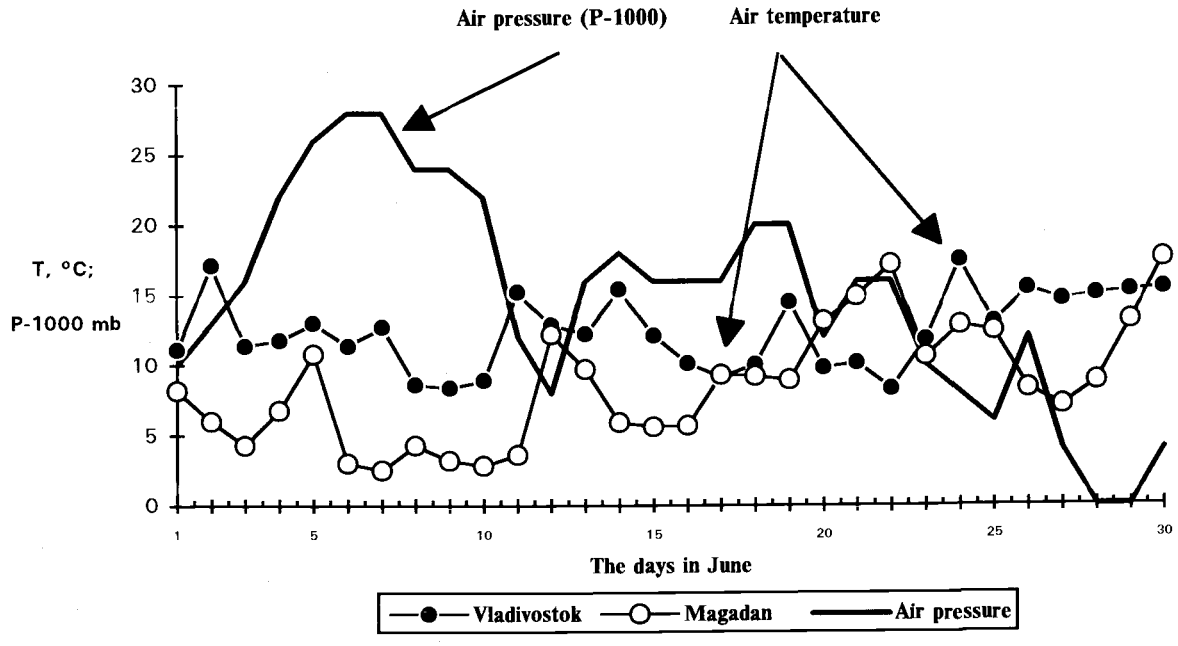

b)

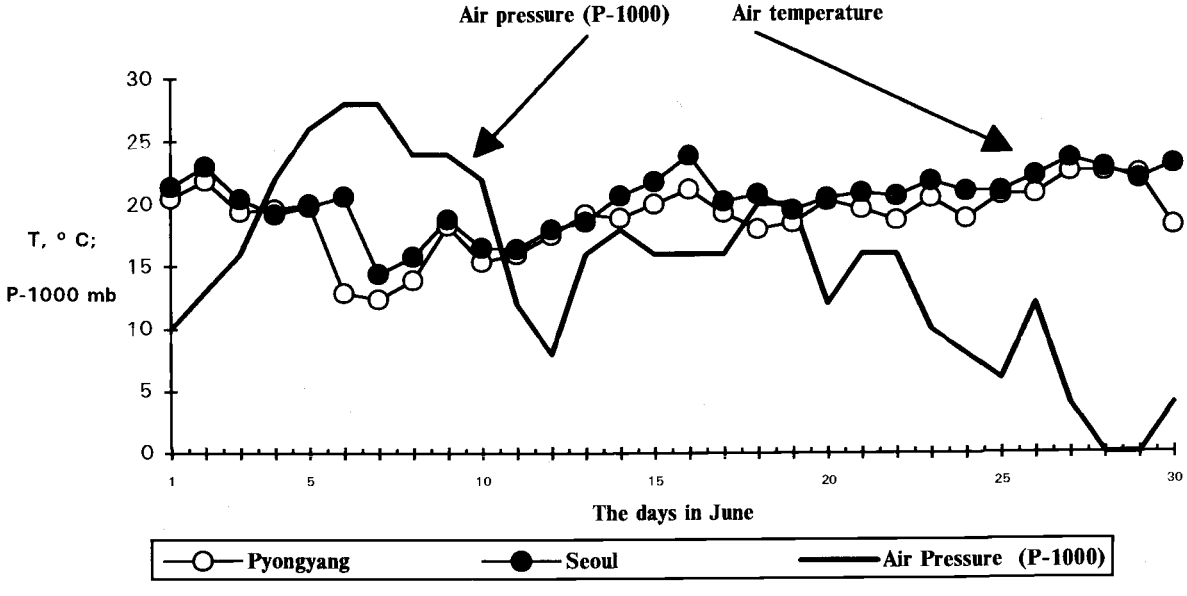

Fig. 4. The daily mean air temperature in June 1992 at the meteorological stations of Primorye (a) and Korean Peninsula (b) and mean air pressure over the Okhotsk Sea.

Research of Water Structure and Dynamics in the Okhotsk Sea and Adjacent Pacific

Boris S. DYAKOV, Alexander A. NIKITIN and Vadim P. PAVLYCHEV

Pacific Research Institute of Fisheries and Oceanography (TINRO-centre)

Vladivostok, Russia.

Water structure and dynamics of the Okhotsk Sea and adjacent Pacific have been studied based on satellite information and CTD data from the section carried out aboard the *R/V Academik Nesmeyanov* in September 3-12 1993. Spatial variability of geostrophic currents and hydrological conditions in the layer of 1,000 m have been investigated. It was established that the most complex dynamic zone was situated near the Kuril Islands.

The international expedition organized by the Pacific Oceanological Institute (Vladivostok, Russia) and the Institute of Ocean Sciences (Sidney, Canada) was performed in September 3-12 of 1993 aboard the *R/V Academik Alexander Nesmeyanov*. The oceanographic section along the WOCE P1W line has been carried out. A total of 30 stations, separated nominally by 30 nautical miles, were occupied.. The section started in the Pacific at 44°00'N and 153°30'E and ended on the northern Okhotsk shelf at 58°30'N and 141°48'E. On the way section passed through the Bussol Strait and crossed the basin and the shelf region of the Okhotsk Sea. A total length of the section was 870 miles (Fig. 1).

CTD data from this section and satellite information were used to investigated the water structure and dynamics of the Okhotsk Sea and adjacent Pacific. Velocities and volume transport of the geostrophic currents in the layer of 1,000 m were calculated applying the standard procedure (Zubov, 1979).

In September the cyclonic activity in the Okhotsk Sea and adjacent are of the Pacific strengthed. Also, the intrusion of water from the Pacific through the Bussol and Fourth Kuril Straits in the Okhotsk Sea increased (Luchin and Darnitsky, 1993; Luchin, 1987). Satellite images indicated the complex horizontal water structure near the Kuril Islands and on the northwestern shelf of the Sea (Fig. 1). The main features of this structure are: thermal front, currents, eddies of different scales and rotations (cyclonic and anticyclonic). Within the Kuril Islands area the intrastructure of the Kuril front and seasonal and synoptical secondary fronts have been revealed (Gladyshev, 1994). The cold Kuril current was observed along the Kuril Islands, and the warm Soya current was detected near the northern coast of Hokkaido. Six anticyclonic eddies were found in the region, five (A1-A5) in the Okhotsk Sea and one (A6) in the Pacific. The transverse streamers branched from topographical upwelling near the Central Kuril Islands (Darnitsky and Bulatov, 1995). The formation of Okhotsk sea eddies and streamers is a result of the interaction of large-scale tidal currents with the bottom topography (Gladyshev, 1994; Darnitsky and Bulatov, 1995).

The anticyclonic eddy A6 was found to the southeast from the Bussol Strait at 45°00'N and 152°00'E. The eddy was not stationary but was a type of eddy usually observed in the area of current convergence or divergence (Bulatov and Lobanov, 1983). The main formation mechanism of this eddy is the displacement of currents (Ginzburg, 1992). At the same time Lobanov (1993) considered all Kuril anticyclones as old Kuroshio rings. He suggested that in result of water transformation the warm core of these rings was destroyed and the cold core was formed.

The oceanographic section crossed the northeastern periphery of the eddy A6 (Fig. 1). In the layer of 50-350 m (stations 1-5) the cold water core with temperature less than 2°C was found (Fig. 2). During the survey more eddies were established in the Okhotsk Sea as compared with the adjacent Pacific, similar to that was observed in 1991 and 1994 (Darnitsky and Bulatov, 1995). Eddy formation is connected to general water circulation of the Okhotsk Sea and the water exchange between the Sea and the Pacific (Gladyshev, 1994). Analysis of the satellite information demonstrated the entry of the Pacific waters through the Bussol Strait in the Okhotsk Sea (Fig. 1).

Some structural zones were revealed on the section "Pacific Ocean-Okhotsk Sea". The most complex dynamic zone was situated near the Kuril Islands. The cold Kuril current of 100 miles width moved along Simushir Island (Fig. 3). In the center of this current (20-300 m) geostrophic velocity was 18.0-19.8 cm/s. The discharge of the Kuril current ws equal to 10.2×10^6 m^3/s (near normal), but in July 1993 the discharge was 6×10^6 m^3/s.

The speed on the periphery of the eddy A6 was 5.2-8.9 cm/s and increased to the center to 12.8-15.9 cm/s (Fig. 3). The diameter of eddy A6 was equal to about 70 miles and the discharge changed from 6.8 up to 8.4×10^6 m^3/s which compared with the intensity of the Kuril current. The Kuril current and anticyclone A6 spreaded approximately up to 700 m (depth of speed isoline of 5 cm/s).

To the northwest from the Kuril current the Northeastern current (stations 8-12) of 140 miles width and speed in the center 6.3-7.5 cm/s was traced (Fig. 3). The discharge of this flow was 7×10^6 m^3/s and water temperature in the upper layer of 20 m was 10-12°C (Fig. 2). In central deep water part of the Okhotsk Sea a calm halistatical zone was found where the current velocity of different directions did not exceed 2.5 cm/s in the upper 50 m layer and the volume transport in the layer of 1,000 m between separate stations fluctuated from 0.1 to 0.7×10^6 m^3/s. Water temperature of the upper homogeneous 20 m layer was 12°C (Fig.2).

The increase in the current velocity to 5.5-11.7 cm/s is observed in the north near the continental slope and at Iona Island (Fig. 1). Close to the southwestern part of the Kashevarova bank (stations 23-25) the cyclonic rotation with speeds 9.1-11.7 cm/s was found. The eddy led to the powerful upwelling of the intermediate waters (Chernavsky et al., 1993) (Fig. 2). Near the northwestern shores of the Okhotsk Sea, the Northern Okhotsk current to the west had a speed of 4.5 cm/s (Fig. 1). The more southern current with speed 5.5 cm/s was opposite in direction (Northern Okhotsk counter current). These two currents formed the cyclonic gyre.

The oceanographic section crossed the region of the subarctic hydrological water masses. Typical T, S curves of a variety of subarctic water structures are presented in Fig. 4. For example, T, S curve from station 3 was characteristic for waters from the Pacific (Pacific variety). The region near the Kuril Islands was characterized by T, S curves from stations 6,7,9 (Kuril variety). The subarctic hydrological structure of the deep water part of the Okhotsk Sea was reflected on T, S curves from stations 12, 16, 20, 2, 24. The water structure on the Okhotsk sea shelf was presented by T, S curves from stations 26, 28, 30.

Acknowledgements

The authors would like to express sincere gratitude to Drs. Alexander S. Bychkov and Gennady I. Yurasov (Pacific Oceanological Institute, Far-Eastern Branch of Russian Academy of Sciences, Vladivostok, Russia) and Drs. Howard J. Freeland and Frank A. Whitney (Institute of Ocean Sciences, Department of Fisheries and Oceans, Sidney, B.C., Canada) for providing data from the WOCE Section P1W.

References

Bulatov, N.V., and V.B. Lobanov. 1983. Investigation of mesoscale eddies to the east of the Kuril Islands on the base of meteorological satellites data. Earth Research from Space. 3:40-47 (in Russian).

Chernyvsky, V.I., I.A. Zhigalov, and V.I. Matveev. 1993. Oceanological bases of high biological productivity zone formation in the Okhotsk Sea. Hydrology and Hydrochemistry of Seas. St.-Petersburg. 9(2):157-160 (in Russian).

Darnitsky, V.B., and N.V. Bulatov. 1995. The Okhotsk Sea eddies of the Kuril nearshore area. Vladivostok, POI. (in press).

Ginzburg, A.I. 1992. Non-stationary vertical motions in the ocean. Oceanology. 32(6):997-1004 (in Russian).

Gladyshev, S.V. 1994. Thermohaline fronts near the Kuril Islands. Oceanology. 34(4):504-512 (in Russian).

Lobanov, V.B. 1993. Investigation of synoptical eddies in the Kuroshio-Oyashio region based on satellite and vessel information. Ph.D. Thesis. Vladivostok. POI. 24 p. (in Russian).

Luchin, V.A. 1987. Water circulation of Okhotsk Sea and its specific interannual variability as a result of diagnostic calculations. Trudy DVNIGMI. 36:3-13 (in Russian).

Luchin, V.A., and V.B. Darnitsky. 1993. Climatic eddies current structure of the Okhotsk sea in autumn (part 2). Proc. 9-th conference on catching oceanology. Moscow. p. 219-222 (in Russian).

Zubov, N.I. 1929. Calculation of sea current elements according to information of hydrological section. Morskoy Nauchny Institute. 69 p. (in Russian).

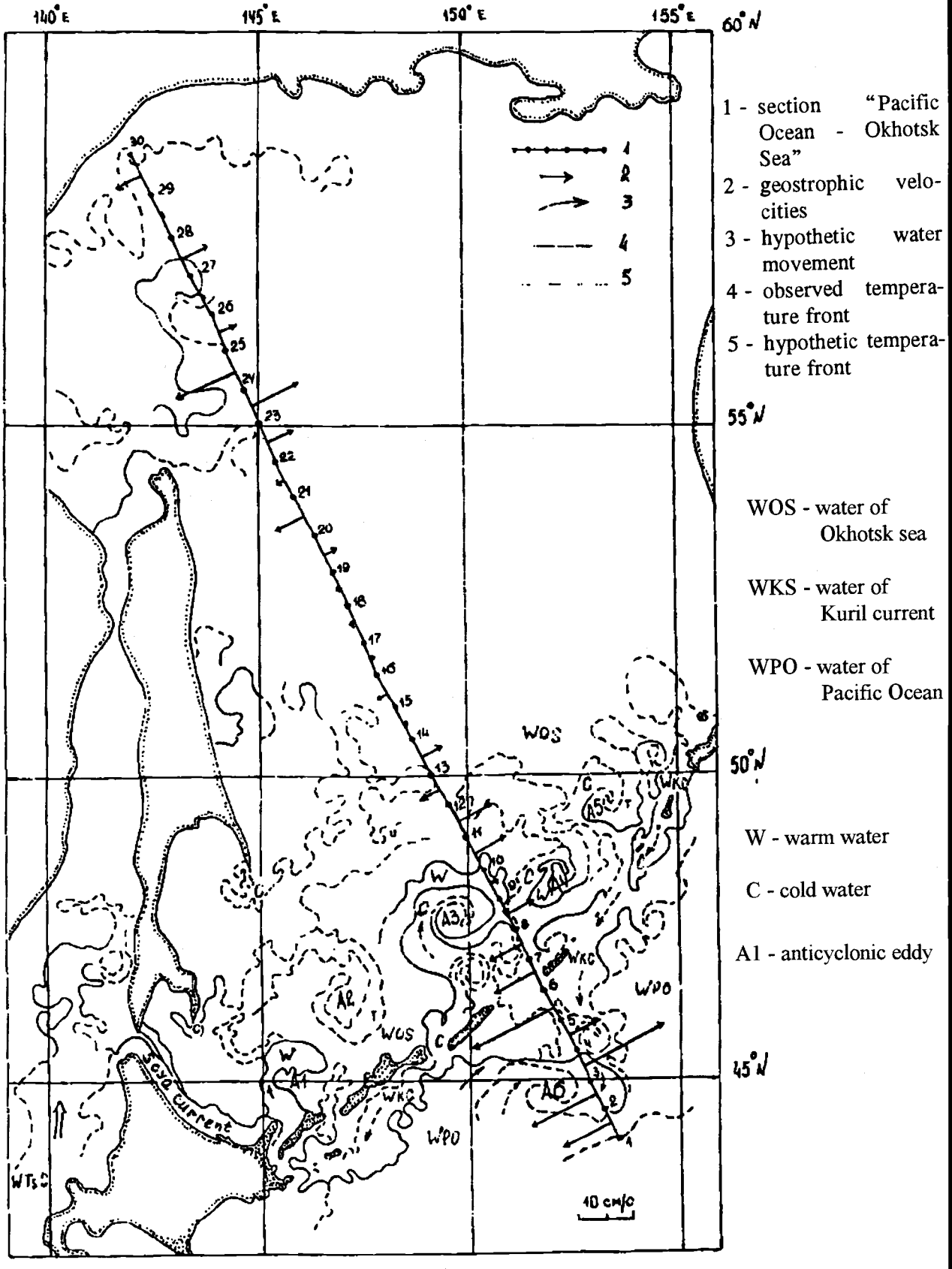

Fig. 1. Oceanographic stations occupied and the Okhotsk Sea water structure (according to satellite data) in September 1993.

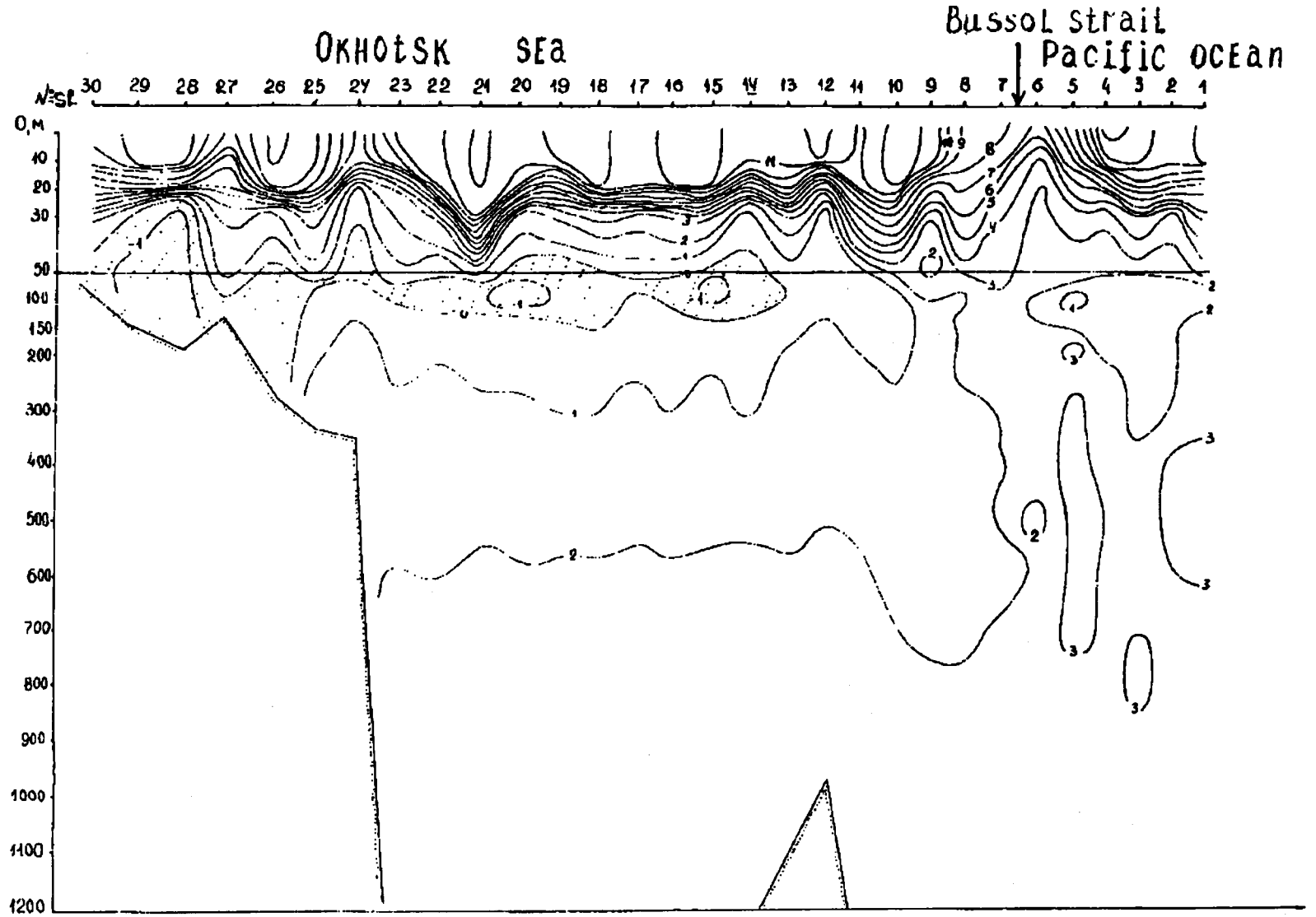

Fig. 2. Temperature distribution along the section "Pacific Ocean - Okhotsk Sea" through the Bussol' Strait in September 1993.

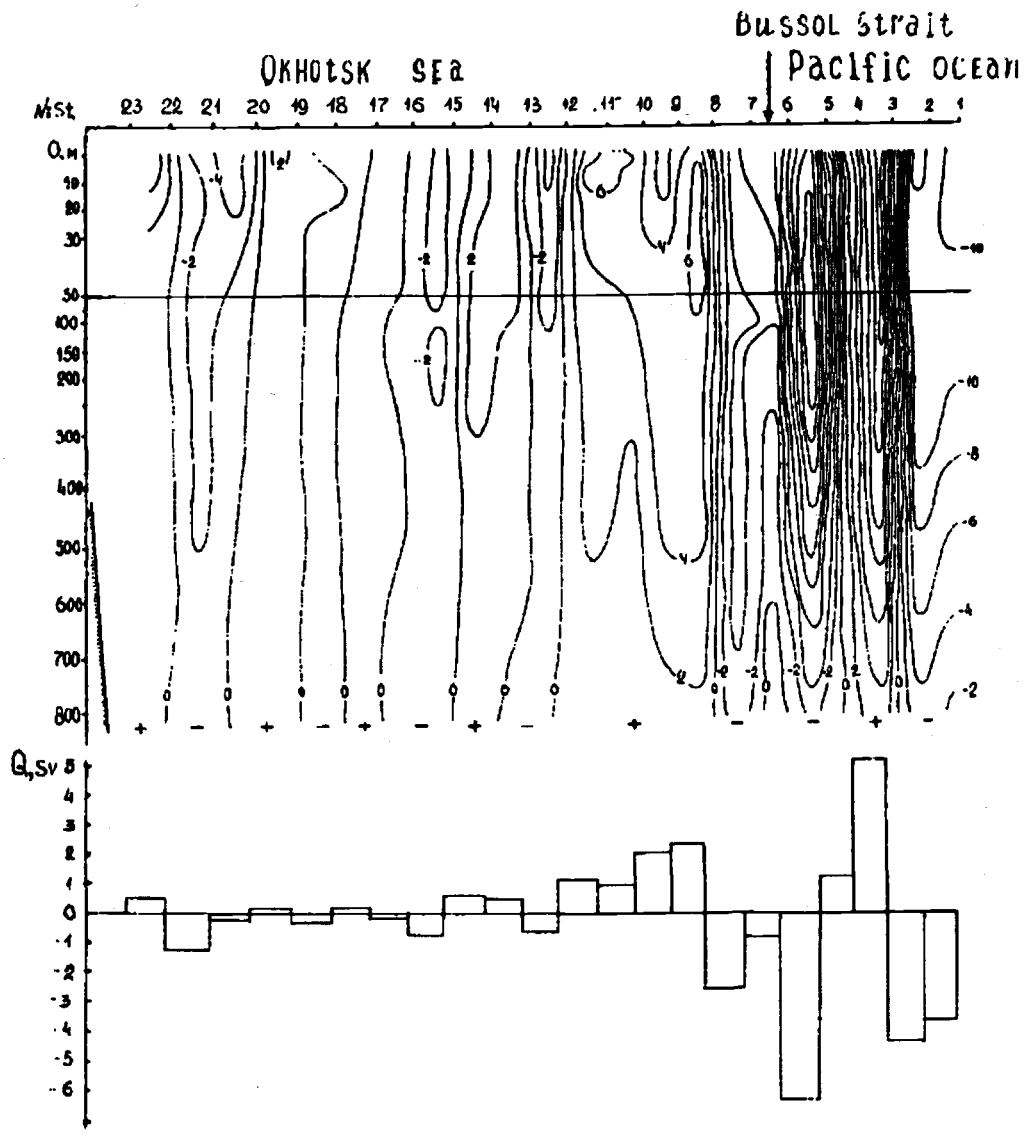

Fig. 3. Geostrophic velocities and water transport along the section "Pacific Ocean - Okhotsk Sea" through the Bussol' Strait in September 1993.

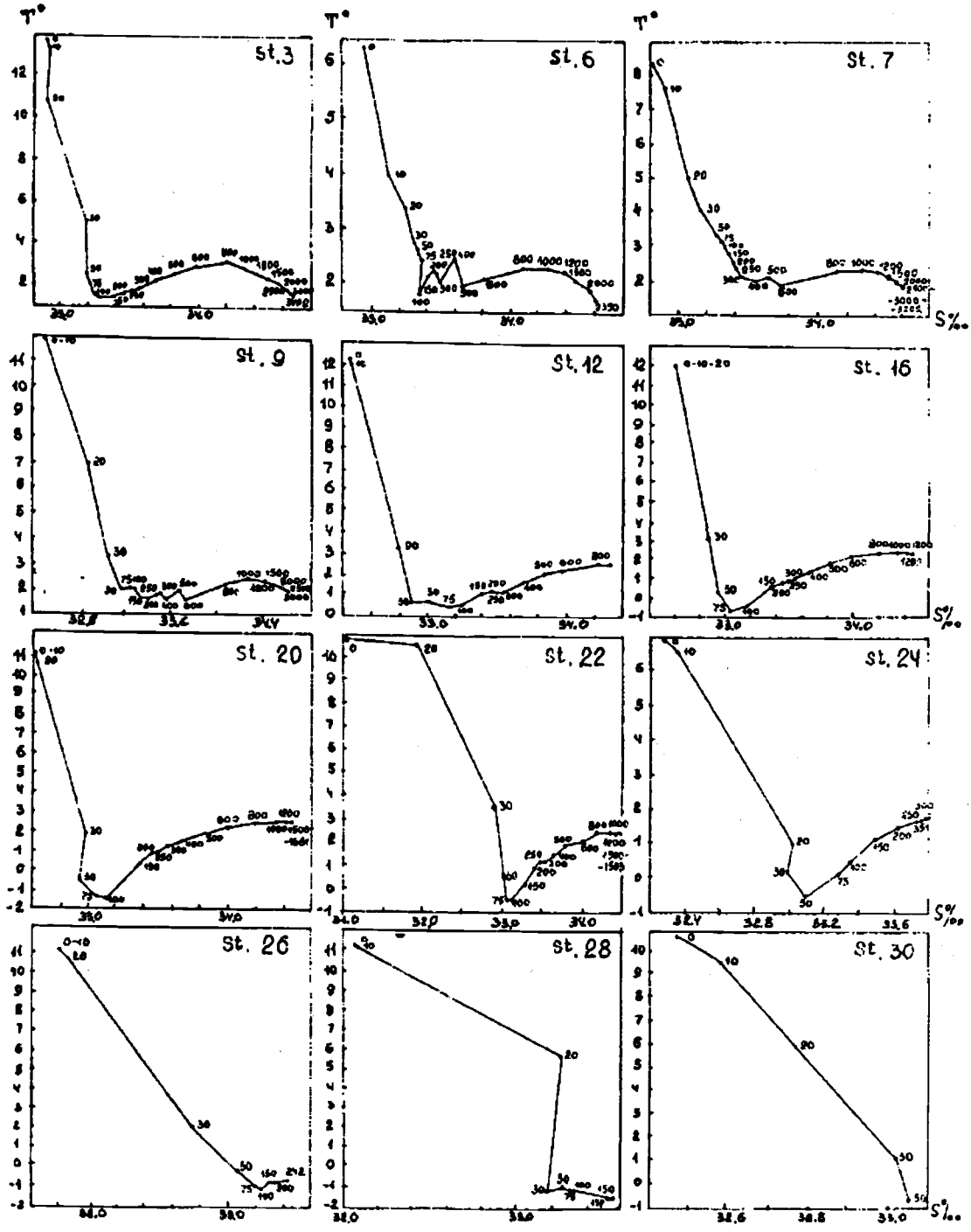

Fig. 4. T, S - curves for selected stations along the section "Pacific Ocean - Okhotsk Sea" through the Bussol' Strait in September 1993.

The Okhotsk Sea Component of Pacific Intermediate Water

Howard J. FREELAND[1], Alexander S. BYCHKOV[2], C.S. WONG[1], Frank A. WHITNEY[1] and Gennady I. YURASOV[2]

[1] Institute of Ocean Sciences, Department of Fisheries and Oceans, Sidney, B.C., Canada
[2] Pacific Oceanological Institute, Far Eastern Branch, Russian Academy of Sciences, Vladivostok, Russia

INTRODUCTION

In the fall of 1993 an opportunity arose to conduct a CTD and hydrographic survey along a line of stations through the Okhotsk Sea. This line of observations was conducted to *WOCE* (World Ocean Circulation Experiment) specifications for the accuracy of sampling and the nominal spacing (30 nautical miles) of stations. The observations were acquired as a joint project involving scientists from Canada and Russia to execute the westernmost leg of the *WOCE* line P1, hereinafter referred to as P1W, from the research vessel *Akademik Nesmeyanov* operated by the Pacific Oceanological Institute in Vladivostok, Russia.

Fig. 1 displays a map of the station locations. A total of 35 stations were occupied to the bottom or 3,500 metres, whichever is shallower. However, for the purposes of this paper only the first 30 stations will be discussed as they included all variables sampled and specifically constitutes the line of observations known as P1W. These are the stations identified with triangles and circles on Fig. 1.

It is well known (Talley, 1991) that the salinity distribution in the top 1,000 metres of the N.E. Pacific is dominated by a salinity minimum tongue. The salinity minimum dominates the salinity distribution between latitudes 45°N to 25°N and is still detectable as far south as 10°N. Talley (1991) reviews some of the history concerning speculation about the possible origin of the NPIW, and some of that material bears repeating here. The Okhotsk Sea does have lower salinity (33.45 psu) and higher oxygen (170 μM/kg) at σ_θ = 26.8 than is encountered in the North Pacific. Typical values along the 165°W section presented in Fig. 2 being 34 psu and 120 μM/kg, respectively. Furthermore, the density of water at the sill in the Bussol' Strait is high (σ_θ = 27.7) suggesting that it could be a source of dense water in the North Pacific. These ideas were pursued by Wüst (1930) who concluded, based on very little information, that the Okhotsk Sea likely was the source of NPIW. Reid (1965, 1973) concluded otherwise. In particular, Reid felt that the Okhotsk Sea could never supply the volume of water required. Favorite et al (1976) disagreed with Reid and actually attributed the sources of both the Oyashio and the East Kamchatka Currents to water formed within the Okhotsk Sea. Kitani (1973) suggested that water mass modification on the Okhotsk Sea shelf could produce water at densities up to 27.05 σ_θ which might subsequently flow into the northwest Pacific. Finally, Talley (1991) concurs with the opinions of Kitani, though is unable to estimate the volume of NPIW that might be formed within the Okhotsk Sea. This paper will demonstrate evidence in support of Kitani's conjecture.

In this paper we will present results from a single section completed from the open Pacific, through the Bussol' Strait and continuing through the Sea of Okhotsk to the coast of Siberia. The data will be described in section 2 and discussion of the implications for the formation of the NPIW mass will be presented in section 3. We will conclude that we have observed the Okhotsk Sea component of

the NPIW water, but that only part of that water mass is formed by direct ventilation from surface processes.

DATA DESCRIPTION

The observations discussed in this paper were completed as part of the cruise designated P1W (western leg of line P1) by the WOCE Hydrographic Program office, 9316 by the Institute of Ocean Sciences (which took a major part in the program), and AN25 by the Pacific Oceanological Institute, Vladivostok, which operates the vessel, the *R/V Akademik A. Nesmeyanov*. In all that follows it will be cited by the WOCE designation, P1W. This survey was a joint endeavour completed by scientists from the Institute of Ocean Sciences (Canada), the Pacific Oceanological Institute (Russia) and the Woods Hole Oceanographic Institution (U.S.A.). The cruise began on the 30th August and was completed on the 21st September, 1993. The Woods Hole interest was in sedimentary processes within the Okhotsk Sea, and none of those observations will be presented or discussed here.

Fig. 2 displays profiles of the primary variables. The indicated bottom is determined from the bottom of each CTD cast. This is reliable as a bottom determination as the CTD was lowered to within a few tens of metres of the bottom with the aid of a pinger suspended below the rosette sampler.

Potential temperature and density are computed relative to the surface. A notable feature is the presence of two lenses of very cold water lying entirely within the Okhotsk Sea. The dichothermal layer, centred at a depth of about 100 metres was contoured in the open water between stations 13 and 24 (Fig. 2a). It is characterized by low salinities 33.0-33.2 psu (Fig. 2b) and densities 26.4-26.6 σ_θ (Fig. 2c) and is supersaturated (up to 360 μmol/kg) by oxygen (Fig. 2d). The latter indicates that winter convection reaches to the depth of the dichothermal layer and that surface heating covers the layer in summer. Temperatures within this sub-zero water mass are as low as -1.1°C near station 20 and represents the temperature of the winter surface mixed layer (Moroshkin, 1966; Talley and Nagata, 1995). The "saline" (about 33.48 psu) water with temperature near the freezing point (-1.71°C), density of 26.85-26.90 σ_θ and oxygen concentration of 250-260 μmol/kg was found just above the bottom on the northwestern shelf on stations 28 and 29 (Figs. 2a-d). This is the so-called Kitani Water originated due to brine rejection during active sea-ice formation (Kitani, 1973; Alfultis and Martin, 1987). We should also mention that in the temperature field there is evident of a discontinuity in properties on opposite sides of the Bussol' Sill. This could suggest either that exchange between the Okhotsk Sea and the open Pacific is restricted at depths from 1,000 m to as shallow as 100 metres, or that the area of the Bussol' Strait is a region where water masses are being modified rapidly, perhaps by tidal mixing.

The potential density structure through the Bussol' Strait and into the Pacific Ocean is interesting (Fig. 2c). Isopycnals at all depths shoal as they are followed from the Okhotsk Sea towards the Pacific. Between stations 5 and 3 they then deepen and then rise between stations 3 and 1. This indicates the presence of a very energetic eddy. In fact there are persistent reports of the presence of a semi-permanent anticyclonic eddy directly outside the Bussol' Strait, and has been named 'The Bussol Eddy' by Russian Scientists. Descriptions of the Bussol' Eddy can be found in papers by: Saitoh, Kosaka and Iisaka (1986); Rogachev and Goryachev (1991) and Rogachev et al (1995). Over the central Okhotsk Sea a general doming of isopycnals is evident, suggestive of a general cyclonic circulation pattern. All of these features are also reflected in the salinity distributions shown in Fig. 2. Between stations 11 and 24 contours of all variables are fairly flat, suggesting little dynamics taking place at the time of the survey. A doming of isopycnals near station 24 may be indicative of a recirculation over the Kashevarov Bank which was close to line P1W.

The dissolved oxygen concentrations in the deep water within the Kuril Basin are more homogeneous than those at similar depths in the open Pacific (Fig. 2d). Oxygen levels throughout the Kuril Basin are similar to values in the Pacific at sill depth. This fits the distribution of other properties, where in all cases the profiles below sill depth inside the Kuril Basin are different from those outside. This suggests that some exchange is occurring in the very deep waters replacing water in the Kuril Basin. But we see little evidence of exchange at other depths. We will return to this point in more detail later in the paper. We see a water mass at the bottom of the Deryugin Basin which is very low in dissolved oxygen, and is also (see Fig. 2) extremely rich in dissolved silicate. This has all of the marks of a very old water mass that is rarely replaced and so sets this basin apart from the Kuril Basin. Water this low in dissolved oxygen is actually found at stations 1 to 4 outside of the Okhotsk Sea where the dissolved oxygen profiles show typical for the northern N. Pacific minimum near a depth of 1,000 metres. However, there can never have been any actual connection between these two water masses as the dissolved silicates are substantially different

The distributions of the nutrients, reveal patterns that are largely reflected in the other, dynamic variables. The notable exception being the presence of very high silicate levels within the Deryugin Basin. The absence of extremely high silicate levels near the bottom of the Kuril Basin suggests that water within that basin is freely exchanged with water in the open north Pacific. The other nutrients (phosphate and nitrate) do not show elevated values in the Deryugin Basin.

Fig. 3 demonstrates details of the potential density distribution around the sill in the Bussol' Strait computed from data at the first 11 stations (shown by the triangle symbols of Fig. 1). This clearly shows that water at a depth of 3,000 metres near the bottom of the Kuril Basin can be exchanged freely with water at a depth of only 2,000 metres in the open Pacific. Examination of other properties indicate that these waters have identical silicate and oxygen profiles, and we will see later that these also have identical θ-S relationships. We presume, therefore, that the properties of the seawater in the open Pacific at 2,000 metres and near bottom in the Kuril Basin are identical, and that deep water is freely exchanged across the Bussol' Sill. Indeed, it appears from Fig. 3 that the survey actually caught a deep water replacement event in the act, so to speak.

The density structure shown in Fig. 3 suggests that the Bussol' Eddy penetrates very deeply. If the eddy intensifies its circulation then the dip in deep isopycnals centred on station #3 must become more pronounced and either isopycnals will rise at stations 1 and 5, or fall at station 3, or both. This suggests that the density of water appearing at the Bussol' Sill from the Pacific Ocean may be determined by the strength of the eddy. In other words, the probability of a deep water replacement event in the Kuril Basin may well be pre-conditioned, or possibly even determined, by the strength of the Bussol' Eddy.

NORTH PACIFIC INTERMEDIATE WATER

Fig. 4 shows θ-S curves for all data collected along the major line of 30 stations indicated in Fig. 1. At the far right of the diagram all curves converge to a single water mass. This is expected from the detailed structure around the Bussol' Sill shown in Fig. 3. The θ-S curves separate into two distinct curves in the σ_θ range of 26.9 to 27.3. The upper branch contains θ-S curves from stations 1 to 5, inclusive, i.e., stations from the open Pacific to the sill in the Bussol' Strait, but no further. The lower branch contains profiles from all the other stations 6 to 30 within the Okhotsk Sea.

A region of θ-S space has been marked with a square. This identifies the profiles that are typical of the Okhotsk Sea, but having θ-S properties (at the same sigma-theta values) distinctly different from water in the open Pacific. Ohtani (1989) identifies this water as the Sea of Okhotsk

component of the North Pacific Intermediate Water mass (NPIW), and Watanabe et al (1991) agree with this conclusion. In the remainder of this paper we will refer to the Sea of Okhotsk component of NPIW as Sea of Okhotsk Intermediate Water, or SOIW. Let us assign an SOIW concentration of 1.0 to the θ-S values that occupy the centre of that rectangle. Allow this concentration to fall linearly to zero at the boundary of the box, and remain zero for any θ-S value outside of the box. We can then search the distributions of θ and S and use this concentration to examine the spatial distribution of the SOIW which is illustrated in Fig. 5. The highest concentrations of this water mass occur between depths of 700 to 800 metres. The water does not penetrate to the bottom in the deepest part of the Deryugin Basin and appears to be cut off very abruptly in the approaches to the Bussol' Strait. We see no evidence of exchange of water through the Bussol' Strait within this water mass. The dashed line superimposed on the contour chart is the path of the contour $\sigma_\theta = 27.05$, discussed above. This, as expected, delineates the upper surface of the SOIW distribution.

If a water mass is formed at the surface and then ventilates a deeper basin, then some properties of this water mass will be carried from the surface and maintained. McDowell et al (1982) point out that for quasi-geostrophic ocean dynamics the horizontal velocity is nearly non-divergent and so at scales larger than the Rossby radius of deformation the relative vorticity is much smaller than the stretching term and so potential vorticity can be estimated from hydrographic measurements alone as:-

$$\bar{q} = \frac{f}{\rho_0}\frac{\partial \rho}{\partial z}.$$

The quantity q is conserved as water sinks below the surface and has been used by Talley and McCartney (1982) to track the penetration of Labrador Sea Water into the deep waters of the north Atlantic by tracking the locations of a tongue of potential vorticity minimum. A ventilated water mass will show up as a minimum in q because a convectively renewed water mass should show excessive vertical homogeneity relative to the water above and below it.

The potential vorticity q is presented on Fig. 6. The contour interval is variable because q has a very large dynamic range. In this plot we have shaded the region of q less than 100×10^{-14} and greater than 50×10^{-14} $cm^{-1}s^{-1}$. Also, the bold dashed lines show σ_θ values of 26.85 and 27.05. The potential vorticity at stations 1 through 4 (in the open Pacific) decreases monotonically from the surface to the deep water and so show no evidence of any recent ventilation. However, the vorticity separates the water masses within the Okhotsk Sea into 4 distinct regions. Starting from the top we find the high potential vorticity region, above 200 metres. Extending from 200 m to a depth of perhaps 450 m we find a region of low potential vorticity. The line $\sigma_\theta = 26.85$ lies down the centre of this potential vorticity minimum. Below this value of σ_θ the potential vorticity increases to a maximum value at a mean σ_θ of 27.05 (region 3) and thereafter decreases steadily to the bottom (region 4). This diagram suggests that a recent convection event has occurred that has ventilated the Okhotsk Sea at a mean density of $\sigma_\theta = 26.85$. The region of ventilation extends to greater densities, perhaps as great as $\sigma_\theta = 27.05$, the maximum density possible indicated by *Kitani*, but certainly no deeper. Thus we have observed ventilation of the Okhotsk Sea essentially to the top surface of the water mass identified as the SOIW, and possibly a short distance into that water mass.

DISCUSSION

What this paper has shown is that if the water mass identified here, and by others, as the SOIW then we have a problem. The calculations of Kitani and the observations here indicate that only

the upper levels of this water mass are ventilated. If we are to move some of this water to higher densities then it is necessary to invoke some form of mixing process that will move water properties selectively downwards. Talley (private communication) has suggested that cabelling might be a significant process. Certainly, if two water masses of equal density are mixed, then cabelling will always increase the density of the mixture so leading to steady sinking. However, the density changes that can be effected by cabelling are rather small compared with the increases of density that we require here, of order 0.2 to 0.3 σ_θ units. Another possibility might be mixing by bottom generated turbulence originating from the very strong tidal flows known to run through the Bussol' Strait. We recommend that the Okhotsk Sea should be subjected to much greater scrutiny than has hitherto been the case. In particular future surveys should have as one object a determination of the role of sub-thermocline mixing processes and the role that these may play in the determination of the properties of the Okhotsk component of the North Pacific Intermediate Water mass.

REFERENCES

Alfultis, M.A., and S. Martin. 1987. Satellite passive microwave studies of the Sea of Okhotsk ice cover and its relation to oceanic processes, 1978-1982. J. Geophys. Res. 92:13013-13028.

Favorite, F., A.J. Dodimead and K. Nasu. 1976. Oceanography of the Subarctic Pacific region, 1960-71. International North Pacific Fisheries Commission. 33, 187p.

Kitani, K. 1973. An oceanographic study of the Sea of Okhotsk - Particularly in regard to cold waters. Bull. Far Seas Fish. Res. Lab. 9:45-77.

Moroshkin, K.V. 1966. Water masses of the Sea of Okhotsk. US Dept. of Commerce, Joint publication service 43.942, 98p. Translation of Vodnye Massy Okhotskogo Morya. Nauka Publ. House, Moscow, 65p., 1965

McDowell, S., P.B. Rhines, and T. Keffer. 1982. North Atlantic potential vorticity and its relation to the general circulation. J. Phys. Oceanogr. 12:1417-1436.

Ohtani, K. 1989. The role of the Sea of Okhotsk on the formation of Oyashio Water. Sea and Sky. 65:63-83 (in Japanese).

Reid, J.L. 1965. Intermediate waters of the Pacific Ocean. Johns Hopkins Press, Baltimore, MD, U.S.A. 85p.

Reid, J.L. 1973. Northwest Pacific Ocean waters in winter. Johns Hopkins Press, Baltimore, MD, U.S.A. 96p.

Talley, L.D., and M.S. McCartney. 1982. Distribution and circulation of Labrador Sea Water. J. Phys. Oceanogr. 12:1189-1197.

Talley, L.D. 1991. An Sea of Okhotsk water anomaly: implications for ventilation in the North Pacific. Deep-Sea Res. 38:S171-S190.

Talley, L.D., and Y.Nagata (Eds.). 1995. The Okhotsk Sea and Oyashio Region. PICES Scientific Report No 2, 227p.

Watanabe, Y.W., S. Watanabe, and S. Tsunogai. 1991. Tritium in the northwestern North Pacific. Journal of the Oceanographical Society of Japan. 47:80-93.

Wüst, G. 1930. Meridionale Schichtung und Tiefenzirkulation in der Westhalften der drei Ozeane. Journal du Conseil, Conseil Internationale pour l'Exploration de la Mer. 5:21p..

FIGURES

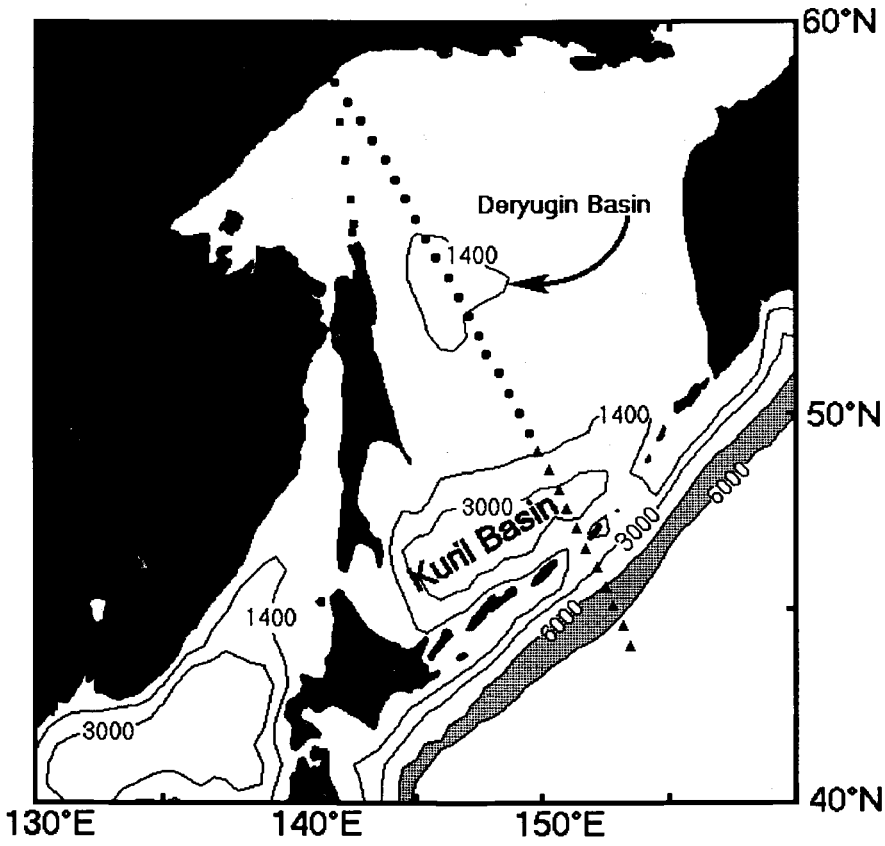

Fig. 1. Map of the station locations.

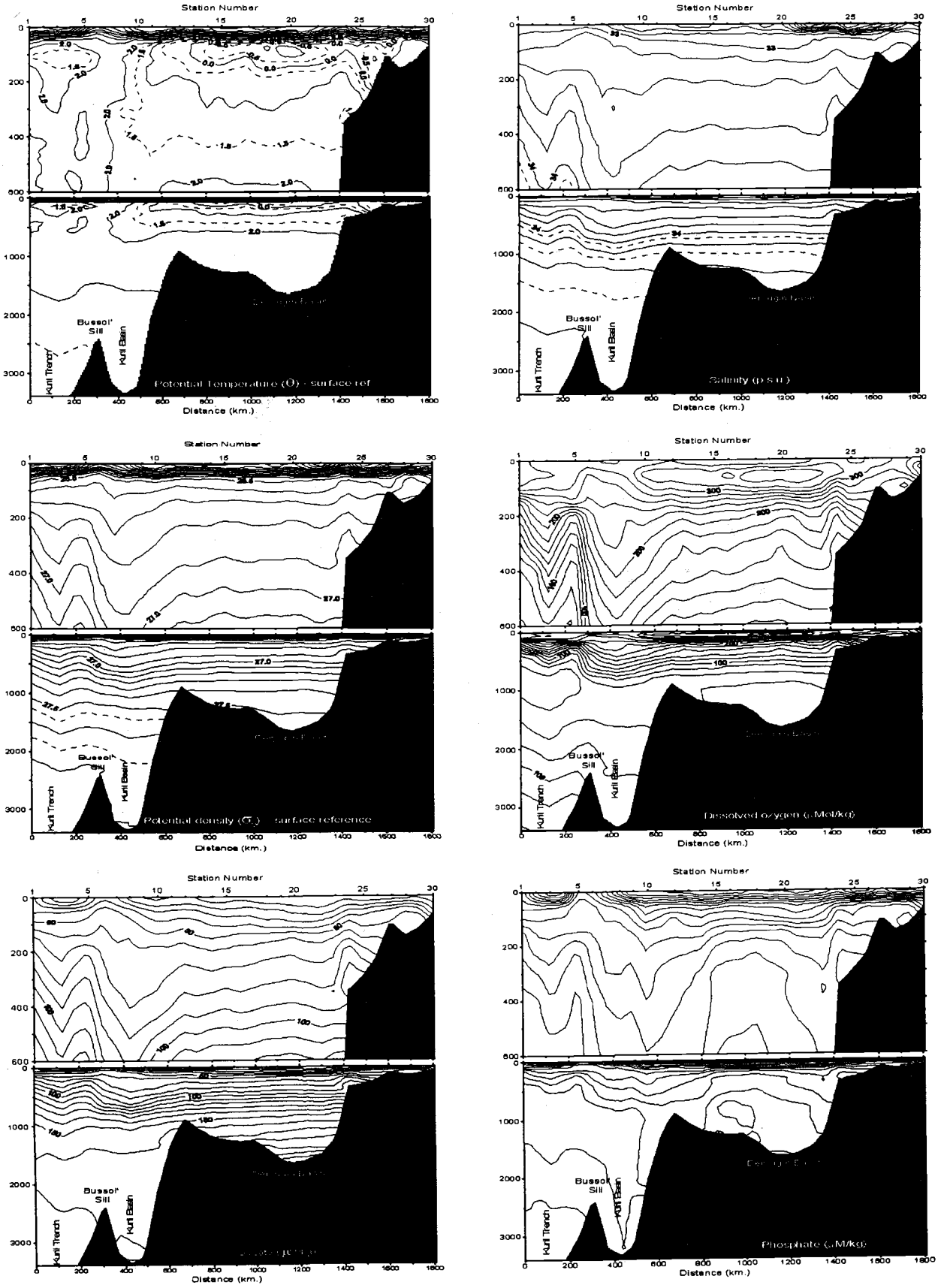

Fig. 2. The distribution of potential temperature, salinity, density dissolved oxygen, silicate and phosphate along line P1W. The upper panel of each plot shows properties in the top 600 metres of the water column.

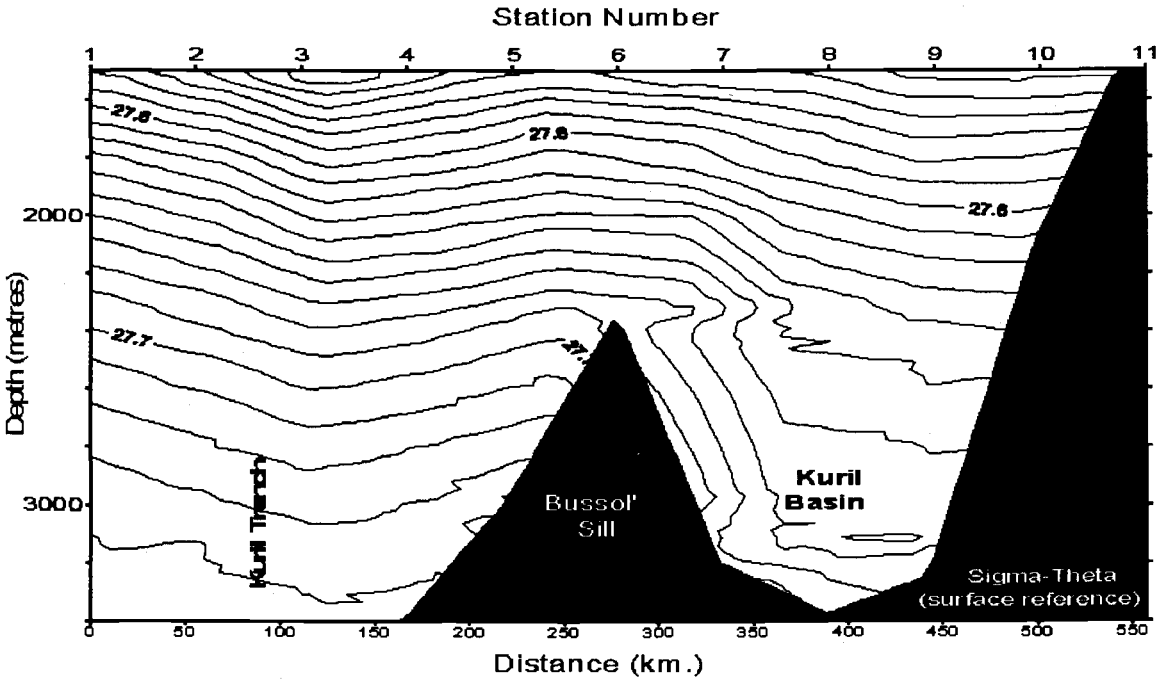

Fig. 3. The distribution of potential density in deep water near the Bussol' Sill.

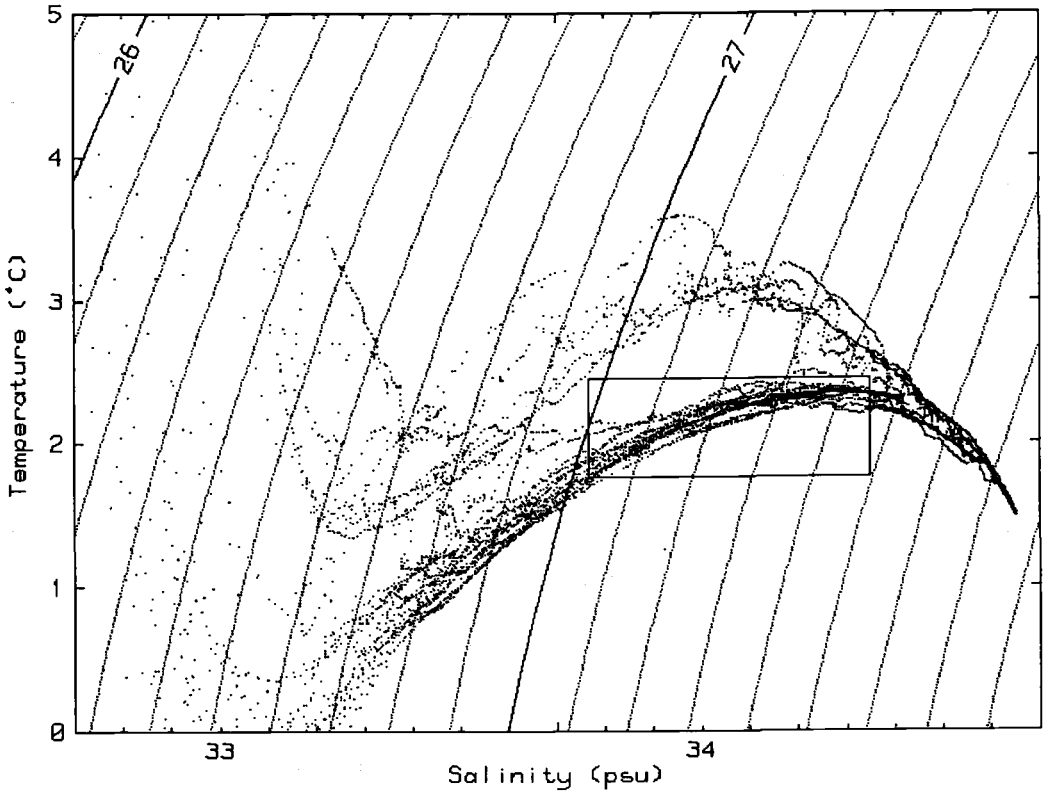

Fig. 4. θ-S curves for the first 30 stations.

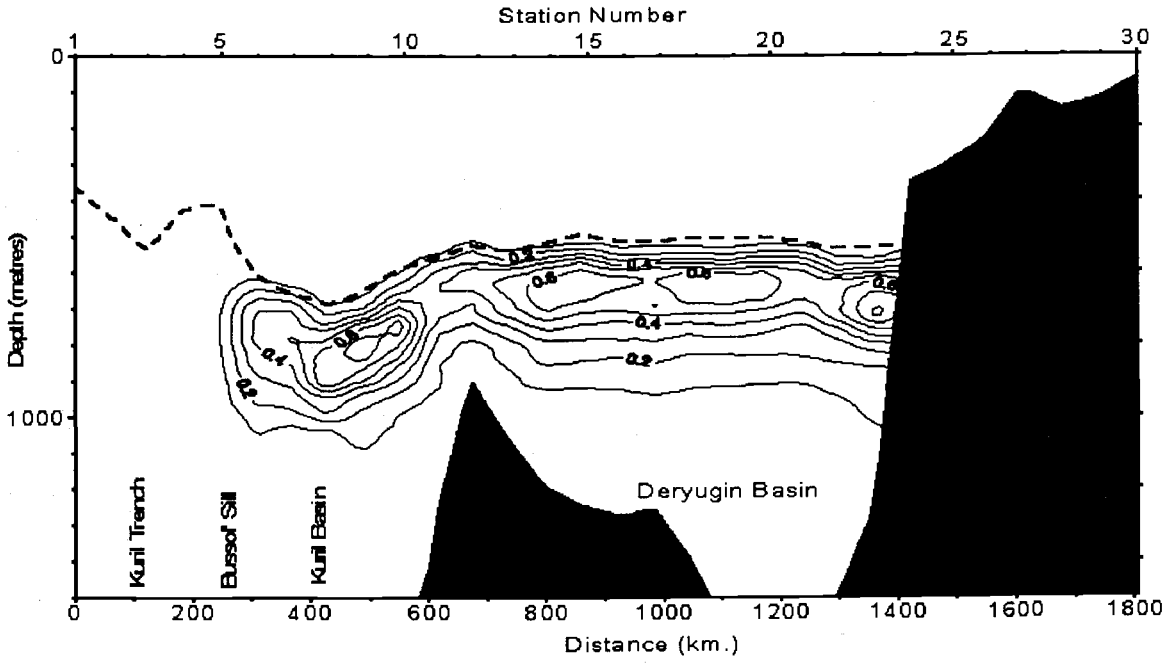

Fig. 5. The distribution of the Sea of Okhotsk Intermediate Water as defined by the box on Fig. 4. The dashed line indicates a potential density of 27.05 σ_θ.

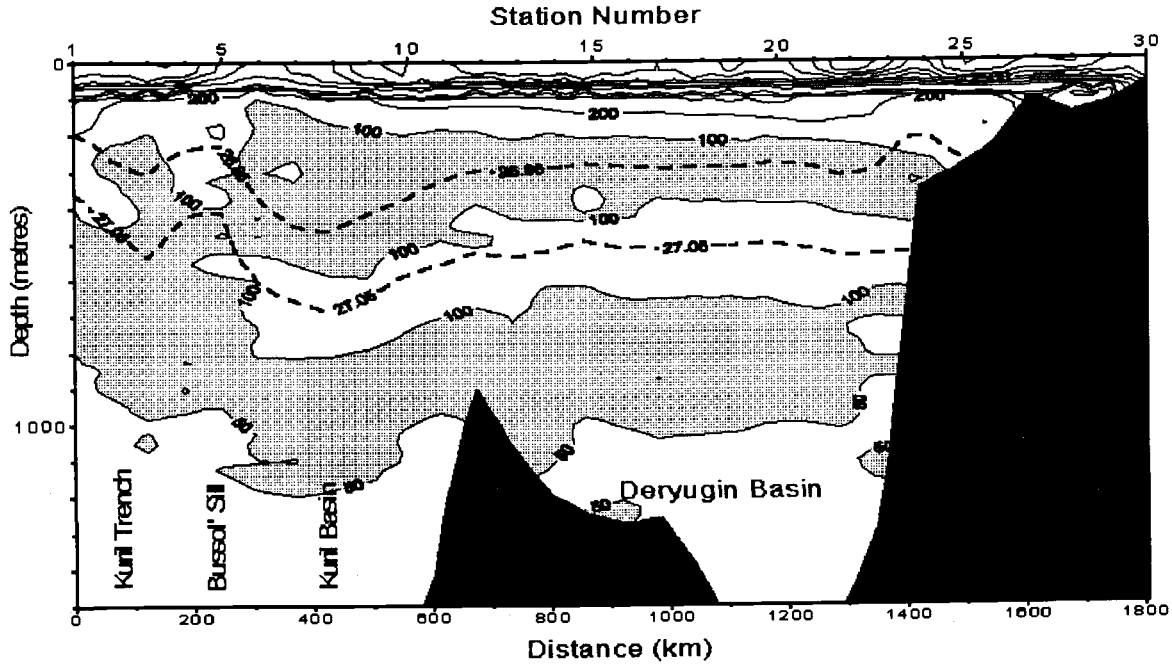

Fig. 6. The distribution of potential vorticity along line P1W. The dashed lines indicate potential densities of 26.85 and 27.05 σ_θ.

Some Experience of the Satellite Environmental Support of Marine Expeditions at the Far East Seas

Emil E. HERBECK, Anatoly I. ALEXANIN, Igor A. GONTCHARENKO, Igor I. GORIN, Yury V. NAUMKIN and Yury G. PROSHJANTS

Institute of Automation and Control Processes, Far-Eastern Branch,
Russian Academy of Sciences, Vladivostok, Russia

1. INTRODUCTION

Geophysical satellite monitoring of the environment becomes a necessary tool for investigation the of seas and atmosphere, especially for such a hard-to-research area as the Okhotsk Sea. It seems that the most interesting results in studies of variable natural objects could be obtained by combining satellite and *in-situ* data. Using the regular satellite information, it is possible to control the *in-situ* data acquisition according to location and development of the object investigated, and thus to increase the productivity and cost-effectiveness of marine expeditions. These are the considerations that determine the direction of our work as well as the objects of interest and methods of data processing. At present moment, we are developing the technology that may be specified as *Regional Environmental Satellite Monitoring* (RESM). The technology includes:

- regular capture of high-resolution multi-channel satellite data,
- extracting of geophysical parameters from the data,
- reconstruction of geophysical fields,
- location and tracing of natural and human-made objects and phenomena at sea surface and atmosphere (eddies, cyclones, frontal zones, currents and its meanders, ice fields, pollution, etc.),
- evaluation of spatial and temporal variability of the fields, objects and phenomena.

Because of high variability of our objects, the data processing should be performed in the quasi-real-time mode and the results should be transmitted to the vessel immediately.

Since 1993, we performed the RESM support for several cruises in the Japan and Okhotsk Seas. The following paragraphs are brief description of our RESM Data System, technology and methods we used, as well as some problems we have met.

2. THE RESM DATA SYSTEM: GENERAL DESCRIPTION

The RESM technology is based on daily capture and processing of data transmitted by meteorological NOAA (HRPT mode) and GMS (digitized LRFAX mode) satellites.

To achieve the goal, the Data System consisting of a 1.7 GHz Receiving Ground Station and local network of five IBM PC compatible computers was built. One of the computers executes a data receiving and antenna control functions; another one (the most powerful) is proposed for the data processing and packing. The rest of the computers are used for both data processing and software development. Being located in Vladivostok our System covers a wide area: from 17 to 62°N and up to 160°E. This area includes the Okhotsk, Japan, Yellow and East China Seas, and some areas of Western Pacific.

At the moment a major part of our work is dealing with sea surface temperature (SST) fields, thermal structures (SSTS), currents (SSC), and ice location and movement. For the last two objects, as well as to provide the fine cloudy filtering and atmosphere correction, both the single images and their series are processed. In the nearest future we plan to work with some atmosphere phenomena, especially typhoons. To research these objects, the System should be upgraded to receive the S-VISSR data from the new geostationary satellite GMS-5.

Main RESM output products include:

a. calibrated IR images, transformed into Mercator projection, both instantaneous and composed (in the last case a cloudy filtering may be performed);
b. SST charts and/or grid information of various resolutions, both instantaneous and composed;
c. SSTS charts;
d. charts of ice cover margins and ice movement;
e. surface current vectors and circulation maps.

3. THE RESM SUPPORT OF MARITIME STUDIES

It is extremely importance to obtain the information regularly during marine expeditions. As a rule, our support was carrying out according to the following scheme:

- day-to-day receipt and pre-processing of the NOAA/HRPT data (2-3 satellites, 4-6 times a day);
- packing the raw and pre-processed data onto a streamer tape;
- processing of the data as described above;
- making of the 5-10 day composed SST, SSTS, and SSC charts;
- transmitting of the charts to the expedition vessels by radio-facsimile channel;
- post-expedition processing of the data collected.

This approach has been used already to support five scientific and fishing cruises to the Okhotsk and Japan Seas.

Apart from the evident advantages, this way has some serious limitation, such as:

- the impossibility of supporting expeditions outside the area covered (e.g., in the central part of the Bering Sea);
- low noise-immunity of the radio-channel used does not allow recognition of small details on the charts;
- low channel capacity hinders transmission of such informative products as images;
- the time of satellite information transmission from the coastal System to a vessel is relatively long, so efficiency may be lost.

But the most significant limitation is that researchers do not have immediate access to the data processing system. As a result, they cannot control (or specify) the satellite data processing according to their observations or changed needs. On the other hand, the absence of *in-situ* information during the satellite data handling decreases the quality of RESM products.

Installation of the RESM System onboard the research vessel eliminates all the difficulties providing the best combination of remote and *in-situ* observations. This was done aboard the *SHIRASE* (Japan) and *POLARSTERN* (Germany) research vessels in the mid-80's. We have a similar experience, where our first RESM System was installed onboard the r/v *AKADEMIK KOROLEV* and took part in several cruises in 1988-1990 (Herbeck et al., 1992). Of course, it was a very difficult and expensive device at that time, because of the high cost of satellite ground stations and due to the

necessity of placing the antenna drive onto a gyro-stabalized platform. But at the present time, both stations and computers have become reasonably priced. Besides, due to the increase of computer capacity it is possible to compensate the vessel motion by using a computer controlled antenna drive over a wide range.

4. THE DATA PROCESSING

Several details and problems of satellite data processing we have met during the RESM support of cruises mentioned above are briefly discussed here.

4.1. Sea Surface Temperature (SST) Fields

Within the framework of our SST field retrieval technology (Goncharenko and Kazansky, 1992) the main output products are SST charts which might be classified according to time-averaging as follows:

- *type A*: averaged SST charts over a period of 5-10 days and 50-100 km resolution (Fig. 1a);
- *type B*: composite charts of 2-3 days / 10-20 km averaging (Fig. 1b);
- *type C*: high resolution charts of 5 km averaging from a single image (Fig. 1c).

In addition SST fields are presented as cartographic Mercator projections of 1 km resolution. These products of digital processing are single images under cloud-free conditions or composite images under partially cloudy conditions (Fig. 1d). The data may be presented both as a picture and as digital grid field information.

A major problem in using satellite measurements for ocean flow visualization is cloud cover. During an expedition, only a few of images can yield usable data (cloud-free images). The Okhotsk Sea region has the most cloudy conditions for satellite surveying. Therefore, it is necessary to make a average or composite map to represent the full SST distribution over the Japan or Okhotsk Seas.

It should be mentioned that SST *type A* fields are used for hierarchical control while products *(B)* and *(C)* are processed. *(A)* is successfully applied to fine cloud filtering of every individual image from the sequence and to normalize images for *(B)* composition. The last procedure is required to avoid artificial defects associated with errors from an atmospheric correction and false thermal front appearances.

The operative linear atmospheric correction MCSST recommended by NOAA/NESDIS for NOAA-11/12/14 satellites was used to make a preliminary SST retrieval. The technique provided an accuracy for SST determination of about 0.5°C. Corrected measurements were filtered to detect obvious cloudy elements and averaged inside 50 km squares to obtain a preliminary SST field *(A)*. Both filtration and correction procedures were based only on satellite data from AVHRR channels 2 (0.9 mkm), 4 (11 mkm) and 5 (12 mkm) without any *in-situ* measurements. The SST field provided test temperature values when the time sequence of all infra-red images was iteratively filtered to eliminate residual cloud contamination. To retrieve the field *(B)*, relevant images must be additionally normalized by *(A)* and averaged inside 10 km squares. Hence, temperature values of *(B)* depend on the time-overlapped 'climatic' field *(A)*. Note, that the accuracy of SST determination is not a limiting factor when a spatially detailed picture is required.

It is advisable to provide the maximal spatial resolution for a SST map obtained from a single image, so AVHRR data were corrected and averaged inside 5 km squares. To retrieve surface current fields from satellite data, the navigated images from the AVHRR band of 10.8 mkm were used. To avoid noise, these images were not corrected pixel-by-pixel.

Fig. 2 illustrates the results of applying of our cloudy filtering technique. There were very hard cloudy conditions as one can see from the images Fig. 2a and Fig. 2b. After the processing of a 7-days imagery sequence, the composed SST fields have been built (Fig. 2c) which are in a good agreement with the momentary SST fields (Fig. 2d) obtained through 4 days (when cloudiness is dissipated).

4.2. Sea Surface Velocity

4.2.1. Methods And Their Accuracy

Two methods were applied to prepare the sea surface velocities charts:

- feature tracing on sequential satellite images (FT);
- maximum cross-correlation technique (MCC) .

The FT procedure was based on a displacement estimation of water submesoscale inhomogeneity (ΔX) and velocity vector calculation (V):

$$V=\Delta X/\Delta T,$$

where ΔT is time interval between two images. The positions of an object are pointed out manually.

The MCC is an automatic method for velocity estimation. The essence of the method is the identification of the maximum cross correlation between search (second image) and template (first image) windows, as the end points of displacement vectors from the window center. Statistical significance of the cross-correlation maxima was used to refuse vectors with a low level of significance.

Instrumental accuracy of velocity estimation was in the range of 2-6 cm/c. It depended on space resolution of satellite images and time interval ΔT. The final accuracy was usually achieved by comparison with another kind of velocity measurements, as a rule with *in-situ* ones.

It should be mentioned that *in-situ* and satellite velocity measurements have different mining. The first are measurements at specific points, while a tracing feature on a satellite image has spatial size of tens to hundreds of square kilometers. Obviously, the short-scale and short-time velocity components are absent in its satellite evaluations, and thus satellite velocity estimations are usually underestimated. The time interval ΔT is comparable with the tide periods and from this reason the satellite velocity measurements should be interpreted correctly.

To consider the accuracy of the satellite technique as a technique for velocity displacement of large-scale water mass, we have to compare satellite and ship measurements (1) for flows with negligible short-scale and short-time velocity components and (2) when the space-time discrepancy between measurements compared is less than the space-time variability of flow.

Some estimation of the FT technique accuracy on the Kuroshio extension flow data has been done:

1. 12 velocities calculated by satellite APT-images (year 1984) have been compared with dynamic method estimations by Alexanin, 1991. The accuracy of comparing scheme was 30 cm/s. Velocities range was 80-160 cm/s and the average difference between two fields was :

   $$\Delta V = [\varsigma(V_i-U_i)]/N = 6.3 \text{ cm/s},$$

   that was less then instrumental accuracy. V_i and U_i are projections of satellite and *in-situ* velocity measurements on the flow direction, N - the number of measurements.

2. The dynamic overfall across Kurosio extension on 142°E has been calculated as 90 cm by satellite HRPT-images of 1990 (Alexanin and Kazansky, 1994) whereas according to Japanese data this value on 144°E was near 100 cm. Such difference could be explained by natural factors.

3. Two sea surface velocities, 124 cm/s and 45 cm/s, were measured in the same region and time aboard R/V KOFU MARU (Japan). The differences between ship and satellite velocity measurements were 26 cm/s and 3 cm/s and the scheme accuracy was about 10 cm/s.

As we can see, the satellite velocity estimations differ from other ones in the limits of the scheme accuracy (not worse then 20% of value).

As a rule, the FT technique was used because this method gives more information about circulation as compared with MCC when measurement accuracy is severe. The MCC method was usually applied for ice velocity calculations.

4.2.2. Observation Conditions And Data Volumes Received

The ability to create sea surface velocity charts is based on the existence of sea regions without cloudiness and mist during 6 hours or more. The results (number of velocity vectors) received naturally depend on the weather conditions (Table 1). For this reason the most difficult place in the Far East region is the central and southeast parts of the Okhotsk Sea in summer. Two expeditions in the region have been supported. Circulation charts were built in operative mode and sent to the ships. The weather conditions during these cruises were difficult (Table 2), nevertheless the detailed charts for the most interesting regions and water objects were built 2-3 times a month using data processing from 3-4 polar NOAA satellites. The longest time interval during which we could not make a chart was 3 weeks. But for the last expedition we could not prepare any chart for the North-Kuril region (approximately 3*3 degrees).

4.2.3. Chart Samples

Fig. 3a displays a chart fragment of the sea surface circulation during April 3-6, 1995. Dynamic topography overfall of the eddy presented in the right and lower corner has been estimated as 45 cm and velocity profile across the eddy was developed. The highest velocity revealed was 70 cm/s.

Fig. 3b presents a chart calculated during the CREAMS expedition, whose main goal was to investigate circulation in the north part of the Japan Sea. Large-scale charts were extracted from the velocity estimations received during August 28-31, 1993. The circulation was in a good agreement with direct *in-situ* measurements.

REFERENCES

Alexanin, A.I. 1991. Geostrophic surface current velocities: comparison of satellite and ship-borne measurements. Soviet J. Remote sensing. 6:55-61 (in Russian).

Alexanin, A.I. and A.V. Kazansky. 1994. Development of a synoptic approach for monitoring oceanic circulation. Proc. OCEANS-'94 OSATES, 13-16 Sept. 1994, Brest, France. 2:II,412-II,417.

Goncharenko, I.A., and A.V. Kazansky. 1992. A hybrid system for monitoring of the sea surface mesoscale features from satellite IR-imagery. Proc. of IEEE International Conference. on Ocean (OCEANS'92). Newport, RI, 26-29 Oct. 1992. Newport, Rhode Island. Vol.1.

Herbeck, E., A. Kazansky, Ju. Proshjants, et al. 1992. Shipboard Complex for Satellite Monitoring of Mesoscale Ocean Variability. Proc. of IEEE International Conference on Ocean (OCEANS'92). Newport, RI, 26-29 Oct. 1992. Newport, Rhode Island. Vol.1.

TABLES AND FIGURES

Table 1. Number of velocity vectors obtained during different expeditions

EXPEDITIONS	NUMBER OF VECTORS
April-May 1995	1551
June-August 1994	2018

Table 2. Example of weather conditions in the Okhotsk Sea during summer period

WEATHER:	CLEAR SKY DAYS (cloudiness 0-3)	CLOUDY DAYS (cloudiness 7-10)	MIST DAYS
MAY	10-20%	70-80%	15-20%
AUGUST	10-20%	70-80%	20-35%

FIGURES

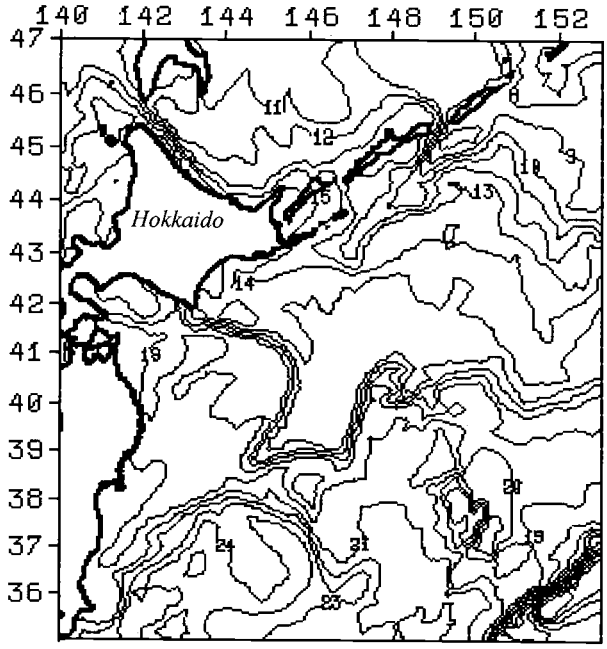

a) 8-day averaged SST chart (8-15 Oct, 1995)

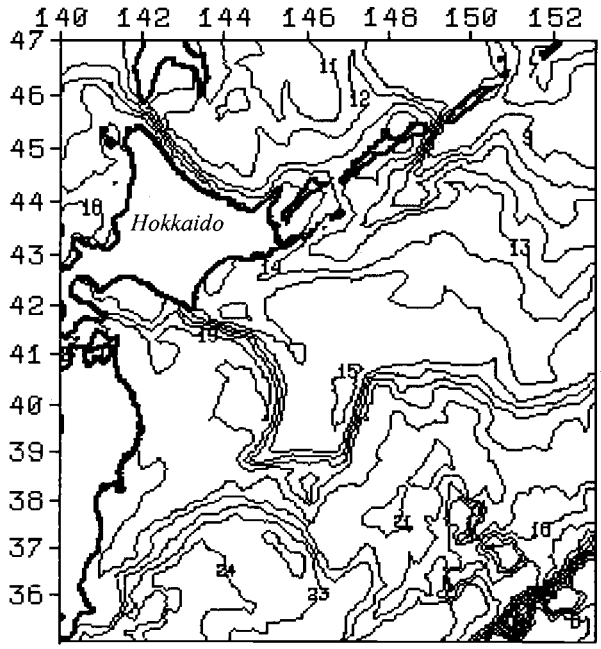

b) 4-day composite SST chart (12-15 Oct, 1995)

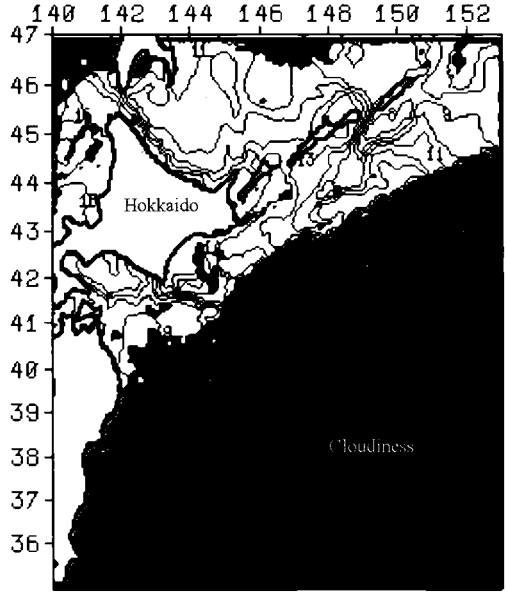

c) momentary SST chart (10 Oct., 1995)

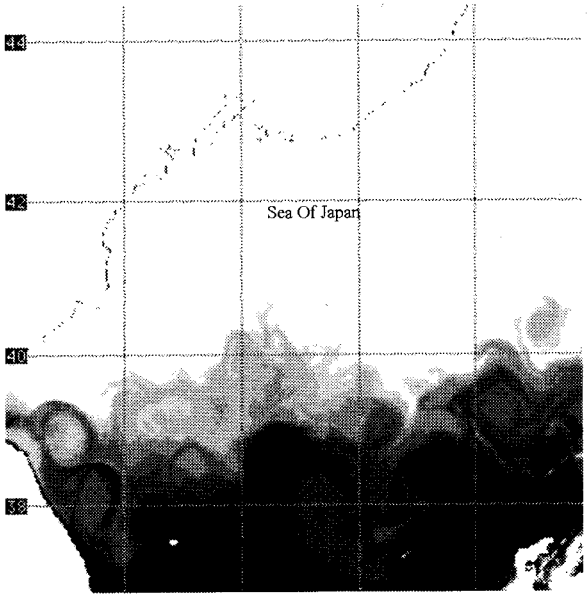

d) SST fields (composite image, 7-9 May, 1994)

Fig. 1. Examples of RESM (Regional Environmental Satellite Monitoring) of SST output products.

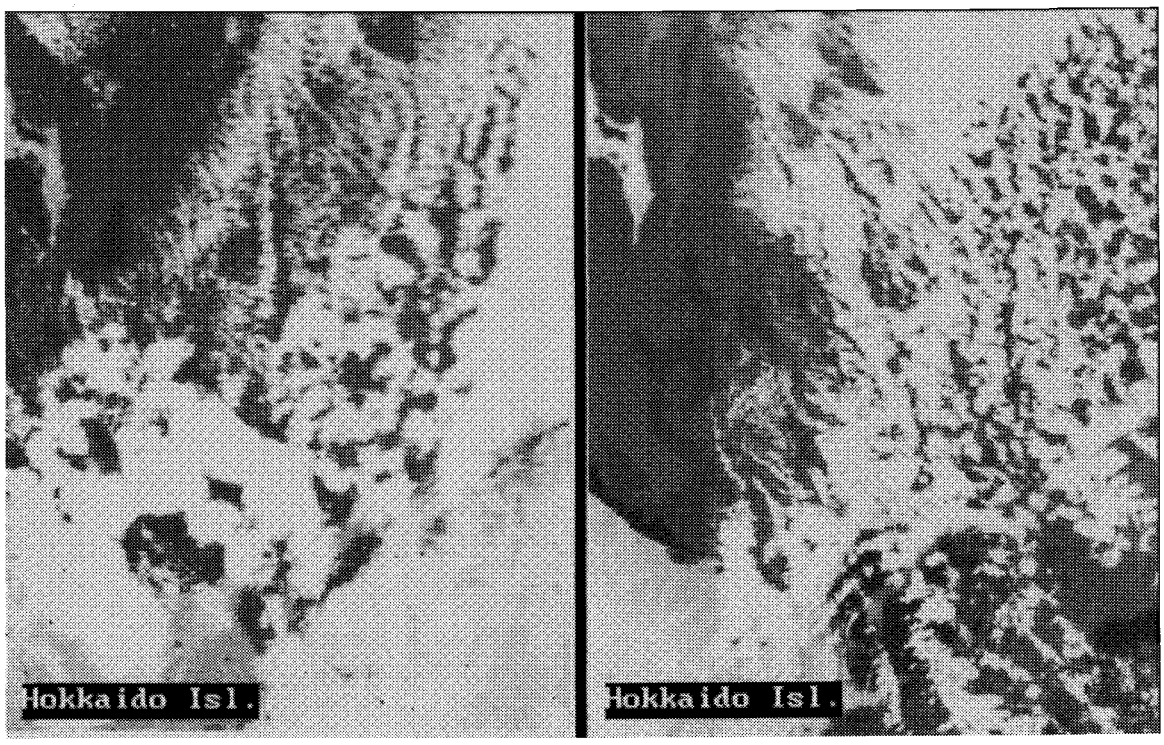

a) b)

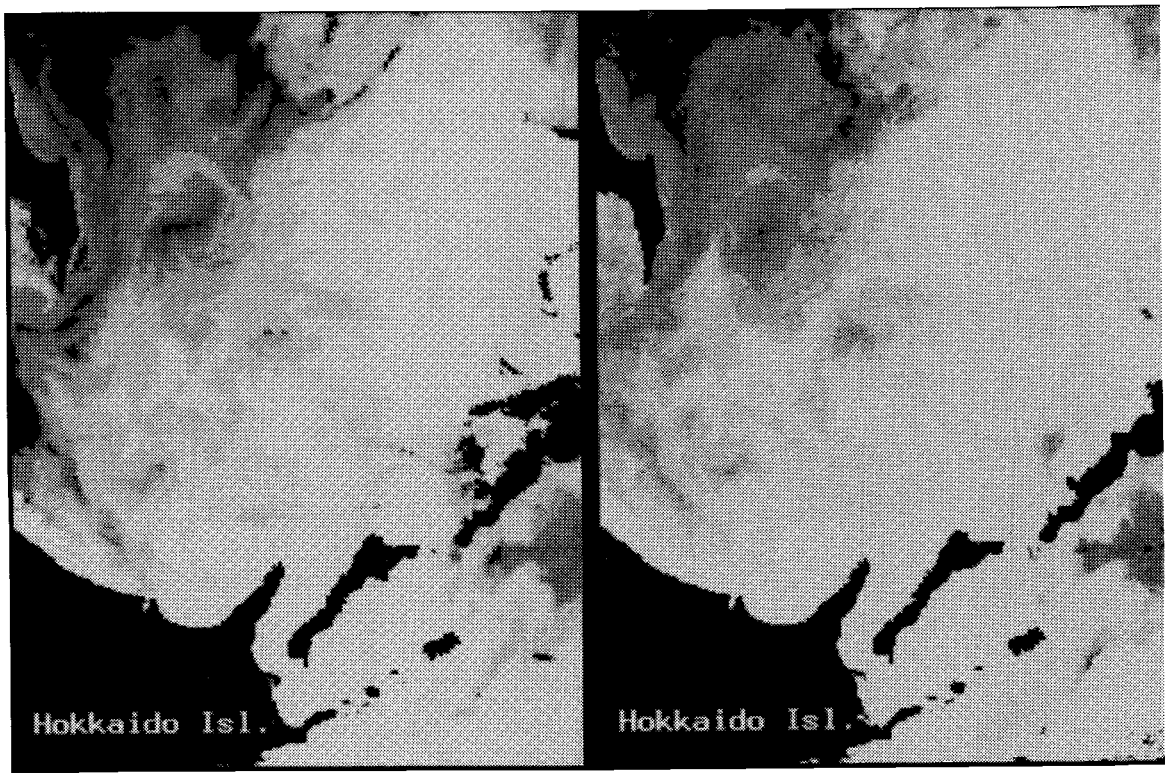

c) d)

Fig. 2. Examples of RESM cloudy filtering technique application.

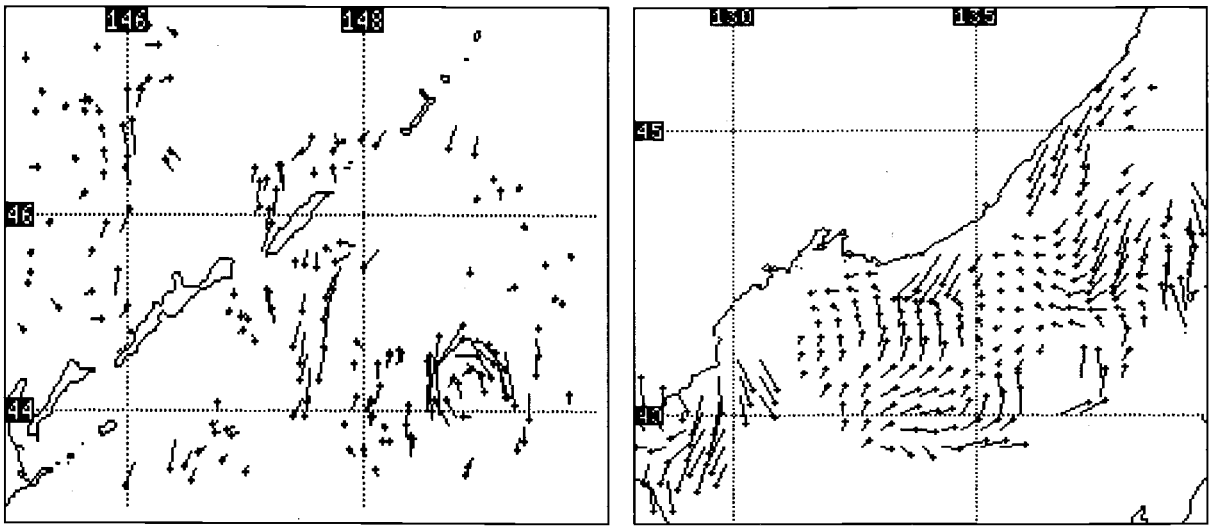

(a) (b)

Fig. 3. Examples of RESM sea surface circulation charts.

The Tidal Influence on the Sakhalin Shelf Hydrology

Alexander A. KARNAUKHOV

Pacific Oceanological Institute, Far Eastern Branch, Russian academy of Sciences, Vladivostok, Russia.

The international ecological expedition aboard the *R/V Academik M. Lavrentjev* was performed on the eastern Sakhalin shelf in October-November of 1994. The character of hydrological observations was determined by small site sizes and the general situation in the studied areas. Sites "C" and "D" were situated in the zone of the influence the East-Sakhalin Current, on the western periphery of the Okhotsk Sea cyclonic circulation (Fig. 1). Water masses, moved by the current, have been formed under the influence of the Amur River drainage in the areas of the Sakhalin Gulf and Nevel'skoy Passage. The gradual salinity increase of these waters is observed southward

All observations were carried out in the beginning of autumn - winter convection characterized by cooling of surface waters and subsequent intermixing. The thickening of the upper homogeneous layer, observed at this time, is accompanied by simultaneous decline of the seasonal layer of abrupt temperature and salinity changes. The process is supported by the wind activity typical for this season. These are the basic conditions forming the thermohaline structures of the East Sakhalin shelf region.

The small-scale spatial - temporal variability is caused basically by two factors: (1) the strong influence of the East Sakhalin Current executed by wind and (2) the influence of tidal motions. The prevailing western winds force the removal of the deep stream current from the shore and the subsequent active upwelling. During our study the wind field was quasi-stationary relative to the period of survey (less than two days) and only tides could determine the dynamics of hydrophysical fields.

Therefore, the full tidal cycle observations are necessary to examine the nature of temperature and salinity variability in the area. Unfortunately, only two day measurements were performed at each site and the actual observational period was only from 8 AM till 10 PM. The corresponding data set makes the interpretation of results more difficult as it does not overlap the tidal cycle. The tidal regime off the east Sakhalin coast is rather complicated. The semidiurnal tides prevail in the southern part of the investigated area, whereas the diurnal tides are dominant in the region of Chaivo.

Observations at sites "C" and "D" demonstrate the significant influence of tidal waves on the temperature and salinity distribution. Based on surface T-S diagrams all stations of site "D" could be divided into two classes with average values equal to 5.15°C - 27.4 psu and to 5°C - 30.0 psu (Fig. 2a.). The average time (ship time) of sampling was approximately 9:30 AM for the first class and 4:30 PM for the second class. A similar situation was observed at site "C"; here all the stations are concentrated in two areas of the T, S plane: 5.0°C - 29.6 psu and to 4.65°C - 31.0 psu (Fig. 2b). The lesser contrast of mean T, S characteristics on site "C" in comparison with site "D", apparently, could be explained by the distant location of the former from the main stream of the East Sakhalin Current. In this area the average time of sampling was about 11 AM for the first and 3 PM for the second group of stations. It should be noted, that the periodicity of measurements of 7 and 4 hours does not adequately reflect the temporal structure of tidal processes, since the time of observations corresponded only to certain tidal phases and does not overlap the tidal cycle. In other words, if the time of

observation is symmetric to the phase of high or low waters, the shorter periodicity will be recorded. If a fewer number of stations is sampled during the ebb phase and more during the high water, the longer periodicity will be fixed. This process plays an important role in the distortion of the tide wave form at a shoal where variations of the sea level become comparable with depth. In this case the crest moves faster than the trough and the forward slope of a wave becomes steeper.

The coincidence of cotidal lines and isohalines (Fig. 3) reflects the significant temporal variability in the region. The subarctic waters (the Okhotsk Sea water belongs to this water type) are characterized by the dominant influence of salinity on water stability and stratification. Therefore the spatial distribution of isohalines is the most representative for comparative purposes. It is remarkable, that for both sites, the variability picture is qualitatively preserved at all horizons (Fig. 3a and 3b). That corresponds to the present conception of current structure in the long progressive waves in the shallow sea, where the reversal fluctuations in longitudinal (horizontal) direction prevail at all depths. Thus, the influence of tides is reflected in horizontal shifting of the whole thermohaline water structure. As it was mentioned, sites "C" and "D" are situated in the area of two spatially homogeneous water masses, which can occupy the region under study in different time periods. During this process the entire replacement of one water type by another occurs. Taking into account the size of the sites "C" and "D" (approximately 6x6 miles), it seems that the amplitude of horizontal transformation of the whole water column exceeds 3 miles. One of the mentioned water structures is under the direct influence of the East Sakhalin Current which provides a salinity contrast forcing the observed variability.

Assuming the tidal nature of T-S variability on the Sakhalin shelf we can conclude that the spatial temperature and salinity distributions on sites "C" and "D" in fact represent the temporal variability of these properties. At 9 AM site "D" was occupied by the water mass of East Sakhalin Current that was reflected in the freshening of the upper homogeneous layer. Hereafter, the shifting of this water structure occurred, and before 4 PM it was completely replaced by a practically non-stratified water mass (Figs. 4a and 4b; St. 23 and 15), conditionally called "background water". The temperature inversions (Fig. 4, St. 15) indicate the active horizontal transformation of water masses. A similar situation was observed at site "C". However, the "background" conditions here were different and were determined by the larger offshore distance and, possibly, by another character of the large-scale circulation. At site "C" the East Sakhalin Current water mass was observed about 11 AM (Fig. 4c, St. 34). The water mass transformation was completed closer to 3 PM and resulted in an increase of salinity of the surface layer and in the deepening of the thermocline from 50-60 to 70-80 meters (Fig. 4d, St. 32).

Investigations of the hydrophysical fields on the East Sakhalin shelf should be planned taking into account the tidal processes in this zone. In future, we have to coordinate the continuous measurements at daily stations with site surveys executed during definite tidal phases. Despite the limited number of representative data, this study expands our understanding of dynamic processes in this region.

REFERENCES

The Atlas of Oceans: The Pacific Ocean. 1974. Moscow, Head Administration of Navigation and Oceanography XIV, 302p. (in Russian)

The Ocean Dynamics (Ed. Yu. P. Doronin). 1980. Leningrad, Gidrometeoizdat, 303p. (in Russian)

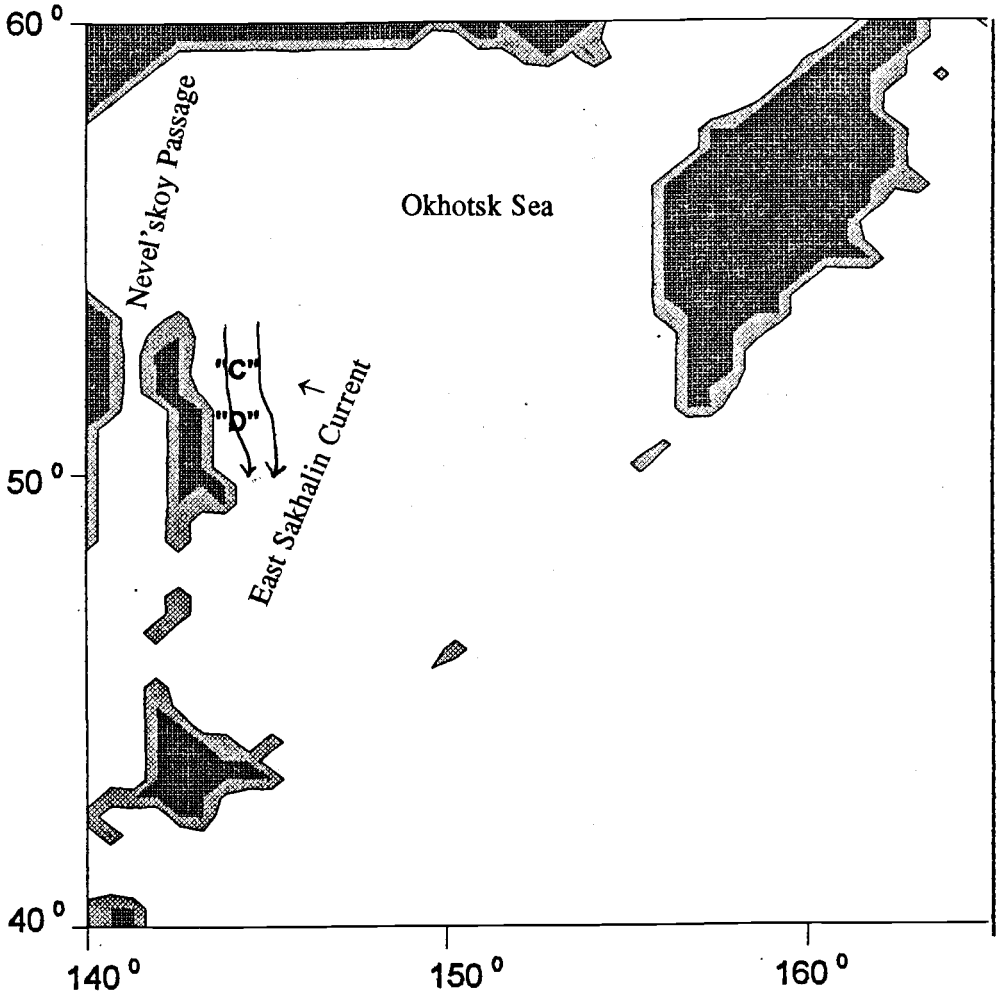

Fig. 1. The observational sites "C" and "D" in the zone of the East Sakhalin Current in October-November 1994.

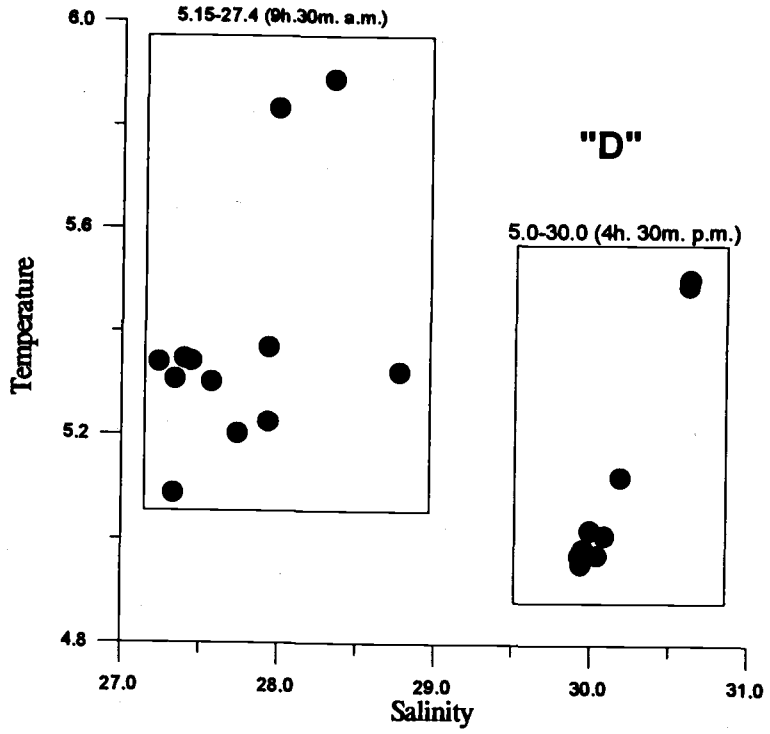

(a)

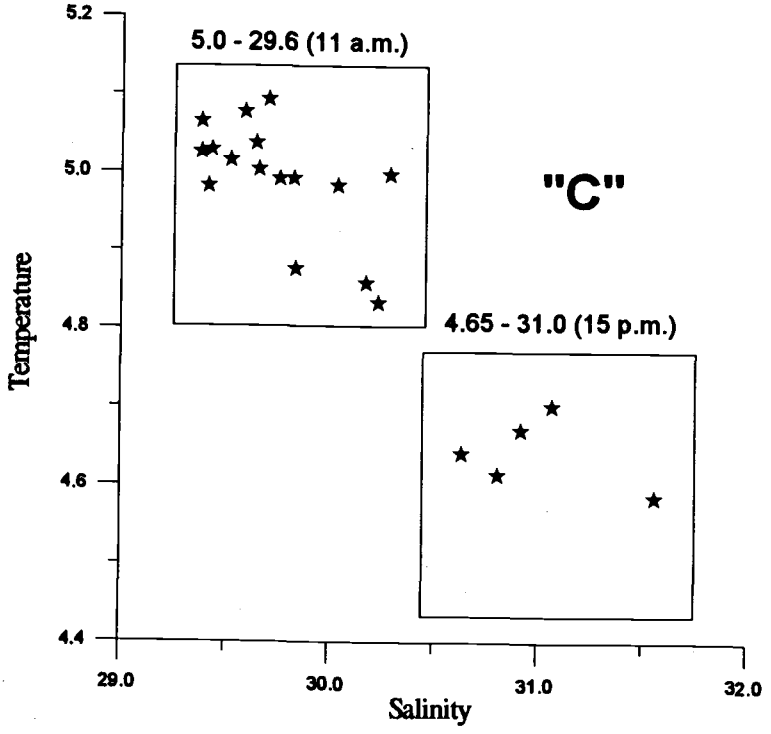

(b)

Fig. 2. Surface T, S - diagrams for sites "D" and "C".

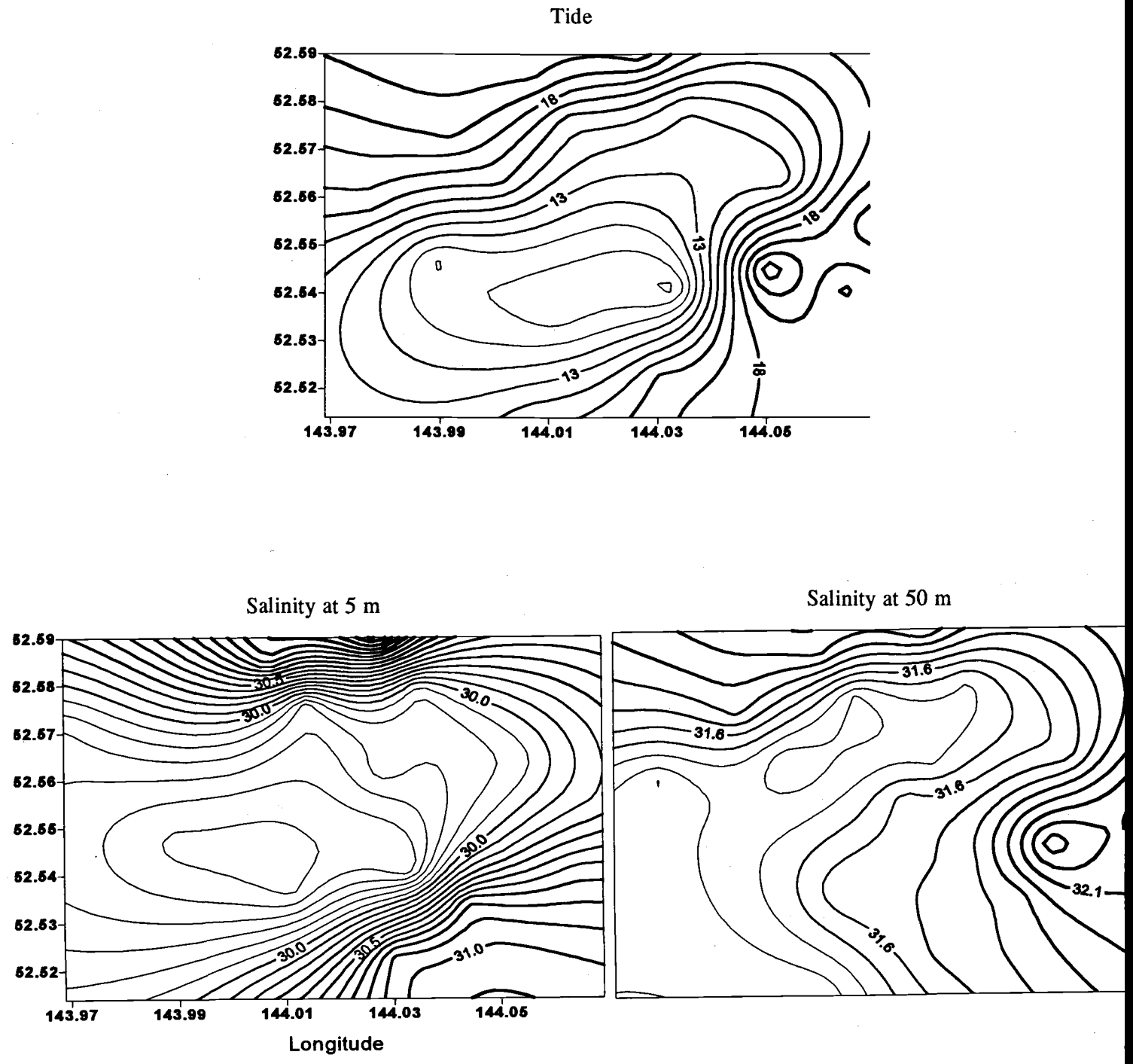

Fig. 3a. Plots of spatial distribution of tides and salinity demonstrating the coincidence of cotidal lines and isohalines for site "C".

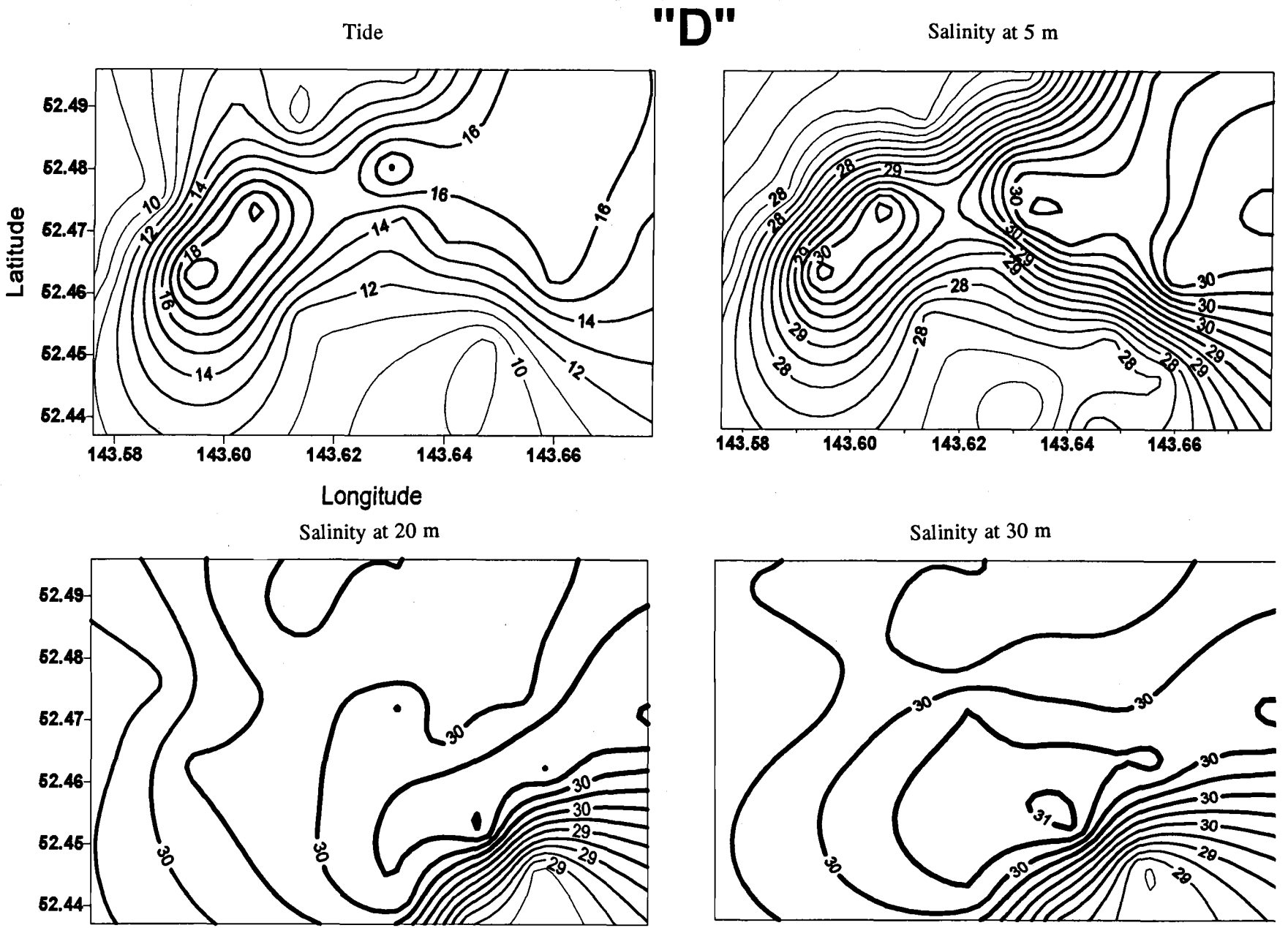

Fig. 3b. Plots of spatial distribution of tides and salinity demonstrating the coincidence of cotidal lines and isohalines for site "D".

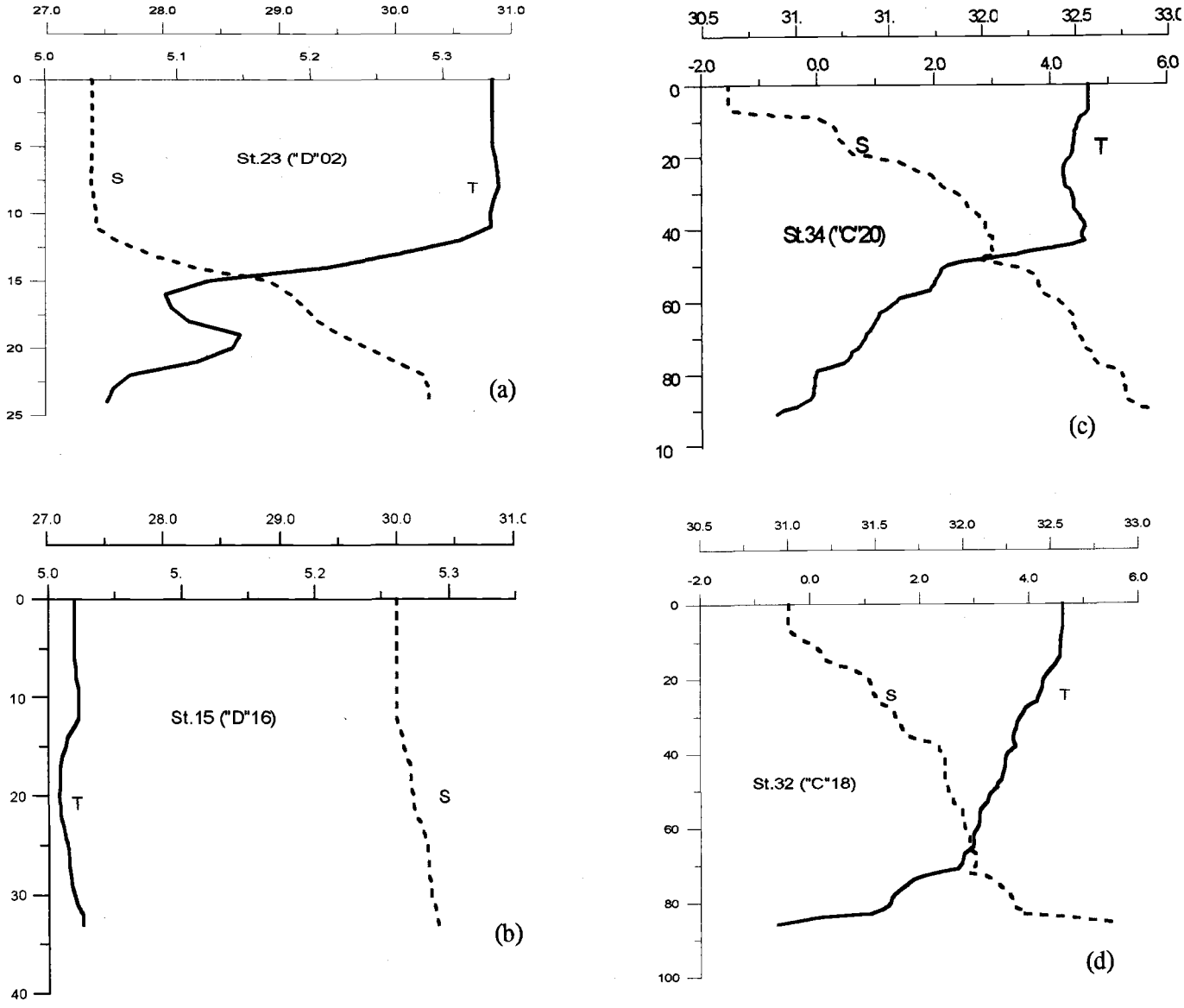

Fig. 4. Temperature and salinity profiles at sites "D" (a - 9 AM; b - 4 PM) and "C" (c - 11 AM; d - 3 PM).

On the Formation Process of the Subsurface Mixed Water Around the Central Kuril Islands

Yasuhiro KAWASAKI

Hokkaido National Fisheries Research Institute, Kushiro, Hokkaido, 085 Japan

The formation of the Oyashio Water (Oy) seems to be related to the mixing of two Subarctic waters: the Okhotsk Sea Water (OW) and the East Kamchatka Current Water (EKCW). On the other hand, near the Central Kuril Islands, a relatively warm and saline Mixed Water was surveyed on the shallow isopycnals lighter than 26.7 sigma-theta (Kawasaki and Kono, 1994). This water shows the vertically homogeneous temperature profile from 2 to 3°C, contrary to the dichothermal (inter-cooled) structure with temperature lower than 2°C revealed for both Subarctic Waters. The surface layer of the Mixed Water has peculiar characteristics: it is cold, saline, dense and rich in nutrient. This suggests that the Mixed Water originates from the deeper layer.

Surface silicate distribution within the study area during the period from late August to early September 1993 is shown in Fig. 1a. High silicate concentrations were found over the bank (hereafter called Bank A) to the east of the Kruzenshtern Strait and to the south of the Bussol' Strait. Sections of potential temperature (deg-C) and salinity (psu) as a function of potential density (kg/m^3 in sigma-theta, cl/ton in thermosteric anomaly) through the Kruzenshtern Strait are given in Fig. 2. The origin of the Mixed Water was observed at the Bank A (Stn. MU5) as isolated warm water with salinity higher than 33.3 psu on the isopycnal layer 26.5-26.6 sigma-theta. This suggests that the effect of bottom topography is an important factor for the formation of the Mixed Water. In the present paper vertical nutrient profiles will be used to discuss the mechanism of the Mixed Water formation.

We assumed that the horizontal supply of subtropical waters, like a warm-core ring (WCR) or Soya Warm Current waters, cause the appearance of saline and warm Mixed Water on the isopycnals lighter than 26.7 sigma-theta. However, this is in contradiction with the nutrient data: the silicate concentration of Subtropical Water is lower than 5 μmol/l. Also, the formation of the Mixed Water cannot be explained by horizontal isopycnal mixing of two Subarctic Waters as they have a dichothermal layer with temperature below 2°C. Therefore, saline and nutrient-rich water has to be supplied from the deeper layer.

During the 1994 summer cruise, CTD and nutrient bottle sampling were carried out concurrently within the Bussol' Strait area. The observation line through the Bussol' Strait and surface silicate distribution are shown in Fig. 1b. Silicate concentrations higher than 40 μmol/l were revealed in the Strait. Sections of potential temperature (deg-C), salinity (psu) and silicate (μmol/l) as a function of potential density (sigma-theta and thermosteric anomaly) through the Bussol' Strait during the period from late August to early September 1994 are presented in Figs. 3a-3c. The warm, saline and nutrient rich Mixed Water is observed in the Strait (Stn. NU1) at density levels less than 26.8 sigma-theta. Stations NU'1, NU1, NU5 and NU9 were selected to compare the characteristics of each water type, i.e. OW, Mixed Water, EKCW, and Subtropical Water, respectively. Silicate and potential density relationships for the different waters are given in Fig. 4. Numerals on the shoulder of each symbol indicate sampling depths in hecto-meters. It should be mentioned that the upper 50 m layer of the Mixed Water is nutrient rich and its silicate - potential density relationship is similar to

that of EKCW. On the other hand, OW is characterized by lower nutrient concentrations at the same density level as compared with other Subarctic waters such as EKCW.

Vertical profiles of silicate (open symbols) and phosphate (closed symbols) for each station on the section through the Bussol' Strait are displayed in Fig. 5. Nutrient concentrations for the Okhotsk Sea Water (Stn. NU'1) do not exceed those within the upper 600 m of the Mixed Water. These data suggest that the Mixed Water can not be produced by vertical mixing of OW itself. Additionally, vertical mixing within the upper 200 m of EKCW can not lead to the Mixed Water formation, as the mean silicate concentration in the 200 m layer of EKCW is about 43 μmol/l, whereas mean silicate concentration in the upper Mixed Water is about 56 μmol/l.

If vertical mixing of EKCW induced by tidal current over the continental shelf is predominant, the upper Mixed Water becomes more warm, fresh, and poor in nutrients. To consider the vertical supply of saline and nutrient-rich water from the deeper layer, relationships between salinity and silicate for selected station are shown as in Fig. 6. Characteristics of the Mixed Water shallower than 200 m coincide with subsurface 100-150 m layer of EKCW. Assuming silicate and salinity are more conservative than a water property such as temperature, the dichothermal layer of EKCW (33.1-33.4 psu in salinity) might be a possible source of the upper Mixed Water. However, in this case a heating process should follow the upwelling. In order to heat up the 30-40 m of water column (see Fig. 4) to about 0.5-2°C, what kind of process should occur?

We presumed that vertical mixing induced by tidal current occurs only over the continental shelf, however, the sill depths for the straits of the Central Kuril Islands are about 400-500 m. Recalculated mean silicate concentration over 400 m water column, EKCW (68 μmol/l) exceeds the mean concentration for the Mixed Water (63 μmol/l). Thus, if tidal currents around the Central Kuril Islands are strong enough to mix the entire water column, vertical mixing of EKCW is another possible forcing mechanism to produce the Mixed Water.

SUMMARY

Around the Central Kuril Islands, a peculiar warm, saline and nutrient rich upper Mixed Water was found on the isopycnals lighter than 26.7 sigma-theta near the Bank A. It seems to be responsible for high primary production of the Oyashio. However, isopycnal mixing of two Subarctic Waters and horizontal transport of the Subtropical Water can not produce the upper Mixed Water.

Vertical transport of the Okhotsk Sea Water is also disregarded as the source of the upper Mixed Water formation based on the nutrient and salinity relationships, whereas upwelling of the subsurface East Kamchatka Current Water appears to be a cause of the upper Mixed Water formation, though the heating process after upwelling remains unknown. The entirely vertical mixing of the upper 400-600m of EKCW is another possibility for the production of the upper Mixed Water.

In future, we have to analyze the water formation process using time resolution tracers or properties and also to carry out model experiments combined with direct current measurements around the Bank A and within the continental shelves near the Central Kuril Islands.

REFERENCES

Kawasaki, Y. and T. Kono. 1994. Distribution and transport of Subarctic Waters around the middle of Kuril Islands. Umi to Sora. 70(2):71-84.

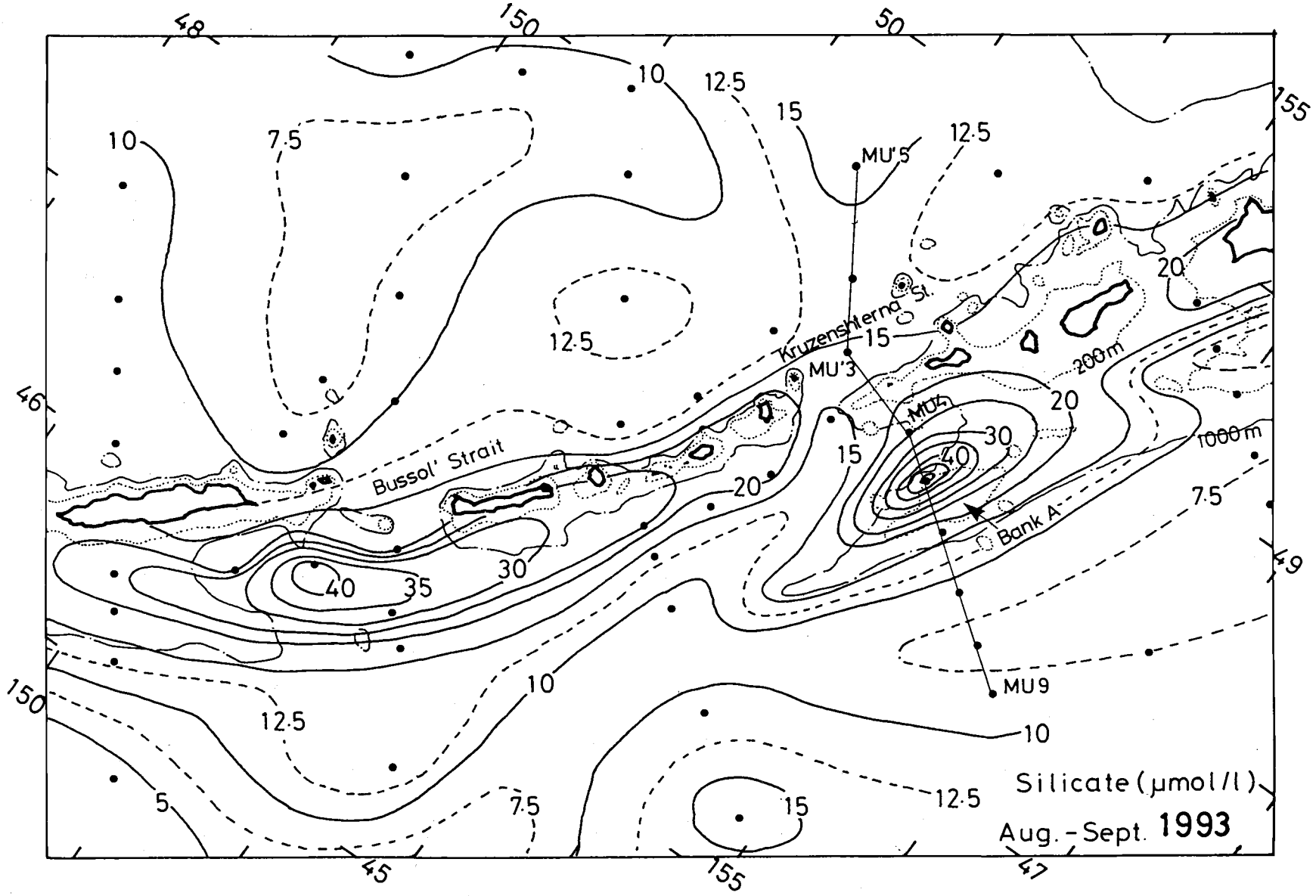

Fig. 1a. Surface silicate distribution (μmol/l) during the period from late August to early September 1993 (a) and 1994 (b). Observational sections through the Kruzenshtern (a) and Bussol' (b) Straits are shown. Study area presented in Fig. 1a is displayed as the dashed rectangular in Fig. 1b.

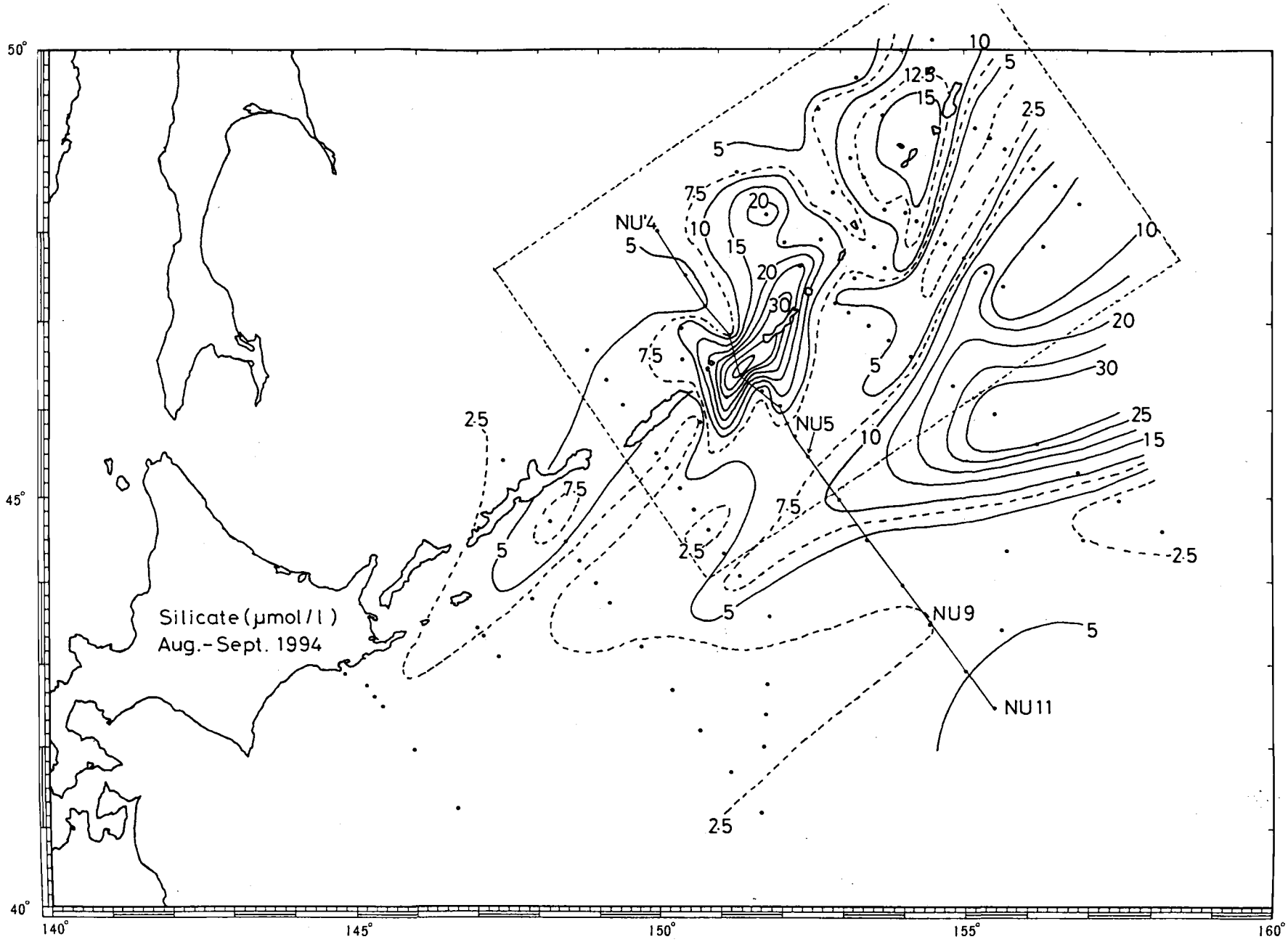
50°
45°
40°
140°
145°
150°
155°
160°
Silicate (μmol/l)
Aug.-Sept. 1994
NU'4
NU5
NU9
NU11
2.5
5
7.5
10
12.5
15
20
25
30

Fig. 1b.

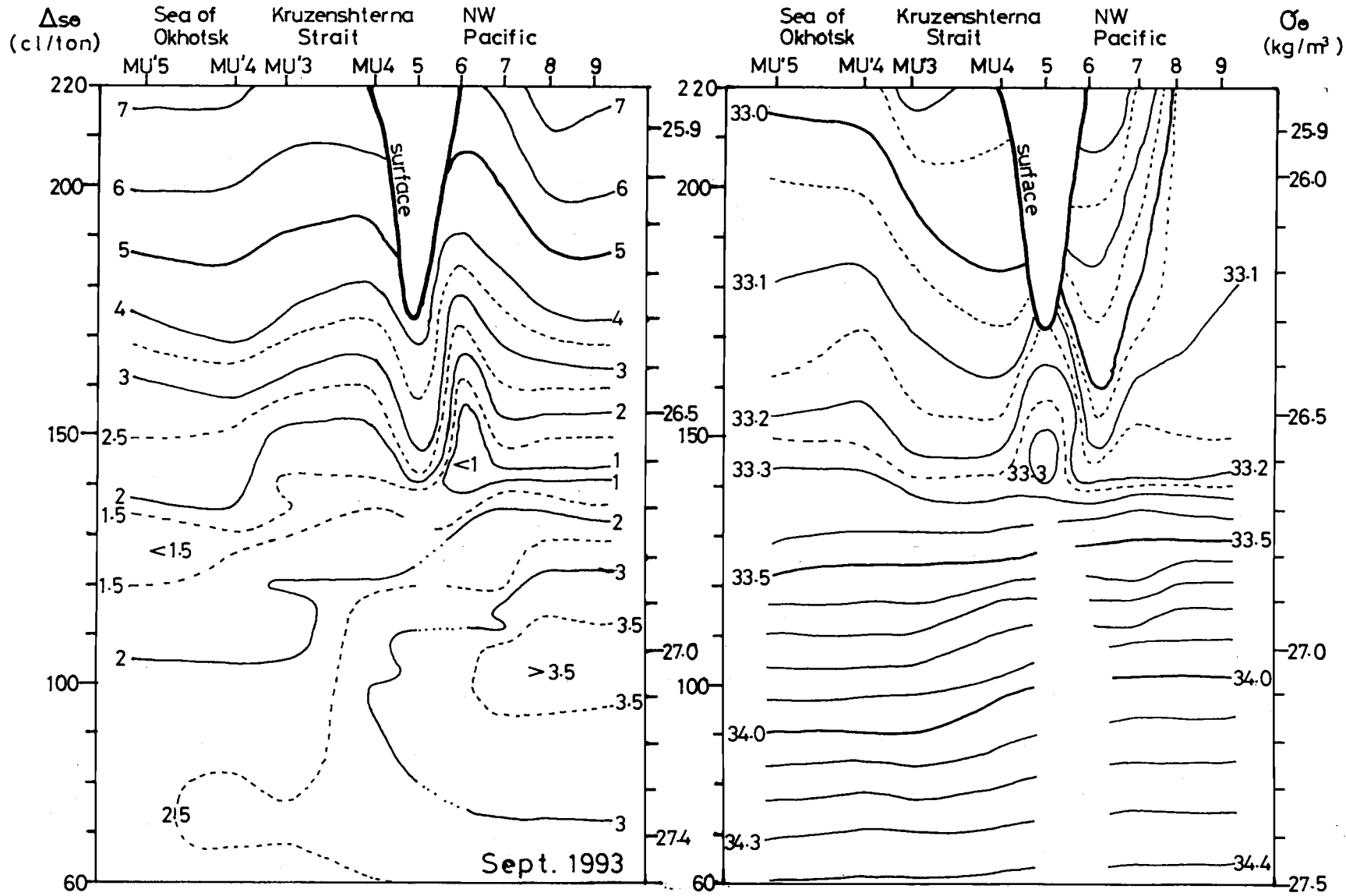

Fig. 2. Sections of potential temperature (deg-C, left) and salinity (psu, right) as a function of potential density (sigma-theta, thermosteric anomaly) through the Kruzenshtern Strait in September, 1993.

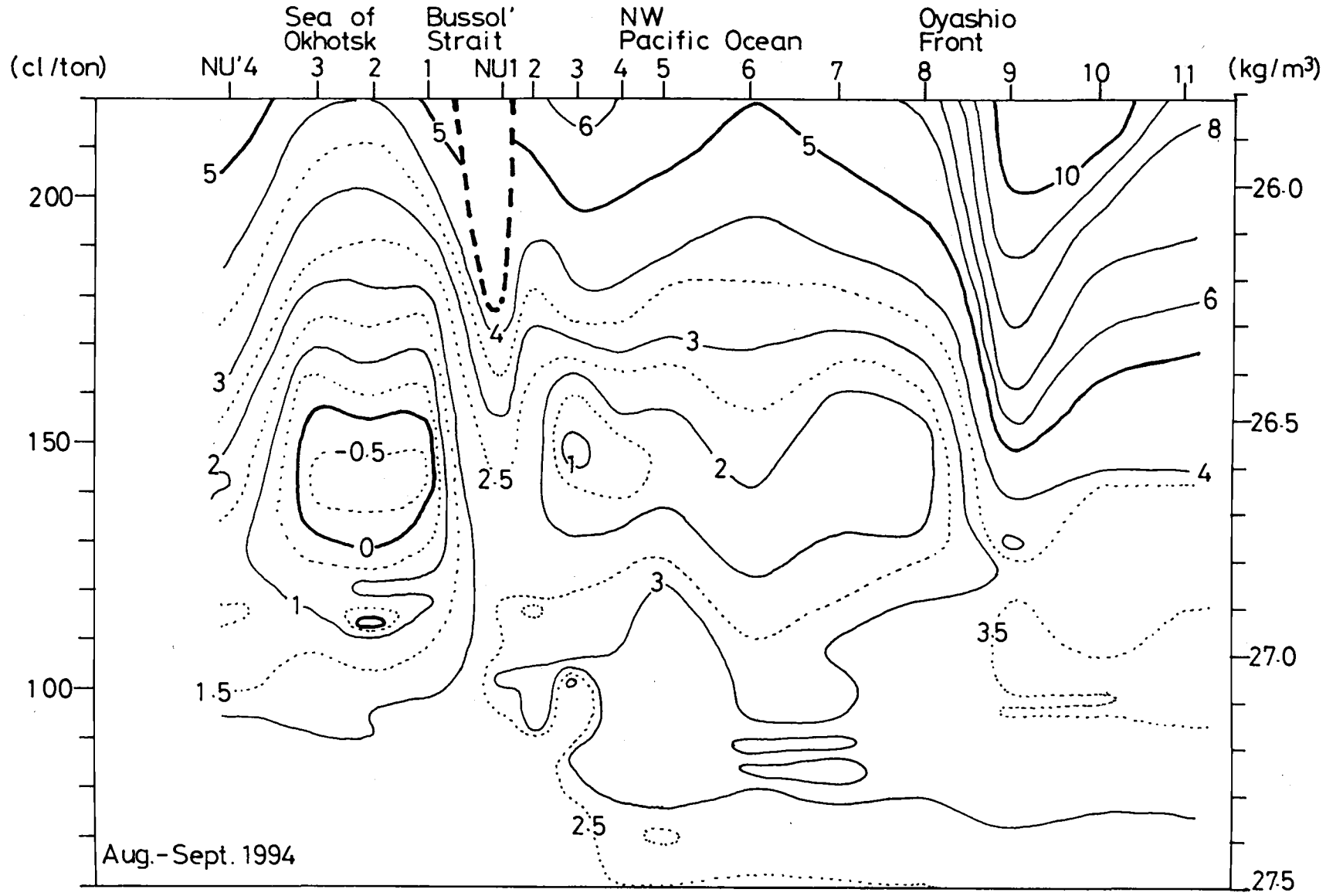

Fig. 3a.

Fig. 3. Sections of (a) potential temperature (deg-C), (b) salinity (psu) and (c) silicate (μmol/l) as a function of potential density (sigma-theta, thermosteric anomaly) through the Bussol' Strait during the period from late August to early September, 1994. Stations NU'1-NU'4 represent the Okhotsk Sea, and stations NU1-NU11 represent the North Pacific. The Bussol' Strait is located between NU'1 and NU1.

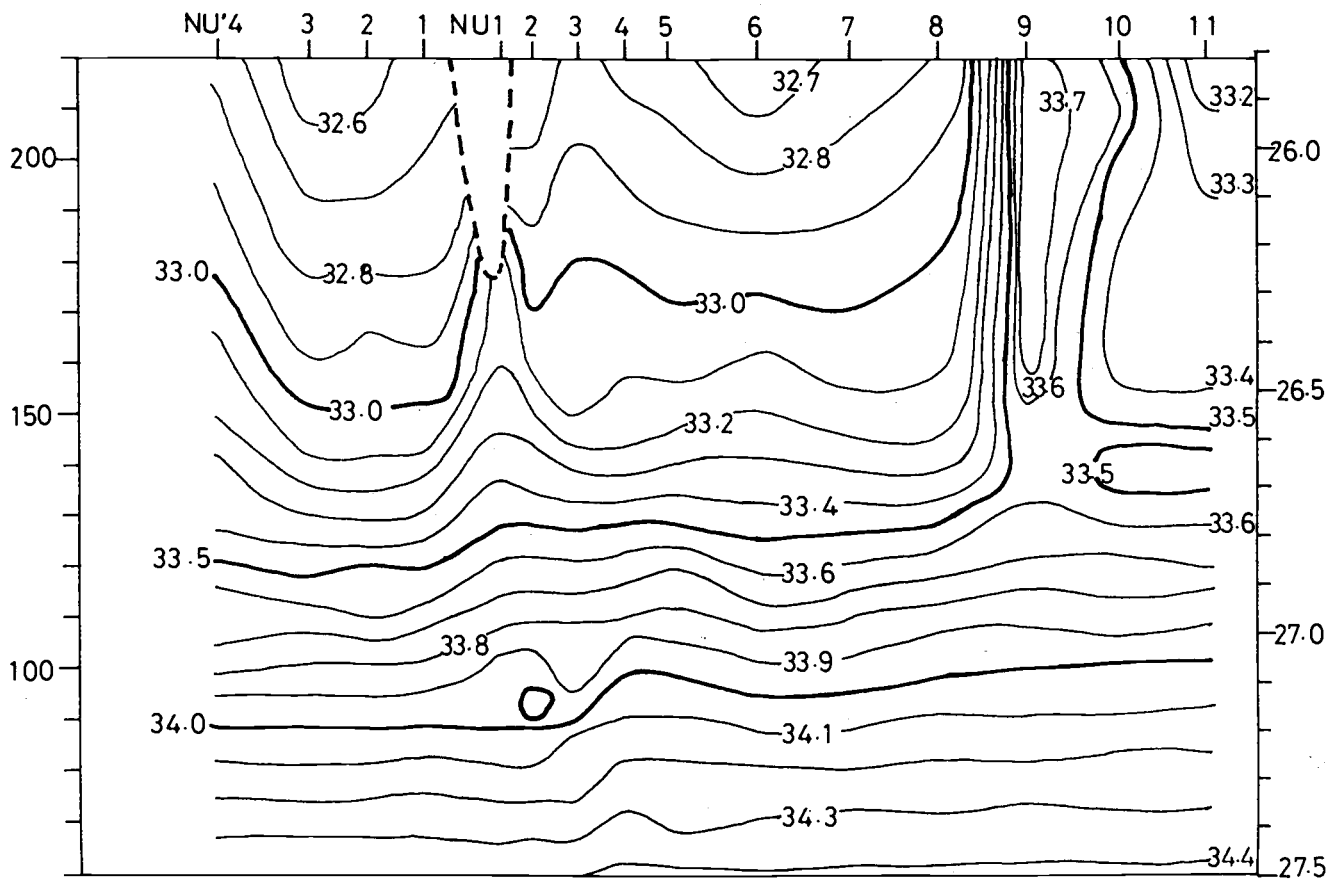

Fig. 3b. (psu)

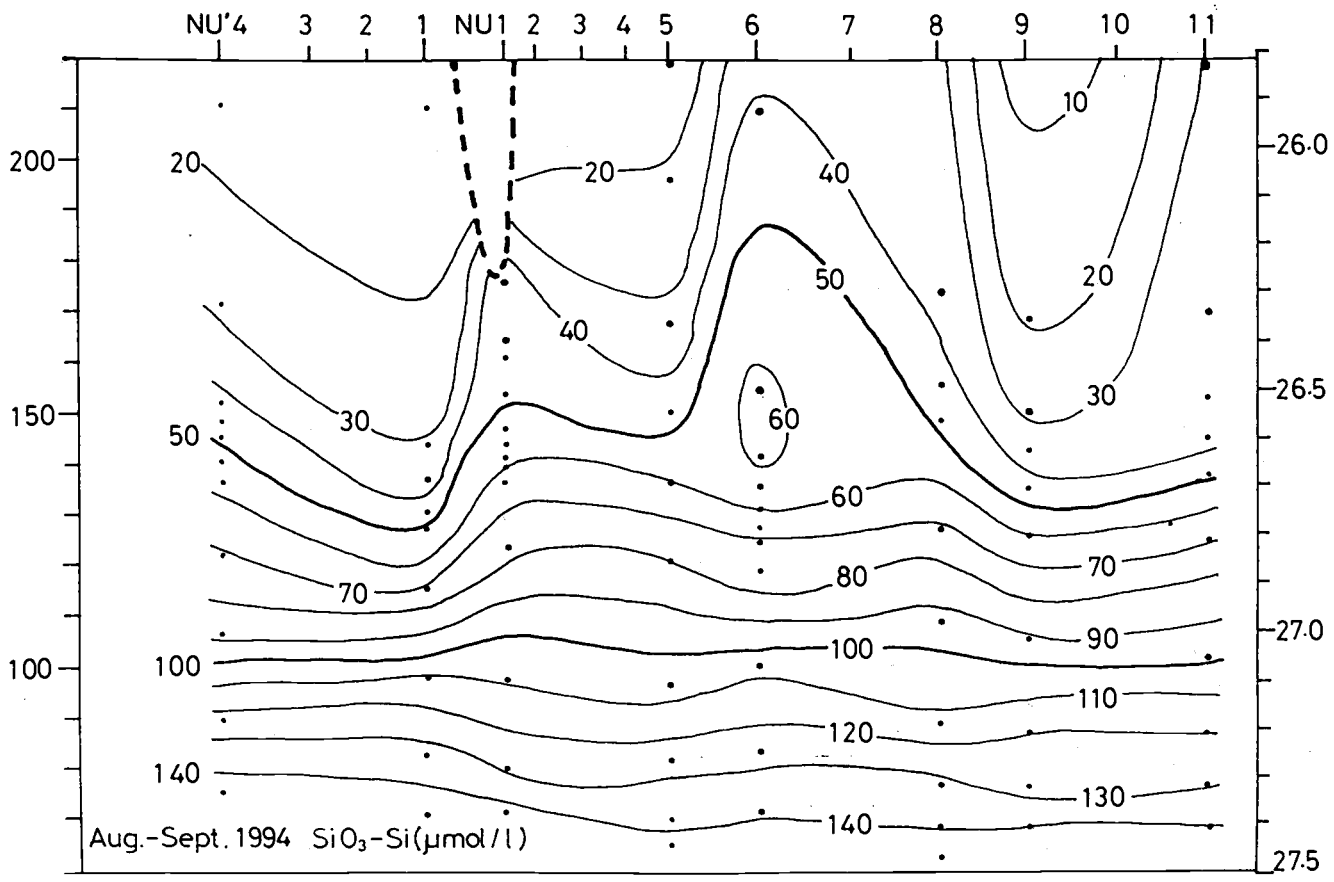

Fig. 3c. (μmol/l)

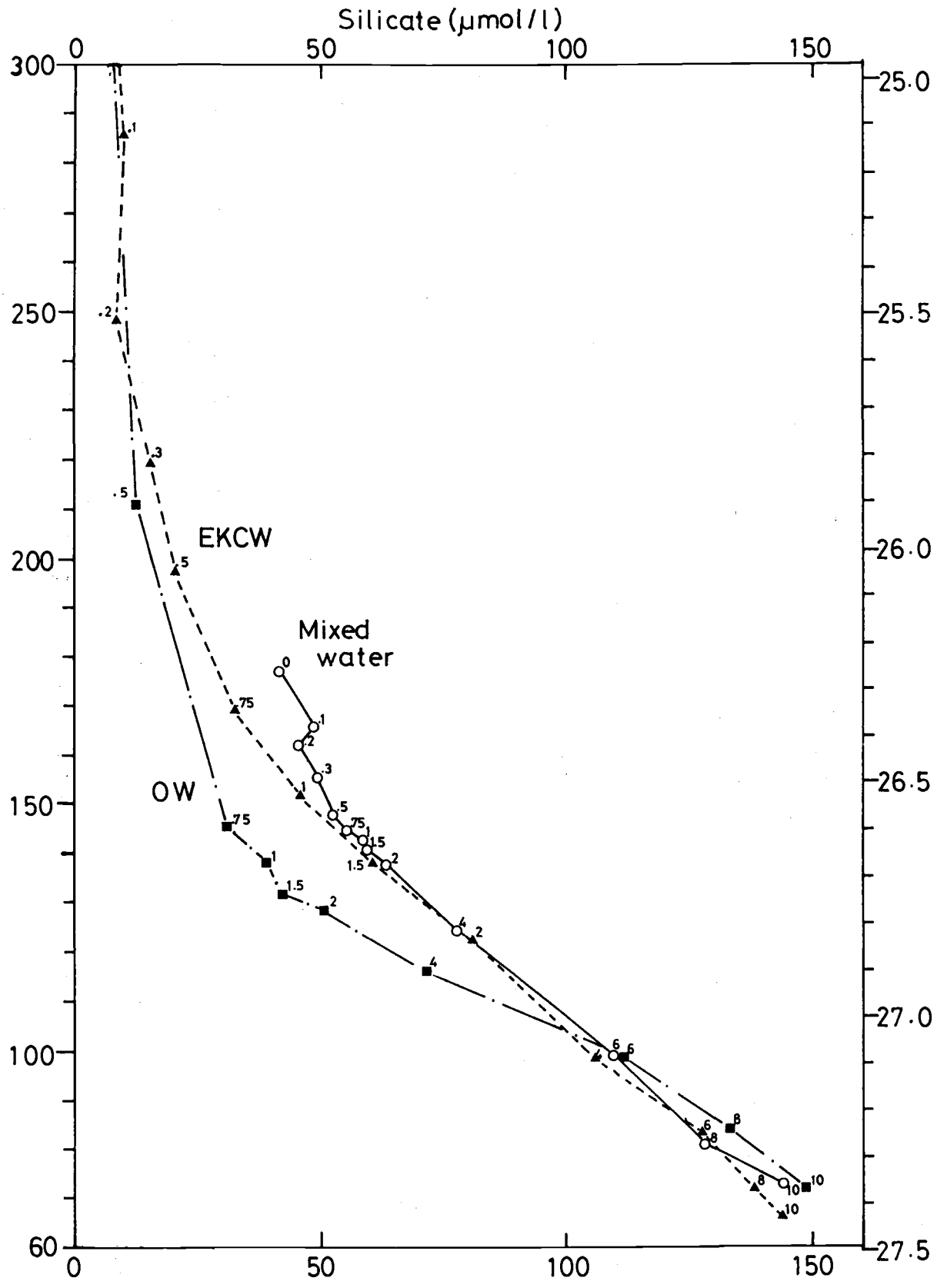

Fig. 4. Plot of silicate concentration (µmol/l) versus potential density (kg/m^3 in sigma-theta, cl/ton in thermosteric anomaly) for OW (closed squares), EKCW (closed triangles) and Mixed Water (open circles) in late August - early September, 1994. Numerals on the shoulder of each symbol indicate the sampling depths in hecto-meters.

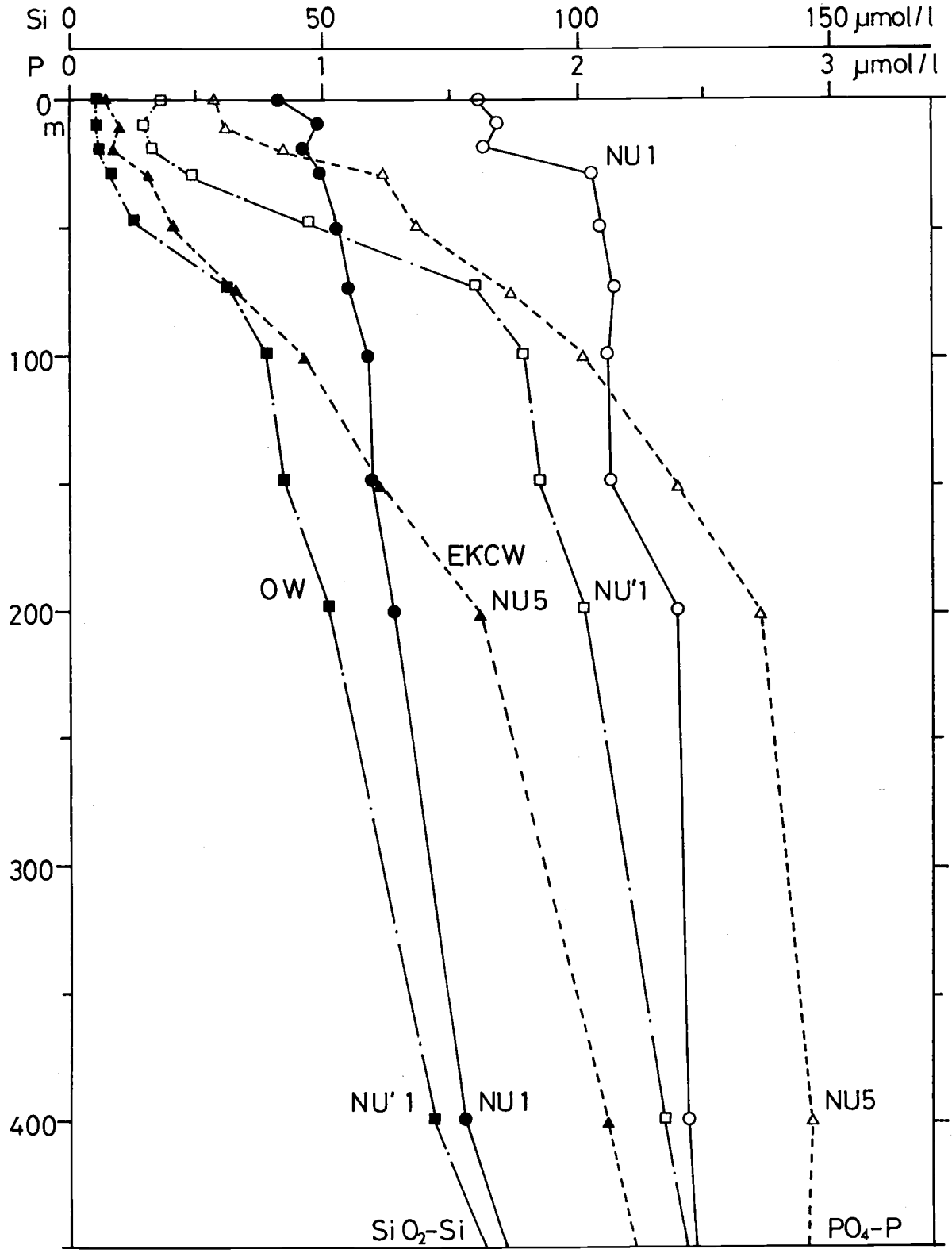

Fig. 5. Vertical distributions of silicate (closed symbols) and phosphate (open symbols) for stations NU'1 (OW, squares), NU1 (Mixed Water, circles) and NU5 (EKCW, triangles) on the section through the Bussol' Strait during the period from late August to early September, 1994.

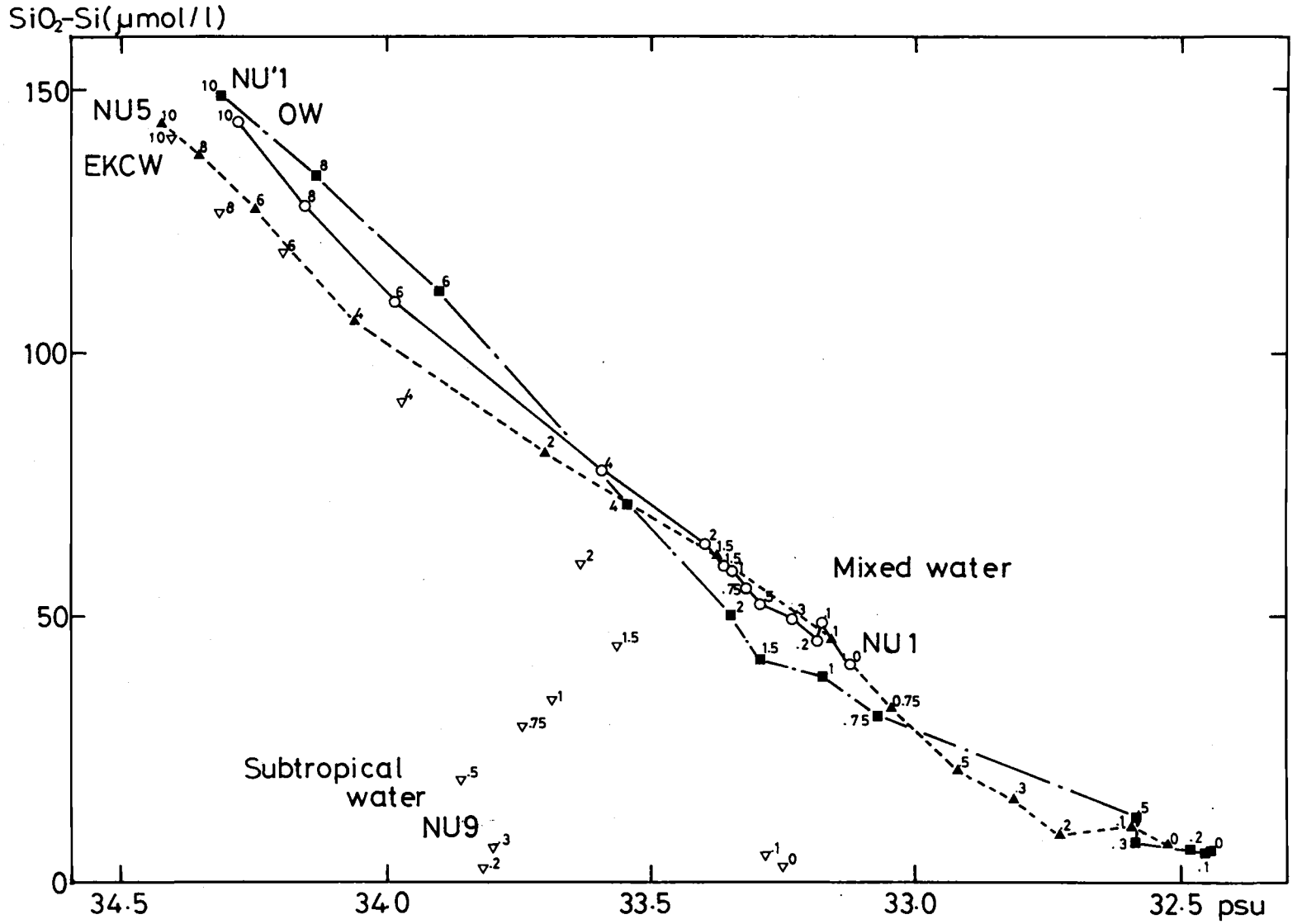

Fig. 6. Plot of silicate concentration (μmol/l) versus salinity (psu) from the surface to the depth of 1000 m for stations NU'1 (OW, closed squares), NU1 (Mixed Water, open circles) and NU5 (EKCW, closed triangles), NU9 (Subtropical Water, open triangles) on the section through the Bussol' Strait during the period from late August to early September, 1994.

Northwest Pacific Paleohydrography

Lloyd D. KEIGWIN

Woods Hole Oceanographic Institution, Woods Hole, MA 02543, U.S.A.

It is important to document carefully glacial-interglacial changes in North Pacific circulation and hydrography in order to understand changes in atmospheric pCO_2 because the Pacific Ocean is the end-member of the modern circulation regime. The modern circulation pattern tends to accumulate CO_2 in the deep Pacific, yet there has been considerable speculation that there may have been a young deep water mass produced in the Pacific during glacial times (Mammerickx, 1985; Keigwin, 1987; Keigwin et al., 1992; Zahn et al. 1991). In addition, it is thought that the marginal seas of the North Pacific contribute to the ventilation of that basin at intermediate depths (for example, Reid, 1973; Talley, 1991). Elsewhere in the world ocean it has been shown that the intermediate depth waters were better ventilated during glaciation, at the expense of the deep ocean (Boyle and Keigwin, 1987; Kallel et al., 1988; Oppo and Lehman, 1993). Could the processes which generate Pacific Intermediate Water in today's ocean have been extended to produce Pacific Deep Water 15,000 years ago?

To answer this and other critical questions about the history of northwestern Pacific circulation, I have been involved in several cruises in the region onboard American and Russian ships to collect new sediment cores and conduct hydrographic investigations. Paleontological and geochemical results from numerous cores on the northern Emperor Seamounts (Fig. 1) support our previous observations based on a single core (Keigwin et al., 1992). For example, the diatomaceous facies centered on deglaciation is found to be widespread (see also Sancetta, 1992) and many new Accelerator Mass Spectrometer (AMS) ^{14}C determinations show that sedimentation rates peaked at that time. The oxygen isotope events in deglacial benthic foraminifera have been confirmed, as has been the evidence for a low salinity event in surface waters. Recently, we have calibrated the $\delta^{13}C$ of the benthic foraminifera *Cibicidoides* against the $\delta^{13}C$ of the total CO_2 in nearby seawater samples, finding that *Cibicidoides* $\delta^{13}C$ is an excellent proxy for the seawater nutrient content in the northwestern Pacific Ocean (McCorkle and Keigwin, 1994). Carbon isotope measurements on *Cibicidoides* of glacial age are uniformly low in the depth range 2,300 m to 4,000 m, supporting the contention that deep ventilation has been low for at least the past 20,000 years. However, the lack of hemipelagic sediment sequences from $<2,300$ m on the Emperor Seamounts denies us a window on the past for shallower depths.

Previous work indicates that the Okhotsk Sea contains appropriate sediment for reconstructing paleoclimate and paleohydrography (Gorbarenko et al., 1988; Morley et al., 1991). Many new cores from that basin reveal that the hemipelagic deposition rates are very high and that, at least during glacial maximum conditions, the benthic fauna contained enough *Cibicidoides* to reconstruct intermediate depth hydrography (for example, Fig. 2). Cores of quality similar to Vulkanolog 34-91 have been recovered at ~100 m spacing in the Kuril Basin along the seaward margin of Akademia Nauk Rise between 1,000 and 3,200 m.

My goal is to combine data from the Okhotsk Sea cores with comparable data from the Emperor Seamounts to produce a composite paleohydrographic profile for the far northwestern Pacific. The two regions are shown schematically in Fig. 3. Various data from hydrocasts in the these regions,

including T, S, $[PO_4]$, $\delta^{13}C$ and $[O_2]$, indicate that water in the Okhotsk Sea between 2,300 m and 1,000 m is in full communication with open Pacific water. This is consistent with modern views of the intermediate depth circulation which show inflow of water to the Okhotsk Sea through Kruzenshtern Strait (sill = 1,600 m) and outflow through Bussol' Strait (sill = 2,300 m) (Figs. 1 and 3).

I suppose that there was no barrier to this circulation pattern during glacial maximum conditions. In addition, because of the general absence of this genus from the modern Okhotsk Sea, it must also be assumed that *Cibicidoides* are as good a proxy for nutrient content of intermediate depth water as they are for deep water. Using the $\delta^{18}O$ of the benthic foram *Uvigerina* to mark the glacial maximum level in our core collection, we have taken additional samples where necessary to extract enough *Cibicidoides* for $\delta^{13}C$ analysis and plotted all those results vs. water depth (Fig. 4).

In Fig. 4, data points connected by the bold solid line are the $\delta^{13}C$ of total CO_2 from the Emperor Seamounts, and the data connected by the fine line are those from the Okhotsk Sea. As noted above, the two hydrocast data sets are indistinguishable between 2,300 m and 1,000 m. It is seen that where the *Cibicidoides* are abundant in modern sediments their $\delta^{13}C$ (open circles) lies close to the water column data. So far, we have found *Cibicidoides* abundant in only one coretop from the Okhotsk Sea, near a depth of 1,000 m off the coast of Sakhalin (BC-32 in Fig. 1).

During glacial times, *Cibicidoides* are present throughout the region. In the open sea the glacial $\delta^{13}C$ data (solid circles) are systematically offset from the coretop data by an amount roughly equivalent to the secular change in seawater chemistry (0.3-0.4 ‰). Those data argue against any major change in deep ocean ventilation, although Cd/Ca data in benthic foraminifera are contradictory (Boyle, 1992). Above 2,300 m, on the other hand, Okhotsk Sea $\delta^{13}C$ data indicate relatively increased ventilation, consistent with results from other locations worldwide. If the glacial data were adjusted by +0.3 to 0.4 ‰ to account for the secular change in world ocean carbon isotope composition, then it would be seen that the change in ventilation begins at the depth of the sill at Bussol' Strait. These results suggest that the Okhotsk Sea was an important source of more oxygenated intermediate waters in the glacial North Pacific Ocean. The influence of this better ventilation may be evident as far downstream as the Gulf of California. There, in Guaymas Basin which is anoxic today at Pacific Intermediate Water depths, glacial bottom waters contained enough oxygen to support an active benthos (Keigwin and Jones, 1990).

REFERENCES

Boyle, E.A. 1992. Oceanic chemical distributions during the stage 2 glacial maximum: Cadmium and $\delta^{13}C$ evidence compared. Annual Reviews of Earth Planet. Sci. 20:245-287.

Boyle, E.A., and L.D. Keigwin. 1987. North Atlantic thermohaline circulation during the past 20,000 years linked to high-latitude surface temperature. Nature. 330:35-40.

Gorbarenko, S.A., N.N. Kobaliuch, et. al. 1988. Okhotsk Sea upper Quaternary sediment and reconstruction of paleoceanographic conditions. Pacific Ocean Geology. 2:25-34.

Kallel, N., L.D. Labeyrie, A. Juillet-Leclerc, and J.-C. Duplessy. 1988. A deep hydrological front between intermediate and deep water masses in the glacial Indian Ocean. Nature. 333:651-655.

Keigwin, L.D. 1987. North Pacific deep water formation during the latest glaciation. Nature. 330:362-364.

Keigwin, L.D., and G.A. Jones. 1990. Deglacial climatic oscillations in the Gulf of California. Paleoceanography. 5:1009-1023.

Keigwin, L.D., G.A. Jones, and P.N. Froelich. 1992. A 15,000 year paleoenvironmental record from Meiji Seamount, far northwestern Pacific. Earth Planet. Sci. Lett. 111:425-440.

Mammerickx, J. 1985. A deep-sea thermohaline flow path in the Northwest Pacific. Marine Geology. 65:1-19.

McCorkle, D.C., and L.D. Keigwin. 1994. depth profiles of $\delta^{13}C$ in bottom water and core top C. *wuellerstorfi* on the Ontong Java Plateau and Emperor Seamounts. Paleoceanography. 9:197-208.

Morley, J.J., L.E. Heusser, and N.J. Shackleton. 1991. Late Pleistocene/Holocene radiolarian and pollen records from sediments in the Sea of Okhotsk. Paleoceanography. 6:121-131.

Oppo, D.W., and S.J. Lehman. 1993. Mid-depth circulation of the subpolar North Atlantic during the last glacial maximum. Science. 259:1148-1152.

Reid, J.L., Jr. 1973. North Pacific Ocean waters in winter. The Johns Hopkins Oceanographic Studies. 5:96 p.

Sancetta, C. 1992. Primary production in the glacial North Atlantic and North Pacific Oceans. Nature. 360:249-251.

Talley, L.D. 1991. An Okhotsk Sea water anomaly: implications for ventilation in the North Pacific. Deep-Sea Res. 38:S171-S190.

Zahn, R., T.F. Pedersen, B.D. Bornhold, and A.C. Mix. 1991. Water mass conversion in the glacial Subarctic Pacific (54N, 148W): Physical constraints and the benthic-planktonic stable isotope record. Paleoceanography. 6:543-560.

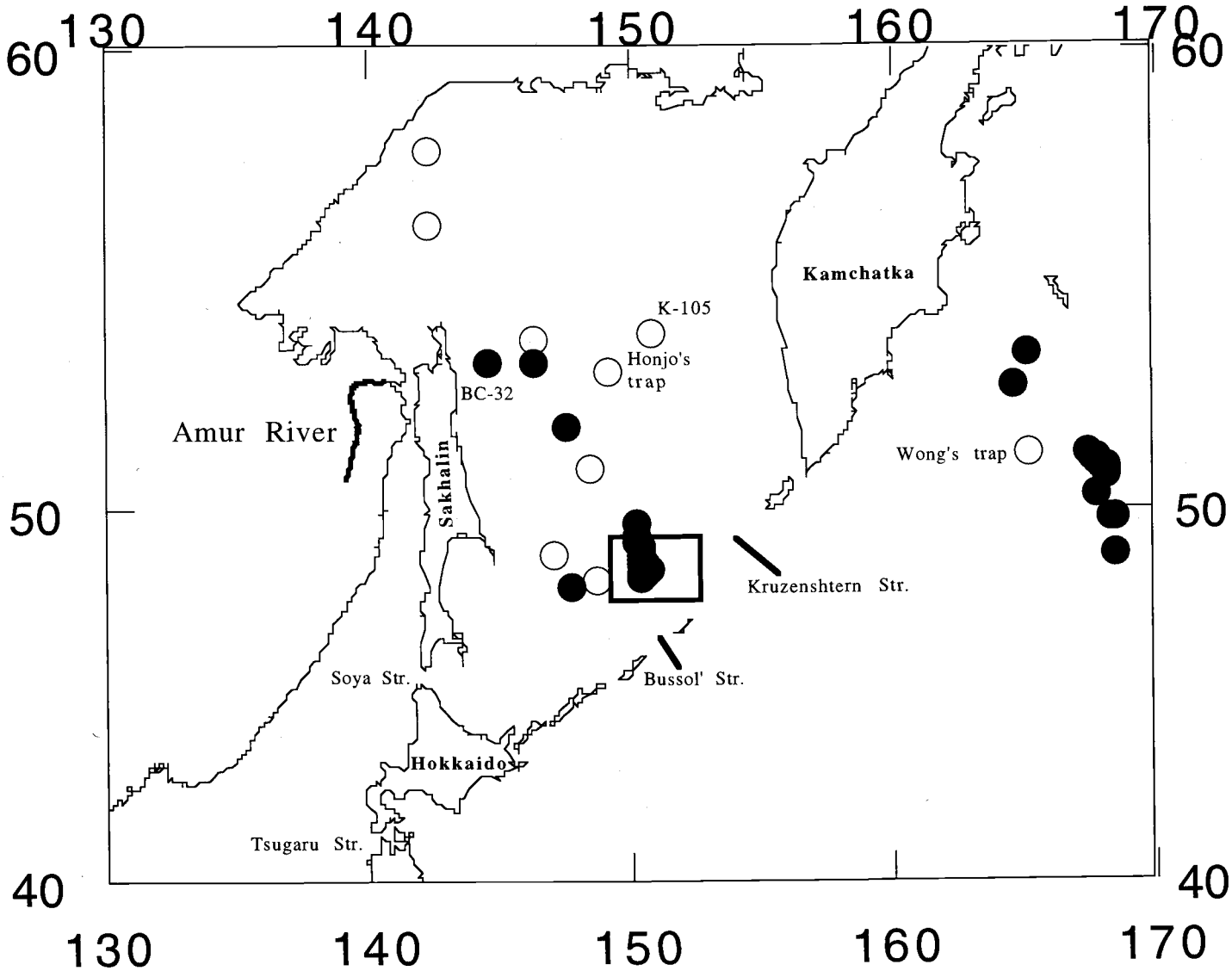

Fig. 1. Some core and sediment trap locations in the far northwestern Pacific Ocean. Solid symbols mark sediment cores in the Woods Hole collection. The box shows the positions of about 20 cores at ~100m depth spacing on the seaward flank of Akademia Nauk Rise in the Kuril Basin.

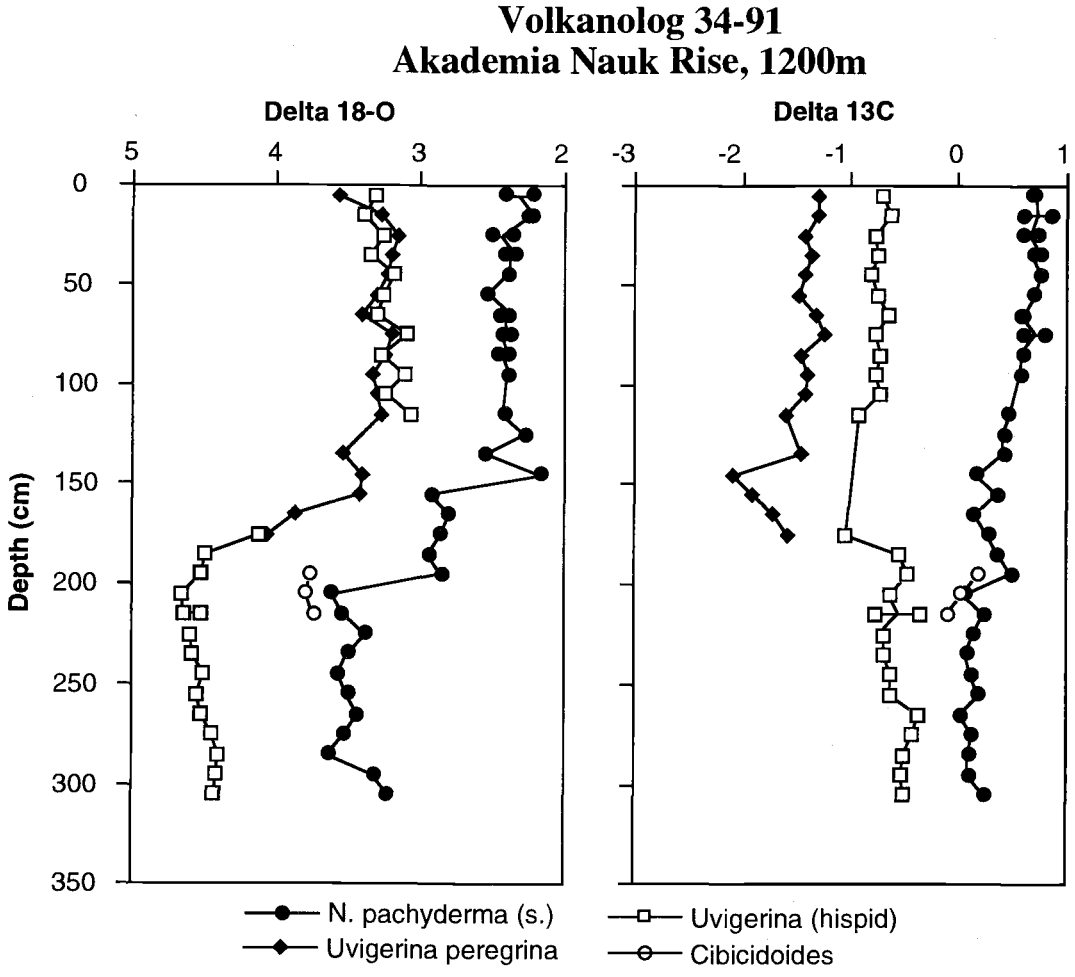

Fig. 2. Stable isotope record from core Volkanolog 34-91 at ~1,200 m water depth on Akademia Nauk Rise. Oxygen isotope results on the benthic foram Uvigerina and the planktonic N. pachyderma (s.) show that there is about 150 cm of Holocene section, with glacial maximum conditions deeper than ~200 cm. Carbon isotope analyses of Cibicidoides from the glacial maximum level at this and many other locations are used in making the paleohydrographic section shown in Fig. 4.

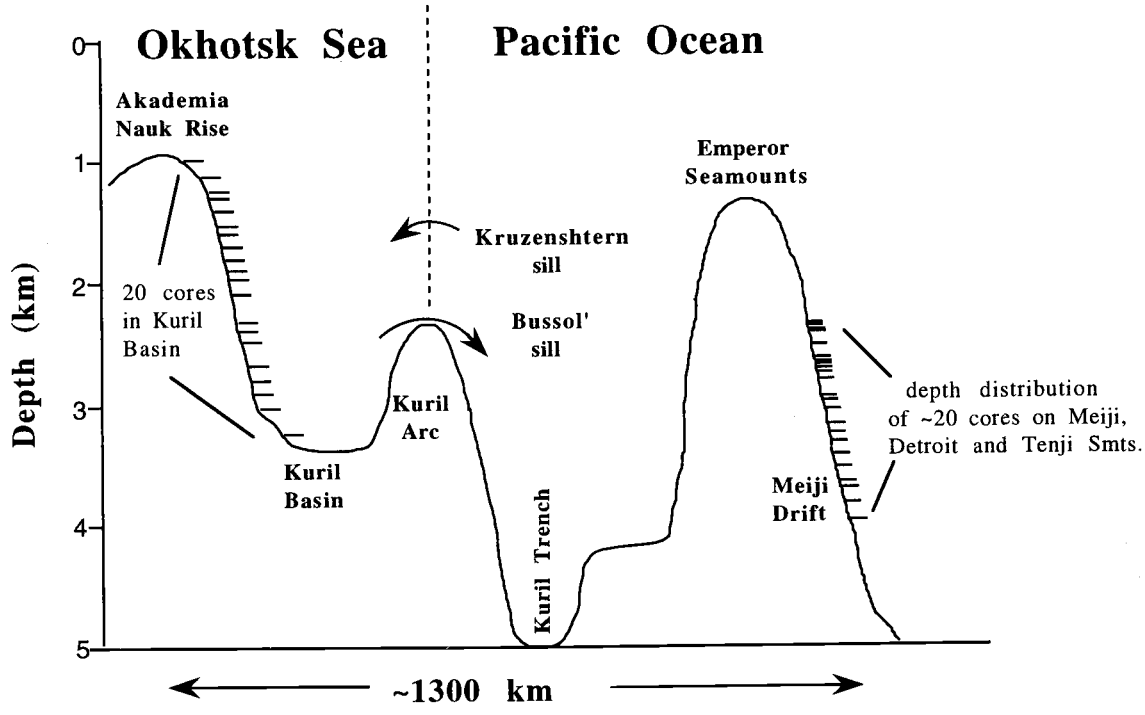

Fig. 3. A schematic diagram illustrating the physiography, circulation and distribution of some sediment cores in the Okhotsk Sea and on the northern Emperor Seamounts in the open Pacific Ocean.

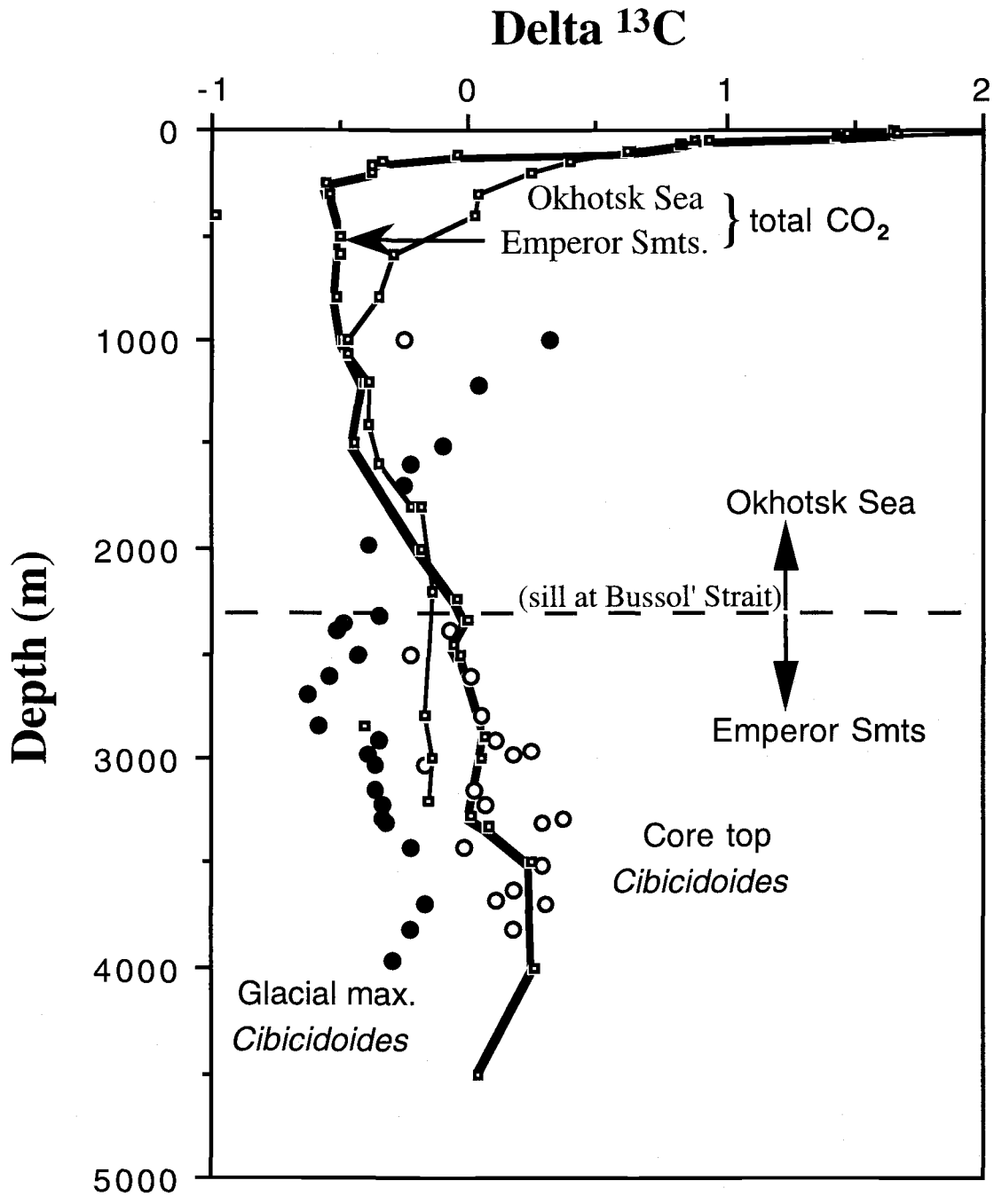

Fig. 4. Modern water column hydrography ($\delta^{13}C$ of total CO_2) in the Okhotsk Sea (thin line) and the open northwestern Pacific (thick line), compared to $\delta^{13}C$ of Holocene Cibicidoides (open circles) and glacial maximum Cibicidoides (filled circles). The paleohydrographic data depart from the modern circulation pattern above ~2,300 m, where $\delta^{13}C$ increases indicating better ventilation. The fact that this change occurs at about the sill depth of the Okhotsk Sea suggests that that sea may have been the source region.

Physical Mechanisms for the North Pacific Intermediate Water Formation

Talgat R. KILMATOV

Pacific Oceanological Institute, Far-Eastern Branch, Russian Academy of Sciences,
Vladivostok, Russia

1. The surface and subsurface fresh water sources for the North Pacific Intermediate Water (NPIW) formation are disposed in the Mixed Water Region between the Kuroshio and Oyashio Currents, especially at the Subarctic Front (SF). The analysis of the salinity fields across this region shows that the connection of the NPIW with surface waters occurs in the SF and this front is the southern border of the subarctic low salinity water distribution. This water moves to the southeast and downward to the intermediate depth in the subtropical part of the North Pacific.

The surface of the North Pacific subtropical zone loses about 40 cm of pure water every year as the result of evaporation. Assuming the low salinity water from the Subarctic Gyre compensates the superfluity of salt in the subtropical zone, the minimum fresh water transport is .5 S_v (10^6 m^3/s) to form the NPIW. The direct estimations of this transport give values of about 6 S_v (Talley and Nagata, 1995). The total volume of the NPIW is approximately $2*10^{6-7}$ km^3 (Kuksa, 1968), and thus its renewal time is 10-100 years. Based on the isotopic measurements the intermediate water longevity is about 10 years. These data clearly demonstrate that the NPIW is an important factor influencing the climatic change of the North Pacific on the time scales of 10-100 years.

The formation of the NPIW is due to the downwelling process. The Subarctic Front is a distinct downwelling zone where dynamic equilibrium keeps the climatic thermohaline front as a sharp border in temperature and salinity fields. In this work we will review several possible physical mechanisms of downwelling at the SF.

2. The Subarctic Front can be roughly described as the axis of the convergence. If the SF is regarded as the longitudinally-uniform thermohaline front, the density ratio ($\alpha\Delta T/\beta\Delta S$) is about 1 and the cross velocity on the convergence axis equals zero. The vertical component of the planetary vortex is the Coriolis parameter $f = 2\omega \sin\varphi = 0.43*10^{-4}\ s^{-1}$, ($\varphi \approx 40°N$), the horizontal component of the planetary vortex is $m = 2\omega \cos\varphi = 0.59*10^{-4}\ s^{-1}$. If the inertial and vorticity forces are balanced along the convergence axis, the following equation is correct (Pedlosky, 1979):

$$u(du/dx) + mw = 0$$

This equation shows that the planetary vortex produces the vertical motion on the convergence axis, and thus, turns the inertial velocity along the SF downward. The estimation of vertical velocity gives

$$w \approx u^2/(m \times L) \approx 10^2\, cm^2 s^{-2}/(5.9 \times 10^{-4}\, s^{-1} \times 10^3\, km) \approx 10^{-4}\, ms^{-1}$$

Besides, there is a link between the latitude advection and the convergence intensity at the climatic thermohaline front.

3. The thermohaline SF is the place of the intensive cabbeling process (Kilmatov and Kuzmin, 1990, 1991). The necessary condition of the downwelling due to the cabelling is $\alpha\ \Delta T/\beta\Delta S = 1$. The

changes in temperature and salinity in the upper layer across the Subarctic Front are $\Delta T \sim 4 \div 10°C$ and $\Delta S \sim 0.5 \div 1.5$ psu. The value of the cabelling can be estimated by the next formula:

$$\delta\rho \approx -0.125 * d^2\rho/dT^2 * \Delta T^2 \approx 0.125 * 10^{-5} g\ cm^{-3}\ °C^{-2} * 10^2\ °C \approx 10^{-4} g\ cm^{-3}.$$

As an example, distribution of basic hydrographic characteristics across the SF at the end of the cooling period is presented in Table 1. The maximum of water density is emphasized.

Cabelling reaches its maximum value in winter due to the favorable conditions (Kilmatov and Kuzmin, 1990). Thus, in the cooling period downwelling occurs at the front to some intermediate depth, where densities of the sinking and surrounding waters become equal. Hence, the cabelling effect in the upper ocean layer at the SF has an annual periodicity with the maximum during the winter. At that time the maximum convergence is observed at the front and its kinetic energy is transformed from the available potential energy of the cabelling process. The vertical velocity produced by the cabelling can be evaluated from the mechanical energy balance equation:

$$w \sim h_M L_M^{-1} (g\ h\ \delta\rho/\rho)^{0.5} \sim 10^2\ m\ (10^5\ m)^{-1} (10\ ms^{-2} * 10\ m * 10^{-4})^{0.5} \sim 10^{-4}\ ms^{-1}$$

4. The cyclic sinking of the ordinary portion of the upper water layer at the SF during winter due to the cabbeling assumes the "spotted" structure of waters in a horizontal direction at intermediate depths. Although the NPIW in the Mixed Water Region of the Kuroshio-Oyashio is characterized by complicated dynamic and thermohaline structure: the horizontal periodicity in values of salinity, temperature and dissolved oxygen at depth about 300 m is observed. The "spotted" structure in the core of the intermediate water mass with decreased salinity at a depth of 600-800 m is also found in the subtropical part of the North Pacific. The observations show that the core of NPIW in the horizontal direction consists of zones with closed isolines alternating at almost equal intervals of about 100-200 miles. Within these zones the decreased salt content takes place. The horizontal and vertical scales of zones are $\Delta L \sim 100$ km, $\Delta h \sim 100$ m, respectively.

Note, that the mechanism of formation of these zones does not exclude such elements as the synoptical deformation fields. In particular, storms, winter convection, ocean rings at the Mixed Water Region of Kuroshio - Oyashio lead to an increase of water exchange between the upper and intermediate waters. But the cabelling process occurs only at the Subarctic Front and it produces the downwelling.

REFERENCES

Kilmatov, T.R., and V.A. Kuzmin. 1990. The Pacific Subarctic Frontal Zone. Vladivostok, FEB RAS. 114 p. (in Russian).

Kilmatov, T.R., and V.A. Kuzmin. 1991. The Effect of Cabbeling and its Season Variations in the Subarctic Front. Izv. Akad. Nauk SSSR (ser. fiz. atm. i okeana). 27:883-887 (in Russian).

Kuksa, V.I. 1968. The Intermediate Waters in the World Ocean. Leningrad, Gidrometeoizdat, 271p. (in Russian).

Pedlosky, J. 1979. Geophysical Fluid Dynamics. N.Y., Springer-Verlag, 624p.

Talley, L.D. 1993. Distribution and Formation of North Pacific Intermediate Water. J. Phys. Oceanogr. 23:517-537.

Talley, L.D., Y. Nagata et al. 1995. North Pacific Intermediate Water in Kuroshio/Oyashio Mixed Water Region. J. Phys. Oceanogr. 25:475-501.

TABLES AND FIGURES

Table 1. Temperature, salinity and conditional density of seawater in the upper (0-5 m) ocean layer across the Subarctic Front along 152°E (April, 1980, R/V "Stepan Malygin").

φ^0 N	θ^0C	S $^0/_{00}$	σ_t	
43°52'	0,9	32,71	26,21	
43 41	0,8	32,66	26,18	
43 05	1,3	32,64	26,13	
42 30	1,8	32,65	26,11	
42 00	6,4	33,66	**26,45**	< SF
41 28	7,6	33,78	26,39	
40 30	9,0	34,04	26,39	
39 28	9,9	34,06	26,26	

Water Masses in the Okhotsk Sea

Vladimir A. LUCHIN

Far Eastern Regional Hydrometeorological Research Institute, Vladivostok, Russia

INTRODUCTION

The cold intermediate layer in the Okhotsk Sea was firstly distinguished by Makarov (1884). The water masses in this marginal sea has been described in details by Kitani (1986), Leonov (1960) and Moroshkin (1966). These surveys contain many illustrations and sufficient analysis of the previous studies. The water structure of the southern Okhotsk Sea has been discussed by Takizawa (1982) and Vakao and Kodzima (1962). The number of papers are devoted to the substantial contribution of the Kuril Straits in modification of the Okhotsk Sea water (Bogdanov, 1968; Bruevich et al., 1960; Leonov 1960; Moroshkin, 1966) and to the considerable influence of the Okhotsk Sea hydrological processes on the North Pacific water structure (Favorite et al., 1976; Kajiura, 1949; Kitani, 1986; Reid 1965; Tally, 1991; Wakatsuchi and Martin, 1991; Yasuoka, 1967).

DATA AND METHOD

The hydrographic (temperature and salinity) data collected at 51,607 stations during the period from 1930 to 1988 were analyzed and classified in times (by months) and in space (trapezia of 1 degree). To distinquish the Okhotsk Sea water masses the TS analysis method was applied and T-S curves were created for each 1 degree square.

RESULTS

The Okhotsk Sea water structure is formed under the influence of the Pacific water advection, fall-winter cooling, river run-off, water mixing in the regions of intensive dynamics, solar radiation as well as the system of the occurring currents. Fig. 1 strictly demonstrates four different water masses in the Okhotsk Sea: the surface layer, the cold intermediate layer, the deep Pacific water mass and near-bottom water mass of the southern (Kuril) basin.

The surface layer is distinquishable only in the warm period. In winter the boundary between the surface and cold intermediate water masses disappears. The influence of the Pacific water is clearly observed within the temperature field: due to the intensive tidal water mixing in the Kuril Straits the Pacific waters are the warmest in winter and the coldest in summer (Figs. 2a, b). The same effect takes place for the low temperature formations in summer near the Shantar Islands and at the entrance to Shelikhov Bay. The temperature anomaly over the Kashevarov Bank is the result of the water rising from below. The warm Soya current in the southern Okhotsk Sea is well pronounced in the summer season.

During the whole year the more saline Pacific waters penetrate into the Okhotsk Sea and fill in its southern and eastern parts. At the same time the coastal dilution is distinctly expressed in summer in the western part of sea: for instance, the influence of Amur river is observed for 100-150 miles from the northern tip of Sakhalin Island (Figs. 2c, d).

In the warm period the cold intermediate water mass can be revealed in the Okhotsk Sea. The distribution of basic temperature and salinity features are preserved in this layer during spring and summer, but the depth of the core location increases by 20-30 m in summer as compared with spring. The deepening of the upper boudary and core of the cold intermediate water mass continues in autumn. Fig. 3 demonstrates characteristics of the summer modification of the cold intermediate water mass. Temperature distribution in the core (Fig. 3c) indicates that the cold waters are transported southward in the western part of the sea. The water flow from the Cape of Terpenie to the southern tip of Kamchatka Peninsula is also distinquished. The intensive dynamic processes at the entrance to Shelikhov Bay promote formation of the positive temperature values here. The salinity isolines show the Pacific water inflow northward in the eastern part of the sea (Fig. 3d).

Fig. 4 presents properties of the deep Pacific water mass. The temperature maximum ($>2°C$) is observed in this water. The T-S distribution in the core suggests that the Pacific water moves from the Kuril Straits towards the Kashevarov Bank. The temperature within the core of the near-bottom water mass of the southern (Kuril) basin does not exceed 1.8-1.9°C and salinity varies from 34.6 to 34.7 psu.

The density (sigma-t) distributions in the cores of the Okhotsk Sea water masses are displayed in Fig.5. In accordance with our estimations density in the cold intermediate water mass varies from 26.0 to 26.75 sigma-t (near the Kuril Straits from 26.3 up to 26.75). In the deep Pacific water mass the density changes from 27.0 up to 27.4 sigma-t and maximum values are observed within the Central Kuril Straits. During the last decades the Okhotsk Sea region has been considered as one of the sources for the North Pacific Intermediate Water formation. Taking into account the water mass parameters (Figs. 2-5) together with the Okhotsk Sea current system (f.e., Luchin, 1995) we can conclude that on the way to the Pacific Ocean the cold intermediate waters from the northern Okhotsk sea (with density of 26.0-26.75 sigma-t) are blocked and transformed at least twice: first, in the anticyclonic circulation system over the southern basin and then within the Kuril Straits Region.

REFERENCES

Bogdanov, K.T. 1968. Hydrological conditions in the Freez Strait in summer period. Oceanological studies. 19:95-104.

Bruevich, S.V., A.N. Bogoyavlensky, and V.A. Mokievskaya. 1960. Chemical characteristics of the Okhotsk Sea. Trudy of Institute of Oceanology of USSR Academy of Sciences. 42:125-198 (in Russian).

Favorite, F., A.J. Dodimead, and K. Nasu. 1976. Oceanography of the Subarctic Pacific region, 1960-1971. Bull. Int. North Pacific Comm. 33:1-187.

Kajiura, K. 1949. On the hydrography of the Okhotsk Sea in summer. J. Oceanogr. Soc. Japan. 5:19-26 (in Japanese).

Kitani, K. 1986. Water mass structure in the Okhotsk Sea. Kaiyo Monthly. 18:93-98 (in Japanese).

Leonov, A.K. 1960. Regional Oceanography. Gidrometeoizdat, Leningrad. 766 p. (in Russian).

Luchin, V.A. 1995. System of currents and peculiarities of temperature distribution in the Okhotsk Sea. The Okhotsk Sea and Oyashio Region. PICES Scientific Report No. 2:211-227.

Makarov, S.O. 1894. R/V "Vityaz" and the Pacific Ocean. St.Petersburg. 505 p. (in Russian).

Moroshkin, K.V. 1966. Water masses of the Sea of Okhotsk. Nauka, Moscow. 65 p. (in Russian).

Reid, J.L. 1965. Intermediate Waters of the Pacific Ocean. Johns Hopkins Oceanogr. Studies. 2: 1-85.

Takizawa, T. 1982. Characteristics of the Soya Warm Current in the Okhotsk Sea. J. Oceanogr. Soc. Japan. 38:281-292.

Talley, L.D. 1991. An Okhotsk Sea water anomaly: implications for ventilation in the North Pacific. Deep-Sea Res. 38 (Supp. 1):S171-S190.

Wakao, M., and I. Kojima. 1962. On the oceanographical conditions in the southwestern region of the Okhotsk Sea. J. Hokkaido Fish. Exp. Sta. 18:1-25 (in Japanese).

Wakatsuchi, M., and S. Martin. 1991. Water ciculation of the Kuril Basin of the Okhotsk Sea and its relation to eddy formation. J. Oceanogr. Soc. Japan. 47:152-168.

Yasuoka, T. 1967. Hydrography in the Okhotsk Sea. Oceanogr. Mag. 19:61-72.

FIGURES

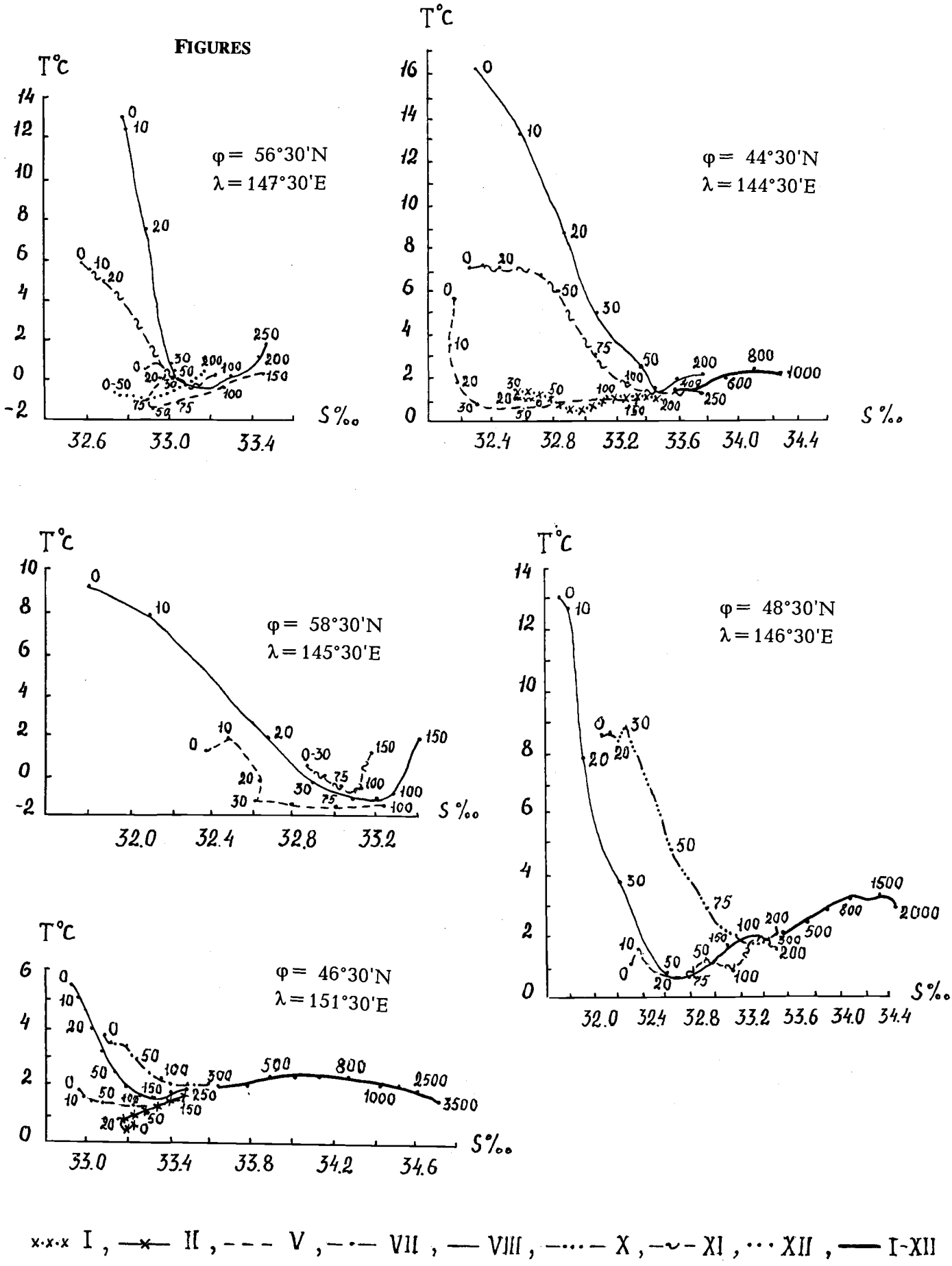

Fig. 1. Typical T-S curves for the Okhotsk Sea.

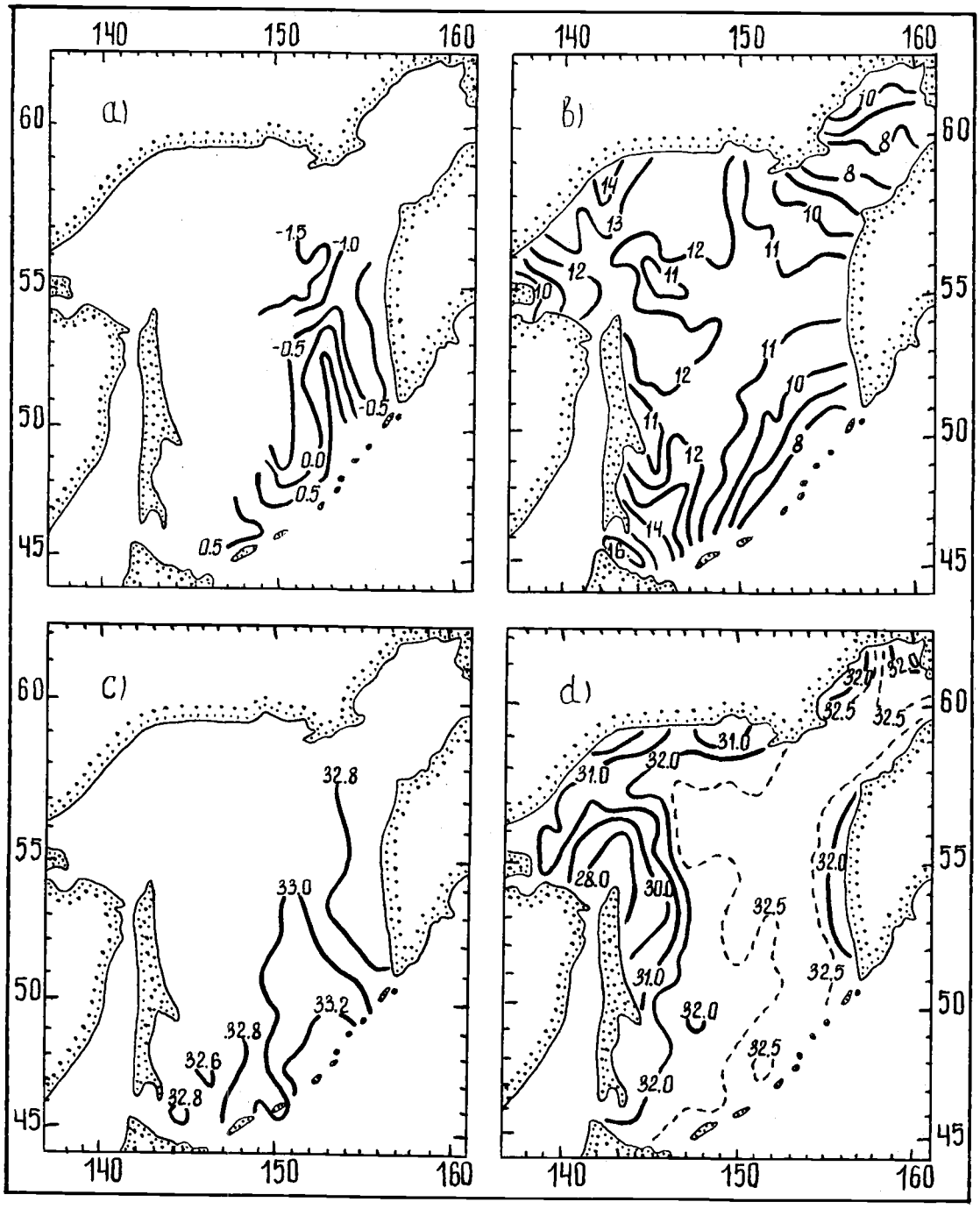

Fig. 2. Surface distribution of temperature (°C) (a - February; b - August) and salinity (psu) (c - February; d - August) in the Okhotsk Sea.

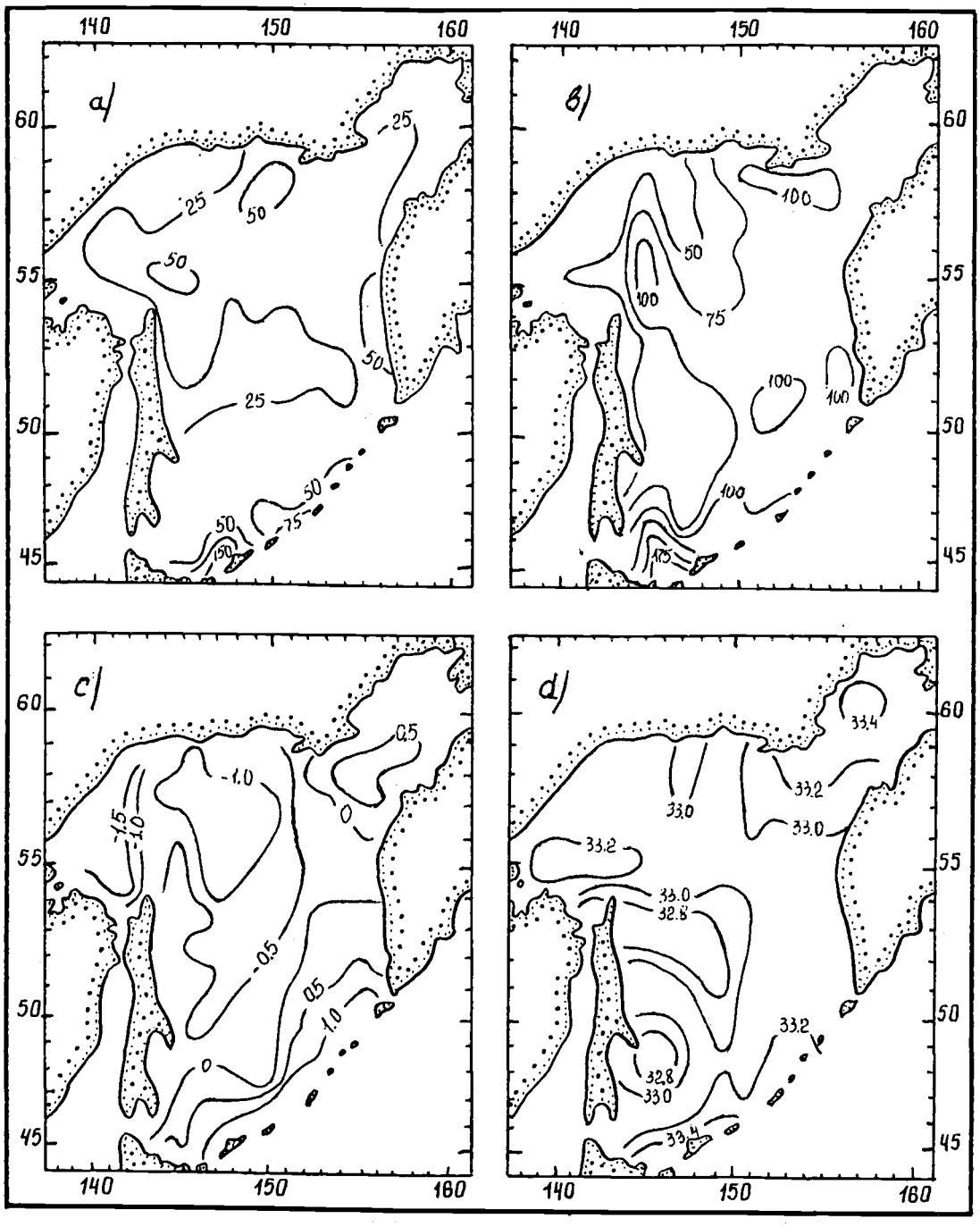

Fig. 3. Characteristics of the intermediate cold water mass (summer modification) in the Okhotsk Sea: a - depth of the upper boundary (m); b - depth of core location (m); c - core temperature (°C); d - core salinity (psu)

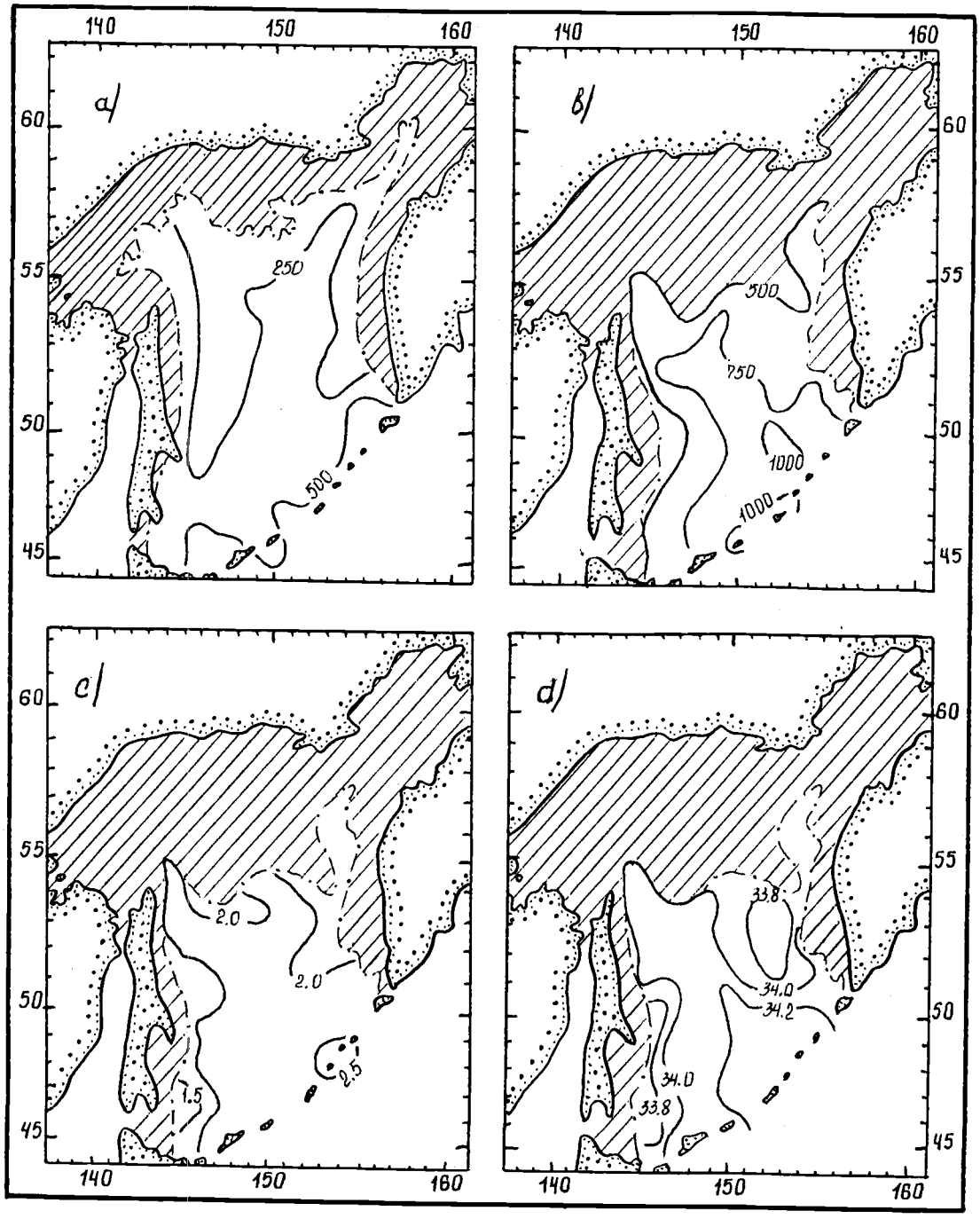

Fig. 4. Characteristics of the deep Pacific water mass in the Okhotsk Sea:
a - depth of the upper boundary (m); b - depth of core location (m);
c - core temperature (°C); d - core salinity (psu)

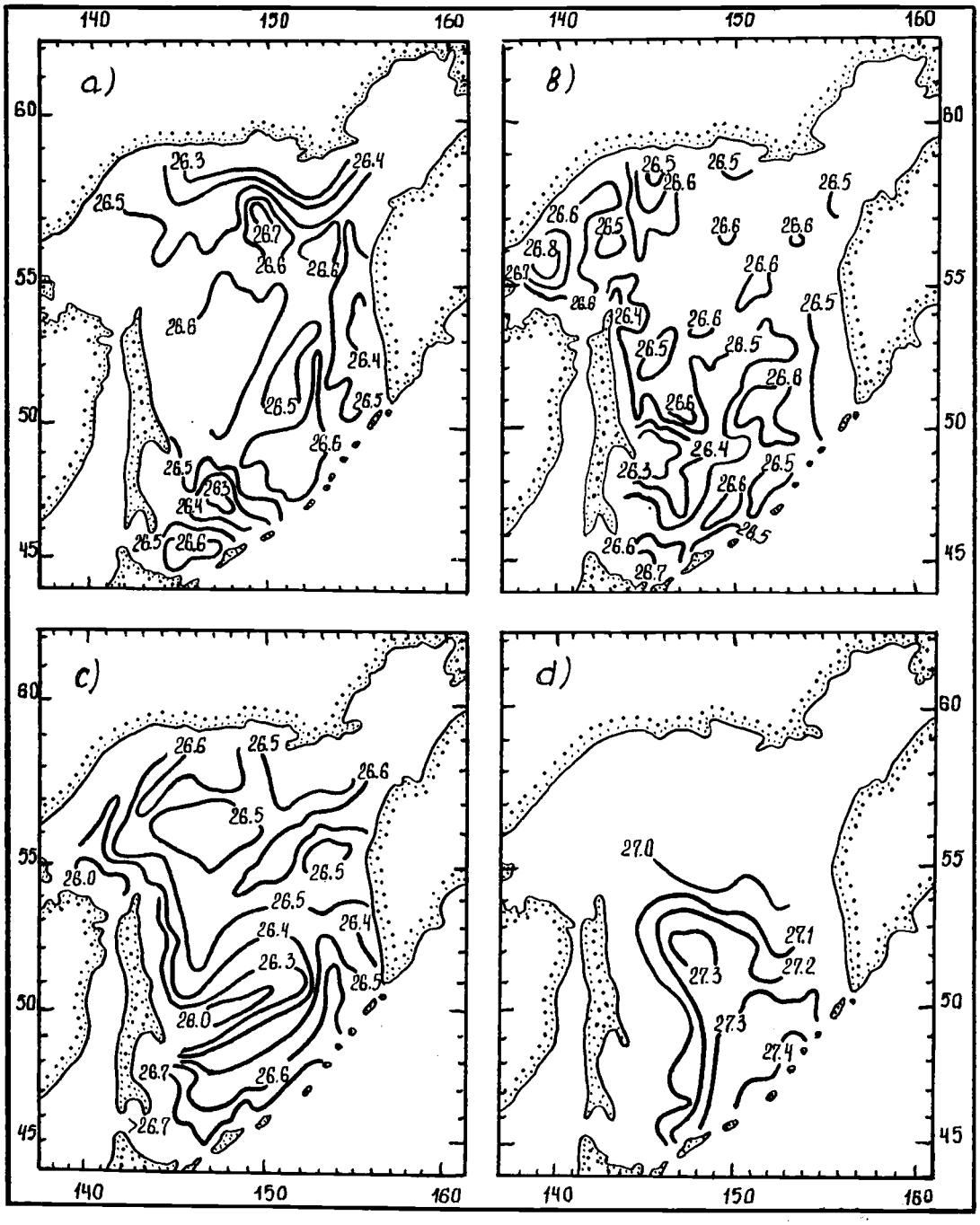

Fig. 5. Distribution of sigma-t in the cores of water masses in the Okhotsk Sea:
a, b, c - the intermediate cold water mass in spring, summer and fall respectively;
d - the deep Pacific water mass.

Numerical Experiments with Finite Element Model of the Okhotsk Sea Circulation

Andrey V. MARTYNOV, Elena N. GOLUBEVA and Victor I. KUZIN

Computing Center, Siberian Branch, Russian Academy of Sciences, Novosibirsk, Russia

INTRODUCTION

In the recent years the coastal areas and marginal seas of the World ocean attract the attention of oceanographers. This interest derives from the fact that these regions are of exceptional importance for the earth's climate and from the point of view that the overwhelming majority of nations' marine activities are performed within 200 mile Exclusive Economical Zones. This special interest did not exclude scientists working in the numerical modeling of oceanic processes. Some well known general ocean circulation models were used as regional models to investigate the circulation of the Greenland and Norwegian Seas (Legutke, 1991), the South China Sea (Shaw and Chao, 1994), the Japan Sea (Holloway et al., 1995), etc. The Okhotsk Sea is the object of the present study.

The general circulation of the Okhotsk Sea consists of a large cyclonic gyre which begins with surface and subsurface northward flow of the North Pacific water through the Kruzenshtern Strait along the Kamchatka Peninsula (the West Kamchatka current), then curves to the northern part of the Okhotsk Sea and flows south along the Sakhalin Island as the Eastern Sakhalin current. The existence of counter currents with the same names one is mentioned for both cases in some recent references (e.g., Zhigalov and Figurkin, 1994). Main features of the current system are the Oyashio inflow through the northern straits and its outflow through the central straits. The warm Soya current inflows through the Soya strait in the southern part of the Okhotsk Sea, comes along the Hokkaido Island and outflows through the Kunashiri strait (Leonov, 1960; Luchin, 1987).

The air circulation above the Okhotsk Sea has a monsoon character which is controlled by the interconnection of the main high and low pressure centers above the mainland and adjacent sea regions during winter and summer. Strong northerly geostrophic winds dominate during the winter monsoon and weak winds from the opposite direction are more typical for the summer monsoon. Investigation of the Okhotsk Sea water circulation response to the seasonal variability of the wind stress in the region is the primary goal of the present study. Analogous numerical experiments were performed by Sekine (1990). The main distinctions of that study from the above mentioned work are connected with some differences in the model formulation. We used different bottom topography as well as wind stress data.

The 3-D ocean general circulation model of the Novosibirsk Computing Center (1986) is adapted to the Okhotsk Sea. This model was earlier applied for the Kuroshio region (Kuzin et al., 1992). The bottom topography used in the model is presented in Fig. 1. The horizontal grid size is 0.25°. The study region covered the entire Okhotsk Sea with the exception of the shelf region with depths less than 30 m.

WIND STRESS DATA

Wind stress is one of the major factors determining the strength of the surface currents. The model was forced using both the monthly climatological wind stress data of Wright (1988) and the seasonal wind stress data prepared based on the same source. These data are sparse and their coverage implies some uncertainty, nevertheless, they were used to increase the wind stress influence because of their higher values in comparison with the analogous data of Hellerman and Rosenstein (1983)(HR):

Source of wind stress data	WINTER		SPRING		SUMMER		AUTUMN	
	Vmax	Vmean	Vmax	Vmean	Vmax	Vmean	Vmax	Vmean
HR, 1983	1.76	1.23	0.38	0.18	0.32	0.18	1.29	0.90
Wright, 1988	2.63	0.92	1.30	0.41	1.32	0.75	2.91	1.65

* All values are in dyne/cm^2.

Numerical experiments were carried out for selected seasons and 12 months separately. The definition of seasons has no rigid "calendar" in this region where the first sea ice forms in November and covers up to 97% of the sea surface in March-April (Wakatsuchi and Martin, 1990). So, the winter period can continue in the Okhotsk Sea for 5-6 months.

The following approach was applied to select the seasonal wind stresses: winter and summer fields were estimated by averaging the monthly mean data of December, January, February, and June, July, August, respectively; spring and autumn fields were estimated by averaging the monthly mean data of April and May, and October and November, respectively. The selected averaging periods were used in order to correctly consider the impact of winds. According to the available wind stress data the winter monsoon begins in October and relatively stable strong northern and western winds are conserved during October and November (Fig. 2d). With the development of a high-pressure center over Siberia a wind stress field is reconstructed and northern winds prevail. The sea ice cover initially forms in northern bays and along the continental shelf. The position of the sea ice edge spreads southward under the influence of cold air coming from the north and due to transportation by the northerly wind. This wind is rather stable for three months but its influence on water circulation is less remarkable compared to the autumn because of the gradual decrease in the open water zone (Fig. 2a). The maximum area of ice is observed in March when transformation of the wind stress field to the summer monsoon begins and the western winds prevail. The influence of the sea ice cover is essentially during the whole spring season including May (Fig. 2b). To specify this influence in numerical experiments, no wind stress was imposed above the ice covered regions for both winter and spring. The mean location of the ice edge was defined from the Pacific Ocean Atlas (1974). A relatively stable southern wind is dominant during June, July and August (Fig. 2c). Mean and maximum (Fig. 2) estimates of the wind stress show that wind strength is higher in the autumn and winter periods, and it is weaker in spring and summer.

GENERAL DESCRIPTION OF THE MODEL

The governing equations of the model are primitive, written for the sphere of radius a in spherical coordinates (λ, θ, z) (z is directed from the surface to the bottom):

$$\frac{du}{dt} - (f-\gamma)v = -\frac{m}{\rho_0}\frac{\partial p}{\partial \lambda} + \frac{\partial}{\partial z}(k\frac{\partial u}{\partial z}) + F^{\lambda},$$

$$\frac{dv}{dt} + (f-\gamma)u = -\frac{n}{\rho_0}\frac{\partial p}{\partial \theta} + \frac{\partial}{\partial z}(k\frac{\partial v}{\partial z}) + F^{\theta},$$

$$\frac{\partial p}{\partial z} = g\rho,$$

$$m\left(\frac{\partial u}{\partial \lambda} + \frac{\partial}{\partial \theta}(v\frac{n}{m})\right) + \frac{\partial w}{\partial z} = 0,$$

$$\frac{dT}{dt} = \frac{\partial}{\partial z}(k_T\frac{\partial T}{\partial z}) + F^{T},$$

$$\frac{dS}{dt} = \frac{\partial}{\partial z}(k_S\frac{\partial S}{\partial z}) + F^{S},$$

$$\rho = r(T,S).$$

Initial and boundary conditions are:

t = 0: $\quad u = u^0, \quad v = v^0, \quad T = T^0, \quad S = S^0;$

at the ocean surface $z = 0$:

$$T = T_0, \quad S = S_0, \quad -\rho k\frac{\partial \vec{U}}{\partial z} = \vec{\tau}, \quad w = 0;$$

at the ocean bottom $z = H(\lambda,\theta)$:

$$\frac{\partial T}{\partial z} = \frac{\partial S}{\partial z} = 0, \quad k\frac{\partial \vec{U}}{\partial z} = -R_H\bar{\vec{U}}, \quad w = mu\frac{\partial H}{\partial \lambda} + nv\frac{\partial H}{\partial \theta};$$

at the solid boundary (all passages are closed in the current version of the model):

$$\frac{\partial T}{\partial \vec{N}} = 0, \quad \frac{\partial S}{\partial \vec{N}} = 0, \quad \vec{U}\bullet\vec{N} = 0, \quad \frac{\partial \vec{U}\cdot\vec{K}}{\partial \vec{N}} = 0;$$

where $\vec{N}$ and $\vec{K}$ are normal and tangential unit vectors to the surface G, respectively.

$$\vec{U}=(u,v), \qquad H\bar{\vec{U}} = \int_0^H \vec{U}dz,$$

The following notations are used in the above equations: t - time, H- depth; u,v,w - the velocity components by λ,θ and z, respectively; $n = 1/a$, $m = 1/(a\cdot\sin\theta)$, a - radius of the earth, $f = -2\omega\cos\theta$, $\gamma = m\cos\theta$, ω - angular velocity of the earth rotation, p - pressure, ρ - density deviation from the mean ρ_0 = const, R_H - drag coefficient; k,μ- coefficients of horizontal viscosity and turbulent diffusion, respectively, $\vec{\tau}$ -wind stress vector, $r(T,S)$ is a sea water function, T-

temperature, S - salinity, F^{λ} and F^{θ} - are the forms parameterizing subgrid turbulent momentum exchange:

$$F^{T,S} = m\left(\frac{\partial}{\partial\lambda}[\mu m\frac{\partial(T,S)}{\partial\lambda}]+\frac{\partial}{\partial\theta}[\mu\frac{n^2}{m}\frac{\partial(T,S)}{\partial\theta}]\right).$$

In system (1) the common notation is used for the time derivative:

$$\frac{d}{dt}=\frac{\partial}{\partial t}+mu\frac{\partial}{\partial\lambda}+nv\frac{\partial}{\partial\theta}+w\frac{\partial}{\partial z}.$$

The governing equations of the model were transformed by separations of the external and internal modes. Equations for the external mode were reduced by the rotor operation to the vorticity equation. This equation in terms of the stream function ψ was solved as a separate 2-D model during barotropic experiments.

$$(\frac{\partial}{\partial t}+R)m\Delta_{\mathrm{H}}\psi - rot((\zeta+f/\mathrm{H})\Delta\psi) = \mu(\Delta\mathrm{H}\zeta+2n^2\mathrm{H}\zeta)+F,$$

in which H is the depth of the sea and F is the wind stress source.

NUMERICAL EXPERIMENTS WITH BAROTROPIC MODEL

The simulation of seasonal situations for the general water circulation clearly shows the presence of cyclonic circulation in autumn (Fig. 3d) which corresponds the most known references listed in PICES report No.2 (1995). Simultaneously, the anticyclonic gyre is formed within the Kuril Basin. The cyclonic circulation is also revealed in winter, but only at the central part of the Sea (Fig. 3a). At the same time, two anticyclonic gyres appear to the north and south of the cyclonic one. Spring and summer distribution of the stream function (Fig. 3b and c) is smoother and does not represent the analogous large-scale formations with the exception of the small cyclonic gyre west off Kamchatka and anticyclonic circulation in the southern part of the Okhotsk Sea during the summer season.

The results of numerical experiments for 12 monthly mean wind stress fields (not presented in figures) suggest that the cyclonic circulation is formed under the influence of steady northern and north-western winds as a main feature of the Okhotsk Sea from October till April. This circulation is replaced by the anticyclonic one from April till September, but its intensity is several times weaker. The Eastern Sakhalin current is expressed best of all in December.

Some other characteristic quasi-stationary features were obtained in the northwestern part of the Okhotsk Sea, west off the Kamchatka Peninsula and north off Hokkaido. In particular, the last two circulations are very important because of their significant influence on the strength of the West Kamchatka and the Soya Currents. The change in rotation is observed during the annual cycle for both cases. The first medium scale circulation is formed near the entrance to Shelikhov Bay. There is the cyclonic eddy at this location which enhances the West Kamchatka Current for June, July and August. The anticyclonic rotation is typical for an eddy situated at the same location from December till May. As a result the intensification of the counter current with the opposite direction (from north to south) is observed west of Kamchatka. In the southern part of the Okhotsk Sea the cyclonic eddy induces the enhancement of the warm Soya current from November till March. The existence of similar cyclonic eddies north off Hokkaido coast has been reported on the basis of the radar imagery data collected during 1969-1988 (Wakatsuchi and Ohshima, 1990). The anticyclonic eddy occurring near the same

location promotes the weakening of the Soya current and decreases the intensity of the western boundary circulation during the period from April till October.

NUMERICAL EXPERIMENTS WITH 3-D MODEL

At the next stage of the study the density stratification was included in the model which has 21 vertical levels. Shelihova Bay was excluded from the domain as temperature/salinity data for this region are not available. The climatological temperature and salinity distributions for summer were used in the initial conditions. These data were prepared on the basis of all observations accessible at the Far Eastern Regional Hydrometeorological Institute, Vladivostok, Russia (V. Luchin, personal communication). The model was spun up by the summer wind stress field prepared on the basis of the monthly mean stresses of Wright (1988). At the diagnostic stage the numerical integration was made with a 15 minute time step. According to the control of the total kinetic energy the equilibrium state was attained after 20 days of model time. The adaptation calculations with the whole system of equations were carried out for another 30 days. Some preliminary results are presented below.

The Ekman drift dominates the flow in the upper layer from the surface to about 30 m. There is no obvious cyclonic circulation on the whole. Although the structure of currents is very complex, some main features of the Okhotsk Sea general circulation are revealed. The north periphery of the anticyclonic gyre above the Kuril Basin is well-developed but the gyre is divided into several cyclonic and anticyclonic eddies. The Eastern Sakhalin current begins to appear below 50 m, it spreads southward to about 50°N, the West Kamchatka current flows north of about 55°N, and strong anticyclonic eddy extends from the upper layers to the bottom near the Kashevarov Bank north of Sakhalin Island. An intense stream in the southern part of the Okhotsk Sea is artificial. The appearance of this simulated stream is connected, probably, with extrapolation of initial data to the southern part of the domain and can not be recognized as the Soya Current directly. Also the formation of two eddies, exactly in the central part of the Sea, is induced by data discrepancy in this region (initial temperature/salinity fields did not smooth to test the model sensitivity for different instabilities).

DISCUSSION

The obvious dependence of the general Okhotsk Sea water circulation on the wind stress field is considered in the present investigation. The reconstruction of atmospheric conditions from the winter monsoon to the summer monsoon induces the essential changes of the whole current system in the region. But this alteration embraces only thin the upper 20-30 meters layer. Some characteristic features of the general circulation and its variability in the annual cycle are obtained in this layer during numerical experiments with the barotropic model. At the second stage of our research some interesting features of the vertical structure of the Okhotsk Sea current system are simulated. For example, the Eastern Sakhalin current is well-developed in the subsurface layer (50-200 m). This current can transport the water generated in the northern part of the Okhotsk Sea far to the south.

Preliminary presentation of in-flow and out-flow through the passages is proposed at the next stage of this study. Winter observations are very sparse even in the open water regions, but during future experiments we hope to prepare some climatic winter fields for comparison with the summer season.

ACKNOWLEDGMENTS

This study was started during Dr. A. Martynov's stay as a visiting scientist at the Institute of Ocean Sciences (Sidney, B.C., Canada). We appreciate the continuous support by Dr. Falconer Henry, Dr. Eddy Carmack and Dr. Mike Foreman. This work was partly supported by grant 93-05-8993 of the Russian Foundation for Basic Research.

REFERENCES

Hellerman, S., and M. Rosenstein. 1983. Normal monthly wind stress over the World ocean with error estimates. J. Phys. Oceanogr. 13:1093-1104.

Holloway, G., T. Sou, and M. Eby. 1995. Dynamics of circulation of the Japan Sea. J. Mar. Res. 53:539-569.

Kuzin, V.I., and E.N. Golubeva. 1986. Numerical modelling of the temperature and currents in the World ocean using finite element method, p. 137-150. *In* Numerical modelling of the World ocean climate. Computer Center Press. Novosibirsk. (in Russian).

Kuzin, V.I., E.N. Golubeva, and A.V. Martynov. 1992. Model of Kuroshio region circulation. Proc. of the Int. Symp. PORSEC-92, Okinawa, Japan. p.1281-1287.

Legutke, S. 1991. A numerical investigation of the circulation in the Greenland and Norwegian seas. J. Phys. Oceanogr. 21:118-148.

Leonov, A.K. 1960. The Sea of Okhotsk, NTIS AD 639 585. Natl. Tech. Inf., Spring-field, Va. 95 p.

Luchin, V.A.. 1987. Water circulation in the Okhotsk Sea and some features of its interannual variability on the base of the diagnostic calculations, in Oceanographic problems of the Far Eastern Seas. 36:3-13 (in Russian).

Pacific Ocean. 1974. Atlas of oceans.

Sekine, Y. 1990. A barotropic numerical model for the wind-driven circulation in the Okhotsk Sea. Bull. Fac. Bioresources, Mie Univ. 3:25-39.

Shaw, P.-T., and S.-Y. Chao. 1994. Surface circulation in the South China Sea. Deep-Sea Res. I. 41:1663-1683.

Talley L.D., and Y. Nagata [ed.] 1995. The Okhotsk Sea and Oyashio Region. PICES Scientific Rep. No. 2. 227 p.

Wakatsuchi, M., and S. Martin. 1990. Satellite observation of the ice cover of the Kuril Basin region of the Okhotsk Sea and its relation to the regional oceanography. J. Geophys. Res. 95(C8):13393-13410.

Wakatsuchi, M., and K.I. Ohshima. 1990. Observations of Ice-Ocean Eddy Streets in the Sea of Okhotsk off the Hokkaido coast using radar images. J. Phys. Oceanogr. 20:585-594.

Wright, P. 1988. An Atlas based on the 'COADS' data set: Fields of mean wind, cloudiness and humidity at the surface of the global ocean. Max-Plank-Institute for Meteorology/ Hamburg, Report 14.

Zhigalov, I.A., and A.L. Figurkin. 1994. Interannual variability of water dynamics in the Okhotsk Sea, p.75. Abstracts of the Third Annual Meeting of PICES in Nemuro, Japan.

FIGURES

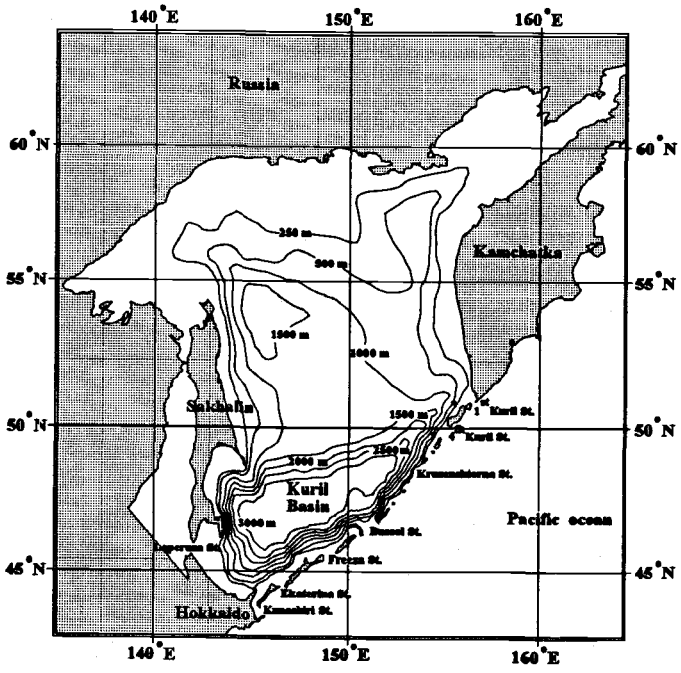

Fig. 1. A map of the Okhotsk Sea with bottom topography contours (in meters).

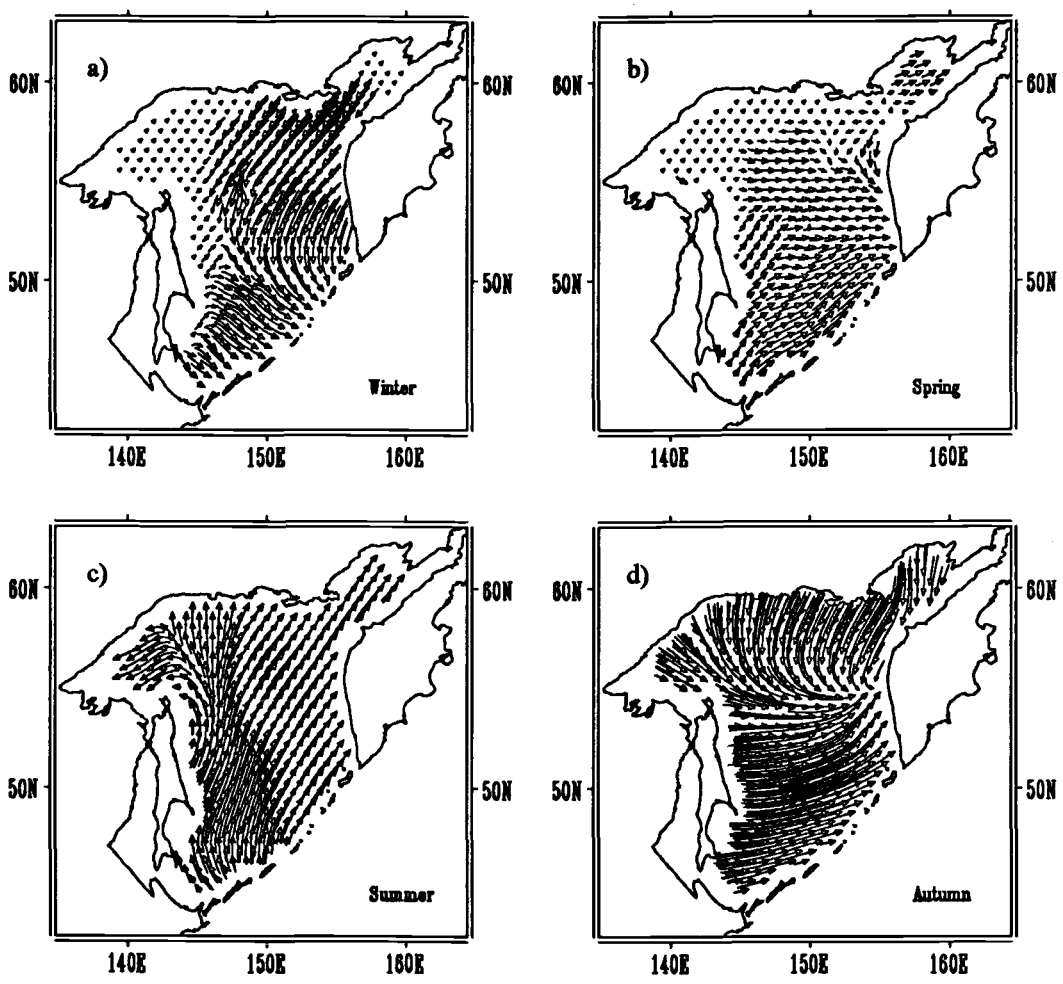

Fig. 2. Wind stress fields for: winter (a), spring (b), summer (c) and autumn (d).

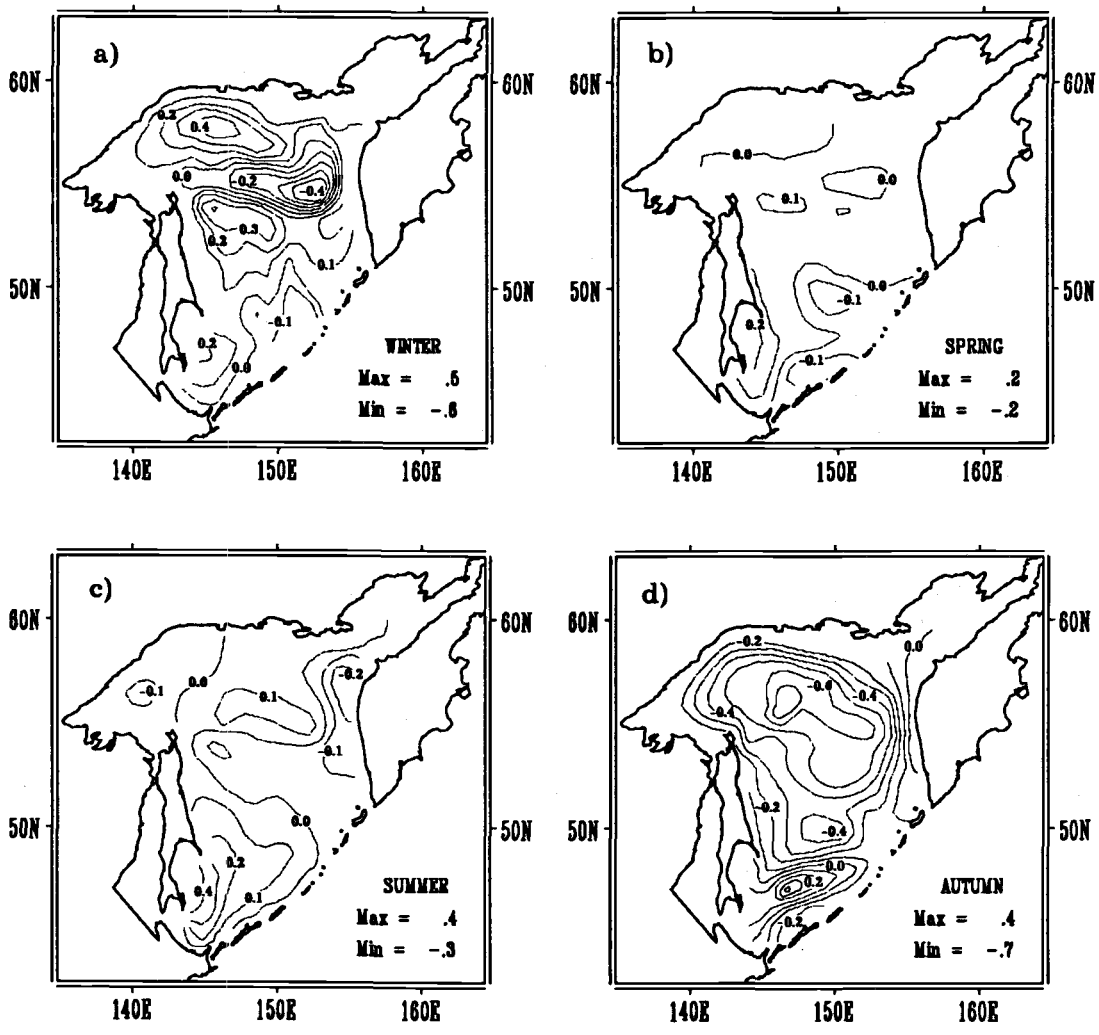

Fig. 3. Volume transport streamlines for winter (a), spring (b), summer (c) and autumn (d) Contour interval is 0.1 Sv (Sv: Sverdrup = $10^6 m^3 s^{-1}$). Real bottom topography.

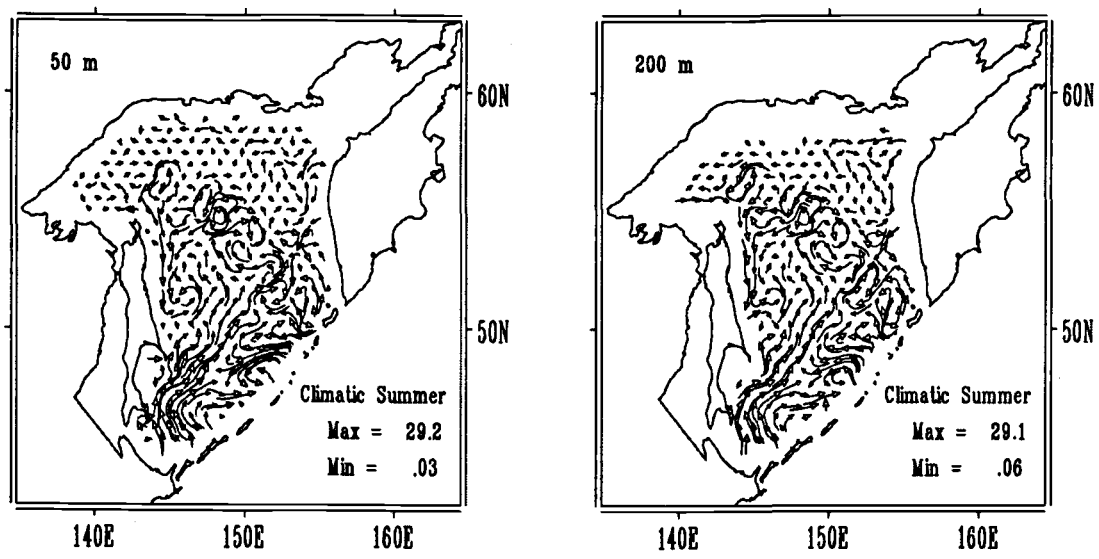

Fig. 4. Current velocity fields at 50 and 200 m after the adaptation. Real bottom topography.

Structure of Intermediate Water Layer in the Northwest Pacific

Nikolay A. MAXIMENKO, Anatoly I. KHARLAMOV and Raissa I. GOUSKINA

Institute of Oceanology, Russian Academy of Sciences, Moscow, Russia

Data collected during Japanese surveys in the northwestern Pacific (Fig. 1) were used to investigate the spatial structure and seasonal variability of the North Pacific Intermediate Water (NPIW) (Talley, 1993). The corresponding information for about 1,300 hydrographic stations in the area contoured by 30-50°N and 140-155°E was published in "The Results of Marine Meteorological and Oceanographic Observations" in 1970-80's. We revealed that although the depth of the salinity minimum and water properties at that depth express significant temporal variations (connected, probably, with eddies activity) their spatial structure is quite stable. The NPIW layer outcrops around 40-42°N where salinity, temperature, potential density and oxygen content are equal to 33.3 psu, 5°C, 26.5 sigma theta and 6.9 ml/l, respectively.

Two principal results were obtained from the general analysis of these data:

1. Spatial variability along the latitude of 41°N did not exceed the accuracy of measurements as well as no reliable difference has been found between sections along 144°E, 148°E and 150°E.
2. Seasonal variability beneath the depth of 100 m was not identified (it was also below the data accuracy).

In the meridional direction the NPIW layer deepens southward to a depth of 800 m at 30°N where the salinity, temperature and potential density reach 34.1 psu, 6.2°C and 26.95 sigma-theta, respectively, but concentration of dissolved oxygen drops to 3.0 ml/l. Typical standard deviations of those parameters are equal to 30 m, 0.03psu, 0.2°C, 0.03 sigma-theta and 0.3 ml/l. Thus, within the NPIW all characteristics are variable and, hence, the layer cannot be traced by any fixed iso-surface (e.g., isohaline or isopycnal). The only distinct tracer of the NPIW is a salinity minimum at an intermediate depth.

The following features of the NPIW layer structure have been determined from the detailed analysis of data along 155°E between 45°N and the equator (Fig. 1):

a) The NPIW outcrops again at 7-8°N around the Subtropical Front (Fig. 2a);
b) At the southern edge of the NPIW layer salinity and temperature increase (Figs. 2b and c), whereas the content of dissolved oxygen and potential density (Figs. 2d and e) decrease southward;
c) Curvatures of vertical salinity (Fig. 2f) and temperature (Fig. 2g) profiles are positive everywhere and express the highest values at the southern and northern edges of the NPIW layer, while the curvature of the dissolved oxygen profile (Fig. 2h) is much noisier and at any latitude it has readings of both signs.

These data were also used to investigate kinematic and dynamic properties of the NPIW layer. Important for our consideration is the fact that the stationary solution of the diffusion equation for salinity may not contain internal extremes without intrusions of "new" water from the boundaries. Since the salinity vertical profile has a minimum in the middle of the layer, the value of this minimum grows towards the equator and the curvature is positive everywhere, we anticipate southward water flow along 155°E.

Mathematically this can be expressed in the following way. Using the above conclusions 1 and 2 (stationary and weak spatial variability of the NPIW layer structure), full equations of salinity, temperature and dissolved oxygen evolution may be presented as

$$V \times S_Y = k_S \times S_{ZZ} \,, \tag{1}$$

$$V \times T_Y = k_T \times T_{ZZ} \,, \tag{2}$$

$$V \times O_Y = k_O \times O_{ZZ} - q, \tag{3}$$

where y- and z-axis are parallel and normal, respectively, to the NPIW layer (traced as a salinity minimum), V is velocity component along y-axis, k_i is corresponding diffusion coefficient, expected to be positive (below we will suggest that effective mixing processes in the NPIW are governed by turbulence and all the k-coefficients are of the same magnitude), q is dissolved oxygen dissipation rate due to biological and chemical processes (also expected to be positive). Thus (1-3) may be rewritten as

$$V / k = S_{ZZ} / S_Y = T_{ZZ} / T_Y = O_{ZZ} / O_Y - q / O_Y \tag{4}$$

and the two last equations of (4) may be checked from the data. A good correspondence between S_{ZZ} / S_Y and T_{ZZ} / T_y and significant difference between S_{ZZ} / S_Y and O_{ZZ} / O_Y were revealed (Fig. 3), that can be explained by a large positive q. Roughly Fig. 3 provides an estimate for meridional velocities

$$V \approx -1 cm^{-1} \times k \tag{5}$$

that gives 1 cm/s for typical value of $k =$ 1 cm^2/s and should be directed everywhere towards the equator.

Thus, we may conclude that the source of a "new" NPIW is located at the southern edge of the layer. The NPIW has a tendency to shift equatorward and must outcrop and "die" at the Subtropical Front. This event was observed by Bingham and Lukas (1994), but the mechanism is not clear yet. Of course, meridional motion should be superimposed on the general large-scale circulation in the North Pacific, however some results suggest that this effect is not so strong (Kilmatov and Kuzmin, 1991).

Our attempts to investigate physical mechanisms of the NPIW formation and dynamics (Maximenko et al., 1995) revealed that the local geostrophic balance can be disturbed by vertical (diapycnal) mixing that in the case of tilted isopycnals will push water particles quasi-isopycnally up or down towards a new geostrophic equilibrium. From traditional 2D dynamic equations we can derive for meridional velocity

$$V = -g \times \tan\Theta \times \rho_t / (\rho_o \times f^2) \tag{6}$$

where g is the gravitational constant, Θ is tilt of isopycnals, f is the Coriolis parameter, ρ_o is seawater density and ρ_t is evolution rate in time. Depending on sign of ρ_t water should sink or rise, what we really observe in the NPIW layer.

Values of ρ_t for the section along 155°E (calculated as a local evolution of ρ_o due to vertical mixing of temperature and salinity) were found to be in good correlation with Figs. 2a and 2e: ρ_t has the same sign as the tilt of isopycnals. Again if k is estimated as 1cm^2/s, V is equal about 1 cm/s and is directed towards the equator.

Quite unexpected results have been obtained from our investigation of the cabbeling effect on NPIW dynamics. We developed an original formal mathematical description of cabbeling rate that for the salinity minimum layer can be written as

$$\rho_t^{cabb} = -\rho_{TT}(T_z)^2 \quad (7)$$

We found that the cabbeling effect is significant everywhere in the NPIW layer and its contribution to local density evolution reaches 30%. That means that analysis of the NPIW should be based on the exact nonlinear equation of state.

ACKNOWLEDGMENTS

This study was supported by grant NDY000 of the International Science Foundation, grant 95-05-14907 of the Russian Foundation for Basic Research, grant NDY300 of the International Science Foundation and the Russian Government, and is a part of the International Research Project "Drifter Investigation of the North-Western Pacific Surface Circulation" supported by the Ministry of Science of the Russian Federation.

REFERENCES

Bingham, F., and R. Lukas. 1994. The southward intrusion of North Pacific Intermediate Water along the Mindanao coast. J.Phys.Oceanogr. 24:141-154.

Kilmatov, T.R., and V.A. Kuzmin. 1991. Cabbeling effect under mixing of seawaters and its seasonal appearance at the North Pacific Subarctic Front. Izvestia Acad. Sciences of USSR (Physics of Atmosphere and Ocean). 27:883-887 (in Russian).

Maximenko, N.A., T. Yamagata, and K. Okuda. 1995. Frontal convection in the Kuroshio and Subarctic Front. Oceanologia. (in Russian, accepted).

Talley, L.D. 1993. Distribution and formation of North Pacific Intermediate Water. J. Phys. Oceanogr. 23:517-537.

FIGURES

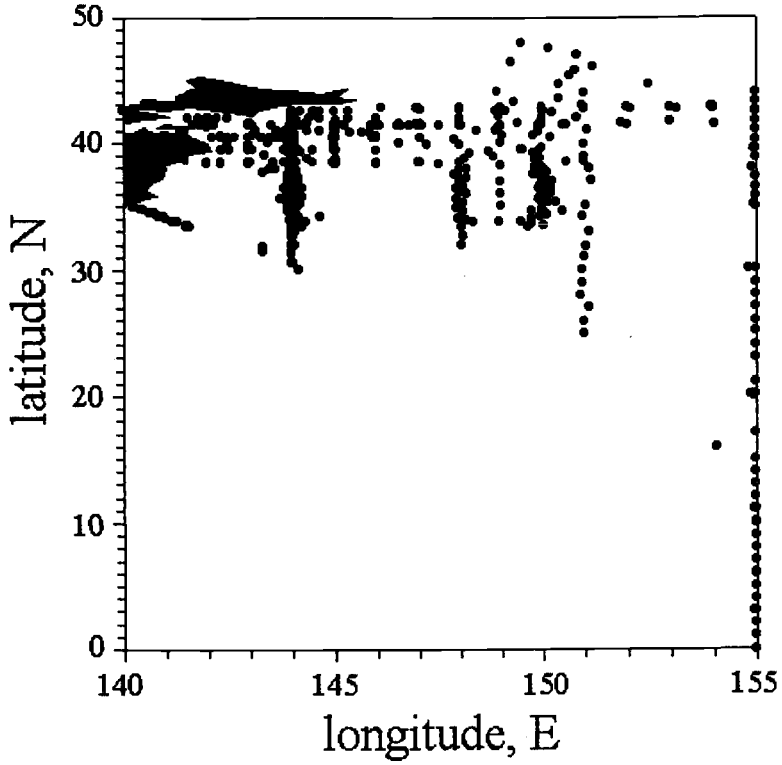

Fig. 1. Location of hydrographic stations used for analysis.

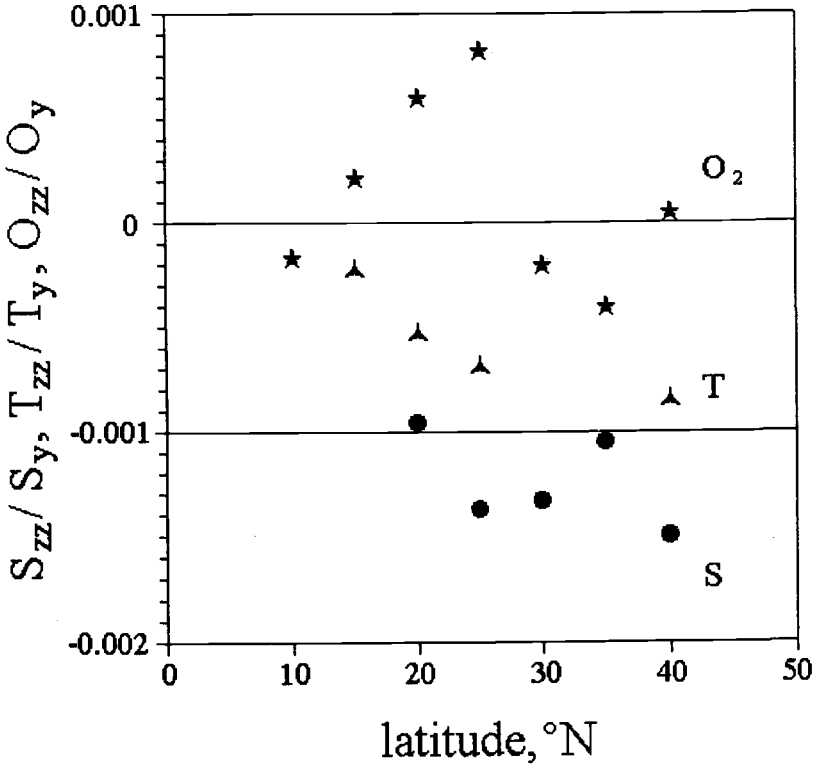

Fig. 3. Meridional distribution of S_{zz}/S_y, T_{zz}/T_y and O_{zz}/O_y calculated from hydrographic data along 155° E.

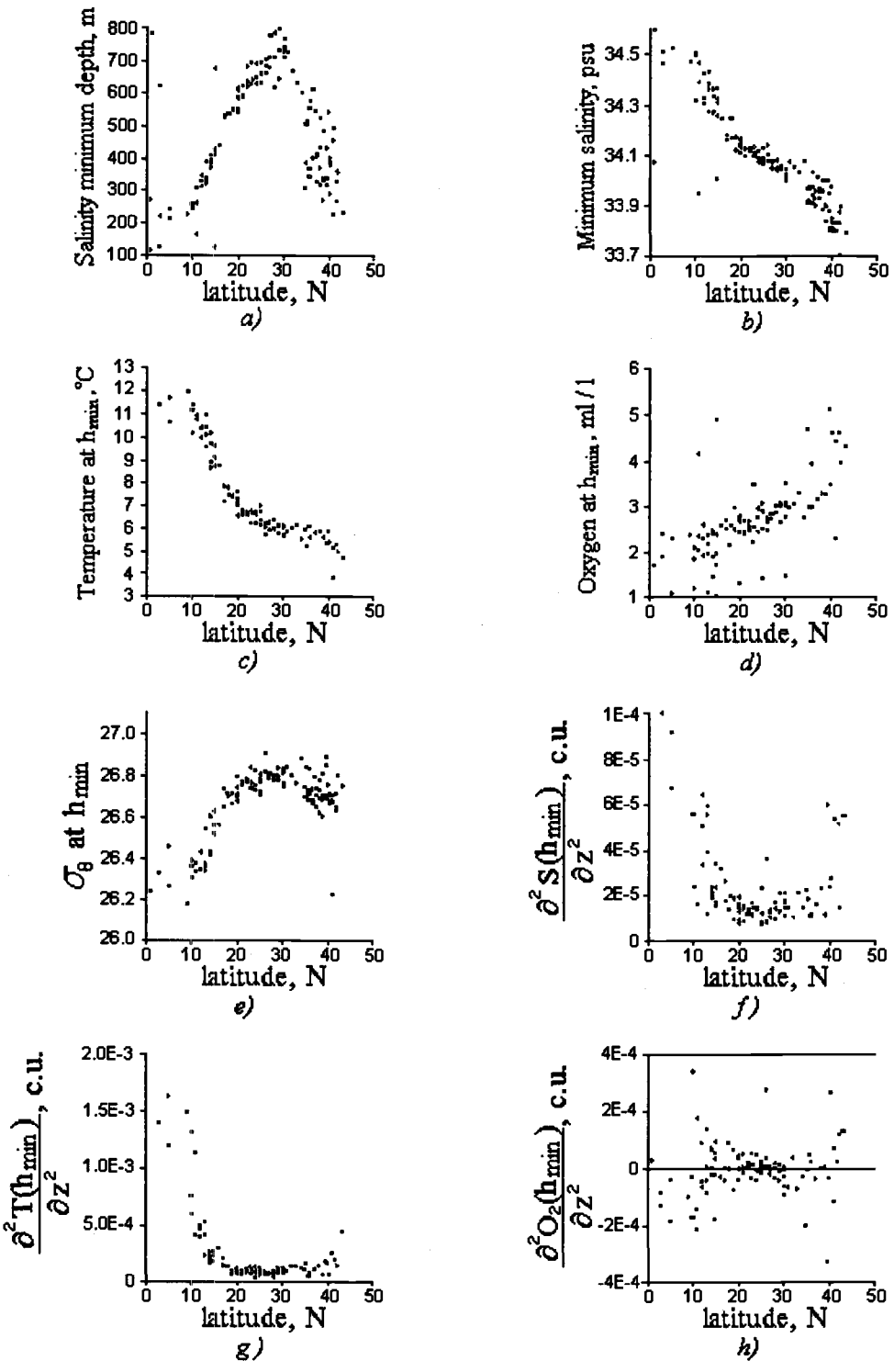

Fig. 2. Distribution of the depth of salinity minimum in the NPIW layer (a), minimum salinity (b), and temperature (c), dissolved oxygen content (d), potential density (e) and corresponding second vertical derivatives (f - h) at the depth of salinity minimum along 155°E .

Fine-structure of the North Pacific Intermediate Water Layer

Nikolay A. MAXIMENKO and Andrey Yu. SHCHERBINA

Institute of Oceanology, Russian Academy of Sciences, Moscow, Russia

INTRODUCTION

The North Pacific Intermediate Water (NPIW), characterized by an obvious salinity minimum and slight increase of dissolved oxygen concentration, is observed within the latitude range 10-40°N (Yang and Nagata, 1992). This layer outcrops at its border contouring the area of the Subtropical water mass distribution. In the north the NPIW is limited by the Subarctic Front (SF). The concept of the NPIW formation by waters of the Okhotsk and Japanese Seas (Yang and Nagata, 1992) coexists with the hypothesis of its role as an interface between the Subtropical and Subarctic water masses (Burkov, 1972). The search for a possible physical processes governing the NPIW formation and evolution is under way.

Role of cabbeling in the frontal zone has been investigated by Kilmatov and Kuzmin (1991). In accordance with Talley (1993), at a narrow front cabbeling breaks the pre-existing geostrophic equilibrium and forces the layer to slip down isopycnically to recover the balance. The proposed mechanism is expected to be the most efficient in the upper ocean at sharp fronts. Data collected from the section along 155°E demonstrated that the dynamics of the NPIW layer in the central and southern parts is determined by the diapycnal (vertical) heat and salt mixing and resulted in an equatorward drift of the layer, superimposed on a subtropic gyre (Maximenko et al., 1995).

DATA

We analyzed numerous CTD data of the "Megapolygon" experiment conducted in the summer-fall period of 1987 in the 500 x 500 km area centered at 40°N and 155°E (Ivanov, 1992). To decrease the effect of the probe calibration, as well as to exclude mesoscale variability of various fields, our primary attention was paid to long longitudinal sections carried out by the same vessel. The section along 152°E, carried out by *R/V "Vityaz"* in October 1987 with 20 miles resolution, is a good example and is discussed below.

RESULTS AND CONCLUSIONS

At least three sub-mesoscale objects are disclosed within the NPIW layer which is clearly seen as a salinity minimum (Fig. 1). These objects are characterized by negative salinity and temperature anomalies of 0.1 psu and 0.6°C, respectively. The horizontal (in the meridian direction) diameter of the anomalies does not exceed 40 miles occupying depths of 200-400 m. Analysis of vertical profiles of 1 m resolution revealed well developed fine-structure inside the mesoscale anomalies mentioned above. Temperature and salinity pulsations are as much as 5-10 times higher than in surrounding waters (Fig. 1). Vertical profiles of water properties at one specific station are shown in Fig. 2. Note, that pulsations of T and S, reaching 0.1 psu and 0.6°C, respectively, do not influence the stability of

stratification, which can be explained by their good inter-correlation (Fig. 3). The vertical scale of the pulsations varies from 1 to 60 meters.

We have discovered that in the horizontal plane the anomalies look like isolated intra-thermocline lenses. Within the "Megapolygon" area we observed simultaneously 3 to 5 such lenses associated with negative temperature and salinity anomalies, each being 40 miles or less in diameter. The actual number of the anomalies could be even greater as not all of them were resolved by the sampling grid. The typical scale of horizontal coherence of T and S pulsations was close to the distance between the stations (20 miles).

Fig. 4 displays the Cox numbers (< > sign shows averaging over the 200 m layer centered at the salinity minimum depth) calculated along the Section as

$$C_T = \frac{< (\nabla T')^2 >}{< \nabla T >^2}, \quad C_S = \frac{< (\nabla S')^2 >}{< \nabla S >^2} \tag{1}$$

C_T exceeds C_S by 1.4 times almost everywhere in the NPIW. Assuming that molecular diffusion plays the leading role at the finest resolved scale and that the mixing process at the larger scale is governed by developed turbulence, we can estimate the turbulent diffusion coefficients as $K_T = k_T \cdot C_T^2 = 2 \cdot 10^{-2}$ cm²/s and $K_S = k_S \cdot C_S^2 = 6 \cdot 10^{-4}$ cm²/s, where k_T and k_S are corresponding coefficients of molecular diffusion. Although this evaluation is very rough, the difference between the coefficients as well as their small values prove the pulsations to be a feature of fossil turbulence rather than of a developed one. The time of dissipation of anomalies with a vertical scale of h = 30m

$$t = h^2 / K \tag{2}$$

is equal to $5 \cdot 10^8$ s » 15 years for the temperature and $2 \cdot 10^{10}$ s » 500 years for the salinity. This means that our lenses may have a long pre-history and still preserve the footprints of the processes which formed the lenses.

Another possible source of the pulsations is the isopycnal intrusions, which are frequently observed on narrow fronts and on the periphery of mesoscale intra-thermocline lenses. Calculations of potential temperature and salinity on the surfaces of constant potential density show that corresponding isopycnal gradients are too weak to provide high values of pulsations. Moreover, water properties viewed in the lenses can be found nowhere except for the vicinity of the Subarctic Front where high mean gradients coexist with high small-scale pulsations of temperature and salinity.

Thus, from both approaches we may conclude:

- the fine-structure of the anomalies revealed contains water relevant to that observed around the SF;
- both the temperature and salinity pulsations are generated by intensive local mixing at the SF, rather than by local dynamics of the sub-mesoscale anomalies;
- those sub mesoscale anomalies represent a "new" intermediate water, which ventilates the layer.

It should be noted, that all three lenses on the section described above (Fig. 1) are located inside the large warm anticyclonic eddy, which is, apparently, a separated Kuroshio meander shifted about 300 km north from the Kuroshio Extension. Such an eddy can create a local narrow high-contrast front essential for effective mixing and cabbeling.

ACKNOWLEDGMENTS

This study was supported by grant NDY000 of the International Science Foundation, grant 95-05-14907 of the Russian Foundation for Basic Research, grant NDY300 of the ISF and the Russian Government, and is a part of the International Research Project "Drifter Investigation of the North-Western Pacific Surface Circulation" supported by the Ministry of Science of the Russian Federation.

REFERENCES

Burkov, V.A. 1972. General circulation of the Pacific ocean waters. Moscow, Nauka. 195 p. (in Russian).

Ivanov, Yu. A. [ed.] 1992. Experiment "Megapolygon", Moscow, Nauka. 415 p. (in Russian).

Kilmatov, T.R., and V.A. Kuzmin. 1991. Cabbeling effect under mixing of seawaters and its seasonal appearance at the North Pacific Subarctic Front. Izvestia Acad.Sciences of USSR. Physics of atmos. and ocean. 27:883-887 .(in Russian).

Maximenko, N.A., R.I. Gouskina, A.I. Kharlamov, and A. Yu. Shcherbina. 1995. Spatial structure and dynamics of intermediate water in the North Western Pacific. Oceanologia. (in Russian, in press).

Maximenko, N.A., T. Yamagata, and K. Okuda. 1995. Frontal convection in the Kuroshio and Subarctic Front. Oceanologia. (in Russian, in press).

Talley, L.D. 1993. Distribution and formation of North Pacific intermediate water. Phys. Oceanogr. 23:517-537.

Yang, S.-K., and Y. Nagata. 1992. North Pacific Intermediate Water in the seas adjacent to Japan. Preprint.

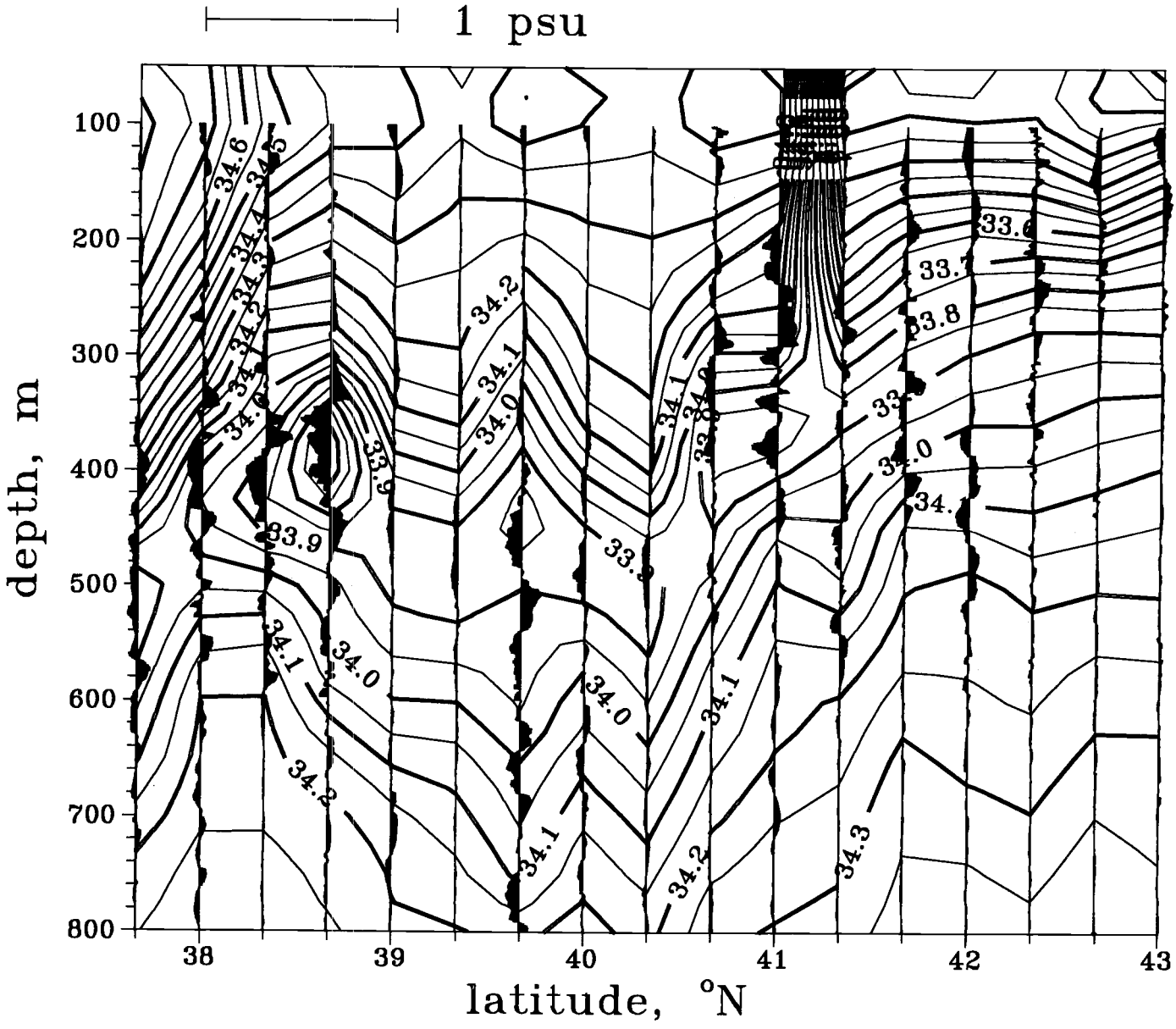

Fig. 1. Salinity distribution and vertical profiles of salinity pulsations of scale less than 100 m. along 152°E in October 1987.

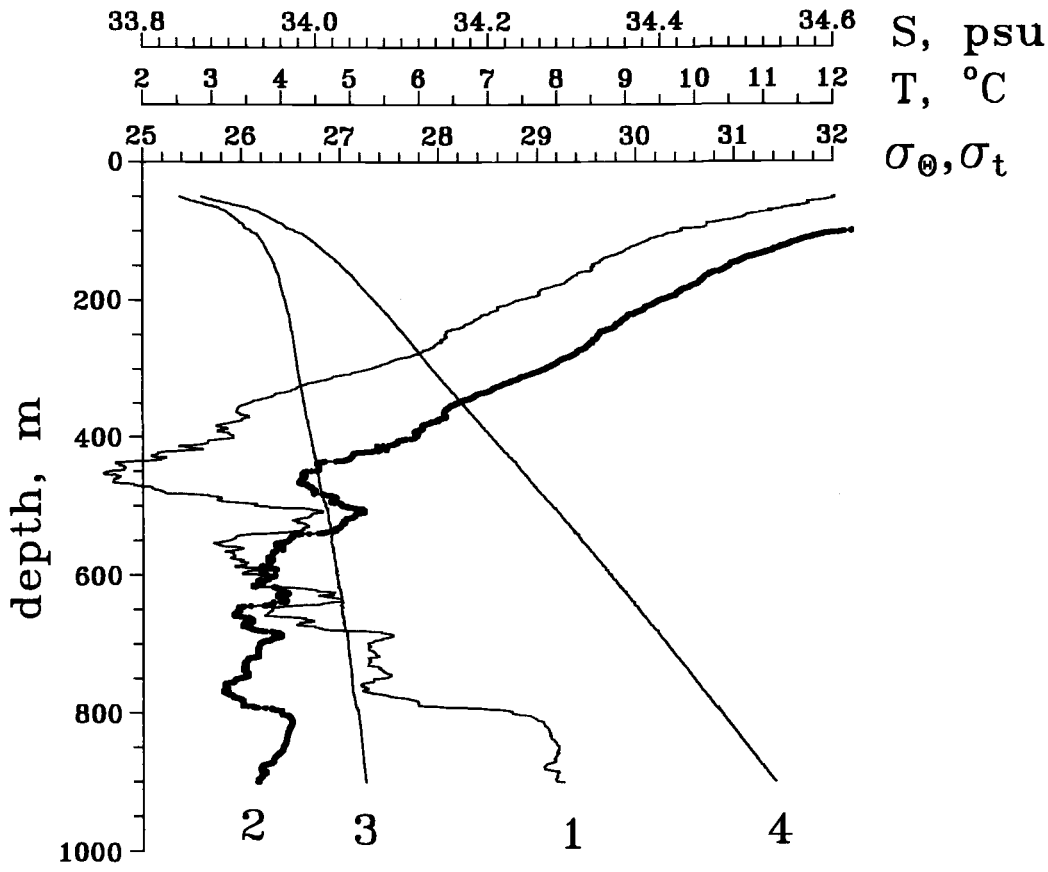

Fig. 2. Vertical profiles of (1) salinity, S; (2) temperature, T; (3) potential density, σ_θ and (4) density σ_t at 39°40'N, 152°E.

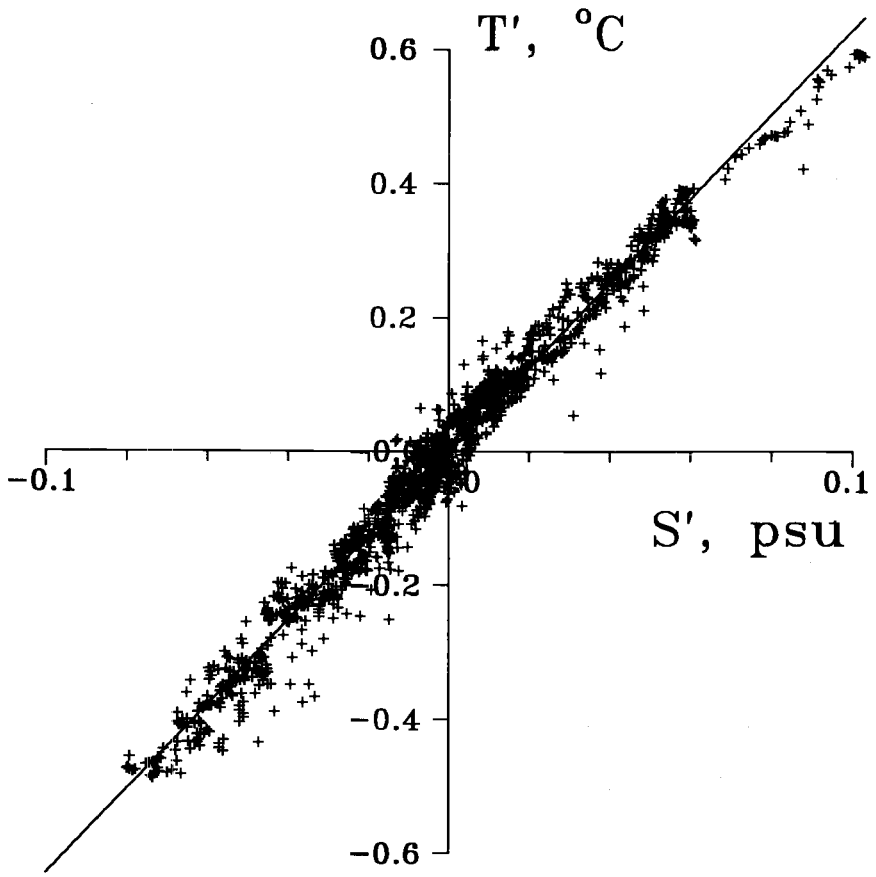

Fig. 3. Relation between T and S pulsations shown in Fig. 2.

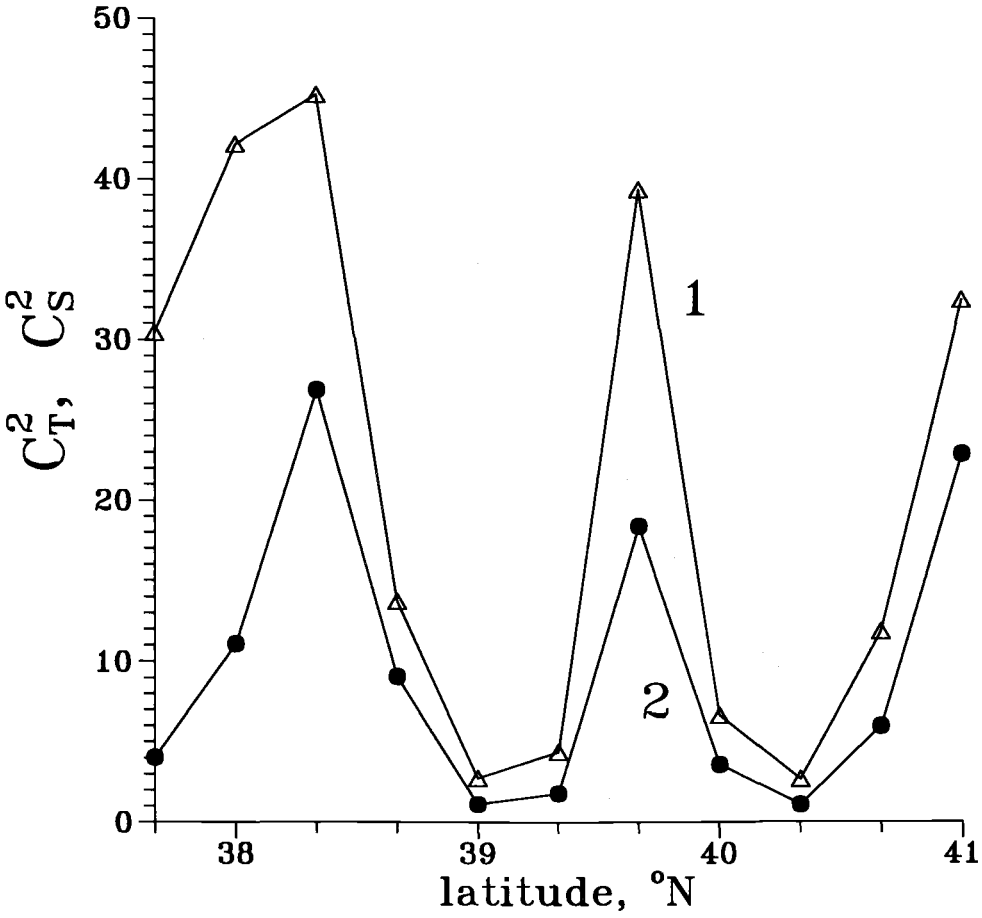

Fig. 4. Meridional distribution of Cox numbers C_T (1) and C_S (2), calculated from (1).

An Experimental Study of Water Transport through the Straits of Okhotsk Sea by Electromagnetic Method

Renat D. MEDJITOV and Boris I. REZNIKOV

Pacific Oceanological Institute, Far Eastern Branch, Russian Academy of Sciences, Vladivostok, Russia

Studies of water dynamics and transport through straits require rapid and accurate observations of water velocities over large spatial scales. Application of standard oceanographic technique is complicated due to hydrometeorological conditions of the area. Significant new information about steady and variable ocean transport can be extracted from the measurements of motion induced electric fields being made with submarine cables and towed electrode systems. Such experiments were performed in the Nevelskoy Strait with the aid of a bottom mounted electrode system that detected the horizontal electric fields at several points of the Strait. Information about lateral and temporal structure of water exchange between the Japan Sea and the Okhotsk Sea was obtained. From these results it is evident that the data were dominated by diurnal and semidiurnal tidal elements. Geomagnetic electro kinetograph (GEK) profiling of the Kuril Straits was realized using towed electrodes to demonstrate the possibilities of this method for future oceanographic investigations.

INTRODUCTION

The depth integral of horizontal water velocity (the transport) in the straits is one of the fundamental characteristics of general water circulation in the Sea. Only two conventional tools to measure barotropic currents are now available. Long-term observations of the velocity fields can be carried out directly with a set of current meters, but this method is usually costly, especially if good resolution is desired. The second method is based on calculations of the bottom pressure records.

An unconventional technology measuring the motion induced electric field is also available for direct observation of transport, but it remains almost unclaimed. This technique detects signals which arise from the motion of sea water through the Earth's magnetic field and contain information about local and regional water velocities. The method of towed electrode pairs or geomagnetic electro kinetograph (GEK) and the utilization of submarine cables are two principal examples of the electromagnetic approach to measuring sea flows. Only a few of that kind of results in straits are known at present, in particular, measurements carried out by Teramoto (1971) in the Sugaru Strait, by Larsen and Sanford (1985) in the Florida current and by Bowden, (1961) near England. This is quite an abnormal situation, since the induced electric fields can yield information on both the spatial and temporal variability of transport in real time scale by using simple, reliable and very cheap tools. This paper presents examples of electromagnetic measurements that have been made in the Straits of Okhotsk Sea.

METHOD AND INSTRUMENTS

The theory of motional electromagnetic induction in the ocean has been refined over the last few decades. In the case where temporal magnetic fluctuations can be neglected, the electric field E

and electric current density J arising from interaction of moving water with Earth's magnetic field F are related by the Ome's law for moving conducting media:

$$E = \nabla f = V \cdot F - J / s \tag{1}$$

where f is the electric potential, V is the velocity vector and s is the electric conductivity.

To define the vector velocity field V, in general case we need to accomplish the simultaneous measurements of F and J at the same points or to determine only one of these parameters and use an adequate theoretical model of induction process based of Maxwell's equations. Usually it is a rather difficult and complex problem, but in some specific situations it can be simplified. Namely, in the low frequency limit when the effect of self induction is weak, the vertical velocity may be neglected by comparison with the horizontal components. Further assuming that the ocean bottom is flat, it can be shown that in the stationary reference frame the induced horizontal electric field is related to the horizontal velocity field by (Sanford, 1971)

$$E_H = C \cdot F_Z \cdot <V_H>^* \tag{2}$$

where C is a constant, F_Z is the known local vertical component of the geomagnetic field, $<V_H>^*$ is the vertically-averaged sea water conductivity - weighted horizontal water velocity determined by

$$<V_H>^* = \frac{\int_0^H V_H(z) \cdot \sigma(z) \cdot dz}{\int_0^H \sigma(z) \cdot dz} \tag{3}$$

and H is the depth.

Due to the cross-product relationship in equations (1) - (2), the north electric field is proportional to the west component of $<V_H>^*$, and the east electric field is proportional to the north component of $<V_H>^*$.

Oceanographic interpretation of equations (2) and (3) depends on the specific effects of the scale factor C and sea water conductivity weighting in (3). The first of these values is principally a function of the local sea floor electrical conductivity structure, and is a measure of the extent to which electric currents induced in the ocean are shorted out by underlying rock. Theoretical predictions suggest that C should lie between 0.9 and 1, and observations give actual values of 0.91-0.94 (Sanford, 1971).

For many oceanic regions, i.e., such as shallow wide straits, it can be shown that the quantity, specified by equation (3) is nearly equivalent to the simple vertically-averaged horizontal water velocity, also called the transport T [m^3/sec], so the expression (2) can be reduced to the following form

$$\Delta f = F_Z \cdot T / H \tag{4}$$

From the other hand, in a reference frame attached to a water element moving at the velocity V, an observer would measure the so-called apparent electric field E_A

$$E_A = J / s = B_Z \cdot (V_H - <V_H>^*) = k \cdot F_Z \cdot V_H \tag{5}$$

where V_H is the local velocity at the depth of measurement, and "k-factor" is an empirical parameter defined as

$$k = |V_H| / |V_H - \langle V_H \rangle^*|$$

So, the GEK data should be interpreted as a vector difference between the surface and vertically averaged velocities (Sanford, 1971).

The surface drift generated by wind and waves generally effects only a very shallow surface layer h in such a way, that h is often small compared to H

$$k = (1 - h/H)^{-1} \sim 1, \tag{6}$$

and therefore, GEK is a very suitable tool to study a shallow surface drifts in a deep sea.

RESULTS AND CONCLUSIONS

The long-term observations of the velocity field were performed in the Nevelskoy Strait with the aid of bottom deployed electrode system that measured the horizontal electric fields at several points of the Strait. This Strait separates the Sakhalin Island from the Main Land and is the place where the water exchange between the Japan Sea and Okhotsk Sea occurs.

The bottom topography with the disposition of electrodes is shown on Fig. 1. Five electrodes in contact with sea water were connected to the measuring circuit by an insulated cable at a distance of 0.2 km, 0.75 km, 2 km, 3 km and 5 km from the shore. This method can be operated to examine the lateral structure of the horizontal electric field, and hence the structure of transport in the Strait. We used the silver-silver chloride electrodes selected in such a way that any pair difference in electrode potential was hundred of times smaller than would be observed in the Strait.

Fig. 2 displays the data (a one-day section) registered by different pairs of the electrodes (curves 1 - 4). Curve 5 shows the potential difference over the whole section (electrodes 1 - 5), while curve 6 represents the sum of the results on separate elements of antenna (curves 1 - 4). It is evident that results of measurements are dominated by irregular diurnal and semidiurnal tidal elements with velocity and transport amplitudes up to 80 cm/sec and $4 \cdot 10^4$ m^3/sec, respectively, and with approximately zero average transport. It should be noted that the presented data were obtained during quiet weather. Under other weather conditions with a strong north wind the southward water transport was found in the Strait. An excellent coincidence of the curves 5 and 6 demonstrates experimental evidence of the theoretical prediction, and thus we can use only two electrodes to measure the total transport through the Strait.

A horizontal GEK-profiling along the Kuril Straits was conducted in August 1983. The results are presented in Fig. 3, where one component of the surface velocity normal to the vessel's course is drawn (k- factor in equation 5 was found being equal to 0.8 from the hydrological soundings).

It is evident from the data, that currents were not uniform, but consisted of a set of individual narrow streams frequently with opposite directions. Besides, this velocity structure is not an instantaneous picture, as it took about two days to cross all these straits and, certainly, the surface currents depend upon the spatial and temporal structure of wind. So, we naturally see that these data do not constitute a considerable global oceanological result, but are presented here only to demonstrate the possibilities of electromagnetic methods for the sea current measurements.

REFERENCES

Bowden, K.F. 1956. The flow of water through the Straits of Dover related to wind and difference in sea level. Phil. Trans. Roy. Soc. London. A, 248 (953):517-551.

Larsen, J.C., and T.B. Sanford. 1985. Florida current volume transport from voltage measurements. Science. 227:302-304.

Sanford, T.B. 1971. Motionally induced electric and magnetic fields in the Sea. J. Geophys. Res. 76:3476-3492.

Teramoto, T. 1971. Estimation of Sea - Bed Conductivity and its Influence upon Velocity Measurements with Towed Electrodes. J. Oceanograph. Soc. Japan. 27:7-19.

FIGURES

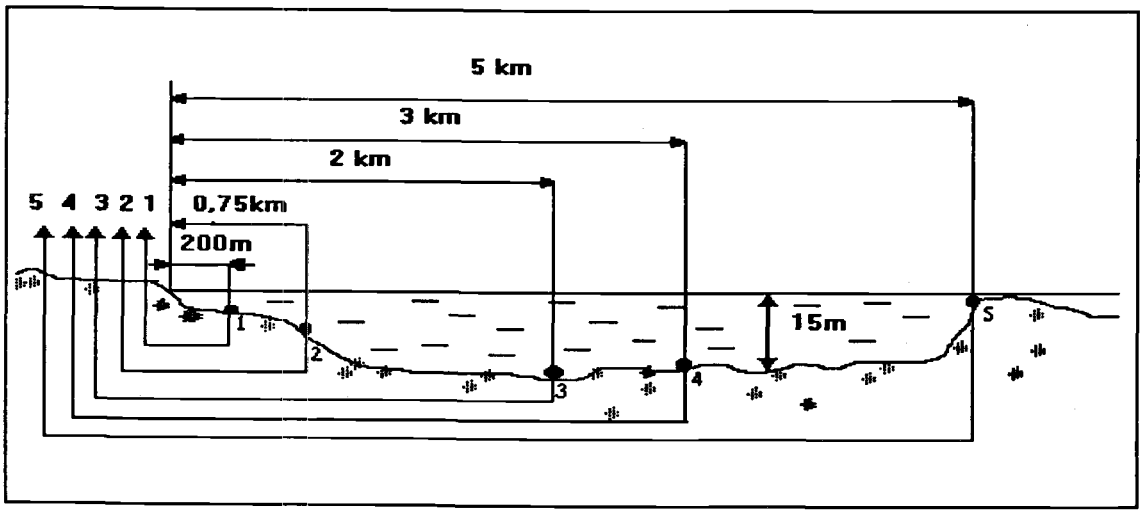

Fig. 1. The topography of bottom with the disposition of electrodes.

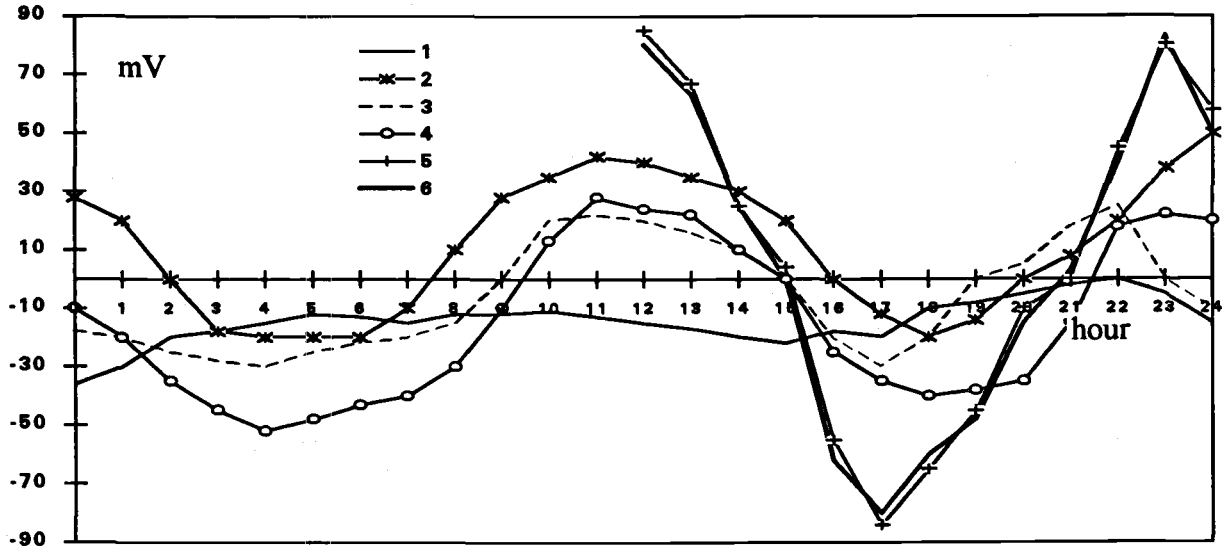

Fig. 2. Data (selected daily section) registered by different pairs of electrodes shown on Fig. 1. See text for details.

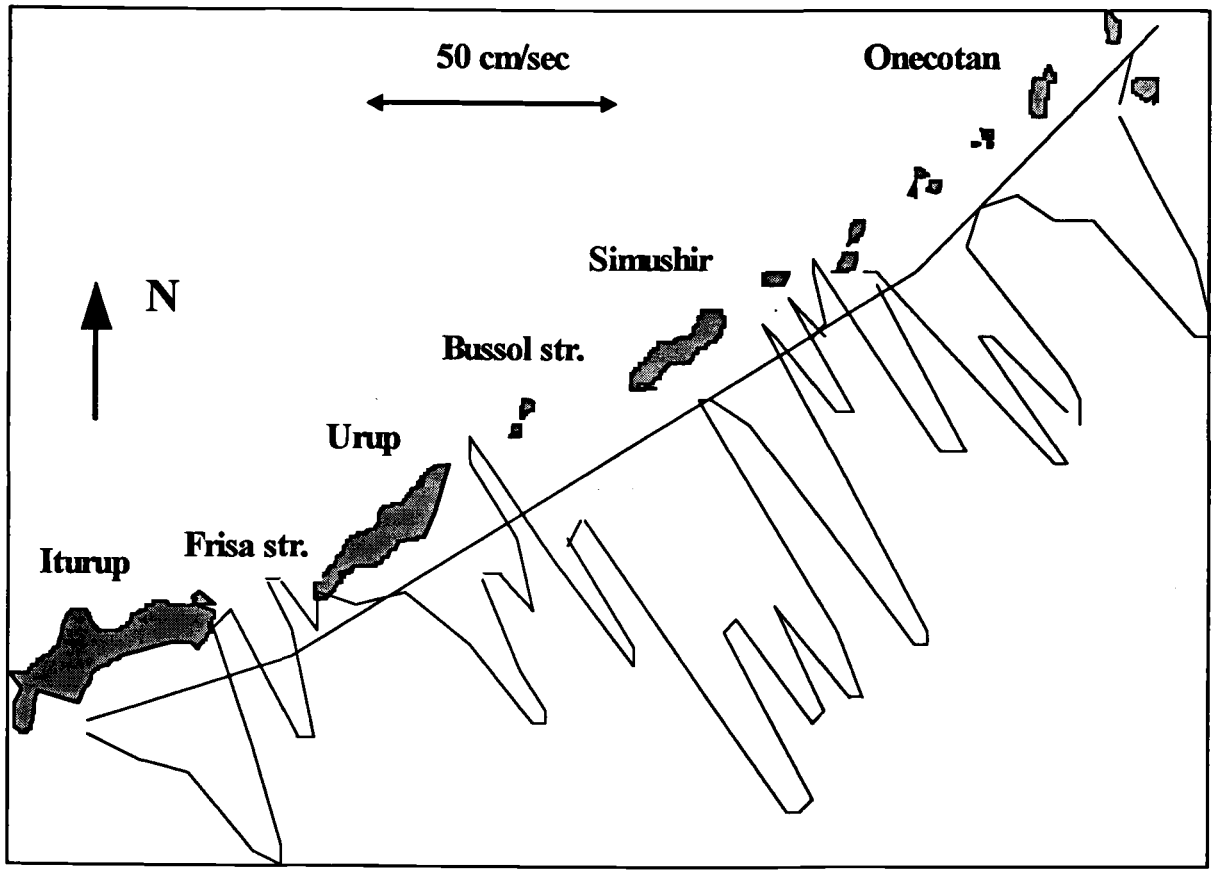

Fig. 3. Normal component of the surface velocity from horizontal GEK-profiling along the Kuril Straits conducted in August 1983.

Oceanological Zoning of the Kuril Islands Area in the Spring-Summer Period

Valentina V. MOROZ

Pacific Oceanological Institute, Far Eastern Branch, Russian Academy of Sciences,
Vladivostok, Russia

In the present paper we provide the regional classification of water adjacent to the Kuril Islands (within a 120-mile zone) in both the Okhotsk Sea and Pacific Ocean for the spring-summer period.

The following materials were considered during this study:

1. Expeditions of the Pacific Oceanological Institute of Far-Eastern Branch of Russian Academy of Siences to the Kuril Straits in the spring-summer period of 1989-1991,
2. Expeditions of the Pacific Research Institute of Fisheries and Oceanography to the South Kuril Islands region in the spring-summer period of 1980-1988,
3. Japanese expeditions to the Kuril Islands area in the spring-summer period of 1963-1972.

Based on systematization of temperature and salinity data and results of T-S analysis, five different thermohaline structures were revealed in the region:

1. Pacific type (Oyashio water)
2. Okhotsk Sea type
3. South Okhotsk Sea type (Soya current zone)
4. Deep straits zone type (Kuril Straits variety of subarctic structure)
5. Islands shelf zone type (homogenized).

Distribution of these water types is shown in Fig.1, while thermohaline indexes of the corresponding water masses are given in Table 1.

It was shown that the water structures displayed above are separated by frontal zones of various intensity, namely by:

1. Oyashio front
2. Okhotsk Sea Kuril front
3. Soya current front
4. Kuril straits fronts
5. Shallow zone fronts.

It was also found, that peculiarities of formation and distribution of different water structure types are not constant and are conditioned by the variable intensity of the current system in the area.

TABLES AND FIGURES

Table 1. Thermohaline structure of Kuril islands area.

Water mass	Spring (April - June)			Summer (July - September)		
	H, m	T, °C	S ‰	H, m	T, °C	S ‰
Pacific type						
Surface	0-30	2.5-4.0	32.4-33.2	0-50	7.0-12.0	32.8-33.0
Cold Intermediate	30-200 core 75-100	min 0-0.5	33.3-33.6	50-200 core 75-100	min 0.5-1.0	33.2-33.3
Warm Intermediate	200-900 core 250-350	**max 3.3-3.5**	33.8-34.0	200-900 core 250-350	**max 3.3-3.5**	33.8-34.0
Deep	900-3000	2.5	34.5	900-3000	2.5	34.5
Bottom	> 3000	1.5	34.7	>3000	1.5	34.5
Okhotsk Sea type						
Surface	0-30	2.0-3.0	32.5-32.8	0-50	6.0-12.0	32.5-32.8
Cold Intermediate	30-150 core 75-100	**min -1.5-0**	32.9-33.0	50-150 core 75-100	**min -1.3-0**	32.9-330
Okhotsk Sea Intermediate	150-600	1.5	33.75	150-600	1.5	33.75
Warm Intermediate	600-1300 core 500	max 2.4	34.3	600-1300 core 500	max 2.4	34.3
Deep	> 1300	1.8	34.7	>1300	1.8	34.7
South Okhotsk Sea type						
Surface	0-30	**5.0-10.0**	33.8-33.9	0-50	**13.0-16.0**	33.8-34.3
Cold Intermediate	30-300 core 75-150	min -0.5-0	33.2-33.3	50-300 core 75-150	min-0.5-0.5	33.2-33.3
Warm Intermediate	300-1200 core 600	max 2.0	34.0	300-1200 core 600	max 2.0	34.0
Deep	>1200	1.5	34.3	>1200	1.5	34.3
Deep straits zone type						
Surface:						
Fourth Kuril	0-20	1.9-2.5	32.7-33.3	0-30	5-8	32.5-33-2
Kruzenshtern	0-20	1.7-2.0	32.5-33.2	0-30	4-8	32.5-33.2
Bussol	0-10	1.5-2.0	33.1-33.4	0-30	3-5	33.1-33.4
Friza	0-20	1.0-2.0	33.0-33.2	0-30	4-14	33.2-33.7
Cold Interm.						
Fourth Kuril	20-600 core 75-200	**0.9-1.3**	33.2-33.5	30-600 core 80-200	**1.1-2.0**	33.7-33.8
Kruzenshtern	30-400 core 75-150	**1.5-2.0**	33.5	30-400 core 75-150	**1.5-2.0**	33.5
Bussol	10-600 core 100-150	**1.0-1.2**	33.5	20-600 core 100-200	**1.4-1.5**	33.8
Friza	20-500 core 75-200	**0.9-1.3**	33.7	30-500 core 100-200	**1.7-1.8**	33.7-34.0
Warm Interm.						
Fourth Kuril	600-bottom	1.3-2.0	33.7-33.8	600-bottom	1.3-2.0	33.7-33.8
Kruzenshtern	400-650 core 500	3.0	33.8-34.0	400-650 core 500	3.0	33.8-34.0
Bussol	600-1200 core 1000	2.3	34.2	650-1200 core 1000	2.1	34.2
Friza	500-bottom	2.2-2.4	34.3	500-bottom	2.2-2.4	34.3
Deep						
Kruzenshtern	> 650	2.5	34.2	> 650	2.5	34.2
Bussol	> 1200	2.0	34.5	> 1200	2.0	34.5
Islands shelf zone type						
Homogenized	0-150	1.0-2.0	33.2-33.5	0-150	3.0-4.0	33.2-33.5

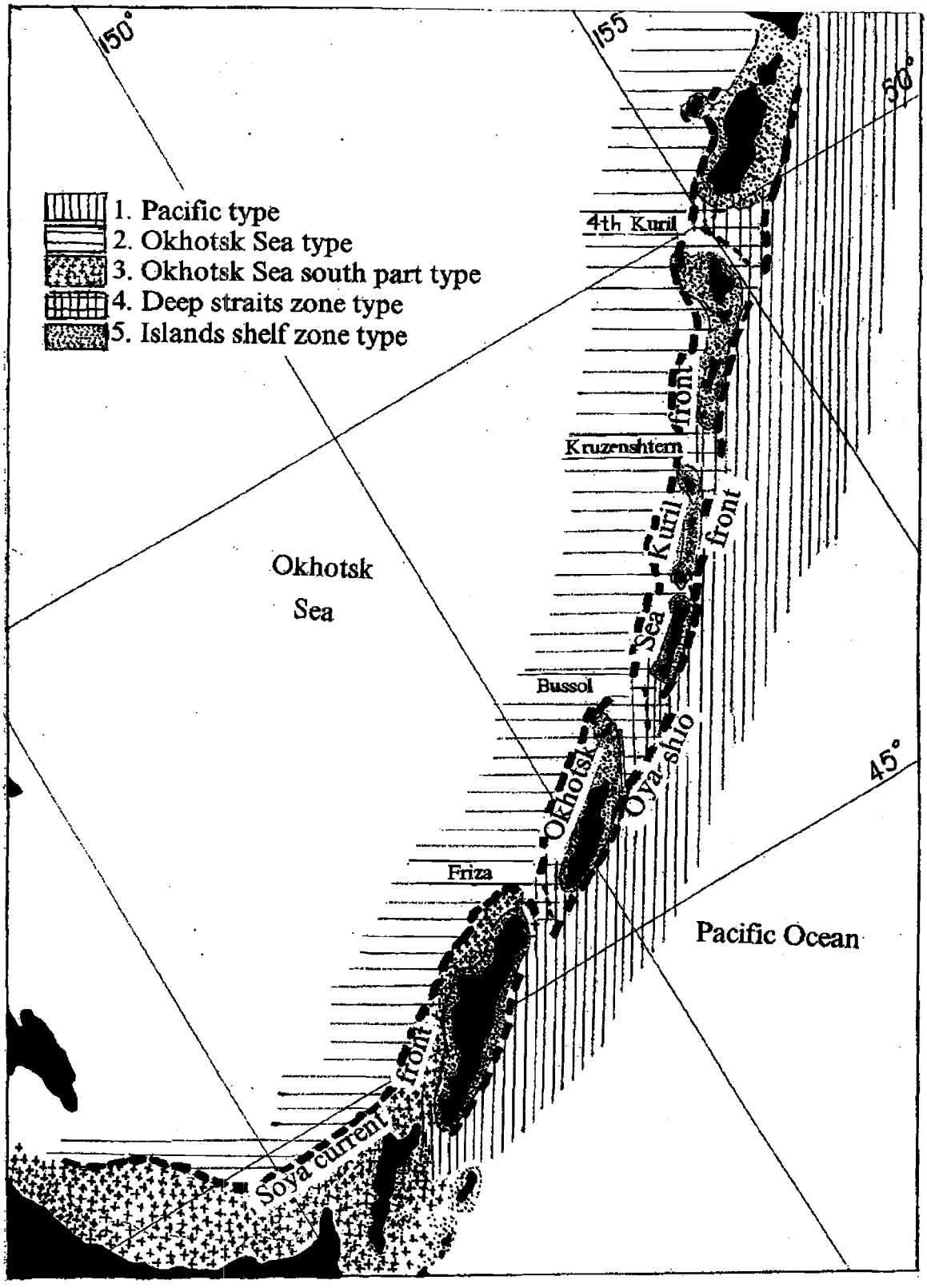

Fig. 1. Distribution of different water structures.

Note on the salinity balance in the Okhotsk Sea

Yutaka NAGATA

Faculty of Bioresources, Mie University, Tsu, Mie-ken, Japan

The source water of the North Pacific Intermediate Water (NPIW) is believed to be generated in the shelf region of the northwestern Okhotsk Sea (e.g. Talley and Nagata, 1995: the figures used in the following discussion will be referred by figure numbers in this report). Sea ice formation occurs actively in the coastal polynya just off the Siberian coast throughout winter season, and the annual rate of the dense water formation is estimated to be about 0.5 Sv by Alfultis and Martin (1987). They urge that the volume of the formed dense water is large enough to maintain NPIW, as it is doubled by horizontal mixing before it flows out into the North Pacific Ocean and reaches to the formation area of NPIW. We shall discuss whether such a formation process of the dense water is physically feasible by considering salinity balance.

Characteristics of the waters and oceanic currents which would affect the salinity balance in the Okhotsk Sea are:

1. The temperature of the dense shelf bottom water is almost at freezing point - 1.8°C, and the salinity is between 33.3 and 33.6 psu (Kitani 1973: Fig.2.3.29). We assume the typical salinity value here as 33.5 psu.
2. The salinity of the surface water in the shelf region is 32.5 psu in summer and between 32.7 and 33.2 psu in winter. Its temperature in winter is -1.8°C (Kitani, 1973 and Reid, 1965). We assume the typical salinity value as 32.5 psu.
3. As to the salinity of the East Kamchatka Current Water near the northern straits of the Kuril Islands, 33.1 psu is selected as the typical value from the figures of Ohtani (1989) (Fig. 2.5.4).
4. The salinity at the temperature minimum (almost at freezing point) in the central part of the Okhotsk Sea is from 32.9 psu (sigma-t 26.5) to 33.1 psu (sigma-t 26.7). We select 33.0 psu as the typical value (Kitani, 1973: Fig.2.3.29).
5. The salinity of the Soya Current Water is about 34.0 psu, and the averaged flow rate is 0.7 Sv (Aota and Ishikawa, 1991).
6. The fresh water supply from Amur River into the region under consideration is of the order of 0.01 Sv (Aota and Ishikawa, 1991).
7. The volume transport from the Pacific Ocean to the Okhotsk Sea through the northern straits of the Kuril Islands is not clear, but is estimated to be 13.2 Sv by Kurashina et al. (1967). The averaged salinity value in the upper 1,900 m layer is about 34.1 psu. The transport from the Okhotsk Sea to the North Pacific through the southern straits of the Kuril Islands is 16.7 Sv (Kurashina et al., 1967). The averaged salinity of the upper 1,900 m is about 33.9 psu. We use these values tentatively.

If we assume the formation rate of the dense water in the shelf region is 0.5 Sv as estimated by Alfultis and Martin (1987), the resulting salinity loss of the surface layer due to ice formation is:

$$(33.5 - 32.5) \times 10^{-3}\ \mathrm{Kg/m^3} \times 0.5 \times 10^{6}\ \mathrm{m^3/s} = 0.5 \times 10^{3}\ \mathrm{Kg/s} \qquad (1)$$

If the salinity loss is balanced with the horizontal transport in the surface layer from the East Kamchatka Current Water, the required transport U is:

$$(33.1 - 32.5) \times 10^{-3}\ \mathrm{Kg/m^3} \times U = 0.5 \times 10^{3}\ \mathrm{Kg/s}, \quad \text{and} \quad U = 1.1\ \mathrm{Sv}. \qquad (2)$$

This value would be considerably underestimated because the distance between the East Kamchatka Current and the shelf regions is about 1,000 km, and because the effective horizontal salinity difference may be one order of magnitude smaller than that used in the above estimation. So, the surface current in the order of 10 Sv is required to be flowing into the region. This is not realistic as we find no eminent current there.

One of the curious behaviors of the dense shelf water is that it looses its high-salinity before it flows out into the central part of the Okhotsk Sea (Kitani, 1973: Fig. 23.2.8-9), though its temperature remains almost at freezing point. This indicates that the water is mixed with low-salinity cold water, which may be found in the surface layer in late winter or in early spring. If we assume its salinity is equal to the typical value (32.5 psu) in the surface layer in the shelf region, the mixing ratio R of the dense shelf water with the cold surface water can be given:

$$32.5\ R + 33.5 \times (1-R) = 33.0, \quad \text{and} \quad R = 0.5. \qquad (3)$$

Namely, the dense water is mixed with the surface water in the ratio of 1:1. This would be reasonable as we find vertically homogeneous water over the Kashevarova Bank which is thought to be generated by strong tidal mixing there (Kitani and Shimazaki, 1971: Figs. 2.3.22 through 2.3.24). This means that half the amount (0.25×10^3 Kg/s) of the salt, which has been given for the shelf bottom layer due to the ice formation, is carried back to the surface layer due to the mechanical mixing in the sea adjacent to the bank.

If net water transport from the surface to the bottom layer due to ice formation is negligible, the dense shelf water would flow out into the central Okhotsk Sea at the rate of 0.5 Sv, and the relatively less saline water would flow into the shelf bottom layer at the same rate. The salinity loss in the shelf bottom layer is given by

$$(33.5 - 33.0) \times 10^{-3}\ \mathrm{Kg/m^3} \times 0.5 \times 10^{6}\ \mathrm{m^3/s} = 0.25 \times 10^{3}\ \mathrm{Kg/s}. \qquad (4)$$

Thus, a half of the salt gain of the bottom layer due to ice formation is carried back to the surface layer, and another half is just carried out from the shelf bottom layer to the intermediate layer of the central Okhotsk Sea.

However, it would be reasonable to assume that some amount of net water mass is transported from the surface to the bottom layer in the process of dense water formation. This would result in the net outflow from the shelf bottom region to the central Okhotsk Sea. If we denote this transport with V, the amount of the salt carried out into the central Okhotsk Sea is 33.5×10^{-3} Kg/m^3 x V. Even if the net water flux is 1/1,000 of the generation rate of the dense water formation rate (0.005 Sv), the resulting salt flux is 0.16×10^3 Kg/s, and of the same order of magnitude as the salt fluxes in the above discussion. This indicates that the accuracy of the present discussion is very limited, and further elaborated investigations would be needed.

The salinity balance in the surface layer of the shelf region is much more complicated as we need to consider the fresh water supply from Amur River. This salinity loss may be estimated as:

$$(33.5 - 0.0) \times 10^{-3}\ \mathrm{Kg/m^3} \times 0.01 \times 10^{6}\ \mathrm{m^3/s} = 0.34 \times 10^{3}\ \mathrm{Kg/s}. \qquad (5)$$

This amount is almost the same order of magnitude as the salinity loss due to the ice formation (0.5 x 10^3 Kg/s). However, the same amount of the water mass in the surface layer should flow out from the shelf region to the central Okhotsk Sea. If the salinity of the out flow is that of the surface shelf water, there would be no net salinity gain or loss. However, most of the Amur River fresh water may spread out over the entire Okhotsk Sea, and additional fresh water would be carried out from the shelf region in the form of drifting ice due to strong westerly winter winds.

It should also be noted that Alfultis and Martin's estimation is based on satellite observation of the coastal polynya, and may include significant error. They assumed that the volume of the dense water would be doubled by horizontal mixing with the surrounding waters before it reaches the Oyashio region, and be enough to maintain NPIW. Recent investigations (see Talley and Nagata, 1995), however, indicate the intermediate Oyashio Water will be modified by horizontal mixing with the old and saline NPIW which is carried by the Kuroshio into the Mixed Water Region (Fujimura and Nagata, 1992). The volume of water is again doubled before it reaches to the formation area of NPIW. The rate of the dense water formation in the shelf region of the Okhotsk Sea, which is required to maintain NPIW, might be much smaller than that estimated by Alfultis and Martin (1987).

If we take the typical salinity values of the Soya Current Water and of the Okhotsk interior water as 34.0 and 33.0 psu, respectively, the effective salt flux carried into the Okhotsk Sea by the Soya Current is:

$$(34.0 - 33.0) \times 10^{-3}\ \mathrm{Kg/m^3} \times 0.7 \times 10^6\ \mathrm{m^3/s} = 0.7 \times 10^3\ \mathrm{Kg/s}. \qquad (6)$$

It should be noted that this effective flux is just in the same order as that produced by ice formation in the shelf region. The Soya Current Water sinks easily by winter cooling due to its high-salinity nature (Talley and Nagata, 1995), and appears to influence directly the nature of the water in the intermediate layers of the Okhotsk Sea.

However, the effective salinity fluxes from and to the North Pacific Ocean through the northern and southern straits of the Kuril Islands are:

$$34.1 \times 10^{-3}\ \mathrm{Kg/m^3} \times 13.2 \times 10^6\ \mathrm{m^3/s} = 450 \times 10^3\ \mathrm{Kg/s} \qquad (7a)$$

and

$$33.9 \times 10^{-3}\ \mathrm{Kg/m^3} \times 16.9 \times 10^6\ \mathrm{m^3/s} = 556 \times 10^3\ \mathrm{Kg/s}, \qquad (7b)$$

respectively. The net flux flows out from the Okhotsk Sea to the North Pacific is of order of 100 10^3 Kg/s, and two orders of magnitude larger than the fluxes discussed above. This means that the salinity fluxes discussed above do not significantly affect the salinity balance in the whole Okhotsk Sea, although they are essential for the formation mechanisms of NPIW.

The accuracy of the present discussion would be very limited, but we may conclude:

1. There would be some efficient mechanisms to maintain the salinity value of the surface water in the shelf region of the north-western Okhotsk Sea. This is essential for the formation of the dense shelf water which is considered as the source water of NPIW.
2. The vertical tidal mixing in vicinity of the Kashevarova Bank plays an important role to carry back salt from the shelf bottom layer to the surface layer.
3. The net water mass transport is a very effective way to carry salt, and so we need to estimate accurately the volume transport of the downwelling associated with the sinking of brine generated by ice formation.

4. The fresh water transport by drifting ice would be important in the salinity balance in the surface layer of the shelf region.

5. The further discussion on salinity balances in various scales is needed: for the northwestern shelf region, for the Soya Current Region and the intermediate layers, and for the whole Okhotsk Sea region.

REFERENCES

Alfultis, M.A., and S. Martin. 1987. Satellite passive microwave studies of the Sea of Okhotsk ice cover and its relation to oceanic processes, 1978-1982. J. Geophys. Res. 92 (C12):13013-13028.

Aota, M., and M. Ishikawa. 1991. Fresh water supply to the Sea of Okhotsk and volume transport of Soya Warm Current. Bull. Hokkaido Nat. Fish. Res. Inst. 55:109-113 (in Japanese).

Fujimura, M., and Y. Nagata. 1992. Mixing process in the Mixed Water and Kuroshio Extension Regions and modification of the intermediate Kuroshio Water. Oceanogr. Magazine. 42:1-20.

Kitani, K., and K. Shimazaki. 1971. On the hydrography of the northern part of the Okhotsk Sea in Summer. Bull. Fac. Fish. Hokkaido Univ. 12:231-242.

Kitani, K. 1973. An oceanographic study of the Okhotsk Sea - Particularly in regard to cold waters. Bull. Far Seas Fish. Res. Lab. 9:45-76.

Kurashina, S., K. Nishida, and S. Nakabayashi. 1967. On the open water in the southeastern part of the frozen Okhotsk Sea and the current through the Kuril Islands. J. Oceanogr. Soc. Japan. 23:57-62 (in Japanese).

Ohtani, K. 1989. The role of the Sea of Okhotsk on the formation of the Oyashio Water. Umi to Sora. 65:63-83 (in Japanese).

Reid, J.L. 1965. Intermediate waters of the Pacific Ocean. Johns Hopkins Oceanogr. Studies. 2:1-85.

Talley, L.D., and Y. Nagata [ed.]. 1995. The Okhotsk Sea and Oyashio Region. PICES Scientific Report No.2, 227p.

Variability of the Kuroshio Front in 1965-1991

Alexander D. NELEZIN

Pacific Oceanological Institute, Far Eastern Branch, Russian Academy of Sciences,
Vladivostok, Russia

The northwestern part of the Pacific ocean is characterized by contact of the cold subarctic and warm subtropical water zones. The Subarctic front, related to the Kuroshio Current, is distinguished by the enhanced bioproductivity and is one of the fishery regions. Doubtless, the fisheries' interest promoted the investigation of the front position and properties (Uda, 1938).

The oceanic fronts are revealed by the enhanced horizontal gradients of the characteristics. The basic frontal zones, or the climatological fronts, are the boundaries of the natural zones in the ocean. They are identified by the multi-year mean (climatic) charts of the oceanographic characteristics distribution. By constructing the climatic fields, the relatively wide frontal zone is charted as a result of the data averaging. This is the region of probable front position fluctuations.

At the present moment only the sea surface temperature data are widely available for the study of fronts (Gulev et al., 1988; Rassadnikov et al., 1987), but deep-sea observations should be performed to analyze the vertical water structure and interannual variability of the front position.

The vertical temperature sections crossing the Subarctic front were constructed along the section of 145°E based on multi-year oceanographic data collected in February and August (Fig. 1). The figure shows that the frontal zone transforms significantly from winter to summer in the upper oceanic layer of 150 m. Moreover, it is difficult to define the front position in August in the upper layer, but it is well distinguished in the layer of 150-300 m.

In order to study variability within the annual climatic period, the monthly charts of multi-year temperature and salinity means were prepared at the standard horizons in the upper layer of 300 m. The front position was marked on each longitude from 140 to 150°E, and then the value corresponding to the average front position eastward from the Honshu Island was calculated. To improve the accuracy of our calculations the characteristic isotherm (isohaline) in zone of maximal gradients was assumed as a criteria of the front.

The preliminary analysis suggested that the isotherm of 13°C and isohaline of 34.6 % at the level of 200 m, located in the Kuroshio current zone, are the most informative for the Subarctic front within the region of 140-150°E. Therefore, for further investigations the term Kuroshio front was used appropriate to the chosen criteria. The Subarctic front concept is broader as it includes the Kuroshio and Oyashio Currents and the Mixed Water Region.

The annual variability of the front position (Fig. 1c) is characterized by the northeast displacement in December and by the southeast displacement in April. During the cold period (December - April) the rapid front displacement southward is observed and then the relatively smooth fluctuation of its northward movement occurs. Perhaps, it can be explained by some changes in the variability of the hydrological parameters within the subarctic and subtropical waters. Southward from the front the semiannual harmonic with maximums in August and

February is distinguished, whereas northward the annual harmonic with maximum in December and minimum in July is revealed.

Interannual front position variations is one of the basic indicators of the ocean thermodynamic regime, but the shortage of information regarding this problem is obvious. The opportunity to solve the above problem appeared as a consequence of the Cooperative Study of Kuroshio (CSK) (The Kuroshio ..., 1972) and the program "Sections" devoted to the monitoring of the energy active zone of the Kuroshio (Expeditional ..., 1989).

To investigate the multi-year Kuroshio front variability, the mean front position (within the region of 140-150°E) and standard deviations were calculated using the seasonal mean temperatures at the level of 200 m from observational data collected in 1965-1991 (Fig. 2). The isotherm of 13°C was also assumed as a criteria of the front. To perform the analysis of the interannual variations the smoothing of the temporary data set was carried out applying the seasonal variation model. To estimate the long-term component the trends were calculated with the help of the parabolic model. The trends with the opposite tendencies in variations of the mean front position and standard deviations were interpreted as meandering of the Kuroshio front.

In 1965-1977 a tendency for the front to move northward from 35.5 to 37°N was observed, then in 1978-1986 the front shifted southward (to 35.2°N) and in the latter period the inverse shearing to 36.4°N (in 1991) occurred. The Kuroshio front was located in the extreme north and south positions in the autumn of 1977 (37.6° N) and in the summer of 1986 (34.7°N), respectively (Fig. 3b). The front meandering decreased in 1965-1977 and increased in 1978-1985.

The front meandering is a wave of the current track deviation (bending) with a consequent eddy detachment, and is considered as one of the basic reasons for the spatial front position variability. Apparently, it is under the influence of quasi-stationary meanders and the Rossby waves, associated with the non-stationary Kuroshio. The quasi-stationary meanders were well distinguished by the averaged spatial front positions for all four seasons for the period of study (Fig. 3a). The greatest meander amplitude was observed in winter, while in the warm period the front shear became more sloping. The temporal variation analysis suggested the presence of non-regular processes in the interannual Kuroshio front position variations caused by transfrontal heat and mass transport, as the stationary frontal divisions play the role of barrier for the sea waters located on the opposite sides of the front.

To investigate the Kuroshio front position fluctuations the spectral analysis of the temporal sets along with a preliminary exclusion of the trends was applied. The initial temporal set, including 105 realizations, was approximated by the model of "piece-wise linear trend" and divided on three specified sections of the predominant tendencies. After removal of the trend components the spectra of the residual set were calculated (Fig. 4). The significant interannual fluctuation periodicity of 5-6 years (at the level of 90%) was obtained for the residual smooth set of the average front position. It should be noted that previously the temperature anomaly in the system of the North Pacific circulation with the period of 6 years has been considered and related to the Polar front shear or the Kuroshio Current axis movement (Kort, 1970). Spectrum based on the initial set of standard deviations after separating of the trend component had two maximums corresponding to the periods of 2-3 seasons and about 2 years, respectively.

Multi-year variability of the average front position is under the influence of the water circulation intensity on the western periphery of the subtropic Pacific gyre. Fig. 4a illustrates the results of water transport calculations for the North Trade Current and the Kuroshio along the section of 137°E in 1972-1991. The trends approximated by the parabolic model showed

unidirectional tendencies for the currents associated with the long-period variations of the Kuroshio front position. The running means of the current discharges have been obtained with an averaging interval of 7 seasons (3, 5 years). Fig. 4b demonstrates the residual curves after the trend component is separated. As it was noted, in the Kuroshio front variability the extreme north and south positions were recorded in the autumn of 1977 and in the summer of 1986. This coincides with the enhanced current intensity in the first mentioned period and weakening of the current intensity during the second period. The abrupt increase of the current discharges in 1975 -1977 was due to the rapid front shear northward, while the relatively slow decrease of water transport in 1979-1985 could be explained by a comparatively smooth front shift southward. Thus, the Kuroshio front movements, to a great extent, are related to the multi-year fluctuations of the current intensity within the Subtropical gyre.

REFERENCES

Gulev, S., D. Kadaev, and I. Yashaev. 1988. Synoptic variability of sea water temperature in the Gulf Stream and the North Atlantic currents. Oceanology. 28(5):721-727 (in Russian).

Expeditional investigation results in the Kuroshio energy active zone in accordance with the program "Sections". 1989. Summary of Science and Technology. Ser. Atmosphere, Ocean, Space - program "Sections". 12, 187 p. (in Russian).

Kort, V. 1970. The large-scale ocean-atmosphere interaction (the North Pacific). Oceanology. 10(2):222-240 (in Russian).

Rassadnikov, Y., and A. Nikitin. 1987. Variability of generalized ocean thermodynamic characteristics in the Kuroshio Energy active zone. Summary of science and technology. Ser. Atmosphere, Ocean, Space - program "Sections". 7:288-295 (in Russian).

The Kuroshio and adjacent Pacific regions. 1972. Trudy GOIN. 106: 209 p. (in Russian).

Uda M. 1938. Researches on "Siome" or current rip in the seas and oceans. Geoph. Mag. 2(4):306-372.

FIGURES

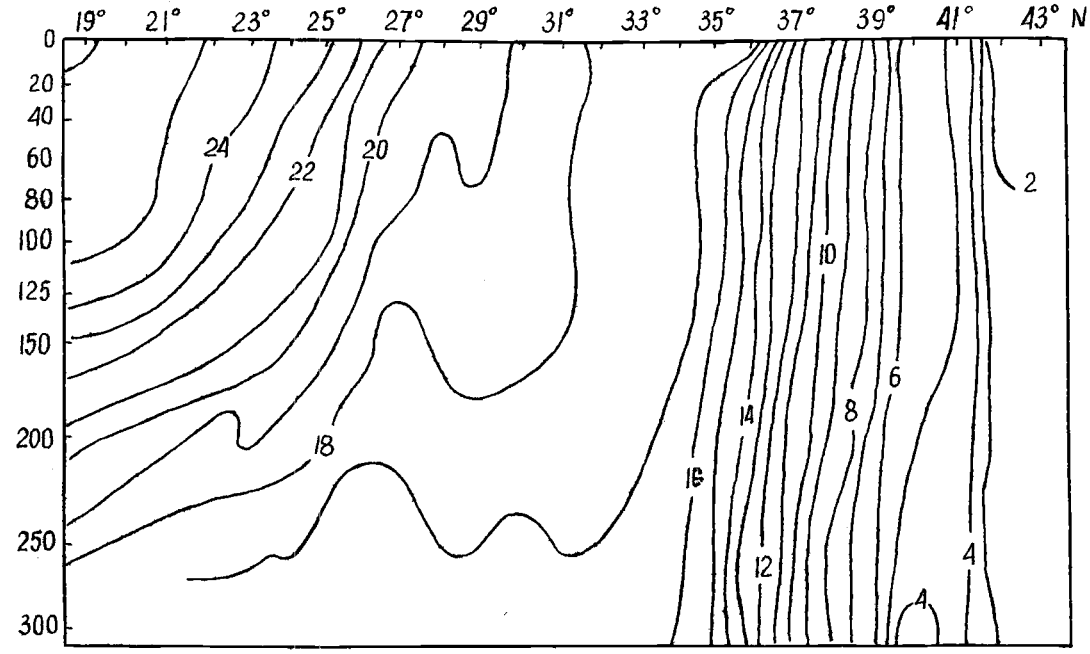

(a)

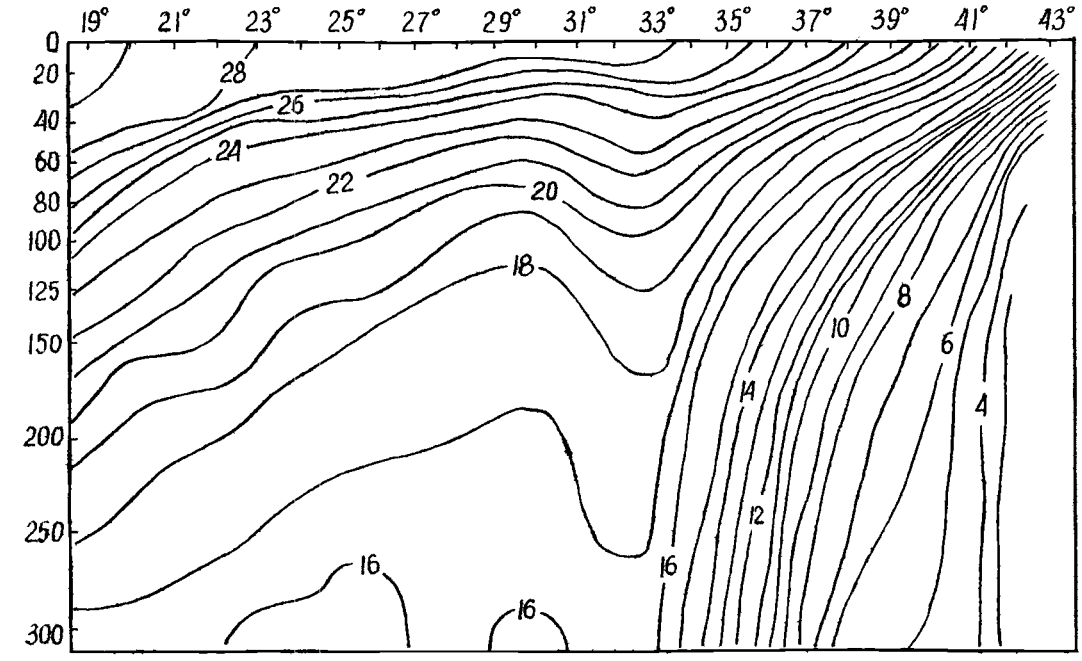

(b)

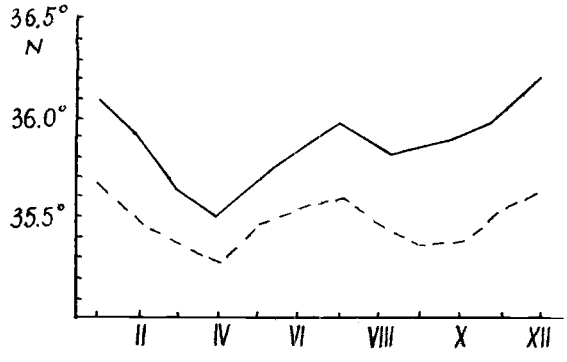

(c)

Fig. 1. Distribution of the multi-year temperature means (°C) along the section of 145°E in February (a) and August (b), and annual variability of mean temperature and salinity (dotted line) front position based on multi-year observations within the region of 140-150°E (c).

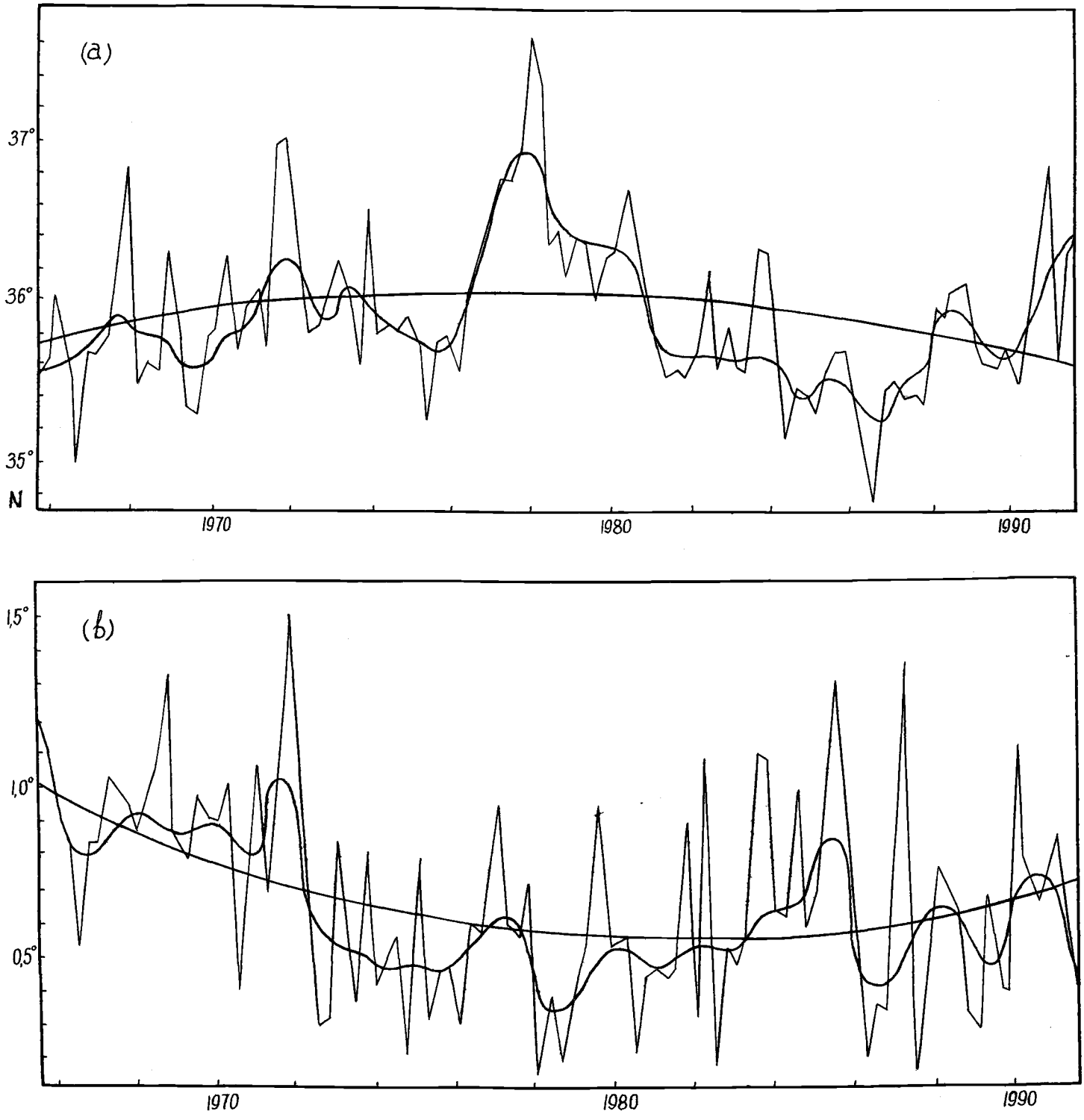

Fig. 2. Temporal variability of the seasonal values for the mean front position (a) and its standard deviation (b) in 1965-1991; components were smoothed by using the seasonal variability and parabolic trend models.

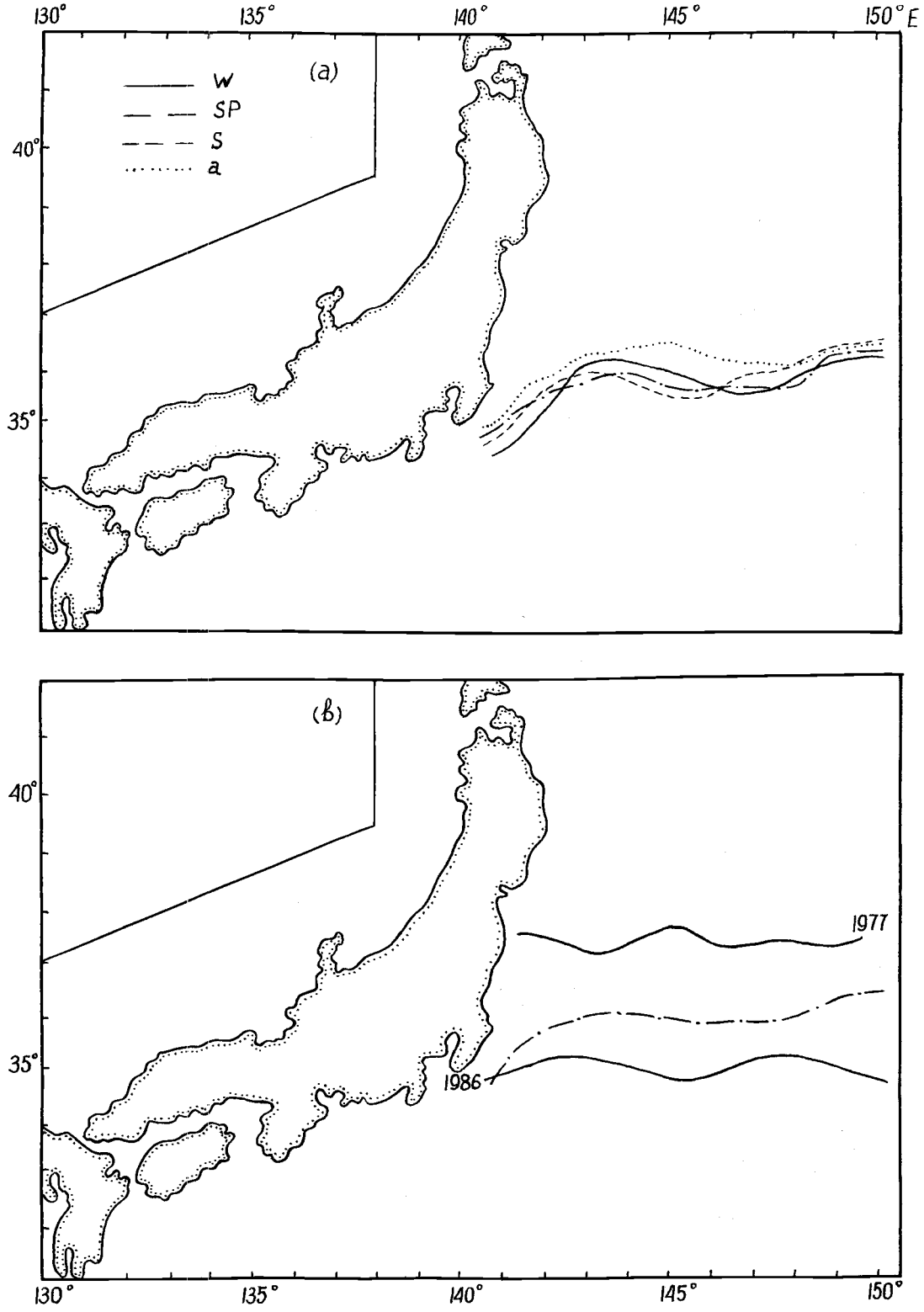

Fig. 3. Spatial seasonal means of the Kuroshio front position in winter, spring, summer, autumn (a); mean and extreme front positions in 1977 and 1986 (b) from 1965-1991 data.

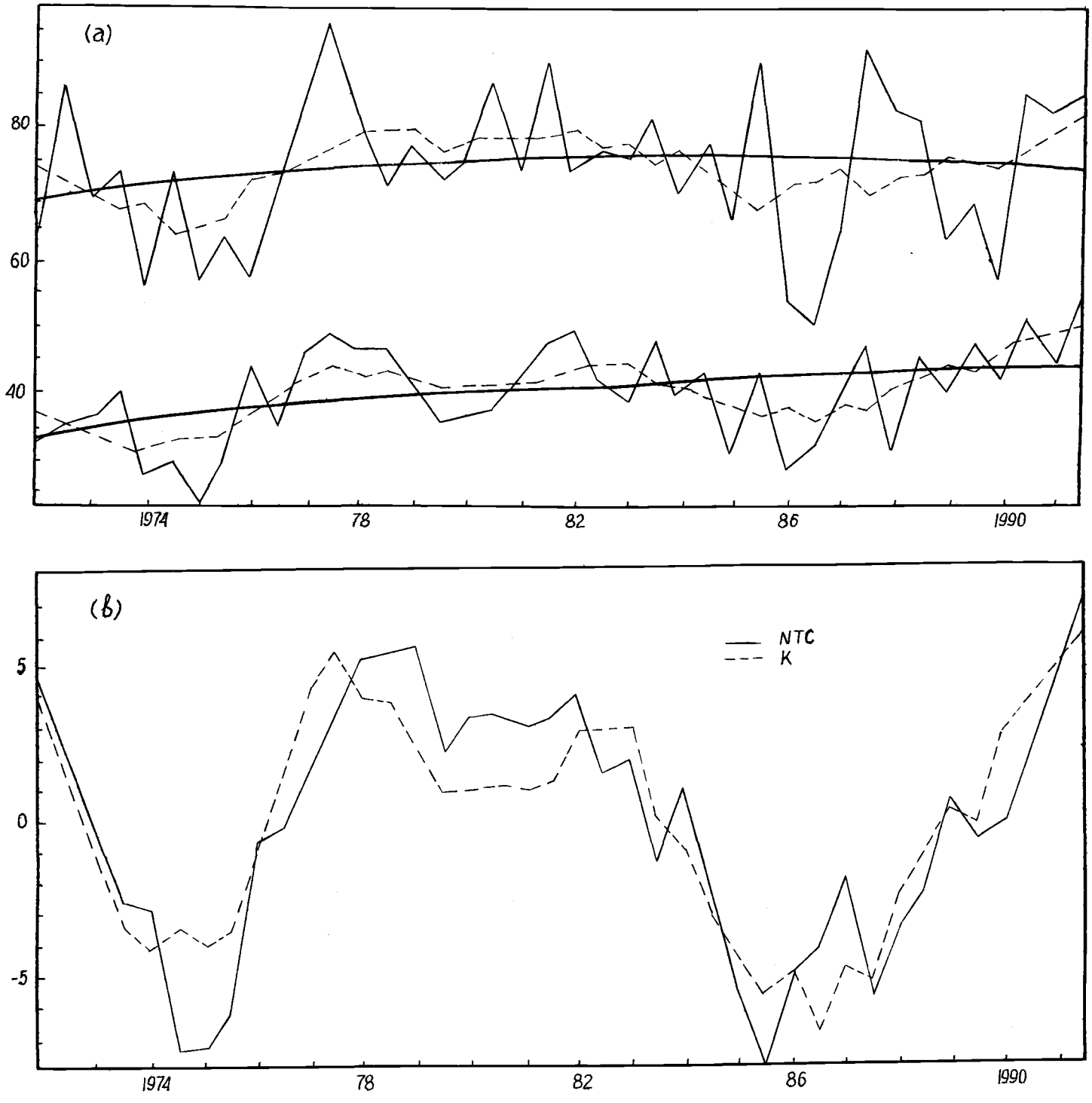

Fig. 4. Temporal variability of the North Trade Current (NTC) and Kuroshio (K) discharges (10^6 m^3/s) along the section of 137°E in the 0-1,000 m layer (a) and residual curves of discharges after filtration and trend component separation (b).

An Experimental Study of Currents in the Near-Kuril Region of the Pacific Ocean and in the Okhotsk Sea

Vladimir I. PONOMAREV, Evgeny P. VARLATY and Mikhail Yu. CHERANYEV

Pacific Oceanological Institute, Far Eastern Branch, Russian Academy of Sciences, Vladivostok, Russia

INTRODUCTION

Direct current measurements in the main pycnocline of the Pacific and the Okhotsk Sea waters adjacent to the Kuril Islands are presented and compared with observations of temperature, salinity, density and dissolved oxygen. These data were collected in July 1993 aboard of *R/V Academik Aleksandr Nesmeyanov* during the joint expedition organized by the Russian Federal Research Institute of Fisheries and Oceanography (VNIRO), the Pacific Research Institute of Fisheries and Oceanography (TINRO) and the Pacific Oceanological Institute (POI) and supported by the Fisheries Committee of Russian Federation. Direct current measurements were carried out by Dr. E.P .Varlaty, Mrs. M.Y. Cheranyev and G.P. Shvetsov from POI.

MEASUREMENTS

Current velocity was determined by the acoustic equipment (complex) designed at the Pacific Oceanological Institute. The equipment and method of measurements were described in details by Varlaty and Tihomirov (1980), and Varlaty and Ozmidav (1981). Current speed and direction were detected synchronically by sinking of the acoustic complex from a drifting vessel. The technique used to measure absolute current parameters included relative velocity sounding and ship drift determination by any available satellite navigation system. Accuracy of velocity, current direction and depth were estimated as 0.5 cm/sec, 3° and 0.25%, respectively. Temperature, conductivity, pressure and oxygen concentration were obtained using Neil Brown MK3 CTD Probe.

A total of 120 stations in the Kuril Islands adjacent areas and the Okhotsk Sea were sampled during the cruise. On the shelf and over the continental slope CTD and current measurements, as well as Rosette sampling, were carried out mostly to the near-bottom. Oceanographic stations in deep areas were taken to a depth of 800-1,000 m

RESULTS

The major patterns of the obtained velocity fields are in agreement with known general circulation of the Okhotsk Sea and the Pacific Subarctic western boundary area in summer, in particular, with the current velocity in August (Fig. 1) estimated by geostrophic balance referenced to 2,000 dbar in deep area and to the bottom on the shelf (Moroshkin, 1964). The Kuril (Oyashio) Current of the Pacific, the Eastern Sakhalin and the Western Kamchatka Currents over the Okhotsk Sea continental slope associated with cyclonic gyre in the central part of the Sea were displayed from the observations.

However, the detailed distribution of current velocity demonstrated some specific features and differences. According to our survey, in July 1993, the jets of the Oyashio Current were situated over the steep continental slope near the shelf break and in the deeper area over the western slope of the Kuril Trench. Meandering, branching and eddy generation off the Boussole and Vriez Straits were typical for the Oyashio Current in summer. The main branch of this Current was located off the Kuril Islands and deep Straits, that was also characteristic of summer situation. The current velocity module of the Oyashio decreased from the northeast (0.7-0.8 m/s) to the southwest (0.3-0.4 m/s) due to disturbances and water exchange through the Straits. In the southwest region the Oyashio turned to the south-southeast off the Small Southern Kuril Islands (Fig. 2).

At all Pacific stations adjacent to the Kruzenshtern, Boussole and Vriez Straits, streams in the layer of 0-800 m possessed a major component directed from the Pacific to the Straits (Fig. 2). The current velocity in this area was 0.4 - 0.8 m/s and its direction demonstrated a good link with bottom topography. At the same time the total flow in the relatively thick upper layer of the Straits (0-800 m) was directed to the Okhotsk Sea only in the Kruzenshtern Strait and in the deep channel of the Boussole Strait adjacent to the Simushir Island shelf slope. The average speed in the Straits was about 0.3-0.4 m/s. In the Okhotsk Sea, along the Kuril Ridge, the current was directed from the northeast to the southwest (or from Kruzenshtern to Vriez Strait). The major inflow to the Sea of Okhotsk through the Vriez Strait occured mainly below the depth of 400-500 m in the deep strait channel and gentle outflow dominated in the upper layer of the Strait.

The dynamic topography (Fig. 3) based on CTD data provided by Verkhunov and Maslennikov (1993) and Moroshkin's geostrophic currents (Fig. 1) revealed the surface inflow stream through the Kruzenshtern Strait and surface outflow current through the southwestern part of the Boussole and Vriez Straits. The current speed in the whole layer of 0-700 m reached maximal values 0.7-0.8 m/s in the area adjacent to Kruzenshtern Strait. The dominated inflow of the Pacific waters to the Okhotsk Sea through the Kruzenshtern Strait was confirmed by both direct current measurements (Fig. 2) and the dynamic topography (Fig. 3), that is in agreement with Leonov (1960) and Moroshkin (1964). The features described above were characteristic for the summer of 1993 and might be typical for summer climate in general.

Regularities of the vertical current velocity distribution were also disclosed for the areas with different water structure, bottom topography and depth. It was shown that the stream current over the shelf break border on the steep continental slope was at maximum speed in the undersurface layer of the pycnocline between 200-300 m. This situation was revealed at stations 276 (Fig. 4c), 283 and 287 in the current over the shelf break of the Small Southern Kuril ridge area. A local velocity minimum was observed in this layer of pycnocline when we move away from the shelf break to the deep offshore area (station 275, Fig. 4a). The velocity maximum shifted to the surface layer at station 275. This phenomenon is related to the vertical and horizontal oscillations of current velocity over the continental slope and also with jet generation and vertical circulation over the shelf break (Johnson and Manja, 1979, 1982).

The main feature of the vertical current velocity distribution on the northern Okhotsk Sea shelf was the two layer structure associated with a two layer density profile. Two current velocity maxima over and under the density interface are typical on the Okhotsk Sea shelf under strong and temperate wind conditions. In this case the current vector turned right with depth from sea surface to the upper maximum and left below this maximum towards the density interface, just as in the surface and bottom planetary boundary layers. In the lower layer the current vector turned in a similar way.

CONCLUDING REMARKS

Thus the important features of the horizontal and vertical current velocity distribution in the main pycnocline of the Kuril adjacent Pacific and in certain areas of the Okhotsk Sea were revealed by direct current measurements. The acoustic measuring complex of POI could be useful in future investigations of currents and eddy dynamics.

ACKNOWLEDGMENTS

We gratefully acknowledge the assistance of Gennady Shvetsov in current measurements and Anatoly Saluk for drawing some figures.

REFERENCES

Johnson, J.A., and B.A. Manja. 1979. Shear layers above a break in bottom topography Geophys. and Astrophys. Fl. Dynam. 14:45.

Johnson, J.A., and B.A. Manja. 1982. Longshore current over the shelf break. Rapp. P.-v. Reun. Cons. Int. Explor. Mer. 180:73-74.

Leonov, A.K. 1960. The Japan Sea. *In* Regional oceanography, Part 1. Leningrad, Gydrometeoizdat. 291-463 (in Russian).

Moroshkin, K.B. 1964. A new surface current map in the Okhotsk Sea. Oceanologia. 4:614-643 (in Russian).

Varlaty, E.P., and V.P. Tihomirov. 1980. Acoustic measuring complex for studying microstructure hydrophysical fields in the ocean. Proc. Symp. "Fine structure and synoptic variability of the seas.", Tallinn, 1980: 48-52 (in Russian).

Varlaty, E.P., and R.V. Ozmidov. 1981. On the values of the local Richardson number in the ocean. Okeanologiya, 21(2):211-216 (in Russian).

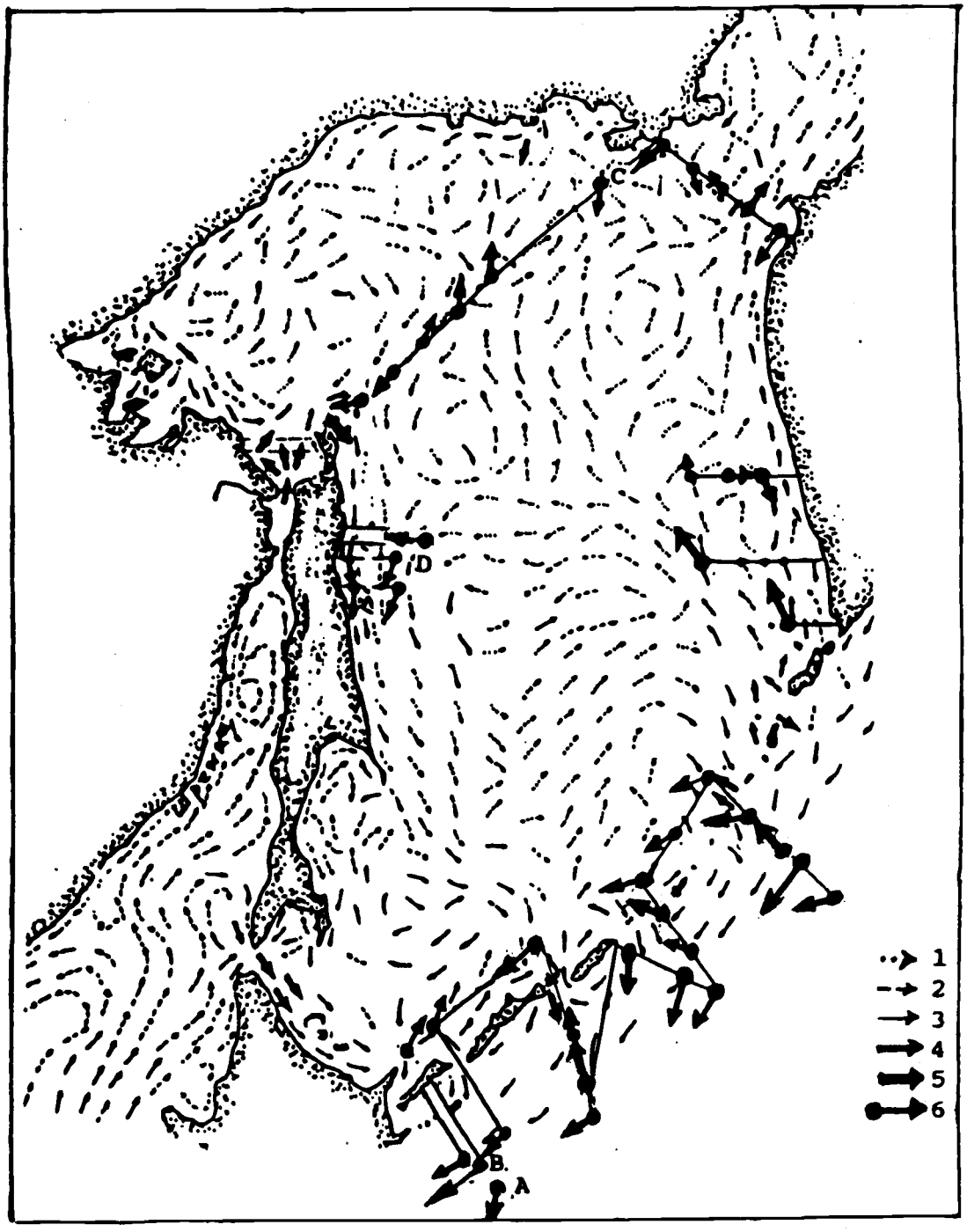

Fig. 1. Surface current velocity in August estimated by geostrophic balance referred to 2,000 db in deep area and to the sea bottom on the shelf (Moroshkin, 1964):
1 - < 5 cm/s; 2 - 5-10 cm/s; 3 - 10-20 cm/s;
4 - 20-30 cm/s; 5 - >30 cm/s;
6 - current velocity measured at 300 m in July 1993.

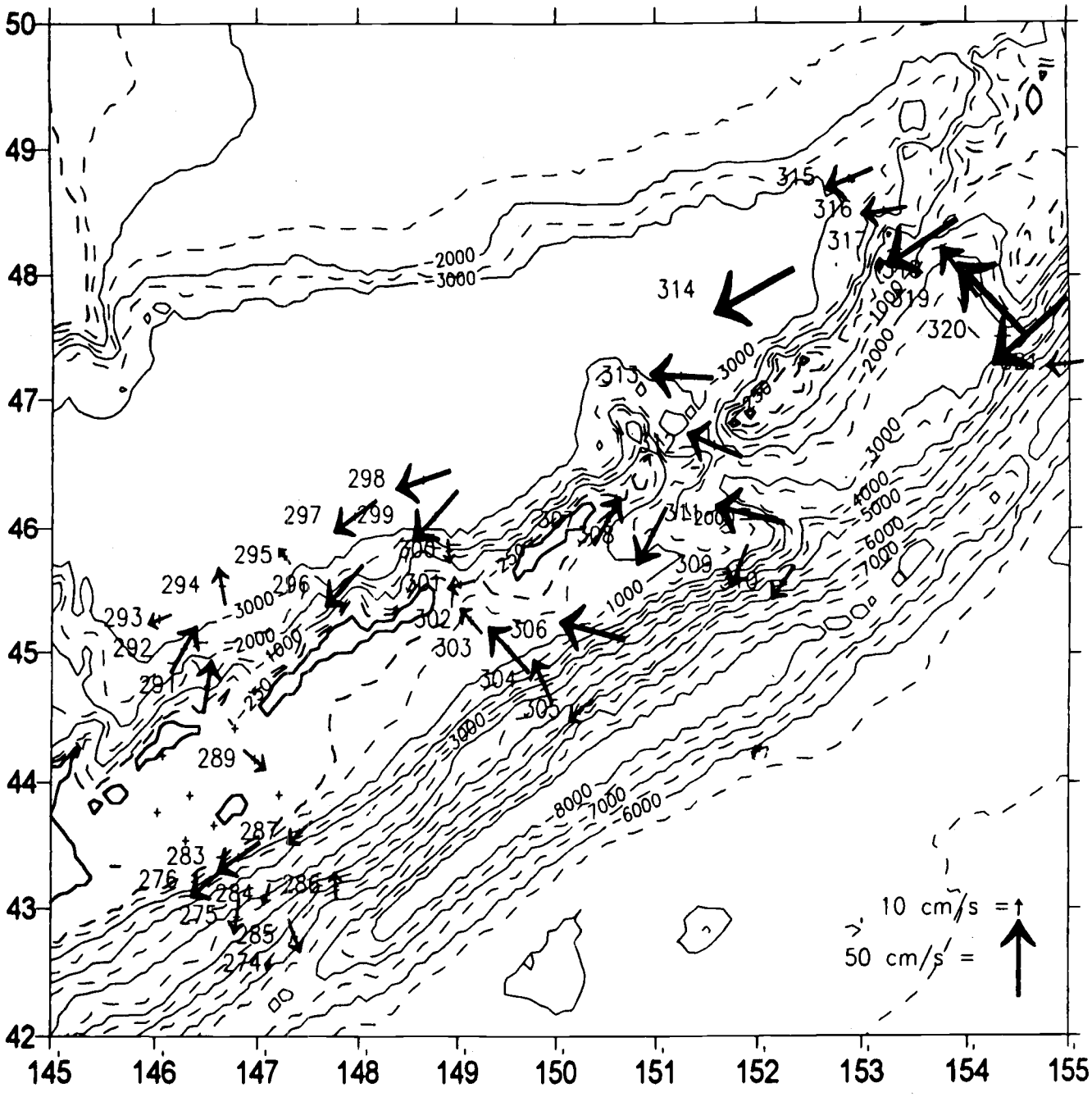

Fig. 2. Experimental currents at 200 m depth.

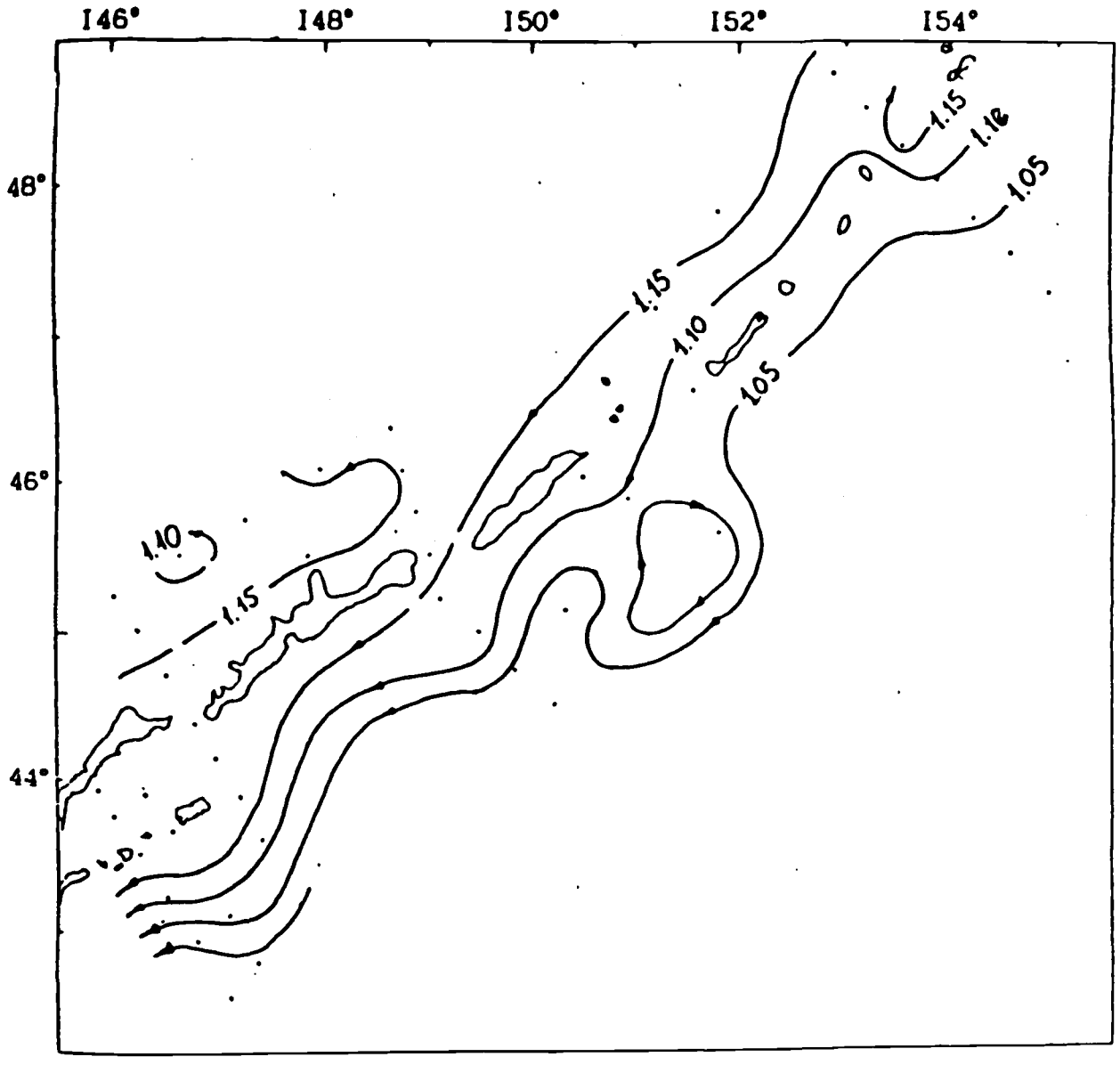

Fig. 3. Surface dynamic topography (in dynamic meters) in July 1993 estimated by geostrophic balance referred to 1,000 dbar.

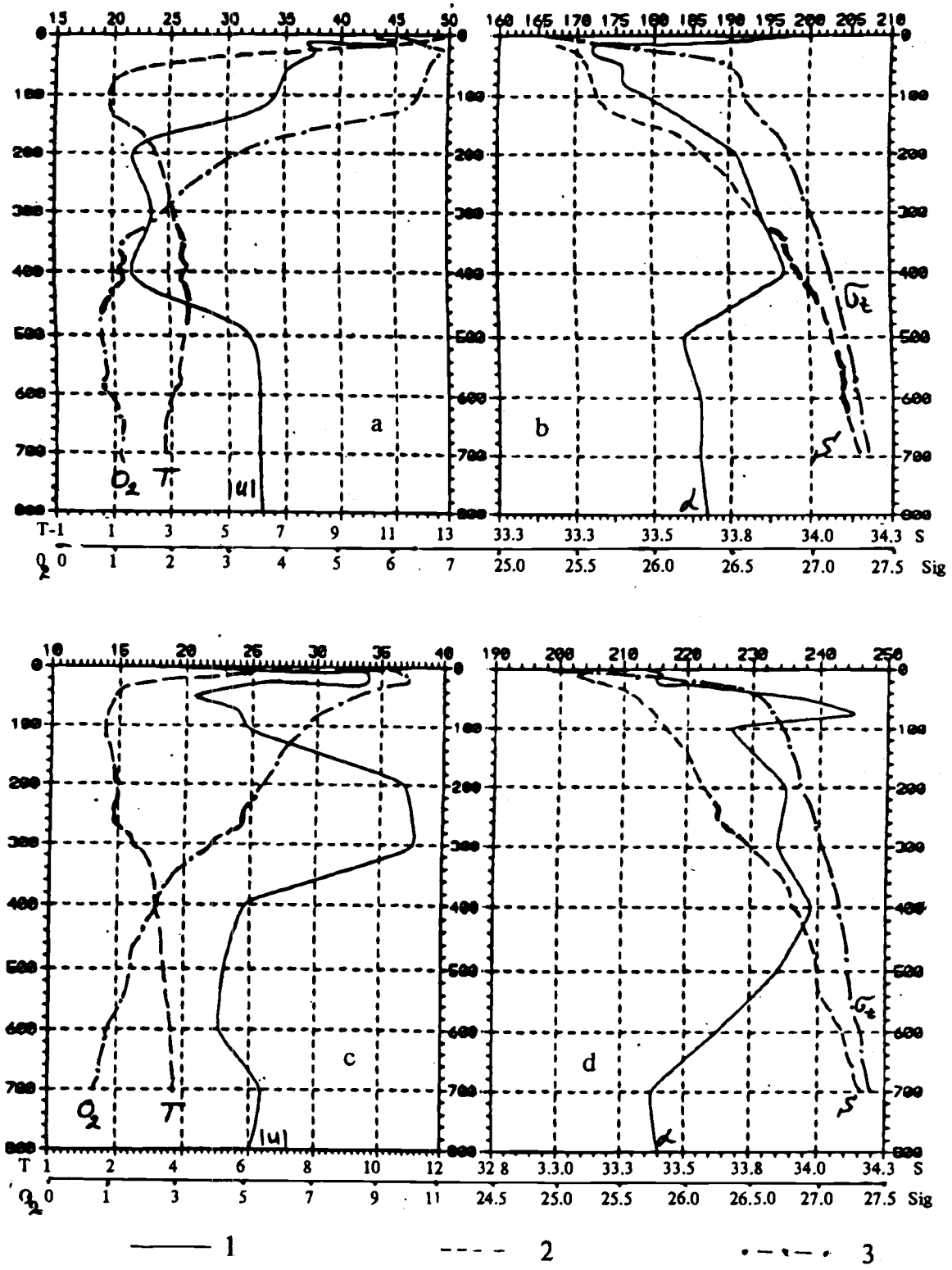

Fig. 4. Vertical profiles of water properties: current velocity (cm/s) - curve 1, temperature (°C) - curve 2, and dissolved oxygen (ml/l) - curve 3 (a, c); current direction - curve 1, salinity (ppt) - curve 2, and density anomaly - curve 3 (b, d) at stations 275 (a, b) and 276 (c, d), points A and B respectively in Fig. 1.

Hydrographic and Tracer Measurements of the Water Mass Structure and Transport in the Okhotsk Sea in Early Spring

Stephen C. RISER[1], Gennady I. YURASOV[2] and Mark J. WARNER[1]

[1] School of Oceanography, University of Washington, Seattle, U.S.A
[2] Pacific Oceanological Institute, Russian Academy of Sciences, Vladivostok, Russia

In April and May of 1995 a detailed survey of the most important portions of the Okhotsk Sea, including the Kuril Straits, the Kuril Basin, and northern part of the Okhotsk Sea was undertaken in a joint USA-Russian expedition aboard the Russian research vessel *Akademik Lavrentjev*. Observations were collected at over 160 stations in the Okhotsk Sea, using both CTD and Niskin bottle methods, with all measurements made over the entire water column. The parameters measured included temperature, salinity, dissolved oxygen, nutrients, chlorofluorocarbons, carbonate chemistry, and tritium and helium-3. A map of the expedition location is given in Fig. 1. Many of the data were collected close to the ice-edge or in regions where ice had been present only a few days or weeks before. The resulting data set represents one of the most complete modern surveys of the Okhotsk Sea in late winter/early spring conditions.

When plotted on a potential temperature-salinity (θ/S) diagram, the CTD data from these 160 stations are suggestive of the regional differences in the character of the water masses of the Okhotsk Sea, as shown in Fig. 2 (note that these are preliminary data, and some editing is obviously required). There are several branches to the main θ/S manifold in the region $1.0°C < \theta < 3.4°C$ and $33.0 < S < 34.6$. At the lowest temperatures in this region lies the main water of the upper 500 m of the Okhotsk Sea; at the highest temperature lies the water of the North Pacific Ocean, just outside Bussol' and Kruzenshtern Straits. Between these curves lie data from a number of stations that suggest the complexity of the mixing between the Okhotsk Sea and North Pacific. It appears that a third water mass, at potential temperatures somewhere between the general Okhotsk Sea and the North Pacific, lies between these extremes and exists as a result of mixing between these two endpoints. Similar properties can be seen in many of the chemical tracers collected on the expedition. It is suggested that the main mechanism responsible for this third curve is tidal mixing through the Kuril Straits.

At the highest densities in the Okhotsk Sea the water mass characteristics are asymptotically similar to the deep water of the North Pacific Ocean. This is due to the fact that the deepest entrance to the Okhotsk Sea is through Bussol' Strait, at a depth of 2,200 m. At depths greater than this within the Okhotsk Sea, in the Kuril Basin, there is no other apparent source of water. Stated differently, although the surface waters of the Okhotsk Sea in winter are among the coldest anywhere in the world ocean, there is no evidence of the occurrence of deep convection within the Okhotsk Sea. The dissolved oxygen concentrations and chlorofluorocarbon ratios in the deepest portions of the Kuril Basin (not shown) appears to preclude this possibility. The chlorofluorocarbon measurements suggest that the deepest waters of the Kuril Basin have not been exposed to the sea surface for 30-50 years, although waters above 1,000 m in the Sea appear to have been ventilated in the past 15 years. In general, the vertical distribution of these variables inside the Okhotsk Sea is quite different from the North Pacific, suggesting that vertical mixing is much stronger inside the Okhotsk Sea, perhaps again due to enhanced tidal activity.

At the lowest potential temperatures in the Okhotsk Sea ($\theta < 0°C$) two main masses of water appear to be present, both formed near the sea surface during the winter, both having some expression close to the freezing point of seawater. At the lowest salinities (< 32.7) and densities ($\sigma_\theta < 26.4$), the remnants of melting ice can be seen. At somewhat higher salinities (> 33.0) and densities ($\sigma_\theta > 26.5$) a second general water mass appears at these cold temperatures. This is the water discussed by Dr. Kitani that is formed by brine rejection under ice shelves. Almost all of this type of water was observed in the northwest Okhotsk Sea, off the northern coast of Sakhalin Island. Taken together, these measurements allow us to make better estimates of the water mass characteristics of the Okhotsk Sea, the residence time of water in the Sea, and the mechanisms that lead to the distributions of these water masses.

A central goal of this expedition was to examine the nature of the flow through the main passages between the Kuriles and the North Pacific, Bussol' Strait and Kruzenshtern Strait. A CTD section across Bussol' Strait was carried out twice over a 3-day period, and a section across Kruzenshtern Strait was run three times over a 2-day period. The repeat times of these sections were chosen to attempt to minimize effects of tidal aliasing. Potential temperature sections across Bussol' Strait are shown in Fig. 3; from the data it can clearly be seen that there is a great deal of change in the subsurface temperature field in Bussol' Strait over time scales of a day or two. Note especially the apparent warming in the western portion of the strait between section 1 and section 2 and the apparent cooling near the central portion of the strait, near the major topographic feature, also between section 1 and section 2. These changes suggest that there is a great deal of tidal energy present at the straits and that the flow near the straits changes on quite short time scales. With this in mind, it is suggested that it will in general be quite difficult to determine the low-frequency (i.e., geostrophic) flow through these straits with any acceptable degree of accuracy in the absence of a dedicated program to carry out direct measurements of currents in the straits for times of a few years or more.

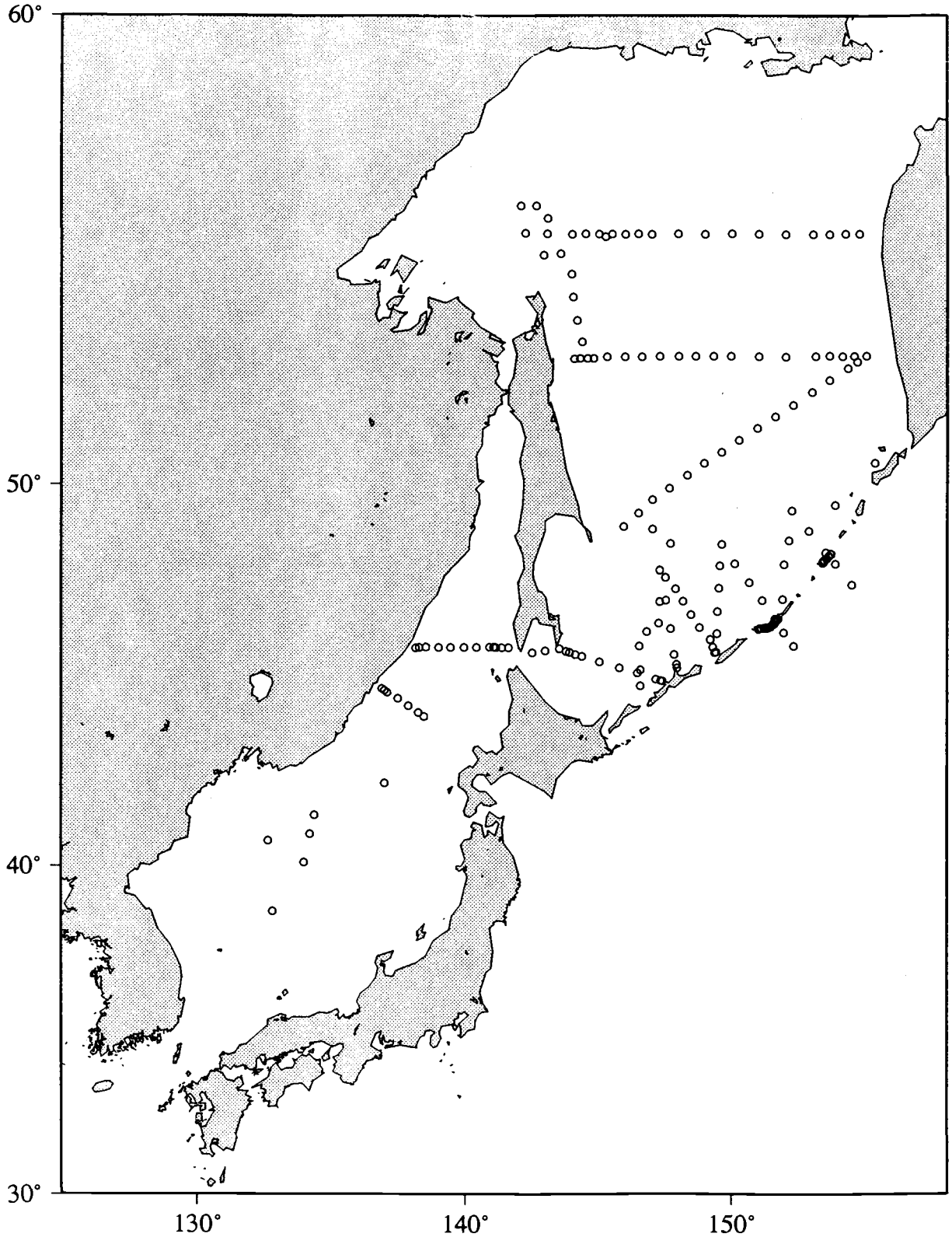

Fig. 1. Map of the expdeition location (R/V Akademik Lavrentjev, April-May 1995).

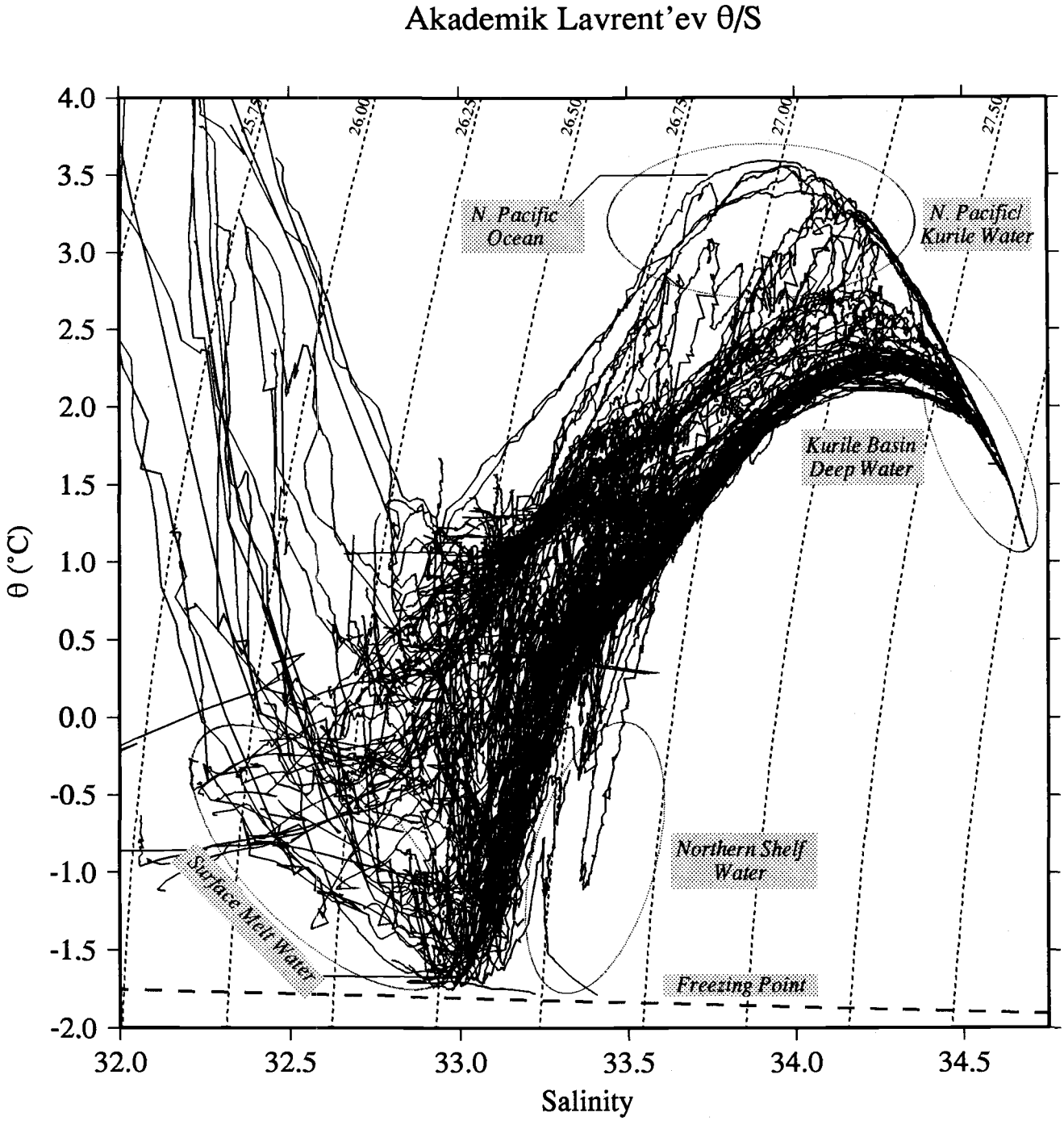

Fig. 2. Potential temperature - salinity diagrams for 160 CTD stations within the Okhotsk Sea in April-May 1995.

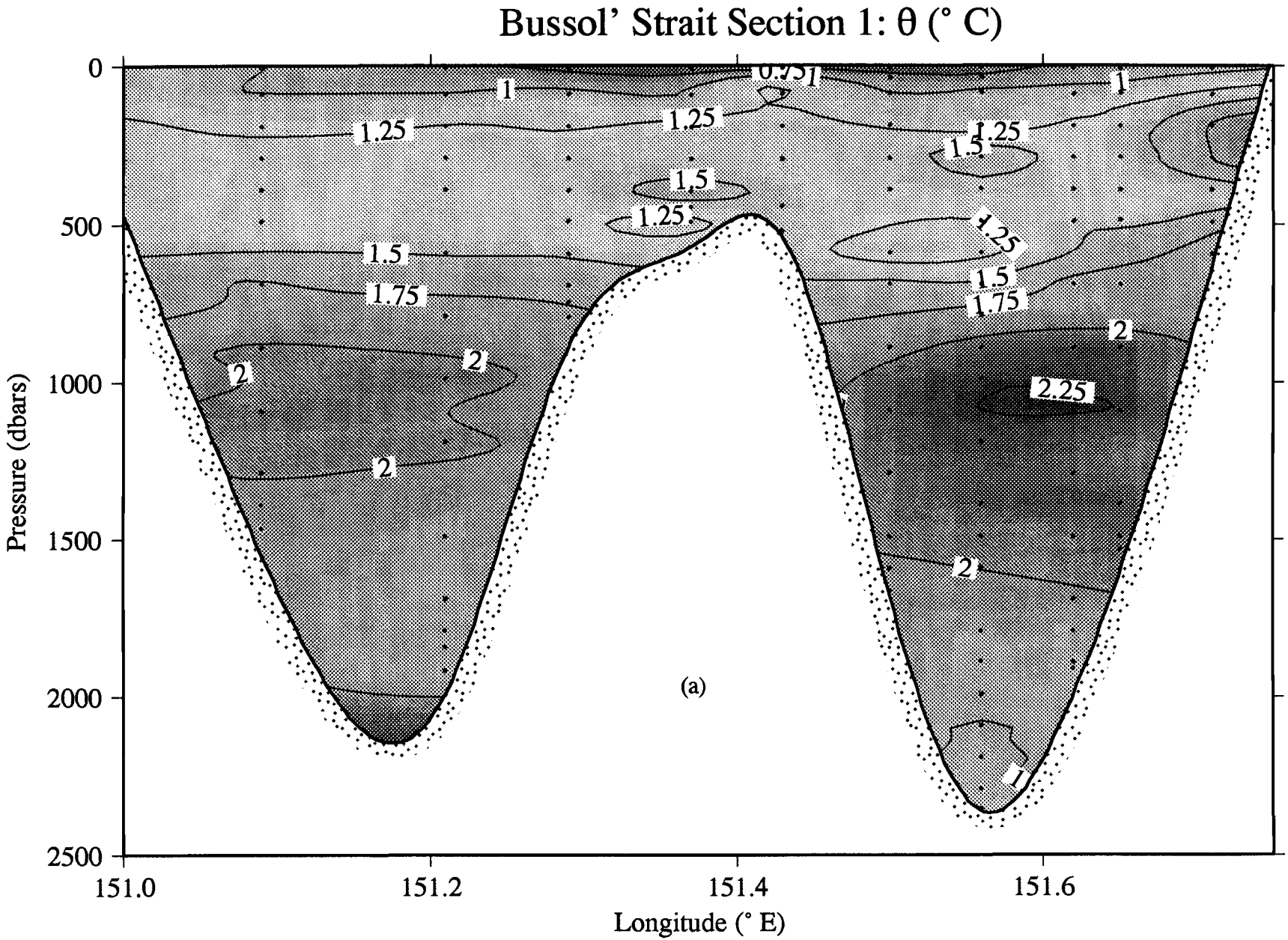

Fig. 3. Potential temperature sections across Bussol' Strait carried out over a 3-day period: (a) section 1; (b) section 2.

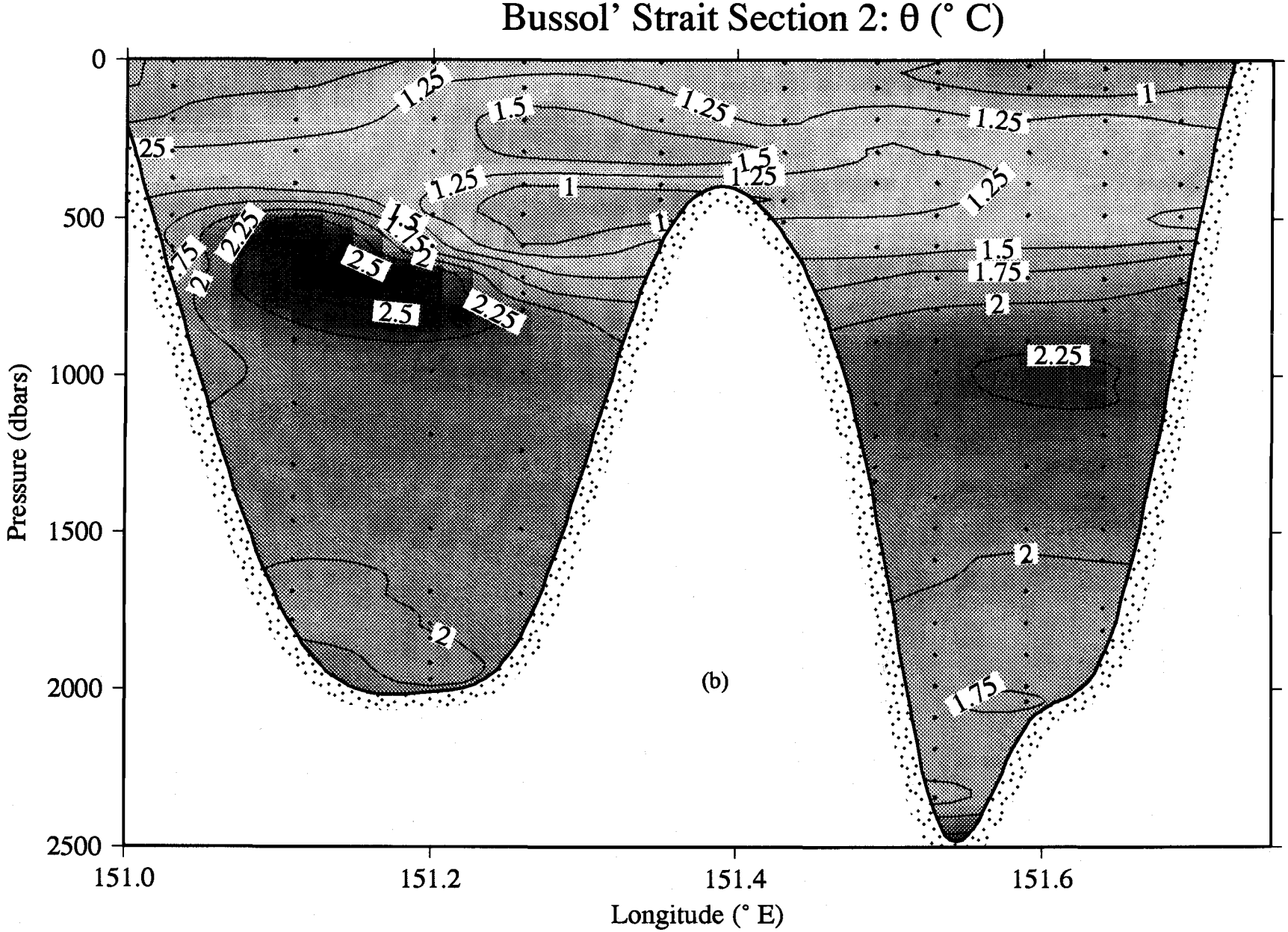

Fig. 3b. Section 2.

Circulation and Water Mass Structure in the Southern Okhotsk Sea, as Observed in Summer, 1994

Konstantin A. ROGACHEV[1] and Andrey V. VERKHUNOV[2]

[1] Pacific Oceanological Institute, Far Eastern Branch, Russian Academy of Sciences, Vladivostok, Russia
[2] Russian Federal Research Institute of Fisheries and Oceanography, Moscow, Russia

INTRODUCTION

Significant transformation of the subarctic water from the northern part of the Okhotsk Sea occurs in the Kuril Basin. Using satellite and a few CTD observations Alfultis and Martin (1987) and Wakatsuchi and Martin (1991) disclosed the anticyclonic circulation in the Kuril Basin in contrast with the large cyclonic Okhotsk Sea gyre by which cold northern shelf waters propagate to the Basin. The detailed synoptic structure of the Kuril Basin is studied insufficiently due to very sparse surveys.

In the present work we describe observations obtained in August 1994 during the cruise of the *RV "Akademik M.A. Lavrentyev"* and demonstrate that anticyclonic circulation in the Kuril Basin constitutes the chain of three anticyclonic eddies with their centers located along the axis of the Basin. Significant water mass transformation and mixing were revealed inside these eddies. Strong inflow of the Pacific warm intermediate waters to the Okhotsk Sea has been detected above 500 dbar (with geostrophic transport through the Boussole Strait of $9.8 \cdot 10^6$ m^3/s), while outflow from the Okhotsk Sea has been found at pressure below 750 dbar.

METHOD OF OBSERVATIONS

CTD survey has been conducted in the period from July 26 to August 26, 1994, using *NBMK3* instrumentation. *Guildline model 8737* probe provided by the Institute of Ocean Sciences (Sidney, B.C., Canada) and calibrated at IOS just before the cruise was used for inter-comparison of the data.

RESULTS

Fig. 1 shows the geopotential anomaly and geostrophic currents at 200 dbar relative to 1,000 dbar for the Kuril Basin area. Three anticyclonic eddies with diameters of 125-300 km in the Okhotsk Sea and one off Boussole Strait are clearly seen. The position of the eddy centers coincide with the Kuril Basin axis, similar to the Kuril Islands anticyclonic rings, which axis lies along the Kuril-Kamchatka trench. The Okhotsk Sea eddies of the Kuril Basin separate cold intermediate waters from the northwest Okhotsk Sea and warm intermediate waters penetrating through the Boussole Strait. The dynamic heights for the Kuril Basin anticyclonic eddies are higher than those in the center of the Boussole ring and have maximum value for the western ring of 12.5 J/kg. The lower boundary of the cold intermediate layer changes from 150 m within the Oyashio to 950 m in the center of the western anticyclone, the biggest eddy of the survey (Fig.2).

Geostrophic transport to the Okhotsk Sea

Recently, Stabeno and Reed (1994) evaluated geostrophic transport through the Aleutian Straits. A similar approach was used in the present work to calculate geostrophic transport (relative to 1,000 dbar) for the Kuril Straits area. We found that transport by the First Oyashio Branch (southward transport to the west of the Boussole ring) was $9.2 \cdot 10^6$ m^3/s, while total transport through the section across the Oyashio First Branch and anticyclonic eddy was $10.4 \cdot 10^6$ m^3/s. The transport through the Boussole Strait to the Okhotsk Sea has been computed as $9.8 \cdot 10^6$ m^3/s. These data contradict the earlier estimations of geostrophic outflow through the Boussole Strait (Reid, 1973). However, despite the uncertainties of geostrophic transport calculations for the Strait area, we assume that the direction of flow reflects the propagation of warm intermediate waters to the Okhotsk Sea. This penetration is clearly seen in the temperature and salinity profiles (Fig. 3).

Penetration of warm intermediate layer to the Okhotsk Sea

A warm intermediate layer to the east of the Kuril Islands was observed at 200-700 dbar. Its maximum temperature was 3.55°C at 300 dbar on station 86. Warm layer with temperature of 3.54°C was also found at 500 dbar on station 82 in the canyon of the Boussole Strait. Simultaneously, water with temperature from 2.6 to 2.68°C was revealed at the other side of the Boussole Strait in the Okhotsk Sea on stations 94 and 95 at 650 dbar. It was the highest temperature of the intermediate waters in the Okhotsk Sea in the area of study. Salinity in the warm core continuously decreased from 33.983 psu (station 86 at 300 dbar) and 33.987 psu (station 82 at 500 dbar) to 33.840 psu (station 94 at 650 dbar) and 33.903 psu (station 95 at 650 dbar). It appears that warm intermediate water penetrates through the Strait deepening gradually from 300 dbar to 650 dbar between station 86 and stations 94-95. Abrupt changes which lead to the temperature and salinity decrease were detected within the Boussole Strait.

Okhotsk water outflow through the Boussole Strait

Our observations in the Boussole Strait canyon (station 82) strictly demonstrated a four-layer vertical water structure (Fig. 4): the surface warm layer (at pressure less than 100 dbar); the cold intermediate layer (typical for summer) with the core at 100 dbar; the warm intermediate subarctic layer (with distinct boundaries at pressures of 450 and 780 dbar) characterized by temperature higher than 3.2°C and salinity over 34.0 psu. However, the most interesting feature of the vertical structure is the lower layer of water which is relatively cold (< 2.3°C), fresh and rich in oxygen. A very sharp dropping of salinity and temperature, as well as an increasing of oxygen concentration take place at a pressure of 780 dbar. Comparison of TS diagrams for stations 82 and 94-97 shows that water of this layer originates from the Okhotsk Sea, i.e. below the warm intermediate layer the TS diagram of station 82 coincides with those in the Okhotsk Sea. Note, that Okhotsk Sea waters in TS diagrams are obviously separated from the Oyashio and Kamchatka current waters with its lower temperature and higher salinity at maximum temperature. Hence, the gap between TS-curves for ocean and Okhotsk Sea stations is evident. Similar signs of the Okhotsk Sea outflow were observed at station 85, however, at station 82 they were more pronounced. The reason could be that this particular station is located exactly in the Boussole Strait canyon.

The CTD results are confirmed by the oxygen bottle data. The Okhotsk Sea water is characterized by high oxygen saturation (up to 15% at pressure of 1,000 dbar) and the absence of an oxygen minimum within the Boussole Strait at pressures less than 1,000 dbar. Meanwhile, oxygen minimum with saturation below 10% and absolute values less than 0.7 ml/l (station 80) exists in the

ocean to the east of the Strait at pressures of 700-850 dbar. Therefore, oxygen concentration of 1.32-1.69 ml/l and saturation of 17-22% at 800-1000 dbar detected at station 82 clearly prove that these waters have originated from the Okhotsk Sea.

Two stations were taken in the Boussole Strait canyon in April 1995, during the joint Russian-USA expedition to the Okhotsk Sea on board of the *RV "Akademik M.A. Lavretyev"*, in which the first co-author participated. These results (not shown here and kindly provided by Dr. S. Riser from the University of Washington and Dr. G. Yurasov from the Pacific Oceanological Institute) definitely indicate the gap between TS-curves for stations at the opposite sides of the Boussole Strait, similar with 1994 data. In particular, vertical structure at station 23 in the Boussole Strait canyon was similar to station 82 (August 1994): cold and relatively fresh layer with high oxygen concentration was found below the warm intermediate layer at pressure 800 dbar. Thickness of this layer was greater than 400 dbar and its thermohaline characteristics coincide with the Okhotsk Sea waters.

Talley (1991) described unusually cold, fresh and rich-oxygen water with sigma-theta of 27.4 at pressure of 800 dbar, observed off the Boussole Strait in August 1985. Isopycnal maps allow the conclusion that this water has an Okhotsk Sea origin. The only station considered by Talley (1991) shows an anomaly of temperature, salinity and oxygen in the layer of 100 m thickness, which is much less than during our survey. It can be explained by the greater distance of this station from the Strait, as compared with our station 82 in August 1994. Moreover, anomalies of temperature and salinity with respect to neighboring waters reached 0.2-0.5°C and 0.07 psu in 1985, whereas anomalies of 0.84°C, 0.08 and 1 ml/l for temperature, salinity and oxygen were revealed in 1994.

Therefore, these observations permit the assumption of the regular outflow from the Okhotsk Sea through the Boussole Strait at pressure below 800 dbar and inflow of warm subarctic waters through this Strait at 300-700 dbar.

ACKNOWLEDGMENTS

We deeply appreciate the efforts of scientific and ship's personnel of the *RV Akademik M.A. Lavrentyev*. We are especially grateful to Drs. Stephen Riser and Gennady Yurasov who provided additional data for the Boussole Strait area mentioned above.

REFERENCES

Alfultis, M.A. 1987. Martin S. Satellite passive microwave studies of the sea of Okhotsk ice cover and its relation to oceanic processes, 1978-82. J. Geophys. Res. 92(C12):13013-13028.

Reid, J.L. 1973. Northwest Pacific Ocean waters in winter. John Hopkins Oceanogr. Studies. 5:1-96.

Stabeno, P.J., and R.K. Reed. 1992. A major circulation anomaly in the western Bering Sea. Geophys. Res. Lett. 19:1671-1674.

Talley, L.D. 1991. An Okhotsk sea water anomaly: Implication for ventilation in the North Pacific. Deep-Sea Res. 38:S171-S190.

Wakatsuchi, M., and S. Martin. 1990. Satellite observations of the ice cover over the Kuril Basin region of the Okhotsk sea and its relation to the regional oceanography. J. Geophys. Res. 95(C8):13393-13410.

FIGURES

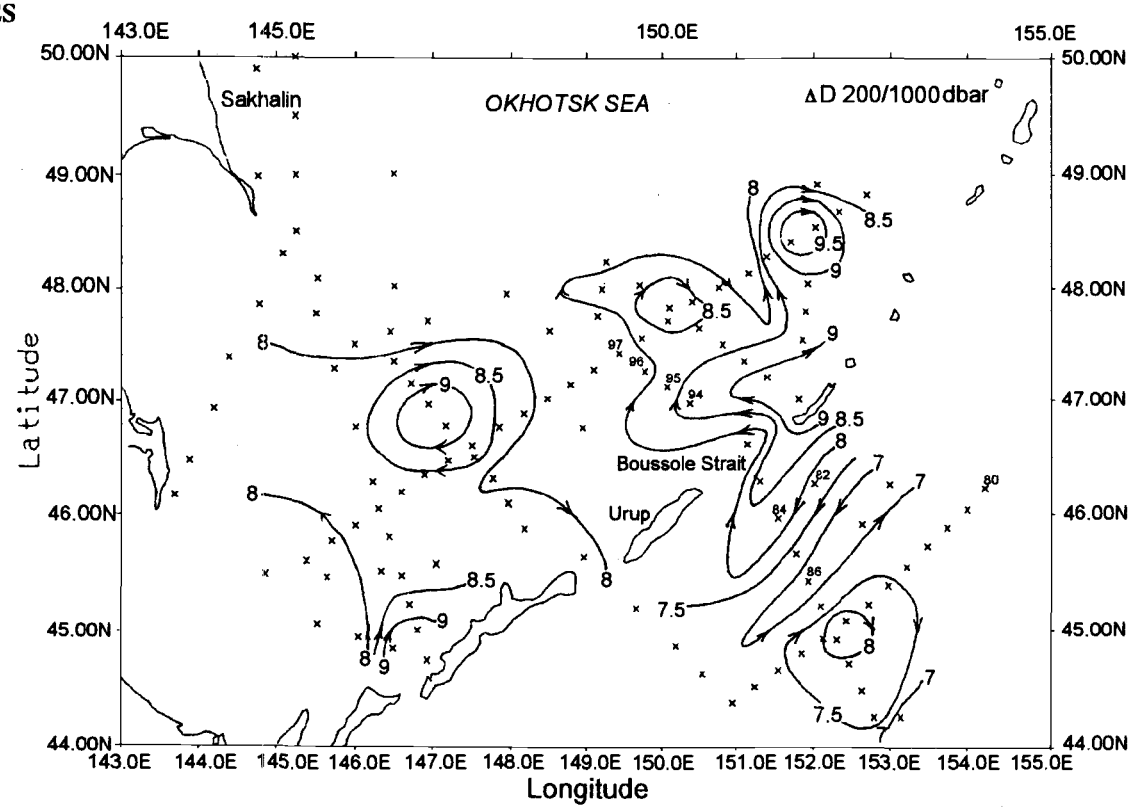

Fig. 1. Geopotential anomaly (J/kg) at 200 dbar, relative to 1,000 dbar, observed in August, 1994.

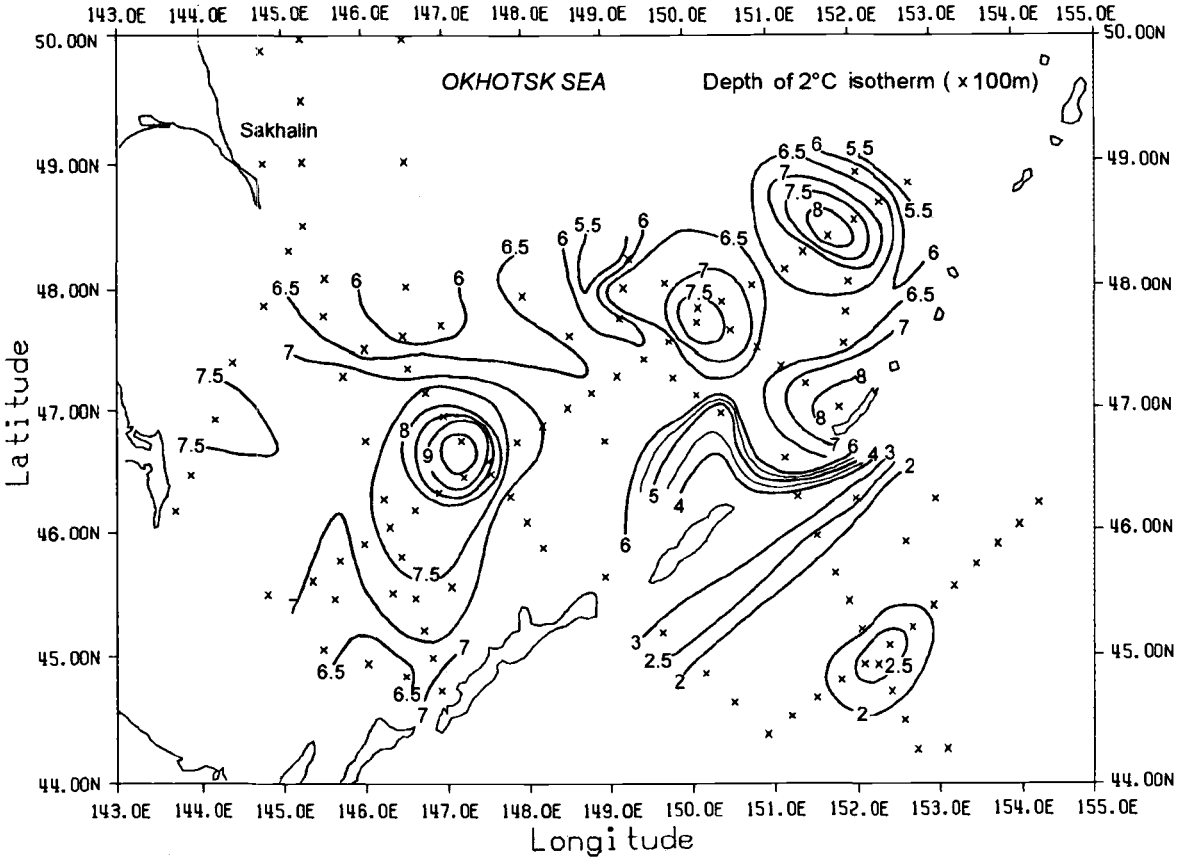

Fig. 2. Depth of 2°C isotherm (x 100m), observed in August, 1994.

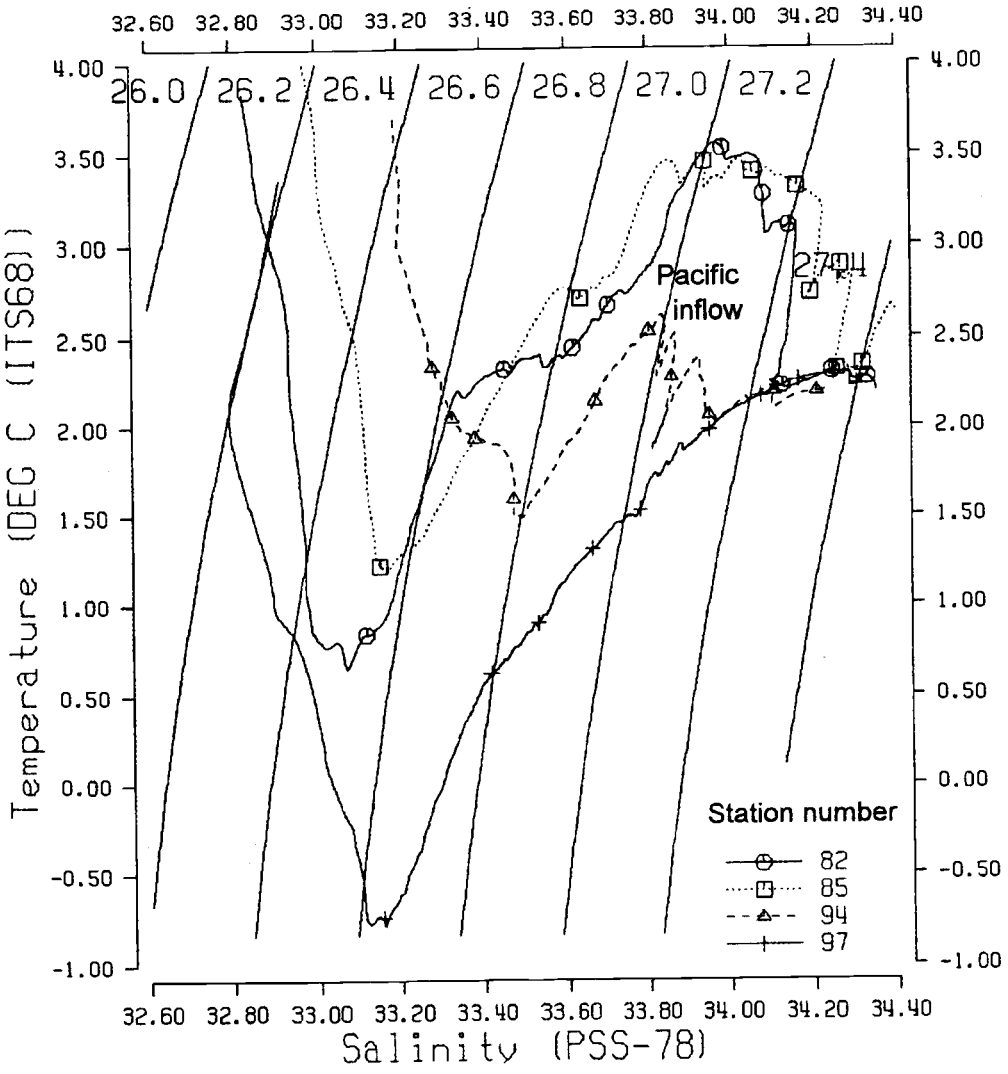

Fig. 3. TS - diagrams for selected stations near the Boussole Strait.

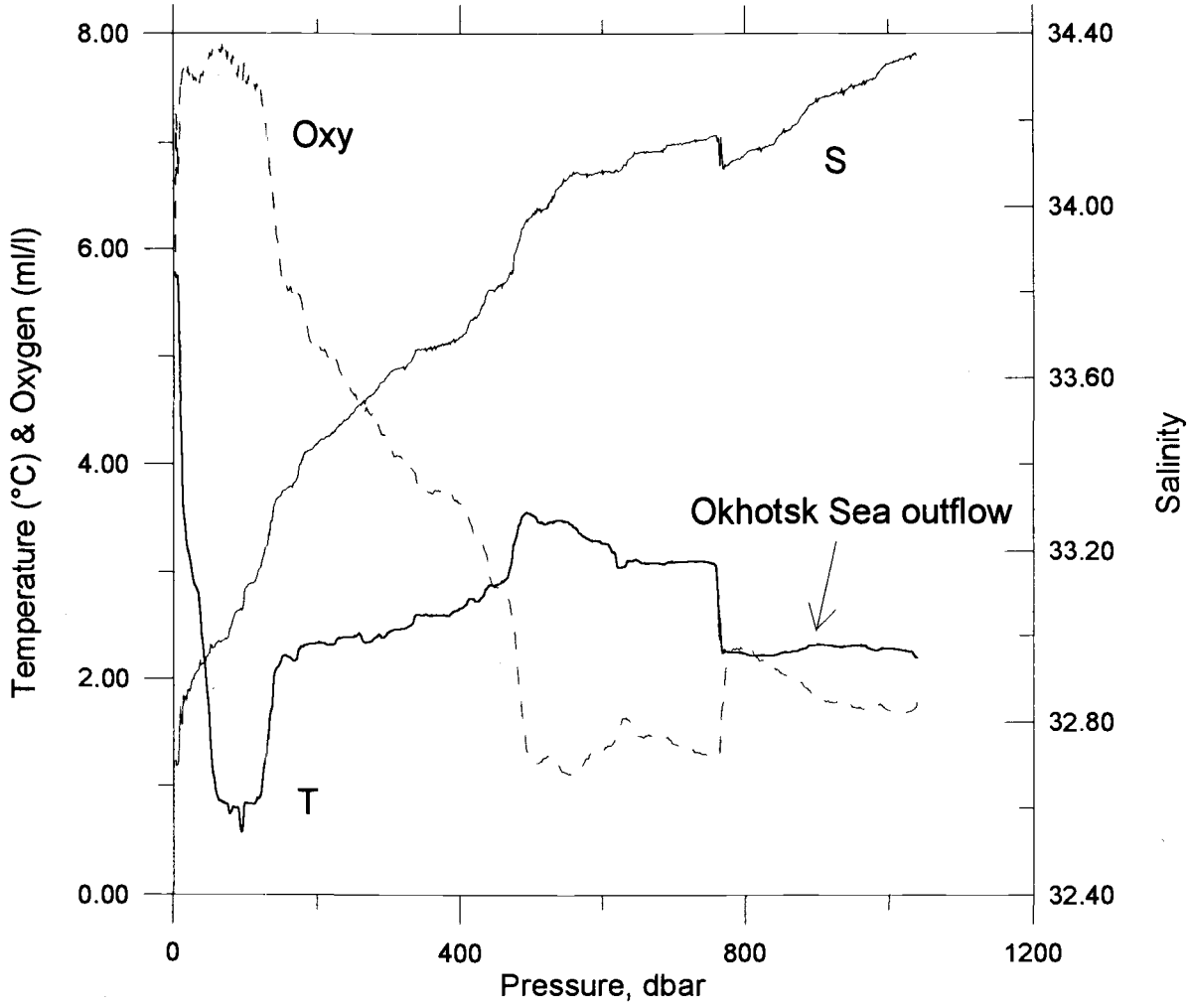

Fig. 4. Vertical profiles of temperature (T), salinity (S) and dissolved oxygen (Oxy) at station 82 near the Boussole Strait. Okhotsk Sea outflow is observed deeper than 780 dbar.

North Pacific Intermediate Water Formation and the Role of the Okhotsk Sea

Lynne D. TALLEY

Scripps Institution of Oceanography, University of California, San Diego, U.S.A.

The following is an extended abstract of a talk which was presented on NPIW, with emphasis on how the salinity minimum forms in the Mixed Water Region. A more general talk, which included more emphasis on the role of the Okhotsk Sea, was presented separately. Because this is an extended abstract, the references are greatly truncated and include primarily my own work. More complete references can be found in those publications.

LARGE-SCALE PROPERTIES OF NORTH PACIFIC INTERMEDIATE WATER

North Pacific Intermediate Water (NPIW) can be defined as either the salinity minimum of the subtropical gyre of the North Pacific, at a potential density of 26.7 to 26.8 sigma-theta, or as the subtropical layer which is freshened by subpolar water with a potential density range of about 26.65 to 27.6. The subtropical gyre's salinity minimum is evident in any vertical section of salinity which crosses it.

The NPIW salinity minimum should be carefully differentiated from the shallower salinity minima which are found in the eastern and tropical North Pacific, and from the Antarctic Intermediate Water (AAIW) found in the tropical Pacific, because their sources differ from that of NPIW. The shallower salinity minima, arrayed around the eastern subtropical gyre, arise from subduction of surface waters as they move southward and encounter less dense surface waters (Talley, 1983; Yuan and Talley, 1992). Antarctic Intermediate Water comes from the south and is found up to the southern boundary of the subtropical gyre, although there is some controversy about whether the salinity minimum in the North Pacific's tropical region really derives more from NPIW than from AAIW.

The NPIW salinity minimum is found only in the subtropical gyre (Sverdrup et al., 1942; Talley, 1993) although isopycnal properties show that its low salinity clearly arises in the subpolar region (Reid, 1965; Talley, 1993). Its northern and southern boundaries are well-defined and coincide respectively with a deep expression of the Subarctic Front and the southern side of the subtropical circulation, which is relatively far to the north at the NPIW depth. Its eastern boundary is less easy to define, but the eastern Pacific's California Current is a region of multiple or missing salinity minima, and it appears that intact NPIW does not extend into this region (Talley, 1993).

The NPIW's salinity minimum has a density of 26.7 to 26.9 sigma-theta in the subtropical Pacific (Fig. 1 from Talley, 1993). Where a portion of the NPIW protrudes southward along the western boundary in the Mindanao Current, it appears to be truncated from below and its density can be lower (Bingham and Lukas, 1994). In the Mixed Water Region (MWR) between the separated Kuroshio and Oyashio, NPIW salinity minima are found in this full range of densities; the denser minima have higher salinity and lower oxygen and are apparently old NPIW which has entered the MWR from the Kuroshio. The lighter minima are considered here and in Talley et al. (1995) to be the newest NPIW.

If low salinity and high oxygen are considered to indicate the most recently-ventilated NPIW, then the region of newest NPIW is the northwestern subtropical gyre, in the MWR, based on salinity and oxygen distribution at the NPIW salinity minimum (Talley, 1993). Away from this location of new NPIW, salinity increases, probably due to vertical diffusion and possibly horizontal diffusion along the eastern and southern sides of the gyre; oxygen decreases due to consumption and diffusion. The highest NPIW salinity is found in the southwestern subtropical gyre and in the Kuroshio and Mindanao Currents. Lowest oxygen is found in these regions as well.

CIRCULATION AND TRANSFORMATION IN THE OKHOTSK SEA

In the wintertime, surface densities in the open North Pacific do not exceed approximately 26.65 sigma-theta except in very localized coastal regions. Even these small regions around Hokkaido and northern Honshu do not ventilate water much denser than 26.7 sigma-theta. What is the source of fresh, oxygenated water at densities greater than 26.65 sigma-theta? It appears that the source is the Okhotsk Sea, and results from direct ventilation of densities 26.6 to 27.2 sigma-theta. On isopycnals which intersect the NPIW salinity minimum, it is clear that the highest oxygen and lowest salinity are found in the Okhotsk Sea (Talley, 1991; hints of this in Reid, 1965, 1972). In fact, the highest oxygen, suggestive of the most recent ventilation are found in the Okhotsk Sea for all densities from 26.7 to 27.6 sigma-theta, which is the density at the greatest sill depth separating the Okhotsk Sea and the NW Pacific. The lowest salinities for this density range and even lower are also found in the Okhotsk Sea. Thus one concludes that the Okhotsk Sea is the site for the densest ventilation impacting isopycnals in the open North Pacific. (While deep water is formed in the Japan Sea, its dense waters do not connect with the open North Pacific.)

Most of the Okhotsk Sea ventilation occurs under sea ice in winter. Winter surface density in open water in the Okhotsk Sea does not appear to much exceed 26.7 sigma-theta, even though waters are clearly ventilated to much greater densities. Brine rejection is a very effective mechanism for increasing the density of near-freezing surface water. Dense, cold water has been observed on the shelves of the northern and western Okhotsk Sea (Kitani, 1973). Based on water properties in the western Okhotsk Sea, it appears that the brine rejection mechanism might be operative to a maximum density of about 27.2 sigma-theta (Talley, 1991). Because this mechanism deposits a very cold water on denser isopycnals, this water is also the freshest on those isopycnals, although there is a net flux of salt downward.

The Okhotsk Sea also contains the North Pacific's freshest, most oxygenated water at densities greater than 27.2 sigma-theta. Based on isopycnal salinity and oxygen distributions, Talley (1991) hypothesized that the principal mechanism for this "ventilation" is vertical mixing primarily within the Okhotsk Sea, and operating most vigorously close to Bussol' Strait. Bussol' Strait is the deepest passage through the Kuril Islands, with a sill depth of 2300 meters, and sill density of about 27.6 sigma-theta. This argument is a refinement of Reid's (1965) argument that vertical diffusion in the North Pacific carries the low salinity surface signature downward - the refinement is to suggest that much of the vertical diffusion is localized. Moroshkin (1966) concluded that there is a great deal of mixing in the Kuril Straits. The primary mechanism for mixing might be tidal flows, which are on the order of 4-5 knots near the surface through the various straits.

In the following few paragraphs the circulation and transformation in the Okhotsk Sea are reviewed; a much more complete review can be found in the PICES Scientific Report on the Okhotsk Sea (Talley and Nagata, 1995).

The Okhotsk Sea is the northwesternmost region of the subpolar gyre (Fig. 2). Much of it is ice-covered in winter, although the ice melts away completely each summer. It is connected to the open North Pacific through the Kuril Island chain, and so the subpolar circulation which enters the Okhotsk Sea must do so through island passages. The two most important passages are Bussol' and Kruzenshtern Straits. Part of the East Kamchatka Current, flowing southward out of the Bering Sea, enters the Okhotsk Sea, and part remains outside. Some of the western boundary current might also enter at Bussol' Strait which is also the primary site of the denser outflow. The outflow turns southwestward and becomes the Oyashio. The net exchange between the open North Pacific and the Okhotsk Sea is on the order of 3-5 Sv, although a very good estimate is not possible using available data.

Within the Okhotsk Sea, the flow is basically cyclonic, but eddy activity is prominent, as are local gyres. In this sense it resembles the Bering Sea, which is also separated by an island chain from the open Pacific. Local circulation features in the Okhotsk Sea which appear to be important for water mass transformation are the northern shelf region where coastal polynyas are often found, Kashevarov Bank around which there is commonly intensified cyclonic flow and above which there is upwelling, the East Sakhalin Current which transports dense, ventilated waters southward from the northern shelf region, the Soya Current which transports saline Japan Sea water into the Okhotsk Sea, and an anticyclonic gyre and anticyclonic eddy field in the Kuril Basin which spreads the saline Soya Current waters into the Okhotsk Sea.

Two important physical elements for dense water formation in the Okhotsk Sea are the input of saline water in the Soya Current, which preconditions the Okhotsk Sea to forming denser water, and sea ice formation which produces dense shelf water through brine rejection. Sea ice forms along the northwestern boundary in December and eventually covers most of the northern and western parts of the sea. A coastal polynya appears in mid-winter along the northwestern side; observations of the densest, saline waters have been along this shelf. Kitani (1973) observed shelf water at nearly 27.05 sigma-theta, and showed that the very coldest waters in the summer temperature minimum, indicative of freezing in winter, were located in the northwestern Okhotsk Sea. The exception is above Kashevarov Bank, where strong tides mix the warmer deep water upwards; a polynya is usually found in this location in winter. Since the surface waters in the coastal polynya are probably near freezing, it is more likely to produce the densest water than would the Kashevarov polynya, whose waters are relatively warm.

The dense waters formed in the northern Okhotsk Sea are advected southwards in the East Sakhalin Current and then over towards Bussol' Strait, based on isopycnic properties (Talley, 1991). Strong tides are found around the Kuril Islands, including in Bussol' Strait. These produce a mixed water around the islands (Kawasaki, these proceedings; Kawasaki and Kono, 1993) which includes components of waters from outside the Kurils and which is also vertically mixed, so that the water which leaves the Okhotsk Sea is not pure Okhotsk Sea water. The newly-ventilated and mixed Okhotsk Sea waters join waters from the East Kamchatka Current and flow southwestward towards Hokkaido.

FORMATION OF THE NPIW SALINITY MINIMUM IN THE MIXED WATER REGION

The ventilated water from the Okhotsk Sea exits primarily through Bussol' Strait and joins the southward flow of the Oyashio towards Hokkaido. The Oyashio separates from the western boundary at the southern end of Hokkaido and flows eastward. It typically meanders at least twice, in well-known locations, after it separates (e.g. Kawai, 1972). Some of the Oyashio water separates off and remains in the MWR while the remainder circulates eastward as part of the subpolar gyre circulation.

The MWR occupies an interesting dynamical niche in the North Pacific's gyre circulations. First, it is bounded to the north and south by vigorous, meandering separated boundary currents, which spawn "rings" or "intrusions" into the MWR, so it is a mixing region between Oyashio and Kuroshio waters. (A third source of water for the region is flow from the Japan Sea through Tsugaru Strait, which affects the uppermost density layers, and introduces extra salinity which preconditions the MWR to have higher winter surface densities, on the order of 26.65 sigma-theta [Talley, 1991].) Second, the MWR is part of the subtropical gyre in terms of Sverdrup transport but it is also a region of Ekman upwelling; these can coexist because of the southwest-northeast tilt of the zero of Ekman pumping over the whole North Pacific (Yuan and Talley, 1992).

The complexity of the MWR is evident in any depiction of water properties in the region. Analyses of temperature at 100 meters are produced monthly by the Japan Meteorological Association; an example during April, 1989 (selected because it was the period chosen for Talley et al.'s [1995] CTD analysis) shows an intrusion of cold water of Oyashio origin down the coast of Honshu, a patch of warm water east of Hokkaido at the usual location between the first two Oyashio "intrusion" or meanders and warm water originating from Tsugaru Strait. CTD sections are occupied regularly along 144°E and show the wall of the Kuroshio, often a warm core ring to its north, and the more density-compensated signature of the Oyashio (e.g. Talley et al., 1995). NPIW is found as a salinity minimum south of the Oyashio front; on the sections which we analyzed it was in almost pure form in the Kuroshio warm core ring.

Temperature / salinity profiles in the MWR away from the near-coastal regions can be classified in four to five relatively well-defined categories (Talley et al., 1995): Kuroshio (subtropical) water, Oyashio (subpolar) water, Tsugaru Water, and one or two classes of mixed water (subtropical and subpolar transitional water), in which the upper part of the T/S relation is dominated by Kuroshio water, the middle by the mixture of Oyashio and Kuroshio water, and the lower by either Kuroshio or Oyashio water. A salinity minimum occurs in all but Oyashio water. The subtropical transitional water is considered to contain the "new" NPIW. A map of the MWR in April, 1989 plus earlier sections at 152°E shows new NPIW in patches through the MWR west of 144°E and completely dominating the MWR by 152°E. Using the definition of the subtropical transitional water as the new NPIW, and assuming primarily isopycnal processes on a large scale, we find that new NPIW is composed of about 45% Oyashio water and 55% Kuroshio water (Talley et al., 1995). This ratio breaks down at densities lower than 26.65 sigma-theta, suggesting that much less Oyashio water is available at lower densities.

New NPIW is therefore formed when the ventilated, freshened Oyashio waters encounter the older, more saline waters of the Kuroshio; their mixture creates a salinity minimum. What sets the density of the actual minimum? The density of new NPIW is slightly greater than 26.7 sigma-theta. The surface density in winter in most of the Oyashio and northern Mixed Water Region achieves 26.65 regularly, implying a steady and large source of newly ventilated water at this density. At a few small coastal patches density greater than 26.7 is achieved but they do not seem to produce enough water to influence the density of the NPIW. A density of 26.7 sigma-theta is also clearly denser than most surface water even in the open Okhotsk Sea in winter.

The robustness of the NPIW density after formation, and its nearness to the Oyashio winter surface density suggests that winter surface density is important, but there must also be a density-increasing mechanism. The obvious candidates are cabbeling and double diffusion. Cabbeling is obviously most effective when the source waters are very different, as they are in the MWR. It is easy to show that a mixture of Oyashio and Kuroshio waters of approximately 45%:55% can produce a density increase of about 0.06 sigma-theta, which is clearly enough to increase the density of the Oyashio's winter surface water to greater than 26.7 sigma-theta after it mixes with Kuroshio water

(Fig. 1). Therefore our hypothesis is that the NPIW salinity minimum density is set by: (1) intrusion of Oyashio waters into Kuroshio waters, with the largest volume of Oyashio water near the surface being at its winter mixed layer density, and (2) mixing/cabbeling of these waters.

How much NPIW is formed? In order to answer this, the question needs to be better posed. It can mean either how much ventilation occurs in the NPIW density range (i.e., how much surface water is converted to water in some specified density range each year), or it can mean how water of this density range enters the subtropical gyre from the subpolar gyre each year? In Talley et al. (1995) we answered the latter question, using a density range of 26.65-27.4 sigma-theta. Subsequent calculations have modified the estimates published in that paper. We used two ways to estimate the exchange of Oyashio water into the subtropical gyre: (1) calculating the eastward transport of new NPIW and the amount of pure Oyashio water included in the new NPIW across 152°E south of the subarctic front, and (2) estimating the amount of Kuroshio water which enters the MWR based on the average number of warm core rings formed each year. Using transports across 152°E (and also 165°E and 175°E), we found that 6.1Sv of new NPIW were moving eastward between the subarctic front and the Kuroshio; thus there were 2.7Sv of Oyashio water included in this.

NORTHWEST PACIFIC TRANSPORT BALANCES

A much better-posed question than the formation rate of "new NPIW" is: what is the total transport of Oyashio water into the subtropical gyre. Since the Kuroshio itself begins to incorporate the new NPIW immediately after it separates from Honshu, and the freshening then begins to spread into the Kuroshio recirculation to the south, a complete estimate of the total of new NPIW must include the Kuroshio and its recirculation. At this point it becomes difficult to define "new NPIW" since various mixtures of old and new are involved. Using the same 152°E sections as in Talley et al. (1995), a new estimate of the total amount of Oyashio water being transported eastward south of the subarctic front is 4-5 Sv.

The total Oyashio transport east of Hokkaido is on the order of 10-15 Sv in the upper 1,000 meters. Therefore 5-10 Sv remain in the subarctic gyre while 4-5 Sv cross into the subtropical gyre. A schematic of upper layer transports through the northwestern Pacific, including exchanges with and transformations in the Okhotsk Sea, and the transport of Oyashio water into the subtropical gyre is shown in Fig. 2. Various estimates of the East Kamchatka Current transport in the upper 1,000 meters yield 15-25 Sv (Talley and Nagata, 1995). Approximately 3-5 Sv enter and circulate through the Okhotsk Sea, in which approximately 1 Sv of surface water is transformed into water in the NPIW density range. The Oyashio carries about 10-15 Sv southward. Thus approximately 1/4 of the Oyashio transport is cycled through the Okhotsk Sea, and of this about 1/4 is new dense water. The ventilation time scale for the subpolar gyre, based on the 1 Sv transformation in the Okhotsk Sea, is on the order of several decades. This seems rather long, and hence the total ventilation rate is probably underestimated. Study of these balances is continuing.

REFERENCES

Bingham, F. M., and R. Lukas. 1994. The southward intrusion of North Pacific Intermediate Water along the Mindanao coast. J. Phys. Oceanogr. 24:141-154.

Kawai, H. 1972. Hydrography of the Kuroshio extension. *In* H. Stommel and K. Yoshida [ed.] Kuroshio: physical aspects of the Japan Current.

Kawasaki, Y., and T. Kono. 1993. Water exchange between the Okhotsk Sea and the North Pacific. Abstract of PICES Nemuro Workshop on western subarctic circulation '93.

Kitani, K. 1973. An oceanographic study of the Okhotsk Sea - particularly in regard to cold waters. Bull. Far Seas Fish. Res. Lab. 9:45-76.

Moroshkin, K.V. 1966. Water masses of the Sea of Okhotsk. U.S. Department of Commerce; Clearinghouse for Federal Scientific and Technical Information, Joint Publication Research service 43, 942, 98 p. Translation of Vodnyye massy Okhostkogo Morya, Nauka publishing house, Moscow. 66 p.

Reid, J.L. 1965. Intermediate waters of the Pacific Ocean. Johns Hopkins Oceanogr. Studies. 2:1-85.

Talley, L.D. 1983. Ventilation of the subtropical North Pacific: the shallow salinity minimum. J. Phys. Oceanogr. 15:633-649.

Talley, L.D. 1991. An Okhotsk Sea Water anomaly: implications for ventilation in the North Pacific. Deep-Sea Res. 38:S171-S190.

Talley, L.D. 1993. Distribution and formation of North Pacific Intermediate Water. J. Phys. Oceanogr. 23:517-537.

Talley, L.D., Y. Nagata, M. Fujimura, T. Iwao, T. Kono, D. Inagake, M. Hirai, and K. Okuda. 1995. North Pacific intermediate water in the Kuroshio/Oyashio mixed water region. J. Phys. Oceanogr. 25:475-501.

Talley, L.D., and Y. Nagata. 1995. The Okhotsk Sea and Oyashio Region. PICES Scientific Report No. 2, North Pacific Marine Science Organization (PICES), Institute of Ocean Sciences, Sidney, BC, Canada. 227 p.

Yuan, and L.D. Talley. 1992. Shallow salinity minima in the North Pacific. J. Phys. Oceanogr. 22:1302-1316.

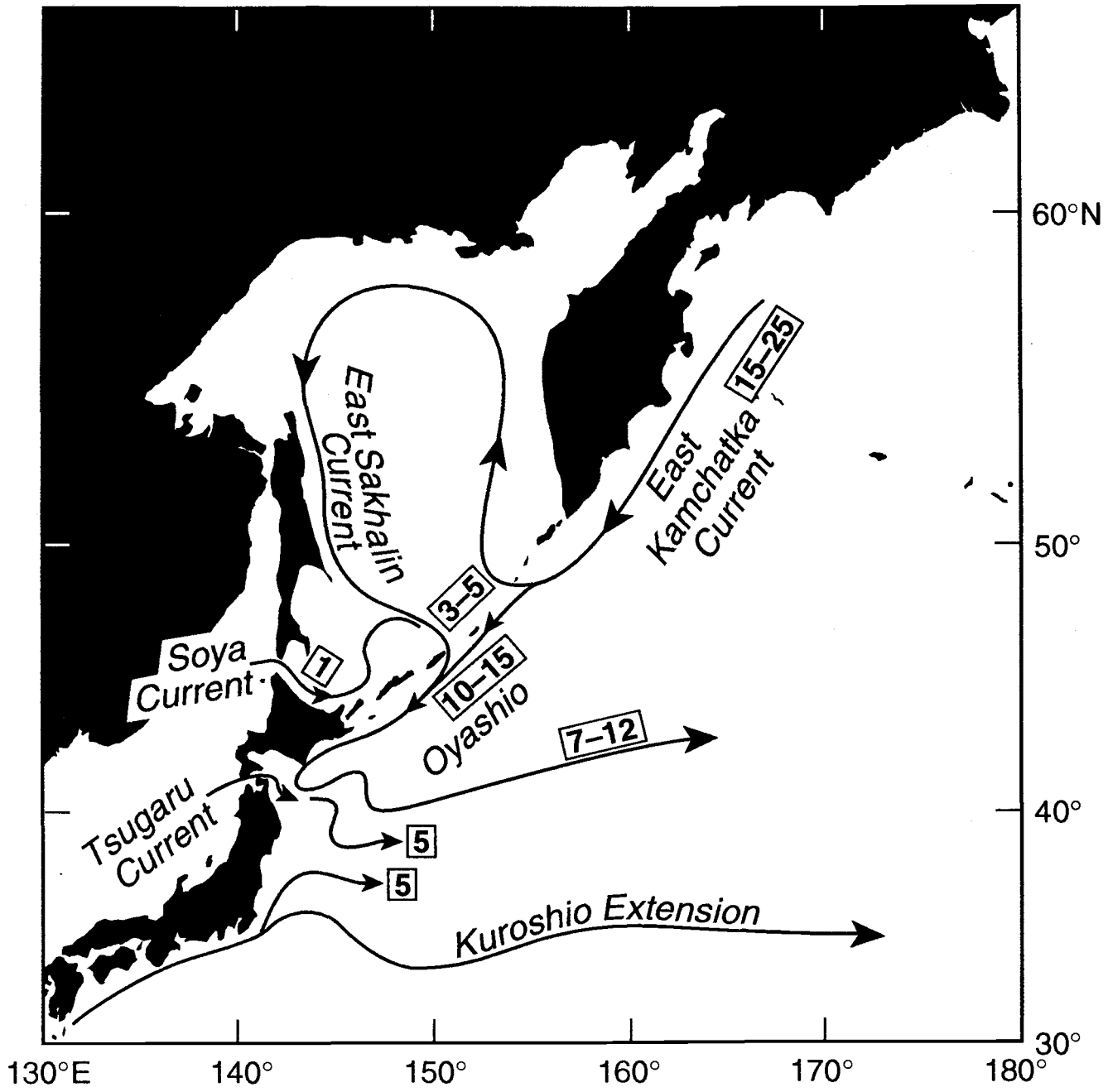

Fig. 1. The influence of cabbeling on the final density of the mixture of Oyashio and Kuroshio water in the Mixed Water Region. Mixing is along straight lines on the potential temperature/salinity diagram. Oyashio water is the cold, fresh curve, based on an average of CTD profiles from a number of stations east of Hokkaido. Kuroshio water is the warm, saline curve, based on an average of a number of profiles within the Kuroshio just east of its separation point. The final mixture is composed of approximately 45% Oyashio water and so obtains nearly the maximum density increase possible.

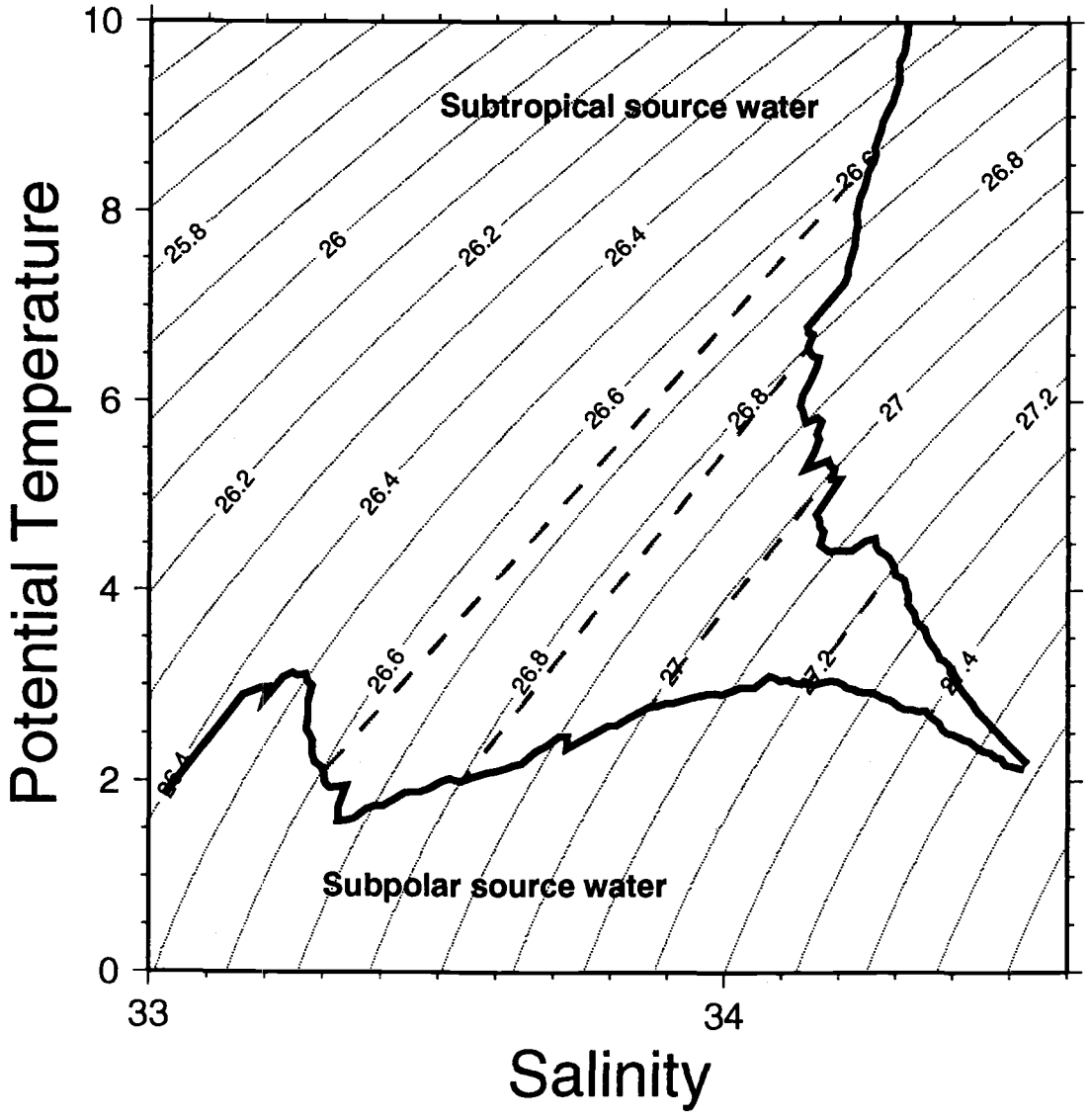

Fig. 2. Schematic of transports and transformations in the upper 1,000 meters in the northwestern Pacific.

Seasonal Variability of Integral Water Circulation in the Okhotsk Sea

Anatoly S. VASILIEV and Fedor F. KHRAPCHENKOV

Pacific Oceanological Institute, Far-Eastern Branch, Russian Academy of Sciences, Vladivostok, Russia

INTRODUCTION

The Okhotsk Sea represents the marginal sea and is separated from the Pacific Ocean by the Kuril Islands and Kamchatka Peninsula, and from the Japan Sea by Sakhalin and Hokkaido Islands. Out of all Far-Eastern Seas the Okhotsk Sea extends farthest into the continent and thus is more influenced by continental conditions. Characteristic morphometric peculiarity of the Sea is the vast shelf which occupies more than 40% of its area. The water exchange between the Okhotsk Sea and the Pacific Ocean is determined by the sizes and depths of the Kuril Islands straits. In the Kuril Islands Ridge there are more than 30 straits with total width about 500 km. The widest and deepest straits are those of Bussol' (the sill depth is 2,318 m and 43.3% of the total width), Kruzenshtern (1,920 m and 24.4%), Freez (900 m and 9.2%) and the Fourth Kuril Strait (600 m and 8.1%). Although the straits are rather deep, even the Bussol' Strait is 1.5 km shallower than the Kuril Basin. The deep water exchange with the ocean is thus restricted. The Okhotsk Sea is connected with the Japan Sea through the shallow strait of La Perouse (the sill depth of 75 m and width of 44 km) and the passage of Nevel'skoy (the sill depth of 14 m and width of 7 km).

Thermochaline structure of the Okhotsk Sea waters is conditioned on the one hand by the intensive water exchange with the Pacific Ocean and, on the other hand, by the strong convective mixing and ice formation during autumn-winter period of the year.

Investigation of the Okhotsk Sea currents started some time ago (Luchin, 1987; Moroshkin, 1966). Most of the known water circulation schemes has been obtained either by the dynamic method with the limited array of the initial data (Moroshkin, 1966) or as a result of diagnostic calculations based on the linear diagnostic model of Sarkisyan (1977) using available water density information and atmospheric pressure fields (Luchin, 1982, 1987). In addition, numerical simulations of currents have been executed applying the simplified baroclinic or barotropic models (Kozlov, 1972; Sekine, 1990).

To investigate the synoptic variability of the Okhotsk Sea currents numerical experiments were performed based on meteorological and CTD observations, and *in situ* current velocity measurements aboard the *R/V Akademik Alexander Nesmeyanov* in September 1993 (Vasiliev and Khrapshenkov, 1994). Seasonal variability of currents has been studied using both the diagnostic Sarkisyan's model for the warm period of the year (Luchin, 1987) and the model of the Novosibirsk Computer Center which takes account of the density stratification (Martynov et al., 1995).

MODEL DESCRIPTION AND INITIAL DATA

The quasigeostrophic model based on principles of self-similarity of the second order was used to reconstruct the sea water circulation by months. It considered spatial distribution of water density, atmospheric effect, bottom topography and coastline, water exchange through the straits, and

b - effect.

The sea water density was taken as the function possessing the natural self-similarity (similarity of the vertical distribution):

$$\rho(x,y,z,t)=\xi(x,y,t)[\sigma(z,t)+\alpha_1 a(x,y,t)(z-h_a^{\vartheta})]+\rho^0(x,y,t), \quad (1)$$

$$where\ \alpha_1=\begin{cases} 0\ at\ z\le h_a^{\vartheta}, & a(x,y,t)=-\dfrac{\partial\sigma(z,t)}{\partial z}\Big|z=H; \\ 1\ at\ z>h_a^{\vartheta}, & \dfrac{\partial(x,y,t)}{\partial x}=\dfrac{\partial(x,y,t)}{\partial y}=0; \end{cases}$$

Here, $\rho\ (x, y, z, t)$ is spatial-temporal distribution of the sea water density; $\rho^0(x, y, t)$ is known sea surface density; $\sigma(z, t)$ is stratification function; $a(x, y, t)$ is discrete-constant function regulating zero flux through the bottom; h_a^{ϑ}- is depth of the near-bottom layer of Ekman friction; $\xi(x, y, t)$ is self-similarity function; x, y, z are coordinates, corresponding to the axes directed eastward, northward or vertically down; t is time, and R is an index related to a characteristic station of the studied region, corresponding to the average vertical distribution of the sea water density.

In a quasistationary statement, computation of currents and density distribution from the tangential stress of wind and surface density leads to the equation for the transport stream function Ψ:

$$-\frac{\partial\Psi}{\partial\nu}+\Delta\Psi=F(T,\rho^0,f);\quad \Psi^L=\Psi^K \quad (2)$$

where L is basin contour; T is tangential stress of the wind; ρ^0 sea surface density; ν is relaxation parameter; f is the errors function related to some additional conditions on surface current velocities (Vasiliev, 1993).

Bringing in the additional conditions on surface current velocities allows calculation of the vertical distribution of currents and components of net fluxes both inside the area and on the liquid margin. Moreover, it permits derivation of the errors function resulting from the need to satisfy the discontinuity equation and water balance in the region. Equation (2) is solved by the method of minimal errors (Marchuk, 1974) by way of reaching a steady state in the time interval corresponding to the period of averaging marginal and surface conditions. The explicit solution of the equation provides the gradients of self-similarity function, the self-similarity function itself, sea water density, level inclinations, and horizontal and vertical distribution of currents.

A more detailed mathematical statement of the problem and the model description are given in (Vasiliev, 1993, 1994; Vasiliev and Dudka, 1994; Vasiliev and Khrapchenkov, 1994). The model has been used for the numerical experiments on dynamic studies in the Northwestern Pacific (Vasiliev, 1993, 1994; Vasiliev and Dudka, 1994; Vasiliev and Khrapchenkov, 1994).

The input data to calculate the integral circulation of the Okhotsk Sea included the real atmospheric pressure fields corresponding to the monthly predominant type of the atmospheric processes (Polyakova, 1994), the average monthly fields of temperature and seasonal surface salinity fields, as well as the monthly averaged stratification function in a characteristic point of the Sea. A uniform mesh with a width of 30' in latitude and longitude, and standard vertical horizons was used for calculations. The ice formation was considered in winter season, but the direct effect of wind was not taken into account for the ice covered area.. Current velocities were determined by the explicit formula, after solving the problem relative to the flow function. Characteristics of the atmospheric influence on the sea surface were computed based on the half-empirical ratios. Discharges in the

straits were either given according to the estimates available (Kozlov, 1972; Luchin, 1982, 1987; Zyryanov, 1974, 1977) or determined from the net fluxes normal to the liquid boundaries of the area, considered while using the given stratification function and the influence function obtained in the solution. The water exchange through the Tartar Strait was not considered. Numerical realization of the model was performed using the method of minimal errors (Marchuk, 1974).

RESULTS

Results of the numerical experiments by months are given in Fig. 1. The cyclonic character of waters circulation, pointed out by many authors studying the Okhotsk Sea currents, was confirmed only for the northern part of the Sea and only for the warm period of the year. A series of not unidirectional gyres which change their sizes and relative location in time was revealed in the southern part of the Sea.

One of the most stable currents of the Okhotsk Sea, namely the East Sakhalin Current, was observed near the eastern coast of Sakhalin Island. Its characteristics, conditioned by the seasonal variability of the atmospheric circulation over the Sea, demonstrated essential temporal changes. During the autumn-winter period (August to May) the current was traced everywhere along the Sakhalin coast. The discharge and velocities were maximal for this season, and reached 1-1.5 S_v and more than 35 cm/s in October. In June-July the current was detected only in the southern part of the Sakhalin coast. Similar changes occurred in the Counter Current, a part of which together with the East-Sakhalin Current forms a cyclonic gyre to the east of Sakhalin Island, and the other part forms the anticyclonic gyre in the central part of the Okhotsk Sea. This dipole structure was well expressed on the maps from October to May, and practically was unobserved in December and June-September, while forming the more complex structures of different vorticity. The maximal discharges and current velocities (more than 2 S_v and 40 cm/s correspondingly) were found in the Counter Current and in the anticyclonic gyre in October.

The North Okhotsk Current of small speed was traced during the warm season and practically vanished for the cold half of the year. This is related probably to generation of the ice cover.

The Kamchatka Current was revealed from January to September, and its core moved gradually (from winter to summer) to the western coast of the Kamchatka Peninsula. For some months we observed the current bifurcation into the northern branch passing to Penzhinsky Gulf and the western branch taking part in the cyclonic gyre to the west of the south-western coast of Kamchatka. The maximal velocities of the Kamchatka Current (exceeded 20 cm/s at 52°N) occurred in November-December. The compensating current near the western coast of Kamchatka was not seen, as it passed on the shelf with water depths less than 100 m. Only in November and December weak flow (with velocities not more than 5 cm/s) directed southward was found near the coast on the section along 52°N.

The Soya Current, with varying level of intensity, was observed during the whole year. In winter it fell into two and sometimes three branches, one of which moved along the coast of Hokkaido Island, the second turned to the north-east, and the last one passed to the east. Both eastward branches were involved into the anticyclonic gyre which shifted to the southern part of the sea in January-February. From June to December, the Soya Current was well manifested as the flow passing along the Hokkaido coast, whereas in July-August and December it turned to the north (not reaching Siretoko Cape) and propagated between two gyres of different vorticity up to the Strait of Freez. In September-November, the main Soya Current branch extended from Siretoko Cape along Kunashir Island as far as the Strait of Freez where it divided into two branches: one of them passed to the

Pacific Ocean through the Strait, another one moved to the north while participating in the anticyclonic gyre.

A series of gyres characterized by different signs of vorticity was observed in the southern part of the Okhotsk Sea during the whole year. From month to month they changed both their sizes and relative location. The Kuril Islands area within the Sea of Okhotsk can be conventionally separated into the northern and southern parts. In January the whole southern part of the Sea was occupied by the anticyclonic gyre with two centers extending along the Kuril Islands up to 48°N. To the north of this structure, a cyclonic vortex of considerably smaller size was located. Together with the anticyclonic gyre it formed a dipole with a meridionally oriented axis. In February the cyclonic gyre was shifted southward to the Islands, while driving back the main anticyclone to the south-west. Their sizes became equal, and the dipole axis extended along the Kuril Islands. At the same time, a cyclonic gyre originated near the southern terminal of Sakhalin Island. In March it displaced the anticyclone from the southern part of the Sea and thus shifted the dipole to the northeast. Such a situation was still preserved in April-May.

In June the anticyclonic gyre moved to the south. It was composed by two centers, one of them was situated to the northwest of the Bussol' Strait, and another to the northwest of the Ekaterina Strait. A cyclonic gyre occurred near the coast of Sakhalin Island and stretched out in the northeastern direction while merging with the cyclone situated to the north of the anticyclonic gyre in the previous months. The similar situation was manifested in July-August when both the anticyclone and cyclone were extended along the Islands to the north-east. Starting from August the cyclonic gyre increased in size from the north to the south and in September it occupied the whole southern part of the Okhotsk Sea up to 49°N and 148°E. Horizontal sizes of the anticyclone grew essentially smaller, and the dipole axis was again oriented to the northwest.

In October the double center cyclonic gyre increased in size, mainly eastward, up to 150°E, and the anticyclone moved to the northeast along the Islands while decreasing in size and stretching out along the meridian. An approximately similar picture was preserved in November-December, but the anticyclone gradually extended along the Islands up to the Strait of Ekaterina.

The cyclonic gyre located near the Kruzenshtern and Forth Kuril Straits was observed during the whole year and its horizontal size was not changed notably. However, during some months, while growing stronger, it merged with the cyclone which moved from the south.

The structure of the main Okhotsk Sea currents, as well as the system of gyres with different vorticity in its southern part, changed considerably from season to season. To the great extent the temporal variability is related to the reconstruction of the atmospheric processes. This allows amplification of existing notions on water dynamics and their seasonal variability, especially in the southern part of the sea.

Based on our calculations it is possible to estimate the integral discharge through the Straits. In practically all the Straits the flows of different orientation were revealed: in the northern straits the Pacific waters inflow being predominant, whereas in the southern straits the outflow of the Okhotsk Sea waters was observed. The total water discharge through the Kuril Straits varied from 0 to -1.0 S_v and was approximately equal to the water discharge through the La Perouse Strait. Table 1 presents the integral discharge of waters through the Kuril Straits for August and December (sign "+" denotes the Pacific waters penetration into the Okhotsk Sea).

Comparison of our numerical calculations with results presented elsewhere (Bobkov, 1992; Luchin, 1982, 1987; Moroshkin, 1966; Sekine, 1990; Zyryanov, 1974, 1977) shows a satisfactory correspondence with the main elements of the Okhotsk Sea circulation schemes. But it should be noted

that the cyclonic character of waters circulation stated by many authors, was confirmed for the northern part of the Sea only. In the southern part the complicated dipole structures changing their sizes and location were observed.

REFERENCES

Bobkov, A.A. 1992. Evolution of notions on water circulation in the southern part of the Sea of Okhotsk. Izvestiya PGO. 124(5):461-470 (in Russian).

Kozlov, V.F. 1972. Calculation of the level surface in the Sea of Okhotsk. Trudy DVNIIGMI. 37:37-43 .(in Russian).

Luchin, V.A. 1982. Diagnostic calculation of water circulation in the Sea of Okhotsk in summer. Trudy DVNIIGMI. 96:69-76 (in Russian).

Luchin, V.A. 1987. Waters circulation in the Sea of Okhotsk and peculiarities of its interannual variability by results of diagnostic calculations. Trudy DVNIIGMI. 36:3-13 (in Russian).

Marchuk, G.I. 1974. Numerical Solution of the Problem on Dynamics of the Atmosphere and the Ocean Using Method of Splitting. L., Gidrometeoizdat. 303 p. (in Russian).

Moroshkin, K.V. 1966. Water masses of the Sea of Okhotsk. U.S. Department of Commerce; Clearinghouse for Federal Scientific and Technical Information, Joint Publication Research service 43, 942, 98 p. (Translation of Vodnyye massy Okhostkogo Morya. Moscow, Nauka, 66 p.)

Martynov, A.V., E.N. Golubeva, and Luchin V.A. 1995. Numerical modelling of the Okhotsk Sea general circulation with the density stratification inclusion. Proc. PICES Workshop on the Okhotsk Sea and Adjacent Areas. Vladivostok.

Oceanographic encyclopedia. 1974. M., Gidrometeoizdat, 631 p. (in Russian).

Polyakova, A.M. 1994 Permanent variations in atmospheric circulation pattern over the Northern Pacific with regard to non-stationarity. Pacific Annual (Part 1). Vladivostok, Far-Eastern Branch of USSR Academy of Sciences.

Sekine, Y. 1990. A barotropic numerical model for wind-driven circulation in the Okhotsk Sea. Bull Fac. Bioresources, Mie Univ. 3:25-39.

Vasiliev, A.S. 1993. Self-similarity of the second order in monitoring of main physical fields of the ocean. Doklady Akademii Nauk. 328(5):613-618 (in Russian).

Vasiliev, A.S. 1994. Application of self-similarity parametrization of thermochaline fields in marine ecological studies. Morskoi Gidrofizicheskii Zhurnal.2:84-88 (in Russian).

Vasiliev, A.S., and K.V. Dudka. 1994. On water exchange of the Sea of Okhotsk and the Sea of Japan with the Pacific Ocean. Meteorologiya i Gidrologiya. 8:64-70 (in Russian).

Vasiliev, A.S., and F.F. Khrapchenkov. 1994. Planning of the oceanological experiment (on the example of the Sea of Okhotsk). Meteorologiya i Gidrologiya. 8:64-70 (in Russian).

Zyryanov, V.N. 1974. To the question on water exchange through the Northern Kuril Straits. Okeanologiya. 14:16-21 (in Russian).

Zyryanov, V.N. 1977. Numerical calculation of stable currents in the Sea of Okhotsk (prognostic model). Trudy VNIRO. 119:24-30 (in Russian).

TABLES AND FIGURES

Table 1. The integral water discharge through the Kuril Straits.

Strait	Discharge in Sv		Width of strait, km	Sill depth, m
	August	December		
Ekaterina	-0.01	-0.01	20	300
Freez	+0.48 -0.99	+0.5 -1.02	40	809
Urup	+0.1	+1.8	24	126
Bussol'	-0.9	-1.8	60	2300
Diana	0	0	18	241
Ricord	0	0	22	450
Nadezhda	-2.0	-2.55	40	500
Kruzenshtern	-0.2	0	72	1945
Severgin	+2.6	+2.65	40	69
4th Kuril	-0.5	-0.7	56	500
1st Kuril	+0.44	+0.5	12	23

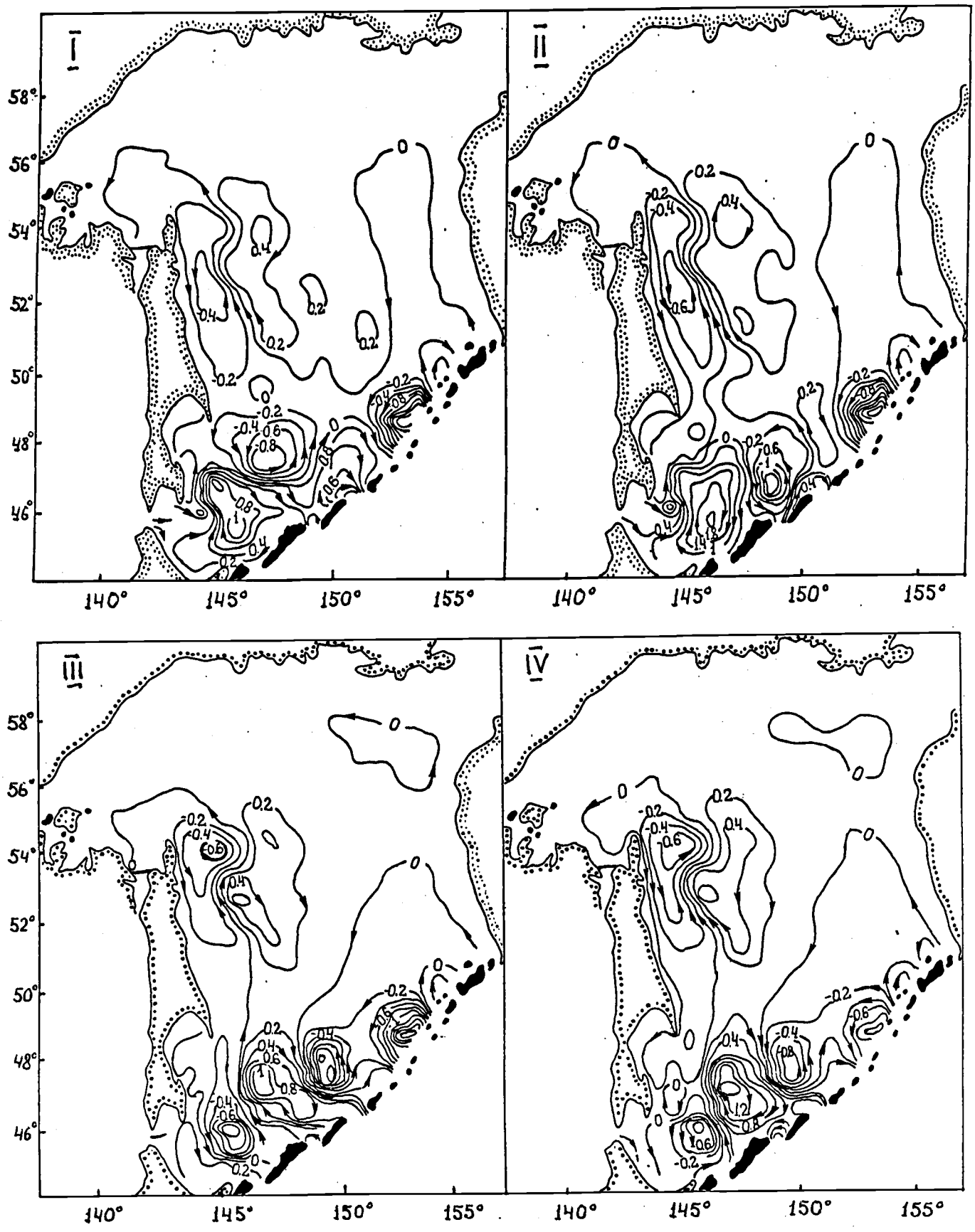

Fig. 1. The monthly transport stream functions (S_v) from the surface to the bottom in the Okhotsk Sea (12 panels).

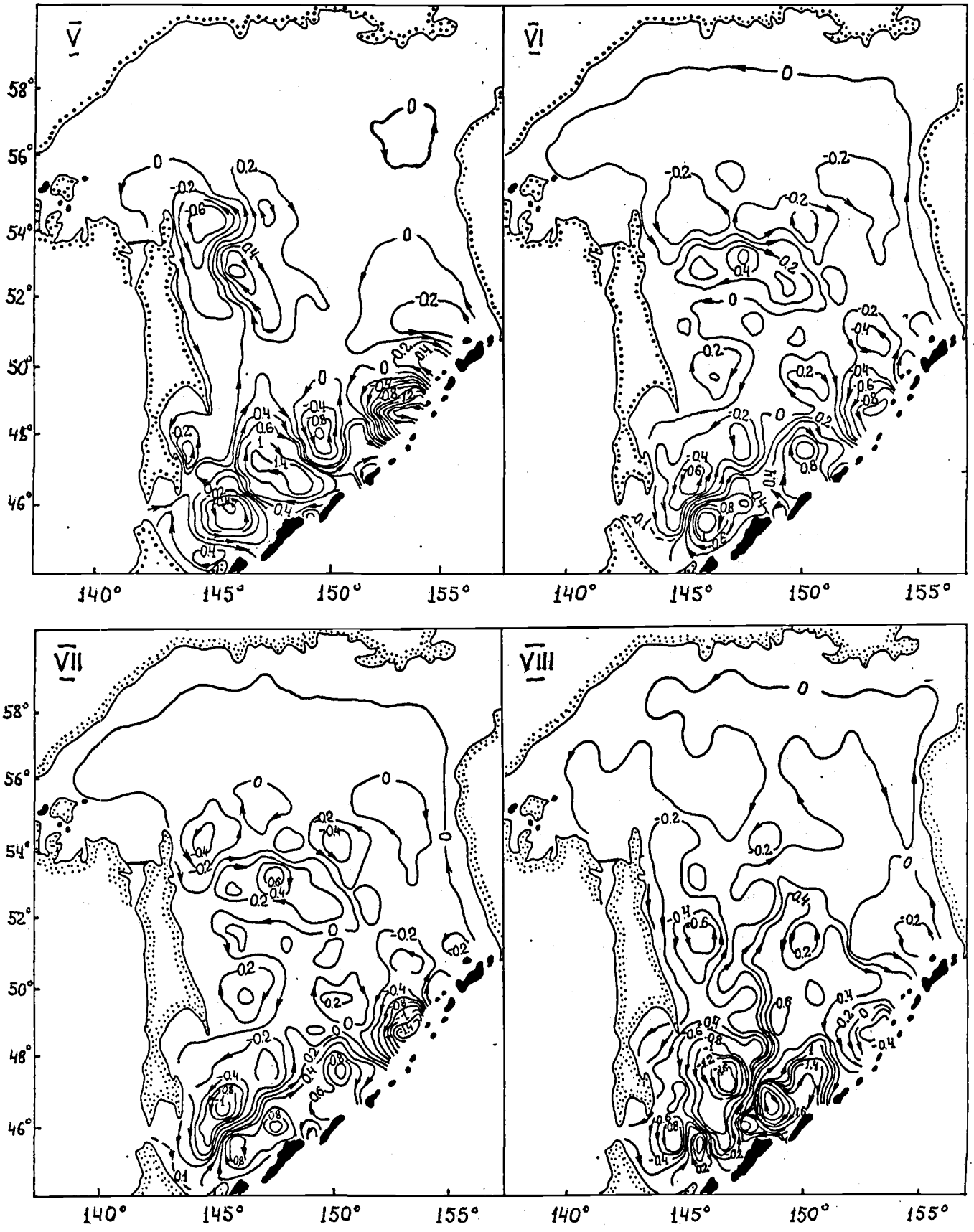
V
VI
VII
VIII
58°
56°
54°
52°
50°
48°
46°
140°
145°
150°
155°

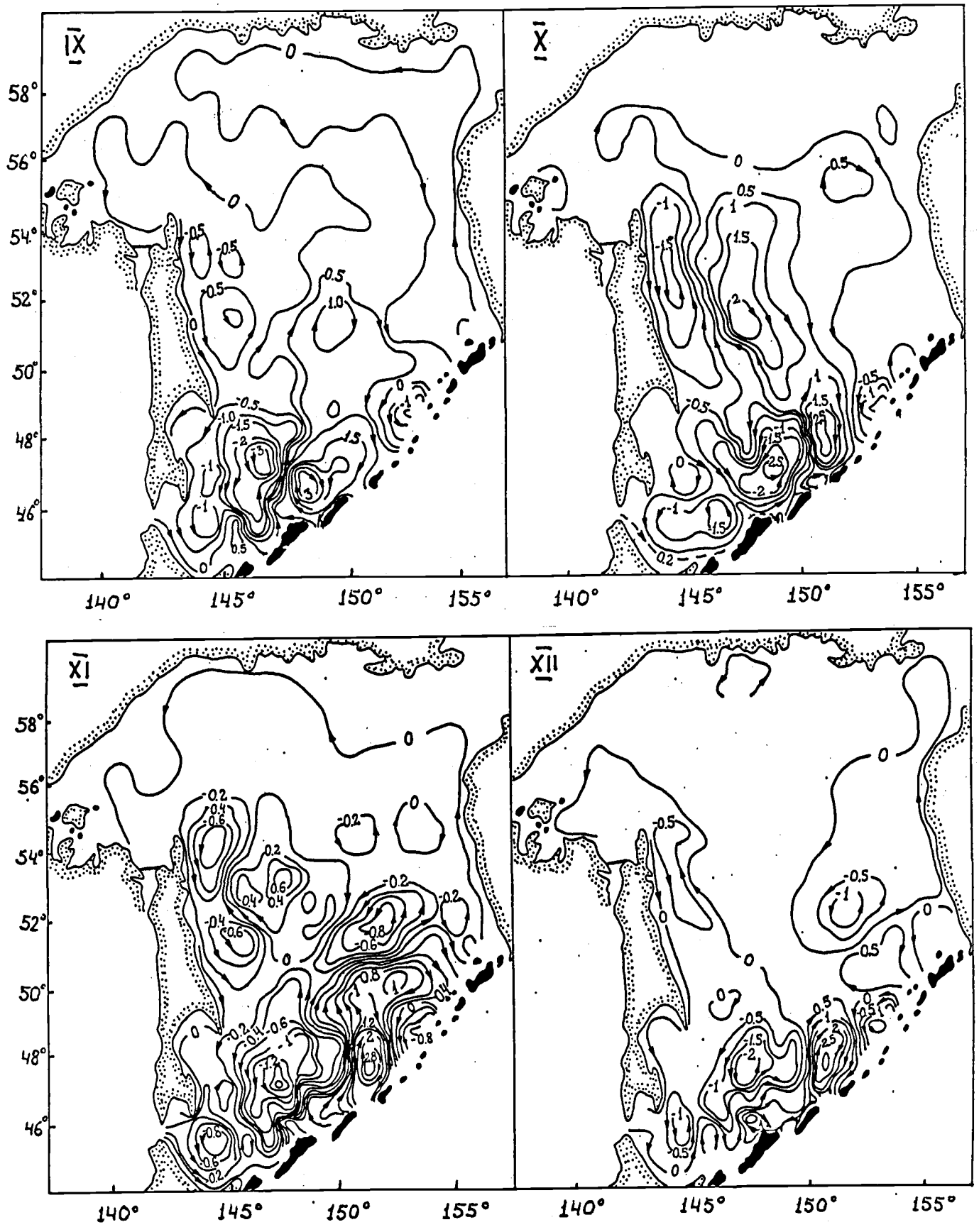
IX
X
XI
XII
58°
56°
54°
52°
50°
48°
46°
140°
145°
150°
155°

Acoustic Methods in Sea Ice Dynamics Studies

V.P. Gavrilo, G.A. Lebedev, A.P. Polyakov

The State Science Center of the Russian Federation
The Arctic and Antarctic Research Institute, St. Petersburg, Russia

The interaction of engineering structures with ice in the regions with fast or drifting ice cover is significant. The most difficult problem is to describe floe interaction, because an ice cover drift depends on external forces acting at some points as well as on the state of ice cover in adjacent areas.

The ice dynamics is determined by hydrometeorological processes. The equation of strength balance on a specific ice surface is based on hydrodynamic theory of ice cover drift:

$$\rho h \frac{\partial V}{\partial t} = \tau_a + \tau_w + C + G + R$$

where V is drift velocity factor; ρ is ice density; τ_a is tangent air pressure on the ice surface caused by wind; τ_w is strength of friction between ice and water; C is the Coriolis force; G is projection of gravity on the sea surface; R is internal resistance caused by interaction between ice flows.

Unfortunately, there are no suitable methods for evaluation of the last parameter R. To overcome this difficulty the following equations were used (Volkov et al., 1971) to describe a spatial irregularity of the ice drift:

$$div\ V = dv/dy + du/dx$$
$$rot\ V = dv/dx - du/dy$$
$$def_1\ V = dv/dx + du/dy$$
$$def_2\ V = dv/dy - du/dx$$

where u and v are projections of vector V on axes x and y correspondingly.

The first equation (divergence) characterizes the intensity of ice cover extension (compacting) at a given point, whereas the second equation (rotation) illustrates the velocity of the turn. It should be noted that both equations are invariant in coordinate axes. The two last equations represent the rate change of ice cover element formation or deformation. So, the third equation gives angular deformation (i.e. the change of angle between the sides of the originally square area) and the fourth shows irregularity of linear deformation along two perpendicular axes. Thus, to solve the problem of the study of sea ice dynamics it is necessary to carry out frequent and accurate measurements of spatial deformation characteristics of the ice cover.

ACTIVE ACOUSTIC METHOD

Two approaches are used to study the ice dynamics. The first is based on the continuous measurements of buoy coordinates installed on different floes. These measurements are performed by a space system designed for observations and radio communication. The second method is based on observations of ice formation characteristics with active and passive sensors from the artificial Earth satellites. Both methods are mainly used to determine the large scale movements of ice cover. To

study the middle scale ice deformations the radiohydroacoustic method was developed in the Arctic and Antarctic Research Institute (Bogorodsky et al., 1975). It is based on measuring (with necessary accuracy) the difference among time intervals corresponding to the propagation of a sound impulse in a water body between several marked drifting flows situated within the distance of one wavelength of acoustic ray propagation.

The change in distance from point A to B for the period between successive observations can be calculated using the sound impulses propagation time:

$$\Delta r = r - r_i = c_w(t - t_i)$$

where t and t_i are the times of sound propagation between A and B, c_w is the sound velocity in sea water. The main limitation of this method is the temporal fluctuations of the vertical sound velocity distribution which can lead to distortions of the refraction sound picture if ray approximation is used.

The relative accuracy of distance evaluation is:

$$\Delta r / r = \Delta t / t + \Delta c_w / c_w$$

The $\Delta t/t$ is the accuracy of sound propagation time registration and $\Delta c_w/c_w$ is the accuracy of known sound velocity. The first parameter is systematic and can be not taken into account. Thus, the accuracy of the $\Delta r/r$ measurement is caused only by $\Delta c_w/c_w$. and is about 0.02% of the measured distance, if Weelson's empirical formula is used to calculate the sound velocity from experimental data (Stashkevich, 1966).

In addition to the seasonal variations of sound velocity, the short period internal waves have an influence on the acoustic signal propagation time. Internal waves are sometimes formed in the zone of the upper thermocline and can induce the distortion of the refraction sound picture. To consider this effect continuous temperature and salinity measurements were carried out in the layer where the main changes of water physical parameters occur.

One of the numerous *in-situ* measurements is presented in Fig. 1, as an example. Here, each point on the experimental curve represents an average r-value determined within the 30-min interval of observation while each marking off was taken every 30 sec. In addition, the results of estimated ice cover linear deformation was obtained with the help of repeated large scale air-photo surveys. Analysis of the independent observations shows their sufficient coincidence as evidence of the high efficiency of the radiohydroacoustic method for the middle scale ice deformation studies. This conclusion justifies the elaboration of a multi-channel radiohydroacoustic automatic station designed for the collection and transmission of information on the strain stress state of the ice cover. Installation of such devices directly on engineering structures will permit exploitation with reduce risk in the regions with fast or pack ice.

PASSIVE ACOUSTIC METHOD

The method is based on the relationship between the energetic and frequency characteristics of ambient noise made during the ice destruction caused by stress state change (which can be explained by the variability of the hydrometeorological processes). Parameters of elastic oscillation (amplitude, frequency spectrum, wave length, sound and vibration velocities, duration of acoustic impulses, sound energy density) can be independent criteria for determination of the ice state before, during and after the moment of ice break up. In particular, the wide spectral maximum at the 50-300 Hz frequency range and 10-12 dB/octave fall of noise level in the direction of high frequency are distinctive characteristics of the noise connected with ice destruction.

The following multi-correlation equation is the result of analysis of the correlation relationships for statistical dependencies linking sound pressure in the water (P), wind velocity (V_w), drift ice velocity (V_i), air temperature (t_a), deformation, divergence and other parameters and their derivatives:

$$P = a*\text{div } V + b*\text{def } C + c*V_w + d*t_a + P_o$$

The coefficients a, b, c and d are functions of the partial coefficients of correlation, dispersion and mean values of the equation parameters, V is the vector of drift velocity. In different seasons some terms of the equation can be neglected (i.e. in winter $P = b*\text{def } C + d*t_a + P_o$). In such cases the reverse task can be solved and def V or div V can be found. These values will characterize the stress state of ice cover in the areas within the radius of spatial correlation.

The practical solution of the task for the Arctic ocean has demonstrated that the proposed method is quite suitable for the estimation of the ice extension or compression intensity. Fig.2 shows fragments of these investigations. The curves 1 (measured) and 2 (calculated) represent temporal changes of noise levels in 20-100 Hz frequency band. The calculated curves 3 and 4 (smoothed) display the deformation of ice cover.

Observations of ice break-up processes, including ice drift at Yenisey, Angara and Daugava rivers also illustrate applicability of acoustic methods for remote studies of ice cover state (Bogorodsky and Gavrilo, 1976). Investigations of ice formation physics during ice destruction performed both in laboratory and *in-situ* have allowed one to obtain the spectrum and energetic characteristics of noise generated at the different stages of ice stress state and during the process of ice drift. Spectral energy characteristics (pressure of underwater ambient noise in the 1 Hz frequency band relative to the zero level $2\ 10^5$ Pa) from the delta region of the Yenisey river are presented in Fig. 3. It clearly shows that extreme dynamic process during the ice drift causes an essential (up to 40 dB) increase of noise level by comparison with the corresponding characteristics for the unmoving ice cover (complete freezing) or for the ice-free river surface (complete ice clearance). Besides, the non-stationary acoustic noise for the river ice break-up differs from the quasi-stationary noise while unmoving ice cover exists on the river. The represented spectra also demonstrate that the wide maximum, caused by the rupturing and crushing of ice, takes place in the frequency band from 0.4 up to 3.0 kHz. The maximum can be widened up to 4.0-5.0 kHz due to friction between snowy ice flows.

The acoustic noise features mentioned above could be the basis for elaboration of methods to control the ice dynamic state at the local river regions in order to improve the ice jam forecast.

REFERENCES

Bogorovsky, V.V., and V.P. Gavrilo. 1976. Possibilities and perspectives of use of acoustic metods in the study of river ice cover. Proc. Coordination Workshop on Hydrotechnik. Moscow, Energoatomizdat. p. 189-193.

Bogorovsky, V.V., V.P. Gavrilo, and A.P. Polyakov. 1975. Radiohydroacoustic method for study of middle scale characteristics of sea ice dynamics. Trudy AARI. 326:219-228 (in Russian).

Stashkevich, A.P. 1966. Acoustic of Sea. Leningrad, Sudostroenie. 363 p. (in Russian).

Volkov, N.A., Z.M. Gudkovich, and D.D. Uglev. 1971. To study of drift irregularity in the Arctic basin. Trudy AARI. 303:76-88 (in Russian).

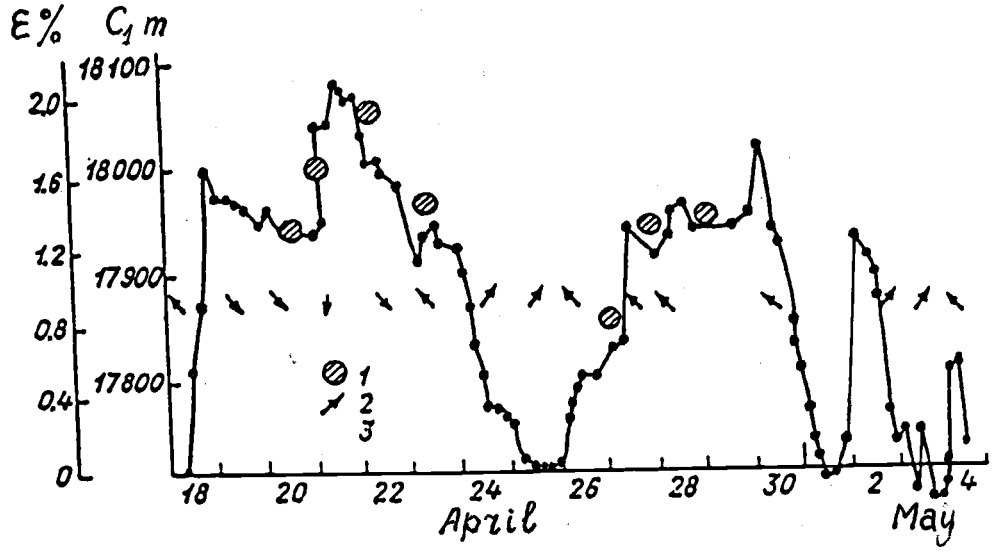

Fig. 1. Time dependence of the distance change (r, m) and linear ice deformation (ε, %) between points A and B:

1 - results from repeated air-photo surveys;
2 - ice drift direction;
3 - results of radiohydroacoustic observations.

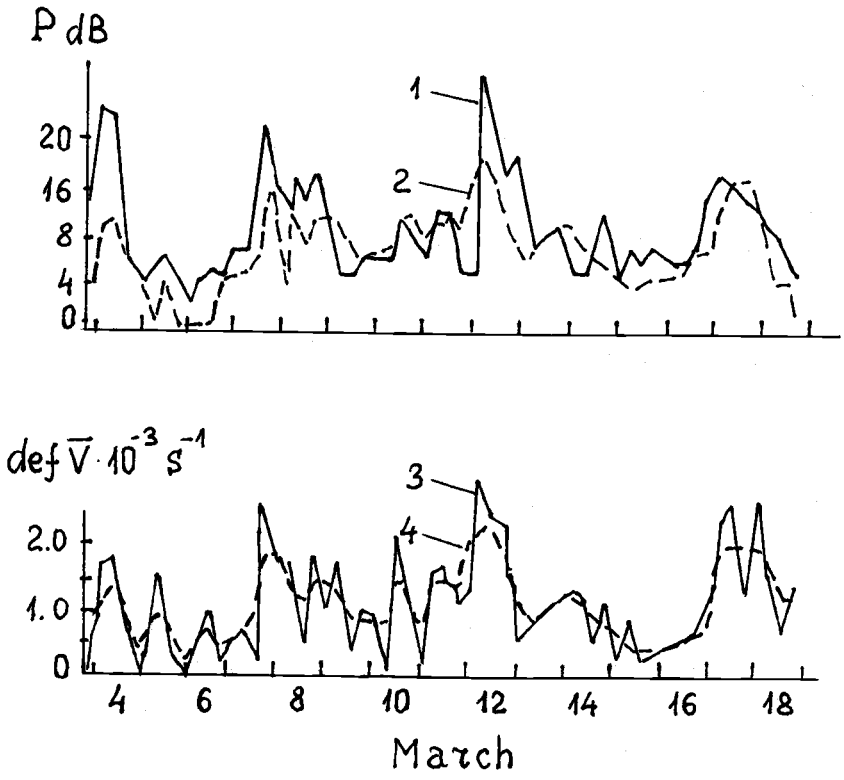

Fig. 2. Temporal changes of the underice noise level in 20-100 Hz frequency band (P, dB) and the ice cover deformation (def $\overline{V}$, S^{-1}) in the Arctic Ocean:
1 - the facts; 2, 3 - calculated curves; 4 - calculated smoothed curve.

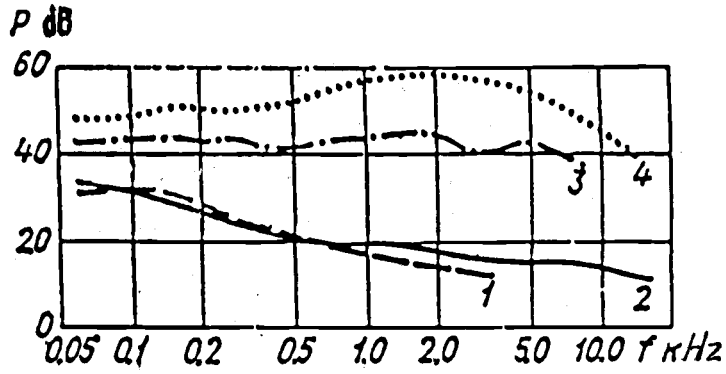

Fig. 3. Spectral characteristics of noise at the different stages of ice stress stage (the delta of Yenisey river, May 20 - June 6).
1 - complete ice clearance; 2 - complete freezing;
3 - ice break-up; 4 - ice drift.

The Role of the Far-East Atmospheric Circulation in the Formation of the Ice Cover in the Okhotsk Sea

Nina M. PESTEREVA and Larissa A. STARODUBTSEVA

Department of Meteorology, Far Eastern State University, Vladivostok, Russia

INTRODUCTION

One of the major characteristics of the intensity of ice formation is the ratio of the ice covered sea area to the whole sea area. In this study we consider a long-term variability of this ratio for the Okhotsk Sea.

The ice cover has a pronounced annual variability explained by natural and, especially during last years, by anthropogenic peculiarities. Natural features include hydrologic factors and the atmospheric circulation in the second natural synoptic region enveloping the area from 80°E up to 160°W.

METHOD AND DATA

Data on the Okhotsk Sea ice cover for the period from 1957 to 1990 have been provided by chiefs of the Sea Forecasting Laboratories of the Primorsky Department on Hydrometeorology and Environment Monitoring. Based on this information the time period was divided on three classes:

(1) years with heavy ice cover;
(2) years with light ice cover;
(3) all other years or years when ice cover of the Okhotsk Sea was normal or near normal.

The years: 1958-59, 1966-67, 1968-69, 1972-73, 1977-78, 1978-79, 1986-87 were regarded as the first class or heavy ice-covered years (Table 1). The second class or light ice-covered years were determined as follows: 1963-64, 1973-74, 1975-76, 1983-84, 1984-85, 1987-88 (Table 2). Features of atmospheric circulation for the second natural synoptic region were analyzed for different year classes.

Snow, as well as ice, are very sensitive elements of the Sun - Earth - atmosphere system and considerably influence both micro- and mesoclimate, weather and atmospheric circulation. Conversely, the atmospheric circulation effects on ice-formation for various classes.

The troposphere circulation anomalies cannot be explained only by the interrelation processes between the troposphere and underlying surface. The stratospheric circulation and its interaction with troposphere also play a key role in the formation of a certain weather regime. The circumpolar gyre is a major synoptic stratospheric phenomenon defining the weather of the northern hemisphere for moderate latitudes. Fluctuations of the intensity and location, to a considerable extent, influence the weather regime in different regions. A detailed description of this approach was given in publications by the distinguished Russian meteorologist Pedya (1976).

The circumpolar gyre trajectories are rather complicated. The cyclonic gyre propagates after the stratospheric cold site, which appears as a result of air cooling during the polar night. Thus, at the first stage we considered the circumpolar gyre intensity and features during the cold period from

November till March for heavy and light ice years using positions of the gyre center and monthly mean data for the geopotential at 100 mbar. In cases where the gyre had two or more centers, we took into account the center located in the Asian sector of the Arctic, or that situated above the Asian continent, and calculated mean values for the first and second year classes.

To reveal the tropospheric circulation features, the data on the Ilyinsky circulation forms were used.

RESULTS

For heavy ice cover years in the Okhotsk Sea, in 60% of cases the circumpolar gyre center shifted to the Asian continent southward of 70°N (e.g. Fig. 1) and the Far Eastern trough stretched to the Khabarovsky Region. The center of the circumpolar gyre was located to the southeast of the usual long-term position in 72% of cases for the period from November till March. Monthly mean distribution of the geopotential at 100 mbar for November 1977 and March 1978 is given on Fig. 1. This map shows that meridional and particularly, western circulation prevailed during this season (it was above normal in 3-11% cases for different years). The planetary high altitude frontal zone was located further to the south in comparison with the long-term mean, which is normally near 40°N. The cyclones moved the southern trajectories. The arctic air mass advection was observed on the western edge of the high-altitude Far-Eastern trough in these circumstances, and negative air temperature anomalies were formed above the southern Far-East, Japanese Islands and Okhotsk Sea. These thermal and dynamic factors contributed to an intensive process of ice formation and maintenance of a severe ice regime in the Okhotsk Sea.

For light ice years in the Okhotsk Sea, the circumpolar gyre shifted to the northwest in comparison with its normal position (Fig. 2). The high altitude Far Eastern trough was weak and an intensive zonal movement was noticed above the region. Meridional processes were below normal up to 5-10% and latitudinal circulation occurred more often in comparison with the normal years. The high-altitude frontal zone stretched to the north from Lake Baikal, to the Amur river and further to the south of the Okhotsk Sea. Simultaneously, with the cyclones movement along the high altitude frontal zone, the drift over of warm air masses towards the Okhotsk Sea was seen. Over the larger part of the Far East, the positive air temperature anomalies at the surface are present followed by less than normal ice cover in the Okhotsk Sea.

Thus, the atmospheric processes in the troposphere and lower stratosphere during fall and the first half of winter are important factors influencing the ice formation in the Okhotsk Sea.

REFERENCE

Pedya, D.A. 1976. O vliyanii kolebaniy circumpolyarnogo vichrya na formirovanie usloviy pogody. Trudy GMC SSSR. 173:45-57 (in Russian).

TABLES AND FIGURES

Table 1. Heavy ice years in the Okhotsk Sea (ice covered area of the Sea, %)

Year/month	1958-1959	1966-1967	1968-1969	1972-1973	1977-1978	1978-1979	1986-1987
December	**30**	**18**	**19**	**26**	**25**	**25**	**28**
March	**85**	**97**	**88**	**94**	**92**	**94**	**90**

Table 2. Light ice years in the Okhotsk Sea (ice covered area of the Sea, %)

Year/month	1963-1964	1973-1974	1975-1976	1983-1984	1985-1986	1987-1988
December	**8**	**16**	**29**	**23**	**11**	**19**
March	**77**	**71**	**66**	**57**	**75**	**63**

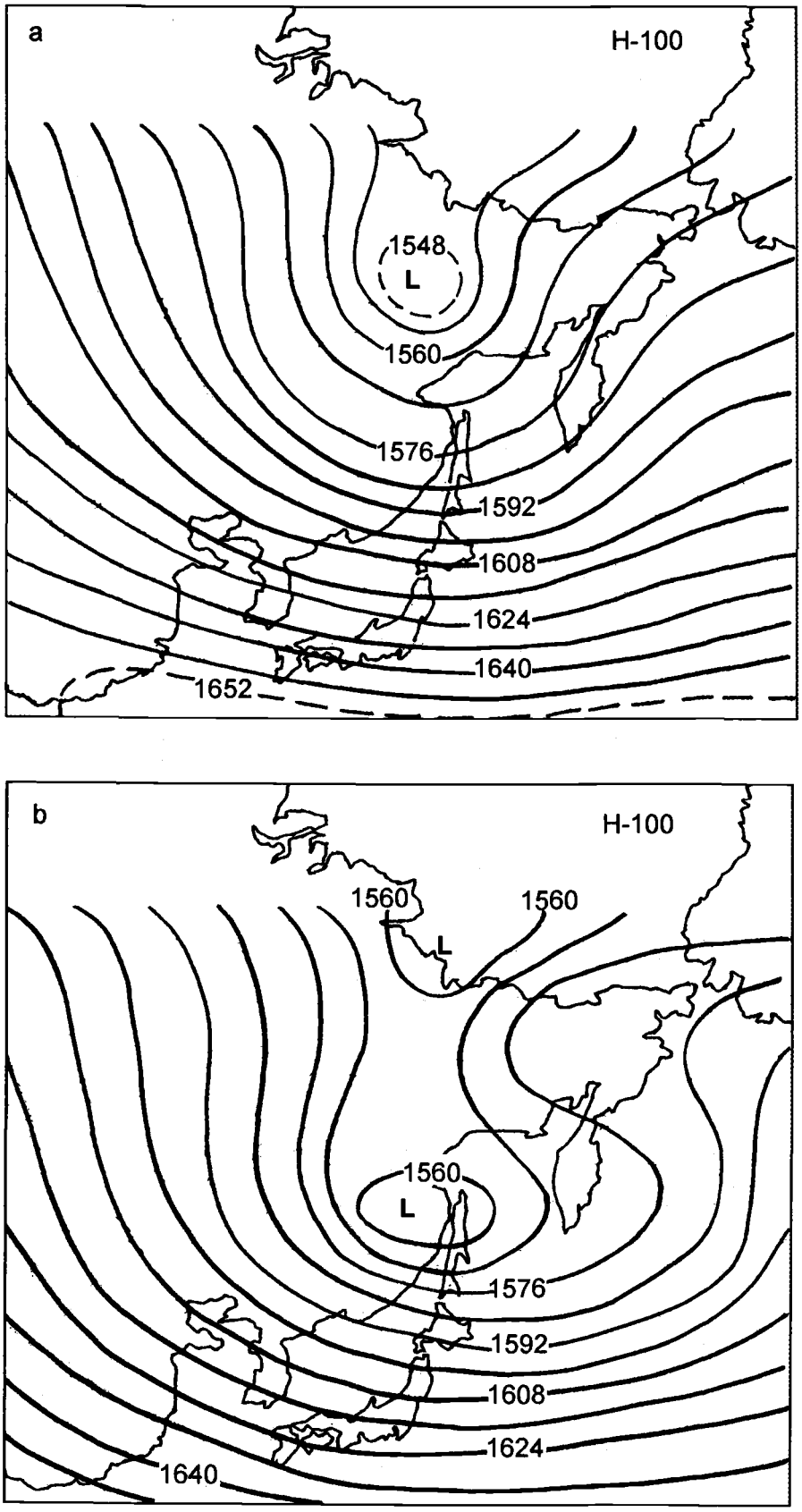

Fig. 1. Monthly mean distribution of geopotential at 100 dbar (x 10m) for November 1977 (a) and March 1978 (b). Heavy ice cover years.

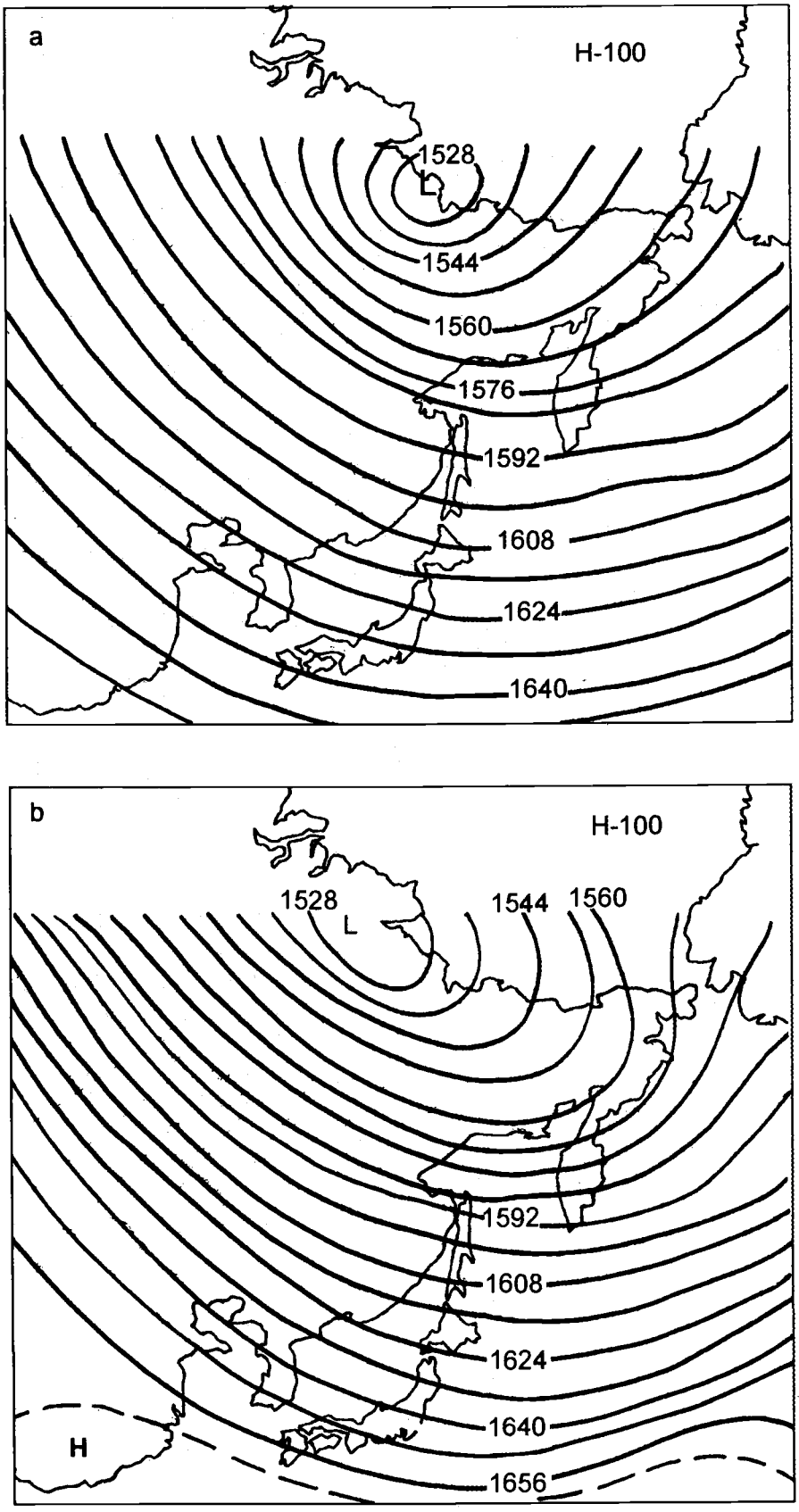

Fig. 2. Monthly mean distribution of geopotential at 100 dbar (x 10m) for November 1984 (a) and March 1985 (b). Light ice cover years.

Anomalous Oyashio Intrusion and its Teleconnection with Subarctic North Pacific Circulation, Sea Ice of the Okhotsk Sea and Air Temperature of the Northern Asian Continent

Yoshihiko SEKINE

Faculty of Bioresources, Mie University, Tsu, Mie-ken, Japan

INTRODUCTION

The subarctic water (known as the First Branch of the Oyashio) extends southward in the surface layer along the coast of Honshu, Japan. Sometimes the Oyashio Water reaches off the Boso peninsula, and then it is often called the Anomalous Oyashio Intrusion. The water near the southern tip of the extended area is considerably modified by horizontal mixing with surrounding waters, but keeps the cold and less saline characteristics of subarctic waters. The Anomalous Oyashio Intrusion usually causes the abnormally cold summer in the northern areas of Honshu, Japan, and influences the coastal fisheries.

The southernmost latitude of the 5°C isotherm at a depth of 100 m is frequently used as an index of this southward Oyashio extension strength. The variation of this latitude is shown in Fig. 1 (the bottom curve). For the period from 1970 to 1988 the eminent Anomalous Oyashio Intrusion occurred in 1973-74, 1981, 1984 and 1986. Charts of the sea surface temperature anomalies in April 1981 and April 1984 taken from the Ten-day Marine Report published by Japan Meteorological Agency are presented on Fig. 2. It can be seen that the Anomalous Oyashio Intrusion is not a local phenomenon, and the low temperature anomalies are widely observed within the subarctic and subtropical waters of the western North Pacific.

In the present work the occurrence of the Anomalous Oyashio Intrusion and its relationship with several oceanographic and meteorological phenomena will be discussed.

THE OCCURRENCE OF THE ANOMALOUS OYASHIO INTRUSION AND WIND CONDITIONS OVER THE NORTH PACIFIC

Based on the wind stress data by Kutsuwada and Teramoto (1987), Sekine (1988a) suggested that the latitude of no wind stress curl is observed in mid-winter just before the occurrence of the Anomalous Oyashio Intrusion. Using a numerical modelling (homogenous ocean model), he also demonstrated (Sekine, 1998b) that change in the wind stress field over the North Pacific Ocean causes the subsequent change in the subarctic circulation pattern: the southward shift of the no wind stress curl is usually accompanied by an increase of the wind stress over the North Pacific. The volume transport of the subarctic circulation is enhanced, and its position at the southern margin is shifted southward. This influences the occurrence of the Anomalous Oyashio Intrusion. In the present paper, only the averaged winter wind stress data just before the Anomalous Oyashio Intrusion (namely the average over late autumns and winters of 1973-4, 1980-81 and 1983-84), and that for the other years are considered.

Here, we numerically examine the year-to-year variations of the subarctic circulation in the North Pacific by using a two-layer ocean model on a beta plane. For simplicity, we consider an ocean

with simplified geometry and bottom topography as shown in Fig. 3a and 3b. The hydrostatic, rigid lid and Boussinesqu approximations are adopted. The governing equations are the same as used by Sekine and Kutsuwada (1994). The grid interval is 1 degree both in the west-east and the south-north directions. The coefficient of horizontal eddy viscosity is set to be 5×10^6 cm^2 s^{-1} in this analysis.

Teramoto and Kutsuwada (1987) compiled monthly mean wind stress fields over the North Pacific Ocean for the period from April 1961 to March 1984. The monthly mean wind stress fields from April 1984 to December 1987 were obtained using the same approach and the wind velocity data supplied by the Japan Meteorological Agency. These monthly mean fields are assumed to represent the field at the middle of the corresponding month, and the daily fields are calculated by interpolating these monthly values. The obtained wind stress data from January 1961 to December 1987 are applied in our model. However, as the ocean is presumed initially at rest and as the time scale of the baroclinic response is several years in our model, baroclinic adjustment may not be completed before 1970. In the later analysis, the comparison with the change of the Oyashio Intrusion strength would be made mainly for the period after 1971.

The distribution of the total volume transport function is displayed in Fig. 4 for January of each year. The western boundary currents are formed even during the first year (January 1961), indicating that such gross features are created through barotropic responses. The portions of anti-clockwise circulation (the subarctic circulation) are shaded in each figure. The area of the subarctic circulation and its strength (the density of the transport function in the shaded area) are characterized by noticeable temporal variability. It can be seen that the area and the strength have a tendency to increase in the years of the Anomalous Oyashio Intrusion: namely, in 1974, 1981, 1984, and 1986.

The southernmost latitudes of the calculated subarctic circulation were obtained for three longitudinal ranges:

1. 142°E - 170°W (the wider domain),
2. 142°E - 170°E (the domain west of the Emperor Sea Mounts) and
3. 142°E - 150°E (the Oyashio region).

Temporal variations of these latitudes for the period from 1971 to 1987 are shown in the upper-top, the upper-middle, and the upper-lower curves of Fig. 1, respectively. The seasonal variation is distinctive for all of three curves, except the period 1972-75 for the wider domain. The southern boundary of the subarctic circulation shifts southward generally in winter and northward in summer-autumn for almost all longitudes under consideration. However, the southernmost latitudes or the strengths of the southward winter shift are very changeable from year to year: the strengths are high in 1974, 1977-1978, 1980-1984, and 1986.

The temporal variation of the Oyashio Intrusion strength (the southern most latitude of the 5°C isotherm at 100 m depth) is also shown in the lower curve of Fig. 1 for the period from 1971 to 1987. The seasonal variability of this curve is not so significant, and variations having longer periods appear to be dominant. As discussed before, the southern shift of the latitude is distinguished in 1974, 1981, 1984 and 1986, and we assume that the Anomalous Oyashio Intrusion occurred for these years. From the same curve, we may conclude that the Anomalous Oyashio Intrusion took place also in 1977, 1978, 1982 and 1983, though its magnitude was somewhat smaller. It should be noted that these years just coincide with the years of the strong southward shift of the southern boundary of the subarctic circulation.

The correlation coefficient between the Oyashio Intrusion strength (the lower curve in Fig. 1) and the latitude of the southern boundary of the subarctic circulation is 0.35 if we chose the Oyashio Region (142°E-150°E: the upper-lower curve in Fig. 1) or 0.38 if we chose the domain west of the

Emperor Sea Mounts (142°-170°: the upper-middle curve in Fig. 1). The latter coefficient is increased to 0.40 if we apply one month lag for the curve of the Oyashio Intrusion strength.

The correlation coefficient between the Oyashio Intrusion strength and the latitude of the no wind stress curl is also calculated for the same period, and the coefficient is 0.31 without lag and 0.40 with one month lag. Though the Anomalous Oyashio Intrusion is a rather local phenomenon along the Pacific coast of the northern part of Honshu, it is strongly suggested that Anomalous Oyashio Intrusion has a close relation to the strength and the position of the global subarctic circulation in the North Pacific and to the position of the no wind stress curl of the wind system over the North Pacific.

OCEANIC AND ATMOSPHERIC PHENOMENA RELATED TO THE ANOMALOUS OYASHIO INTRUSION

Examples of the distribution of the 500 hPa height anomaly over the northern hemisphere are presented in Fig. 5 at the time of the Anomalous Oyashio Intrusion. In these figures, a prominently low pressure area is seen over the North Pacific and high pressure areas over the north Asian Continent (the Siberian High) and over North America. These distributions correspond to the so called PNA pattern, which relates to the ENSO phenomenon or abnormal high sea surface temperatures in the equatorial Pacific (Horel and Wallace, 1981; Shukla and Wallace, 1983). It strongly suggests that the occurrence of the Anomalous Oyashio Intrusion would have a teleconnection with the ENSO phenomenon.

The air temperature anomalies averaged over the nine stations shown in Fig. 6 for the years of the Anomalous Oyashio Intrusion (1974, 1981, 1984, and 1986) were calculated. The anomalies in December and January are positive, and equal to 1.57°C and 1.73°C, respectively. The winter air temperature at the stations surrounding the Okhotsk Sea and in the northern Asian Continent appears to be relatively warmer at the time of the occurrence of the Anomalous Oyashio Intrusion. The similar correlation between the Anomalous Oyashio Intrusion and the sea ice cover of the Okhotsk Sea can be seen: the area of sea ice cover of the Okhotsk Sea were calculated for each month from December to May separately for the years of the Anomalous Oyashio Intrusion and for the years of no Anomalous Oyashio Intrusion (all years from 1970 to 1988 except for 1974, 1981, 1984 and 1986). The obtained results are shown in Table 1. The sea ice cover is clearly larger for the years of no Anomalous Oyashio Intrusion: averaged ice cover area for the whole period analyzed is 61.5×10^4 km^2 for the years of the Anomalous Oyashio Intrusion and 77.1×10^4 km^2 for the other years.

Bhanu Kumar (1988) estimated the area of monthly snow cover of the Eurasian Continent for the period from 1970 to 1986. A significant positive correlation between this snow cover and the Okhotsk sea ice cover areas can be seen for both January data and three months data averaged from December to February (Figs. 7a and 7b). As Yasunari (1990) pointed out the close relationship between the strength of the Asian Monsoon and the occurrence of ENSO phenomena, there is much evidence suggesting the relationship among various oceanic and atmospheric phenomena. Though the Anomalous Oyashio Intrusion is a rather local phenomenon off the Pacific coast of the northern part of Honshu, Japan, but it should be noted that its occurrence is closely related with various large scale phenomena such as the subarctic North Pacific circulation, the wind stress distribution over the North Pacific, the atmospheric pressure pattern like the PNA pattern, the sea ice coverage of the Okhotsk Sea, the snow coverage over the Eurasian Continent, the ENSO phenomenon, and etc. Further investigations are necessary to explain the physical mechanisms of these teleconnections.

ACKNOWLEDGMENTS

I would like to thank professors Y. Nagata of Mie University and K. Ohtani of Hokkaido University for their valuable comments and advice. Thanks are also due to Dr. Kutsuwada of Tokai University and the staff of Japan Meteorological Agency for kind supplying the necessary data. I thank also Mr. F. Yamada of Mie University for his help in data analysis.

REFERENCES

Bhanu Kumar, O.S.R.U. 1988. Interaction between winter snow cover and location of the ridge at the 500 hPa level along 70°E. J. Meteor. Soc. Japan. 66:509-514.

Horel, J. M. and J. M. Wallace. 1981. Planetary scale atmospheric phenomena associated with the southern oscillation. Mon. Wea. Rev., 109, 813-829. Japan Meteorological Agency (1981, 1984): The ten-day Marine Report, nos. 1245 and 1354. (in Japanese) Japan Meteorological Agency (1987): Report on recent climatic change in the world (IV). pp.443.

Kutsuwada, K., and T. Teramoto. 1987. Monthly maps of the surface wind stress fields over the north Pacific during 1951-1984. Bull. Ocean Res. Inst. Univ. Tokyo. 24:1-100.

Sekine, Y. 1988a. Anomalous southward intrusion of the Oyashio east of Japan 1. Influence of the interannual and seasonal variations in the wind stress over the north Pacific. J. Geophys. Res. 93:2247-2277.

Sekine, Y. 1988b. A numerical experiment on the anomalous southward intrusion of the Oyashio east of Japan. Part 1: Barotropic model. J. Oceanogr. Soc. Japan. 44:60-67.

Sekine, Y., and K. Kutsuwada. 1994. Seasonal variation in volume transport of the Kuroshio south of Japan. J. Phys. Oceanogr. 24:261-272.

Shukla, J., and J. M. Wallace. 1983. A numerical simulation of the atmospheric response to equatorial Pacific sea surface temperature anomalies. J. Atmosph. Sci. 40:1613-1630.

Yasunari, T. 1990. Impact of Indian monsoon on the coupled atmosphere/ocean system in the tropical Pacific. Meteor. Atmosph. Phys. 44:29-41.

TABLES AND FIGURES

Table 1. Mean area of sea ice cover (in 10^4 km^2) of the Okhotsk Sea for the years of Anomalous Oyashio Intrusion (1974, 1981, 1984 and 1986: the left column) and for the years of no Anomalous Oyashio Intrusion (the other years: the right column). The standard deviations are also shown.

Month	Anomalous intrusion years	Weak intrusion years
Dec.	27.6 ± 6.7	36.2 ± 8.5
Jan.	69.0 ± 13.2	89.6 ± 12.6
Feb.	98.9 ± 18.4	117.1 ± 11.8
Mar.	94.9 ± 18.8	114.1 ± 16.6
Apr.	60.4 ± 14.8	78.8 ± 16.2
May	17.9 ± 2.9	26.9 ±8.8

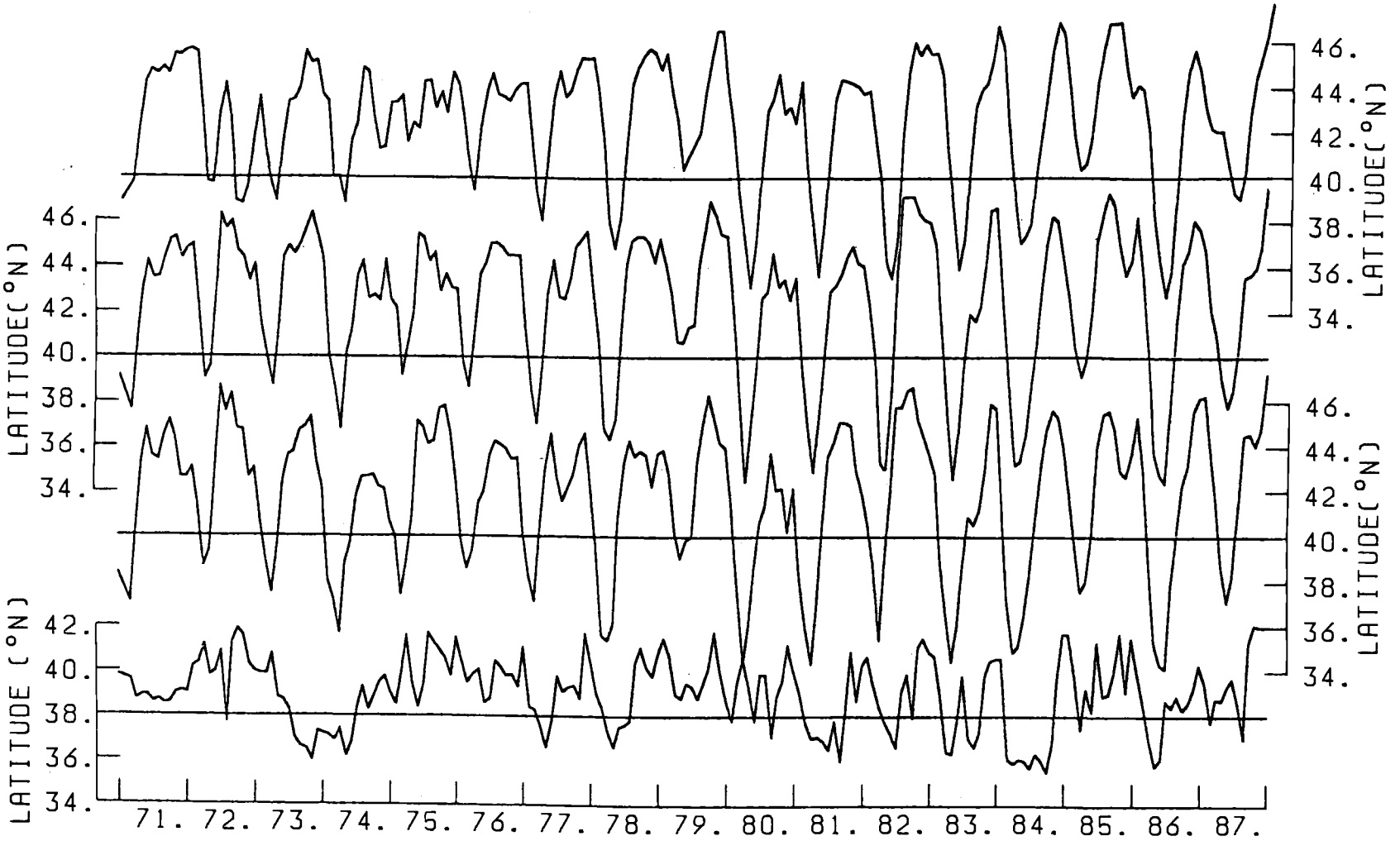

Fig. 1. Temporal variations of the southernmost latitude of the 5°C isotherm at the depth of 100 m (the bottom curve). This latitude is usually used as an index of the Oyashio Intrusion strength. Three other curves demonstrate temporal variations of the latitude of the southern boundary of the calculated subarctic North Pacific Circulation: the upper-top curve indicates that in the longitudinal range between 142°E and 170°W, the upper-middle curve that between 142°E and 170°E (west of the Emperor Sea Mounts), and the upper-lower curve that between 142°E and 150°E (the Oyashio region), respectively.

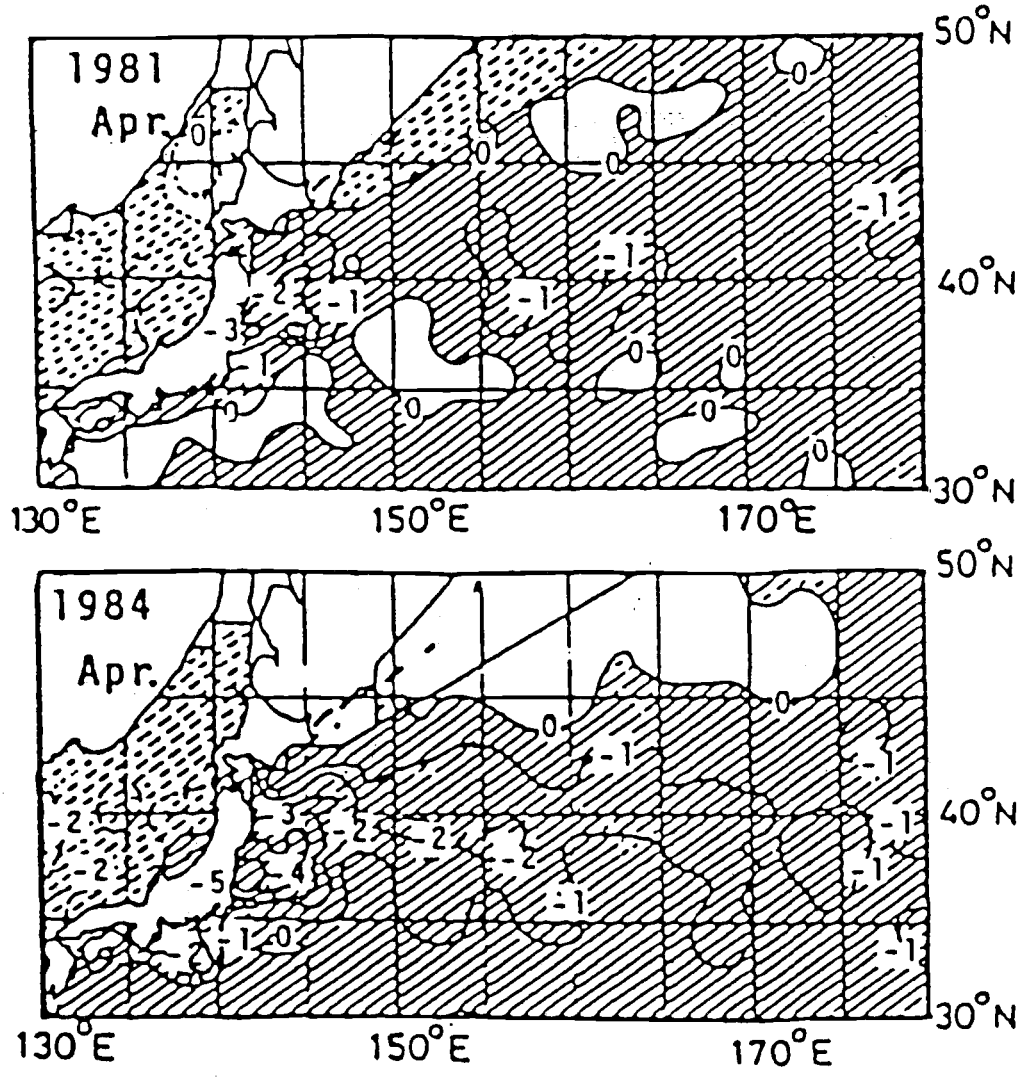

Fig. 2. Sea surface temperature anomalies in April 1981 (upper panel) and April 1984 (lower panel). Conspicuous Anomalous Oyashio Intrusions were observed in these years. The low temperature anomalies (hatched area) are widely seen in the western North Pacific area.

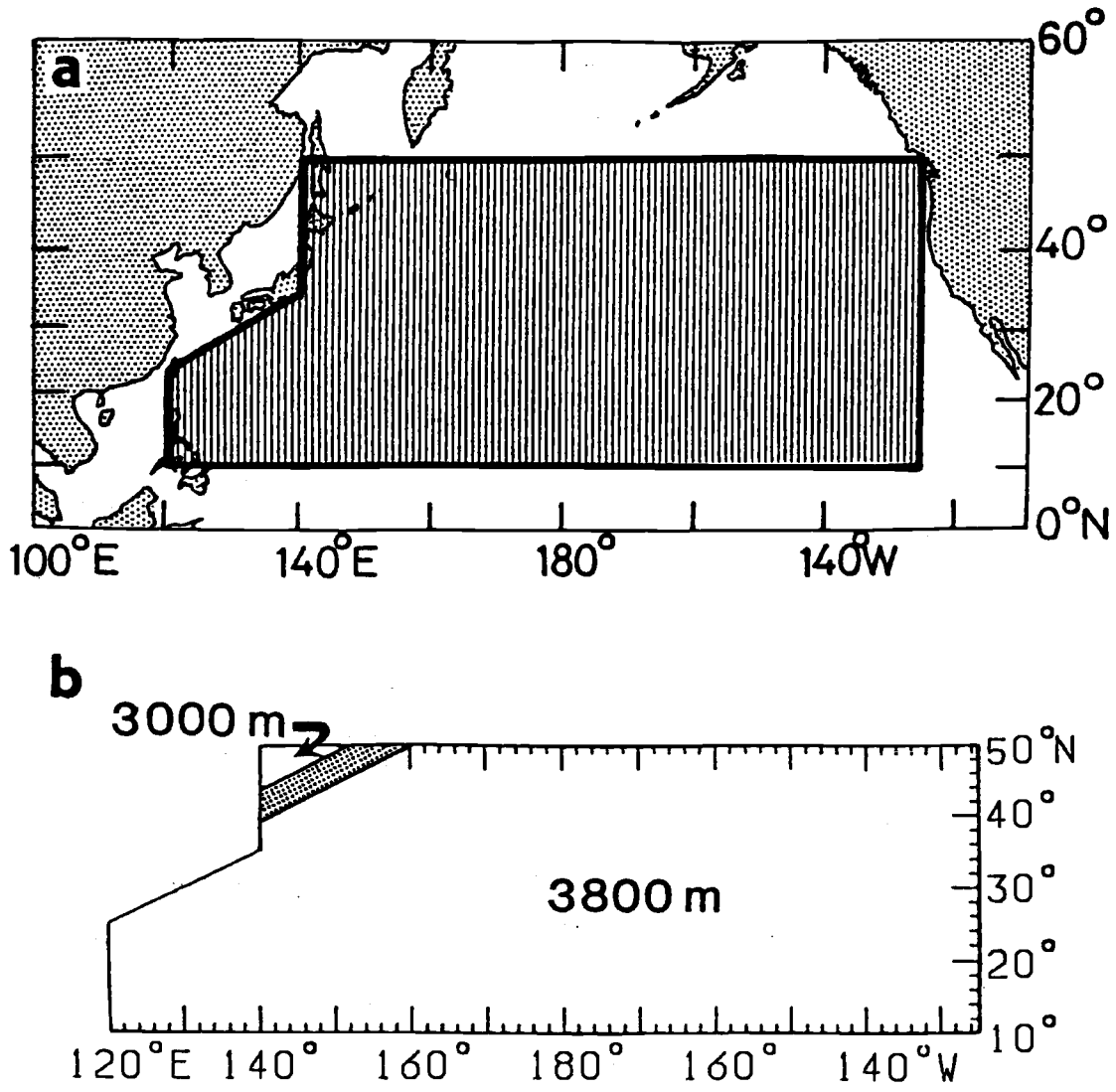

Fig. 3. Geometry of the ocean domain (a) and assumed bottom topography (b) used in the model.

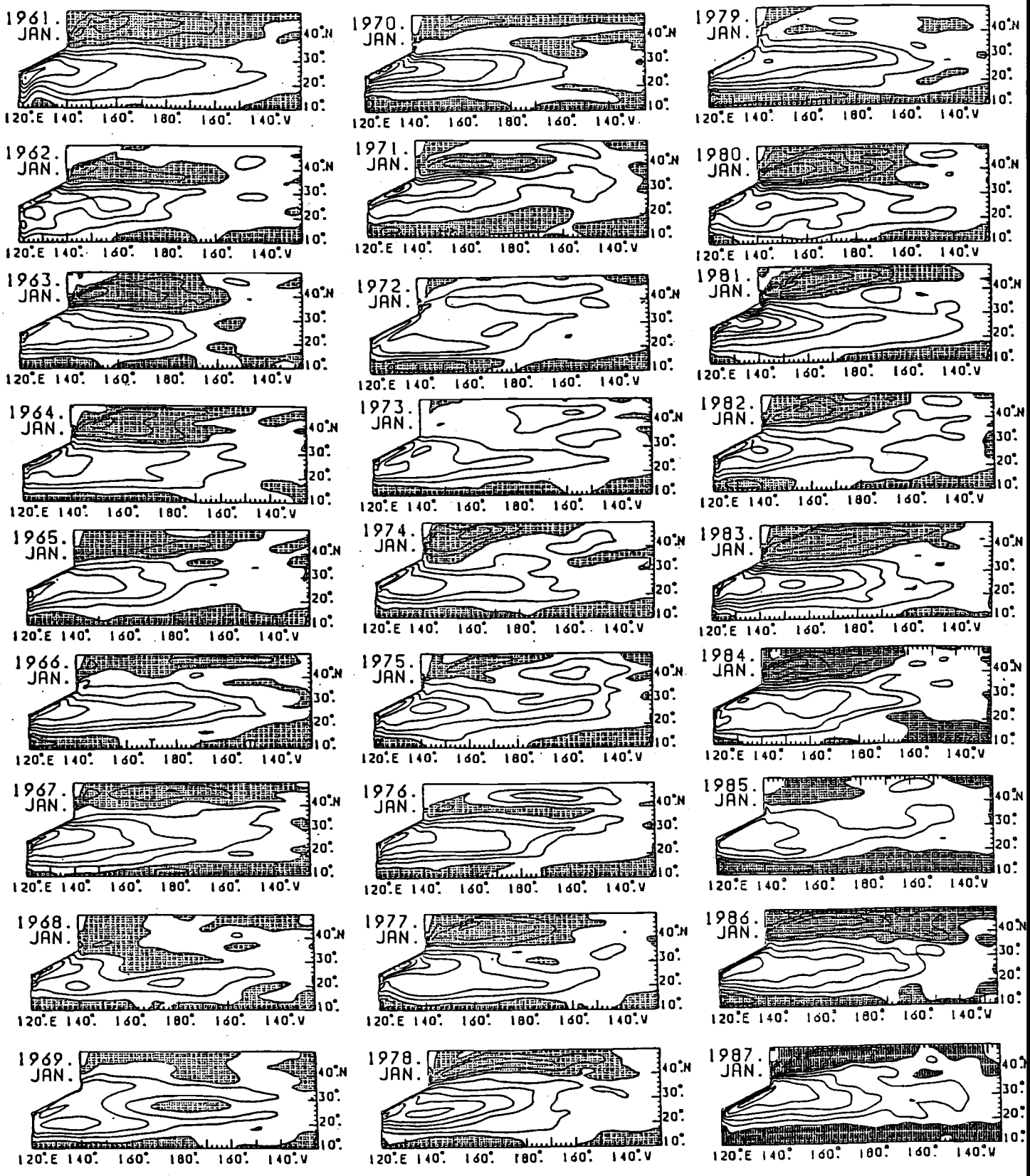

Fig. 4. The calculated total volume transport function at the middle of January of each year. Contour interval is 10 Sv. The shaded area indicate the portion of anti-clockwise circulation.

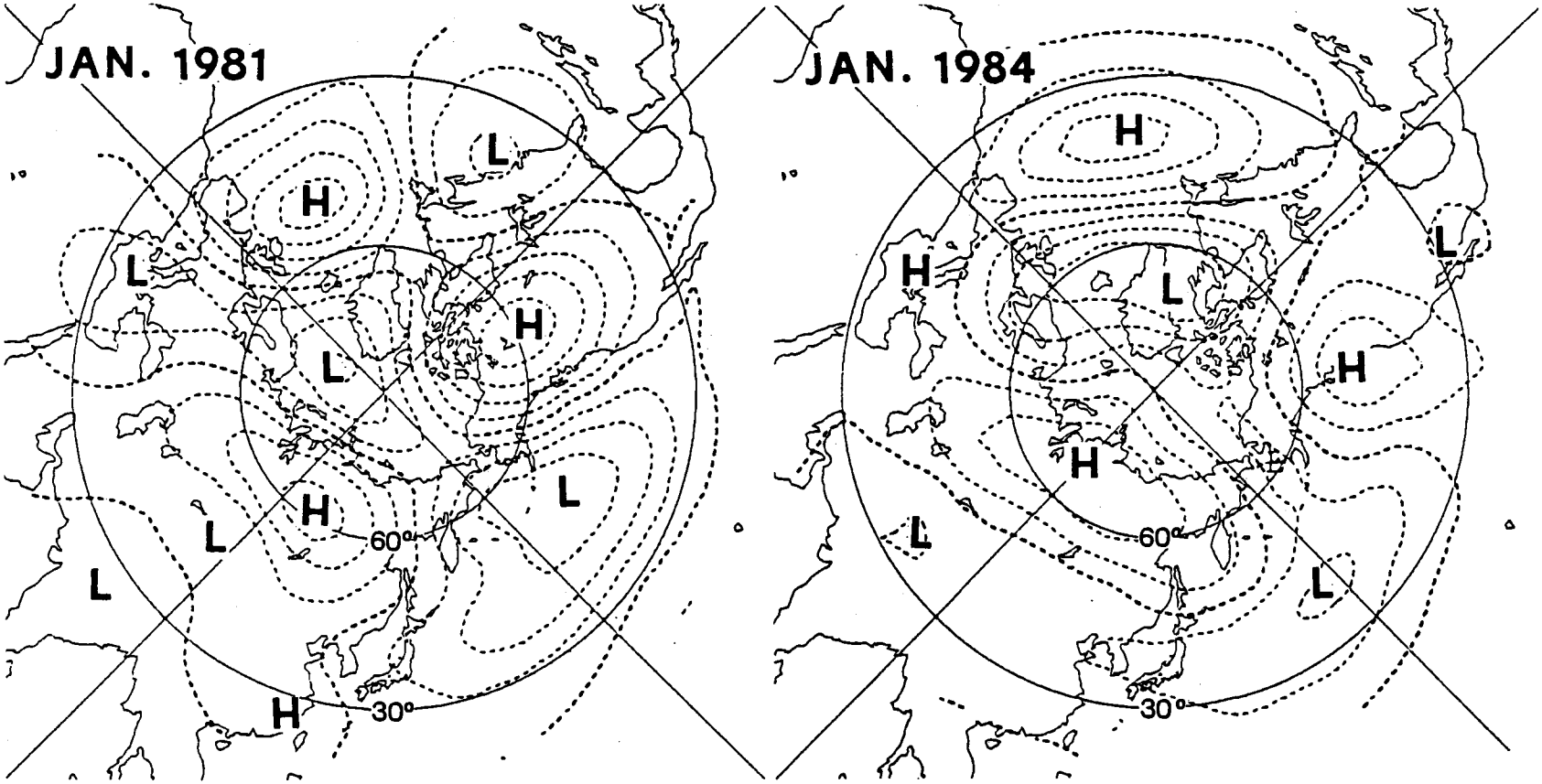

Fig. 5. Examples of the 500 hPa height anomaly distributions over the northern hemisphere at the time of the Anomalous Oyashio Intrusion: January 1981 (left) and January 1984 (right). Contour interval is 50 m.

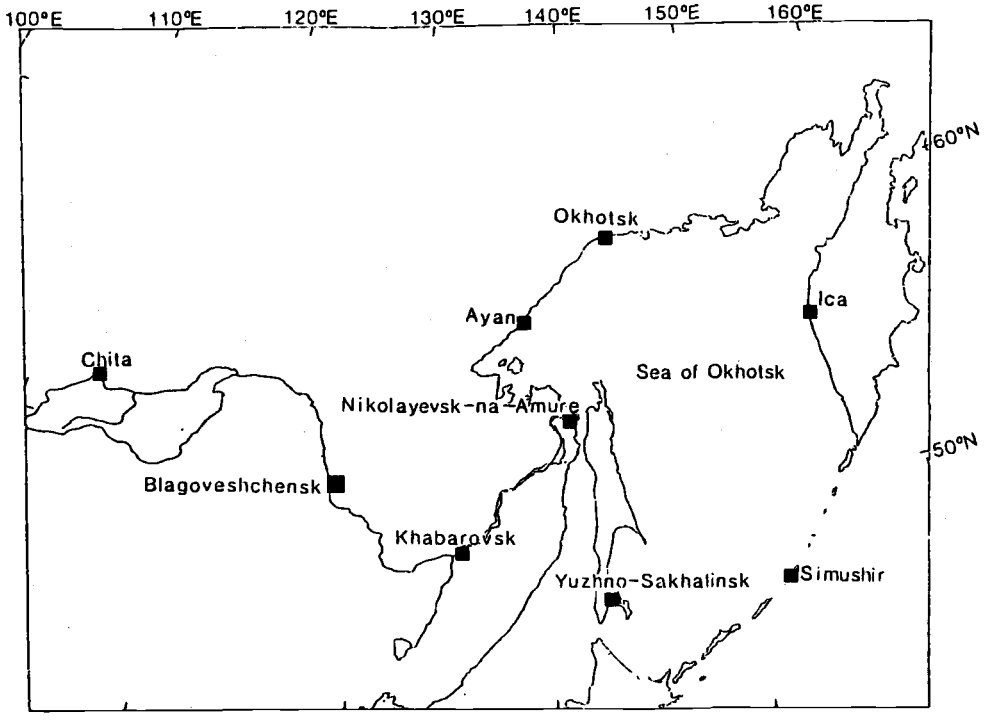

Fig. 6. Meteorological stations used for the air temperature anomalies analysis.

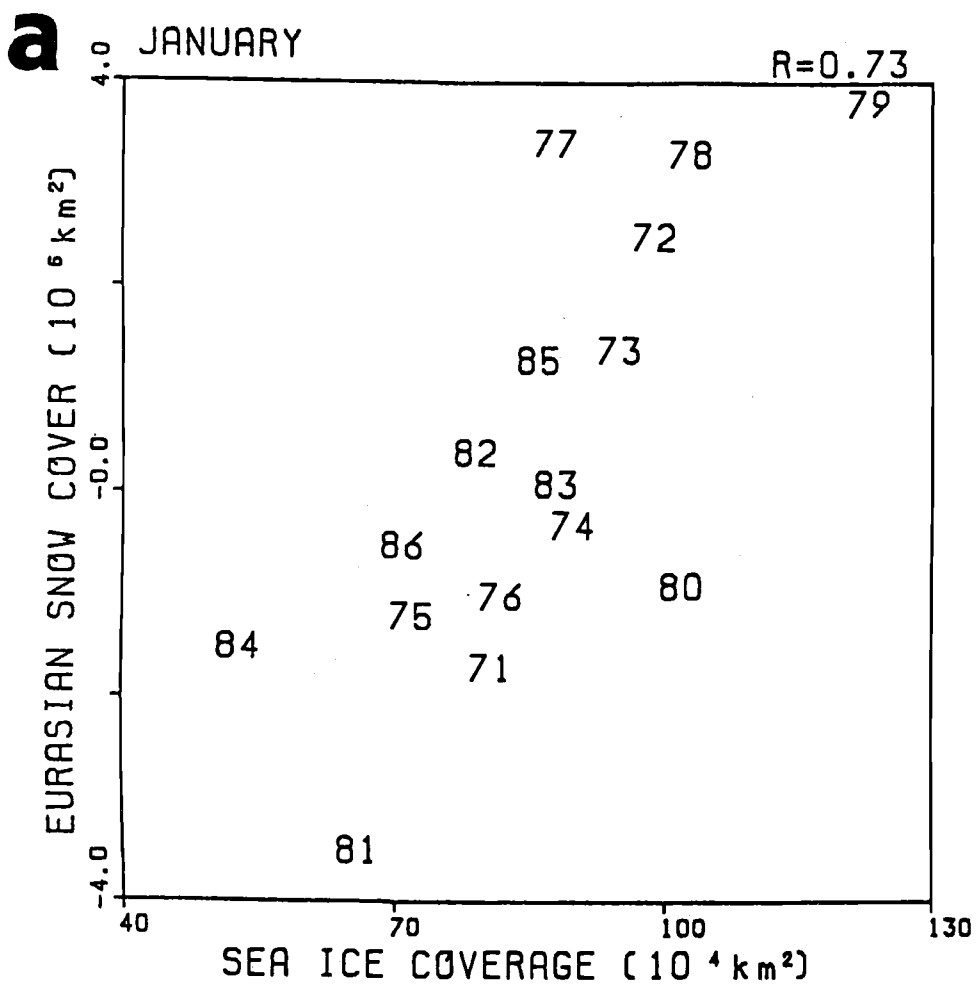

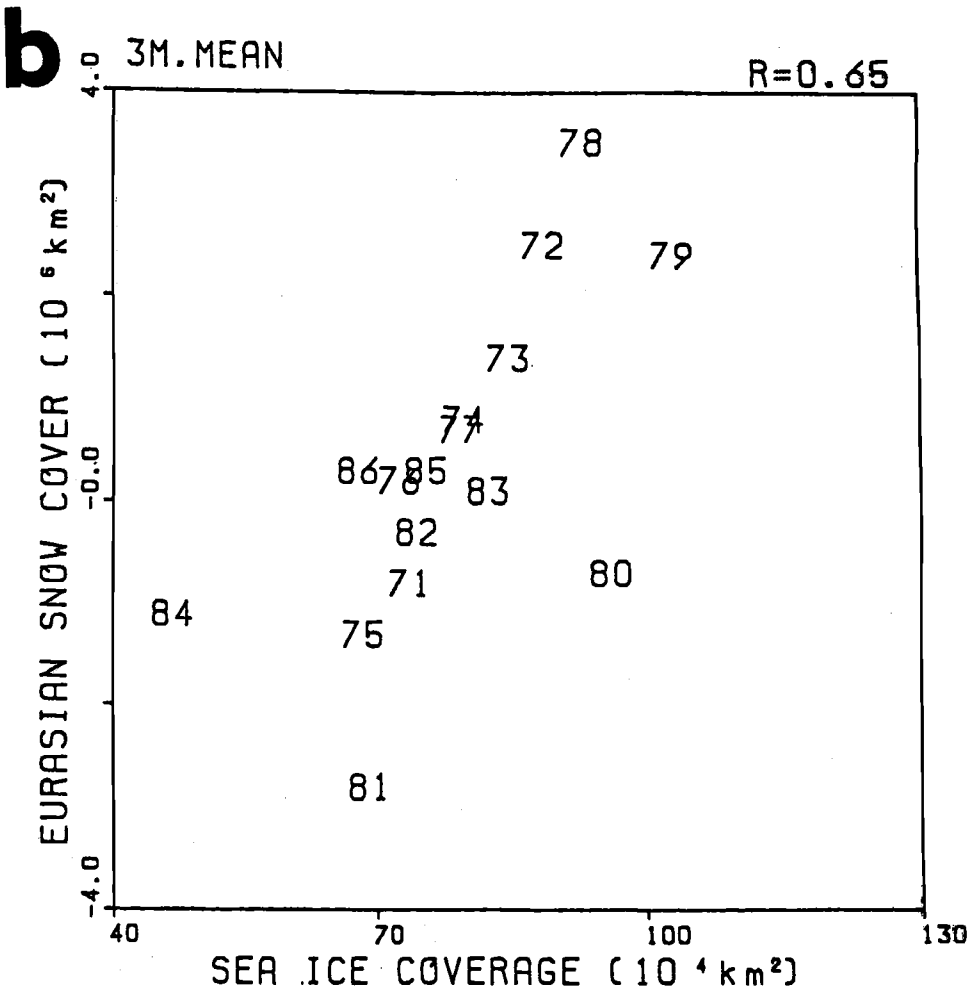

Fig. 7. Correlation between the areas of the Okhotsk Sea ice cover and the Eurasian Continent snow cover: for January data (a) and for three months data averaged from December to February (b). Numbers indicate the corresponding years.

Characteristics of the Tidal Motions in the Kuril Straits

Vladimir A. LUCHIN

Far Eastern Regional Hydrometeorological Research Institute, Vladivostok, Russia

INTRODUCTION

The tidal currents increase considerably their velocity in the Kuril Straits and create favorable conditions for intensive vertical and lateral water mixing leading to a decrease of the vertical gradients of the water properties observed in the region.

Results from previous investigations and data collected from 66 buoy stations within the Kuril Island area were recently examined by Luchin (1995). Tidal constants from 20 island positions were used to calculate yearly sea level fluctuations. All data obtained demonstrate that the main part of the Kuril region is characterized by predominant diurnal tidal currents and sea level fluctuations. These tides and sea levels are in phase: during the low water time it is clearly seen that observed differences in the onset time of tidal extrema do not exceed 1-2 hours and depend mostly on the geographical position and local bottom topography of sea level observational points. The diurnal tidal sea level fluctuations are dominant during both summer and winter and the maximum tidal amplitudes are detected in these seasons. Semidiurnal sea level fluctuations are the most pronounced in March and September.

The major ellipse axes of tidal currents are directed mainly along isobaths, whereas in the straits they are oriented along the troughs. In narrow straits, under specific astronomic conditions, maximum tidal currents can reach 5-8 knots.

DATA AND METHOD

The instrumental current measurements were collected from 516 stations in the Kuril region. Unfortunately, their duration at 450 stations did not exceed 1 day and was from 3 to 15 days only at 66 buoy stations (38 of which have been located in the narrows of straits). Sea level fluctuations along the Kuril Islands have been considered at 20 coastal stations. The hourly sea level heights were calculated using tidal constants for 8 main constituents.

RESULTS

Analysis of available observations show that vertical structure of tidal currents in the Kuril Straits is quite homogeneous (Fig. 1). Variations of current parameters with depth are insignificant and demonstrate that the barotropic component dominates in tidal flow. Certain variations in the current directions at specific depths are probably related to the topographic peculiarities within the straits. The weakest tidal current velocities are observed in the Bussol Strait. Therefore, water structure here is less transformed and the effect of non-periodic and baroclinic disturbances increases in the tidal flow.

Simultaneous current measurements were also performed at several points spatially divided up to 26 miles. These data show that spatial variations of tidal flow (in the absence of abrupt topographic changes) are insignificant.

The sea level temporal variations and tidal current features demonstrate the existence of a certain interaction between them. Temporal sea level fluctuations simultaneous with current observations were calculated using tidal constants from the nearest sea level station and the following results were obtained. In the Bussol Strait (sill depth 2,318 m) tides have a progressive wave character. The maximum tidal currents penetrating into the Pacific occur in the period of low water or about 1 hour before.

Standing fluctuations are observed in the deep part of the Kruzenshtern Strait (sill depth 1,920 m). The maximum currents occur 1-3 hours before low water (Fig. 2). The standing fluctuations dominate also in the shallow straits and over the shallow parts of the deep straits. For instance, the tidal currents move into the Okhotsk Sea over the shallow part of the Kruzenshtern Strait as sea level rises and reverse into the Pacific Ocean as sea level falls (Fig. 3).

The anomaly relation between sea level and the currents is observed in the deep trough of the 4th Kuril Strait. Standing fluctuations are dominant in this case, but the maximum currents into the Okhotsk Sea occur 6-8 hours after the low water (Fig. 4). Further investigations under different astronomic conditions are required for this region.

Thus, in the straits with complicated morphometry different contributions of progressive and standing wave components were observed. It can lead to generation of eddy disturbances within the tidal flow. This event should also be expected in the regions of abrupt depth changes.

RECOMMENDATIONS FOR FIELD OBSERVATIONS

1. Current measurements in the main Kuril Straits should be conducted simultaneously and duration of observations has to be not less than 15 days. Sea level fluctuations should be recorded nearby at the same time.
2. Tidal observations in straits with complicated topography should be simultaneously assessed in both troughs and shallow water regions.
3. Observations have to be carried out in the periods of prevailing diurnal currents as well as when semidiurnal currents are dominant.

REFERENCES

Luchin, V. A. 1995. System of currents and peculiarities of temperature distribution in the Okhotsk Sea. The Okhotsk Sea and Oyashio Region. PICES Scientific Report No. 2:211-227.

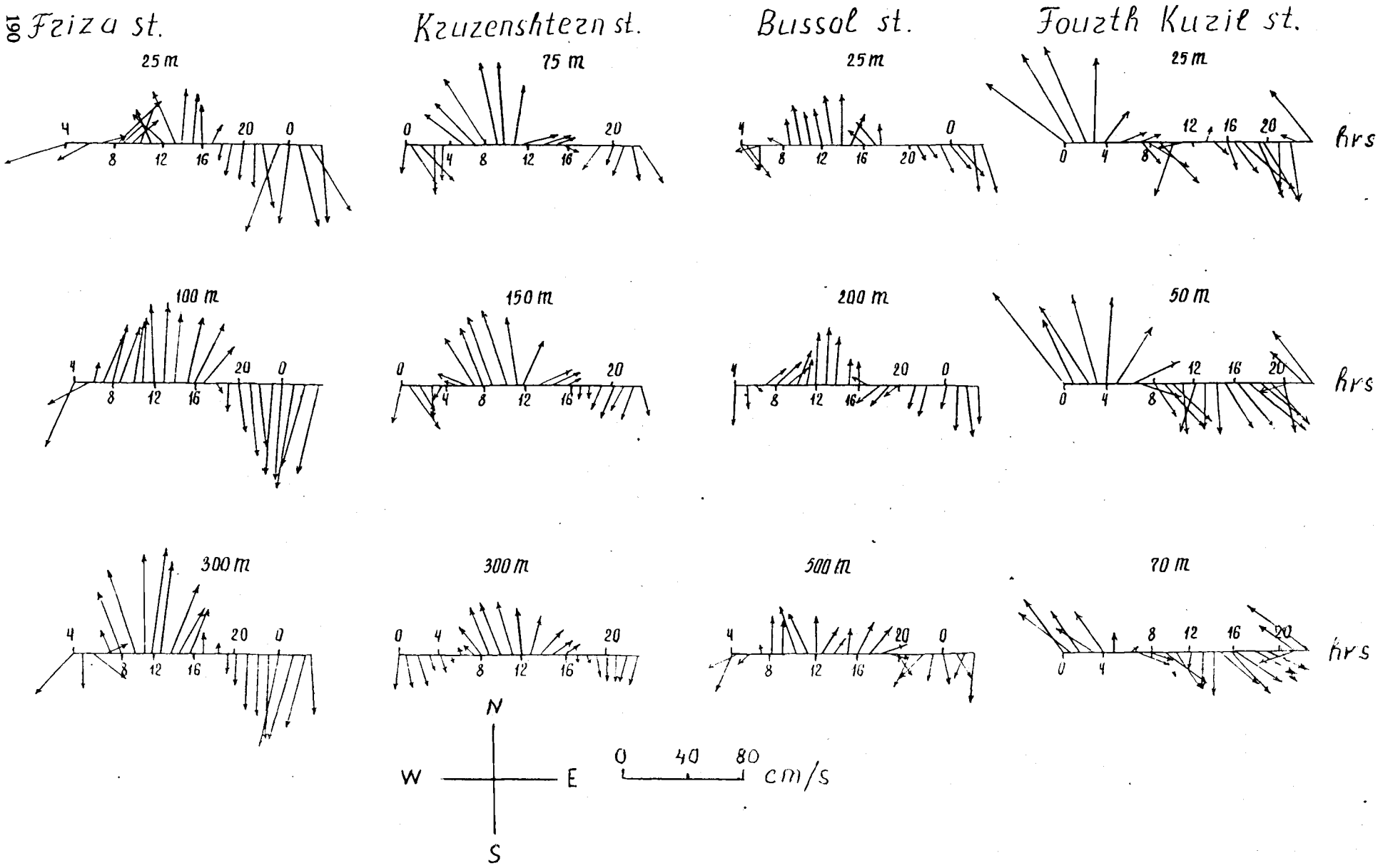

Fig. 1. Temporal variations of tidal current velocities at various depths in the Kuril Straits.

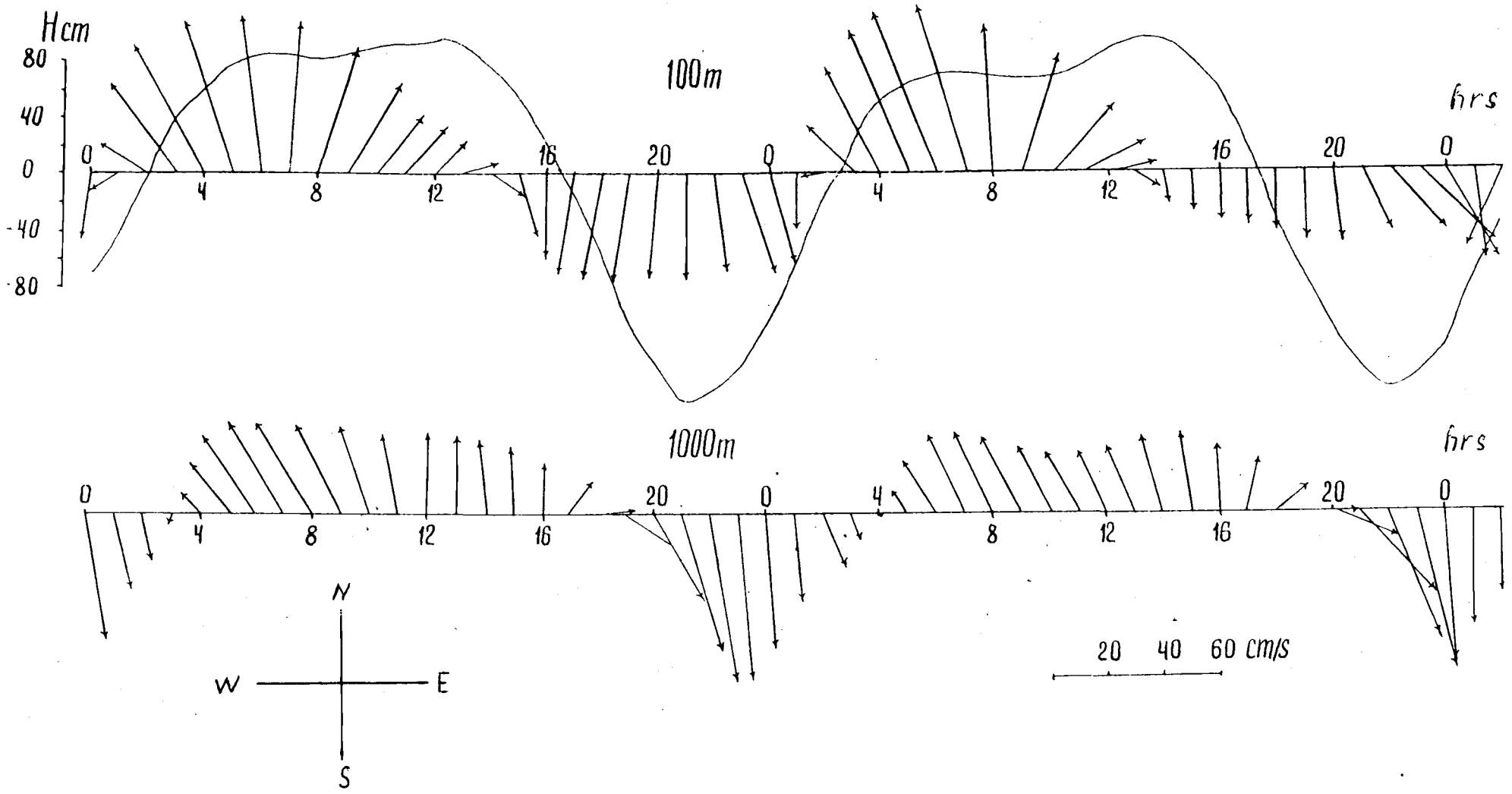

Fig. 2. Temporal variations of tidal current velocities and sea level fluctuations in the deep part of the Kruzenshtern Strait.

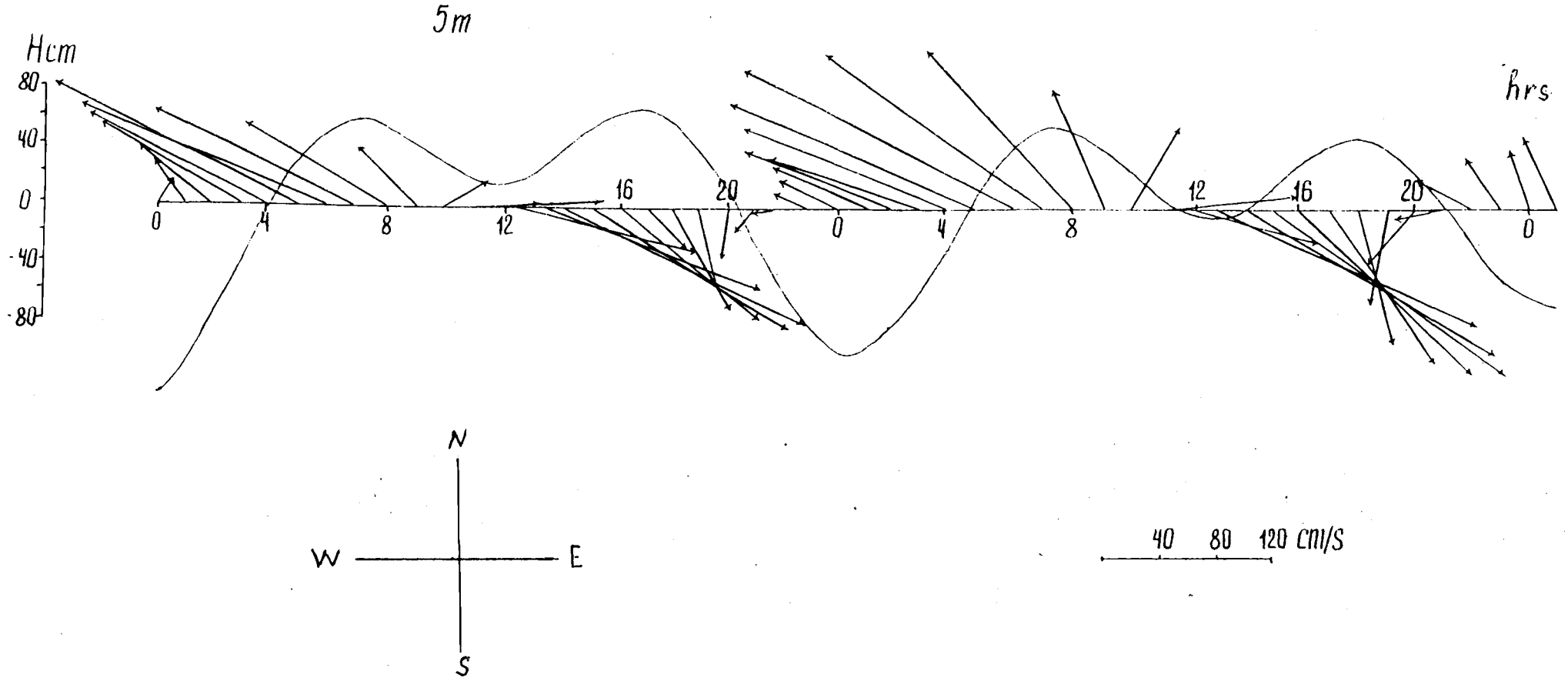

Fig. 3. Temporal variations of tidal current velocities and sea level fluctuations in the shallow part of the Kruzenshtern Strait.

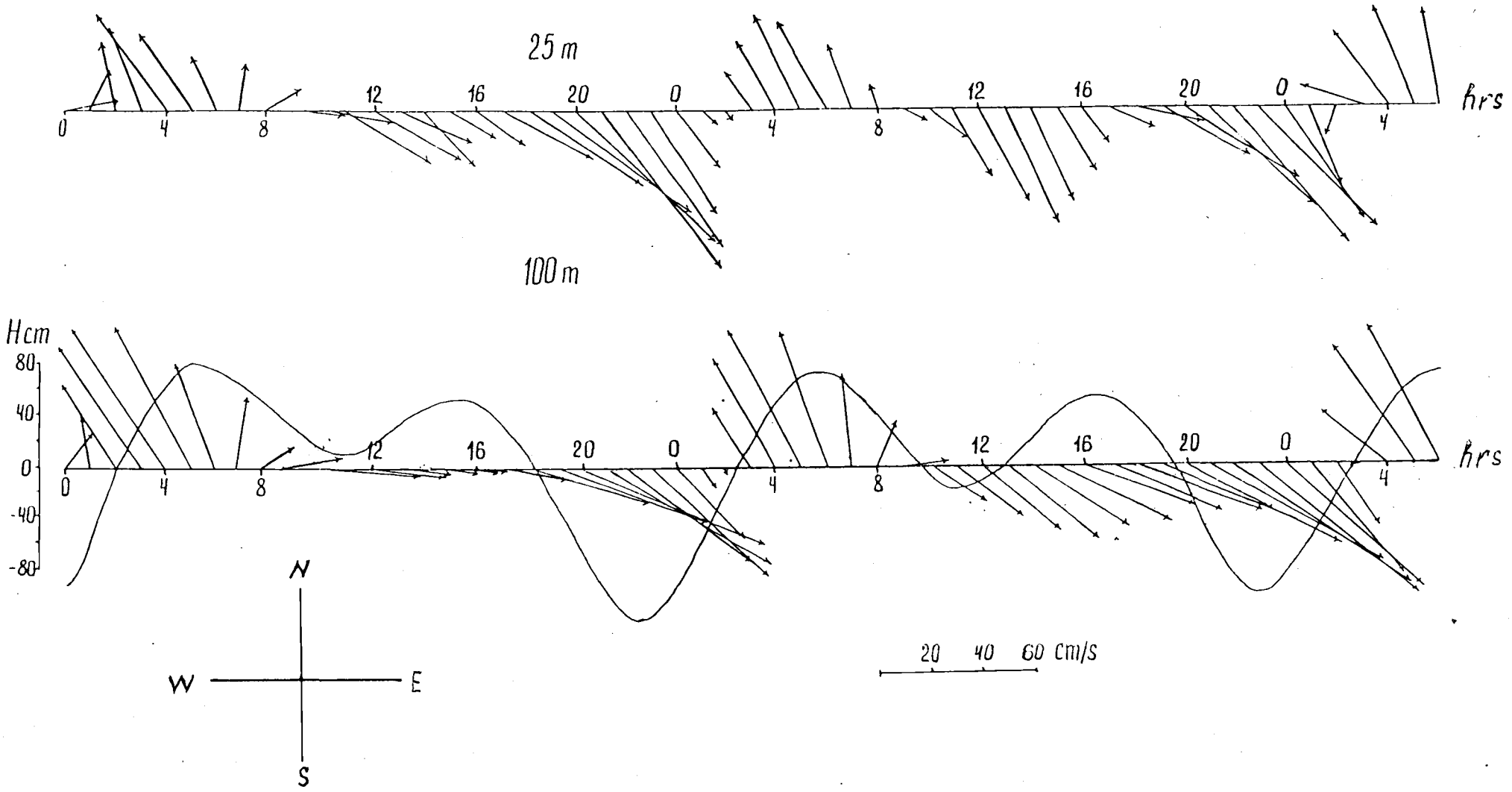

Fig. 4. Temporal variations of tidal current velocities and sea level fluctuations in the 4th Kuril Strait.

On Seasonal Variability of Tidal Constants in the Northwestern Part of the Okhotsk Sea

George V. SHEVCHENKO

Institute of Marine Geology and Geophysics, Far Eastern Branch,
Russian Academy of Sciences, Yuzhno-Sakhalinsk, Russia

INTRODUCTION

The main problem of tidal regime research could normally be reduced to the determination of tidal constants (amplitude h and phase g) from the available sea level observational series. Tidal sea levels and currents for any moment of time can be predicted using these constants. In most cases a monthly observational series is enough for reliable estimation of h and g, and as a rule, a corresponding long-term forecast can be made with sufficiently high accuracy, satisfying practical requirements for hydrology surveys, port activities, coastal engineering, etc.

However, in some ocean regions this method does not work properly for various reasons, such as, change in water circulation, bottom friction, influence of ice, outflow of energy into internal waves, etc. As a result, temporal variability of tidal constants is observed (Pugh and Vassie, 1976; Sgibneva, 1981) and prediction of tides turns into a more difficult problem.

A correct prediction of tidal currents and sea levels is highly important for the northwestern part of the Okhotsk Sea because of planned development of the oil and natural gas industry in this area. In the present work the seasonal variability of tidal constants is studied based on hourly sea level data at three stations: Nabil Bay (Katangli), Okhotsk and Moskalvo. Seven year average tidal constants were used to calculate the amplitude and phase "systematic corrections" for each month.

DATA ANALYSIS

Hourly sea level data from tide gauges in the Okhotsk Sea [Korsakov (1977-1990), Poronaisk (1977-1988), Kurilsk (1977-1985), Magadan (1977-1988), Okhotsk (1982-1988), Moskalvo (1965-1966, January-May) and Katangli (1987-1993)] were analyzed. Tidal sea level constituents were determined by least square method for all years. Significant difference between observed and predicted sea level series has been found at three stations in the northwestern part of the Okhotsk Sea (Okhotsk, Moskalvo, Katangli) where spectra of residual sea levels had prominent peaks at tidal frequency bands). For these stations, tidal constituents were determined for each month separately as in Pugh and Vassie (1976). Since for monthly series some tidal constituents (such as K_1 and P_1 or S_2 and K_2) could not be separated, they were estimated using values obtained from the whole year. Our results (Figs. 1 and 2) clearly demonstrate that the amplitude and phase of main constituents change from month to month.

Similar phenomenon was also revealed in some other Okhotsk Sea regions, in particular for Penzhinskaya Guba (Sgibneva, 1981) and in Amursky Liman (Lyubitsky, 1989).

SEASONAL VARIABILITY OF TIDAL CONSTANTS

Seasonal variability of tidal constants at Okhotsk and Moskalvo stations is very strong. For the principal semidiurnal constituent M_2 variances in amplitude and phase are over 30% and 25°, respectively. Maximum amplitudes are observed in March and April and maximum phases are found in September and October when amplitudes are small. The diurnal tides have maximum amplitudes and minimum phases in January, whereas minimum amplitudes are observed in August and maximum phases in October. Thus, seasonal variability of tidal amplitudes and phases of the main constituents is almost in counter-phase.

Variability of tidal constants on the northeastern coast of Sakhalin Island is not evident. Although the maximum amplitudes (in April and December) mainly correspond to minimum phases, but maximum phases (in September for diurnal tides and in July for M_2) do not coincide with minimum amplitudes observed in June for diurnal tides or in January - February for M_2. It should be noted that variability of tidal constants at Katangli station is not so significant and clearly emphatic as at the Okhotsk station where it has almost periodic character.

"SYSTEMATIC CORRECTIONS" OF TIDAL CONSTANTS

Seven year average tidal constants for Okhotsk and Katangli stations were used to calculate "*systematic monthly corrections*". The amplitude corrections have been estimated as a ratio of the average monthly values to the whole year value, while the phase correction was computed as a difference between monthly and the whole year values. These corrections may be used in analysis of relatively short off-shore measurements of currents and sea levels, and also for more accurate tidal predictions.

To characterize the importance of "systematic corrections" three variances and corresponding ratios (%) have been calculated for each tidal constituent (Table 1):

1. *Factoral (or intergroup) variance* (D_f) related to deviations of the mean monthly values from the mean yearly value;
2. *Average group variance* (D_g) associated with deviations of mean monthly values for every year from the average (over 7 years) monthly values caused by various reasons, considered as casual;
3. *Total variance* (D_t) equals to the sum of two previous.

The relative contribution of the intergroup variances demonstrates the importance of regular events in comparison with the casual elements caused by fluctuations inside the groups. It is also evident, that in the Okhotsk region seasonal fluctuations of tidal constants are the most essential, and casual deviations are insignificant compared to "systematic monthly corrections".

CONCLUSIONS

1. Significant seasonal variability of tidal constants in the northwestern part of the Okhotsk Sea has been revealed based on analysis of tide gauge data.
2. Seasonal variability is high and steady in the Okhotsk region and rather less on the northeastern coast of Sakhalin Island.
3. Use of "*systematic monthly amplitude and phase corrections*", calculated from seven year average tidal constants, reduces errors of sea level prediction up to 0.5 m in the Okhotsk region and up to 0.2 m at Katangli station.

4. Obtained results could be used for more accurate forecast of tidal sea levels and currents in the northwestern part of the Okhotsk Sea.

REFERENCES

Lyubitsky, Yu.V. 1989. Sea level at the river mouth. Trudy DVNIGMI, Vladivostok. 38:69-104 (in Russian).

Pugh, D.T., and J.M. Vassie. 1976. Tide and surge propagation off-shore in the Dowsing region of the North Sea. Deutsche Hydrographiche Zeitschrift. 29:163-213.

Sgibneva, L.A. 1981. Variability of tidal constants as consequence of non-linear effects. Trudy GOIN, Moscow. 156:33-40 (in Russian).

TABLES AND FIGURES

Table 1. Total (D_t), factoral (D_f) and average (D_g) group variances of 7-year average monthly tidal constants (corresponding ratios D_f/D_t and D_g/D_t are given in brackets).

		VARIANCES (Deg^2, cm^2)	
STATION/CONSTITUENTS	*FACTORAL*, D_f	*AVERAGE GROUP*, D_g	*TOTAL*, D_t
KATANGLI			
M_2 (phase)	21.8 (61%)	14.4 (39%)	36.2
M_2 (amplitude)	0.8 (53%)	0.7 (47%)	1.5
K_1 (phase)	10.3 (65%)	5.5 (35%)	15.8
K_1 (amplitude	2.9 (43%)	3.8 (57%)	6.7
OKHOTSK			
M_2 (phase)	59.0 (93.8%)	3.9 (6.2%)	62.9
M_2 (amplitude)	49.4 (84.7%)	8.9 (15.3%)	58.3
K_1 (phase)	15.7 (86.7%)	2.4 (13.3%)	18.1
K_1 (amplitude	6.2 (87.3%)	0.9 (12.7%)	7.1

FIGURES

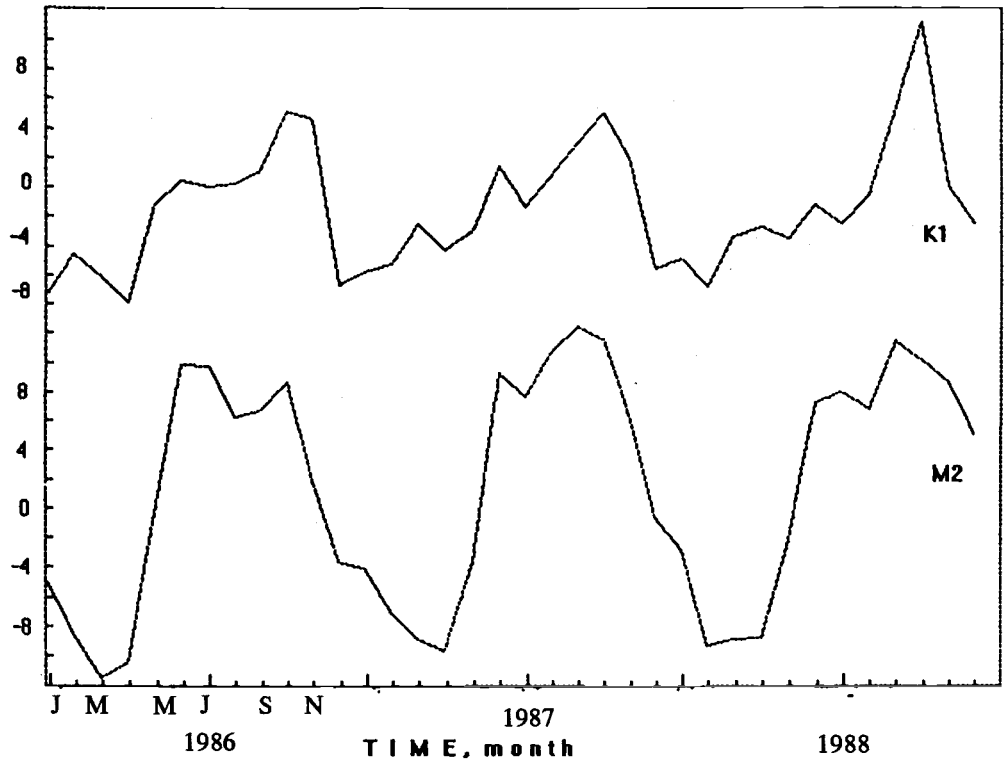

Fig. 1. Phases of the main diurnal and semi-diurnal constituents determined for each month separately (difference between monthly and whole year values). Okhotsk, 1986-1988.

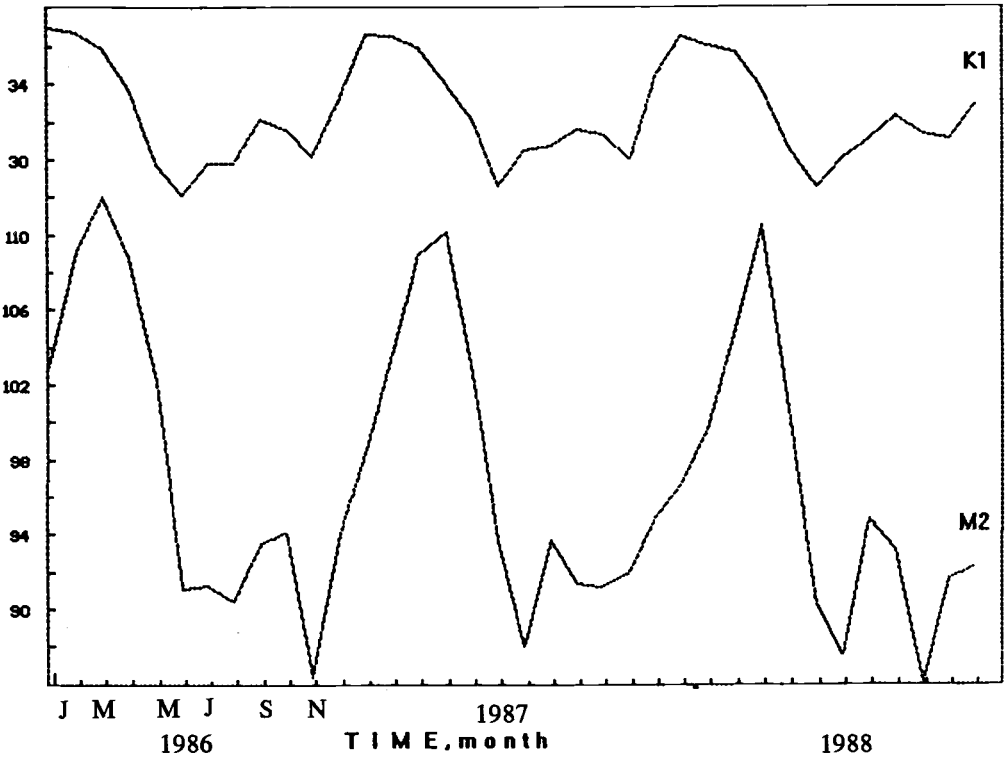

Fig. 2. Tidal amplitudes of main diurnal and semi-diurnal constituents determined for each month separately (in percentage, related to M2 amplitude obtained for whole year). Okhotsk, 1986-1988.

A "Chimney" of Cold Salt Waters near Vladivostok

Mikhail A. DANCHENKOV[1], Kuh KIM[2], Igor A. GONCHARENKO[1] and Young-Gyu KIM[2]

[1] Far Eastern Regional Hydrometeorological Research Institute, Vladivostok, Russia
[2] Research Institute of Oceanography Seoul National University, Seoul, Republic of Korea

INTRODUCTION

It is generally believed that the Japan Sea Proper Water (JSPW) is formed in the northwestern part of the Japan Sea. Nevertheless, this area was investigated very poorly in comparison with the southern part of the Sea. Almost twenty five years ago Nitani (1972) noted that the winter situation in the northwestern Japan Sea is unknown and suggested a survey in Peter the Great Bay just before and during the period of ice formation. None the less, after fifteen years, Gamo et al. (1986) mentioned a lack of information about the spatial and temporal variations of water properties in the northern Japan Sea regarded as a regional source of the bottom water and emphasized the need to research the northern and northwestern Japan Basin, especially in the winter season. According to Sudo (1986), the most probable source of the JSPW formation is the region north of 41°N between 132°E and 134°E. This statement was amplified by Senju and Sudo (1993) who advised that the upper portion of the JSPW is formed by winter convection, likely off the Siberian coast west of 136°E between 40°N and 43°N.

Now the opportunity arose to discuss the process of water formation in the northwestern part of the Japan Sea based on new temperature and salinity data collected during two consecutive winters in 1994 and 1995.

DATA

During the winter of 1994 research vessels of Far Eastern Regional Hydrometeorological Research Institute repeated temperature and salinity measurements nine times on the section along 132°E from Vladivostok to 36.5°N. In March 1995 seven one-time sections were performed from the coast to 41.0°N between 131.5°E and 133.6°E. The total number of stations sampled was 116.

Note the interesting feature of bottom relief in the area of investigation: just south of Vladivostok between 41.5°N and 42.5°N there is a bottom rise with a minimum depth less than 1,000 m contoured by a 2,500 m isobath.

VERTICAL DISTRIBUTION OF WATER CHARACTERISTICS IN 1994 AND 1995

The "chimney" - area of homogenous vertical water properties near the bottom rise - was revealed for the first time in March 1994 along 132°E between 41.5°N and 42.5°N. In March 1995 during the winter CREAMS cruise the meridional boundaries were determined as 131.8°E and 133.2°E. The "chimney" was bordered from the south and west by the Subarctic (Polar) thermal front, from the north by a coastal saline front and from the east by a coastal thermal front.

In March 1994 the temperature in the "chimney" changed from -0.7°C to 0.7°C and was lower than in neighboring waters. Salinity in this area varied between 34.02 and 34.19 psu and was lower than in the northern part of Peter the Great Bay, but higher than in surrounding waters by 0.03-0.10 psu. Density (sigma-t) in the "chimney" was in the range 27.30-27.44, almost uniform in vertical direction and also differed from density of adjacent waters. Seawater homogeneity was observed from the surface down to 1,500 m (the lowest horizon of observations).

In March 1995 measurements at section along 132.3°E were performed with better accuracy and just above the bottom rise, and the characteristics of seawater were found in a good agreement with our previous survey (Table 1). Depth of salinity maximum was situated at 300-500 m and depth of temperature minimum at 1,700-1,900 m.

At 132°E (western border of the "chimney" area) and at 133°E (its eastern edge) the sigma-theta surface of 27.32 was located at depth above 100 m. In the center of the "chimney" near surface sigma-t was higher than 27.32 (Fig. 1). Between the surface and 1,000 m water temperature changed from 0.5°C to 1.0°C and salinity from 34.05 to 34.07 psu. Even during summer, sigma-t of 27.3 was closer to the sea surface than anywhere else in the Japan Sea.

HORIZONTAL WATER STRUCTURE

At the sea surface in winter the "chimney" area was bordered from the south and west by the Subarctic (Polar) front and from the north by the coastal Primorye front. The Subarctic front was best revealed by temperature distribution and the coastal front by salinity distribution. According to satellite images (e.g., November 28, 1983) water of in the "chimney" was colder than surrounding waters, and that cold pool is detected in the area every winter. It should also be mentioned that extremely high salinity (more than 34.15 psu) was observed in the pool at the end of 1994.

CONCLUSION

The "chimney", an area of homogeneous vertical temperature and salinity distribution, was found in winter above the bottom rise near Vladivostok. The "chimney" water is characterized by temperature 0.5°C - 1.0°C, salinity - 34.05-34.07, and density (sigma-t) higher than 27.3.

REFERENCES

Gamo, T., Y. Nozaki, H. Sakai, T. Nakai, and H. Tsubota. 1986. Spatial and temporal variations of water characteristics in the Japan Sea bottom layer. J. Marine Res. 44:781-793.

Nitani, H. 1972. On the deep and bottom waters in the Japan Sea, p.151-201. *In* D. Shoji [ed.] Researches in hydrography and oceanography. Tokyo Hydr. Dept. of Japan.

Senjyu, T., and H. Sudo. 1993. Water characteristics and circulation of the upper portion of the Japan Sea Proper Water. J. Marine Systems. 4:349-362.

Sudo, H. 1986. A note of the Japan Sea Proper Water. Progr. Oceanogr. 17:313-336.

TABLES AND FIGURES

Table 1. Temperature (°C), salinity (PSU) and depth of 27.32 sigma-t (Zs-t) above bottom rise in winters of 1994 and 1995.

Time	Coordinates	Temperature and salinity					Zs-t
		0m	200m	400m	1,000m	2,000m	
22.03.94	42.2°N, 132.0°E	0.89	0.61	0.35	0.18	-	60 m
		34.046	34.066	34.063	34.060	-	
	41.8°N, 132.0°E	0.75	0.58	0.44	0.22	-	100m
		34.046	34.069	34.065	34.061	-	
03.03.95	42.0°N, 132.3°E	0.66	0.67	0.62	0.24	0.19	0m
		34.060	34.068	34.071	34.063	34.063	
	41.8°N, 132.3°E	0.90	0.63	0.53	0.23	-	50m
		34.049	34.066	34.070	34.063	-	

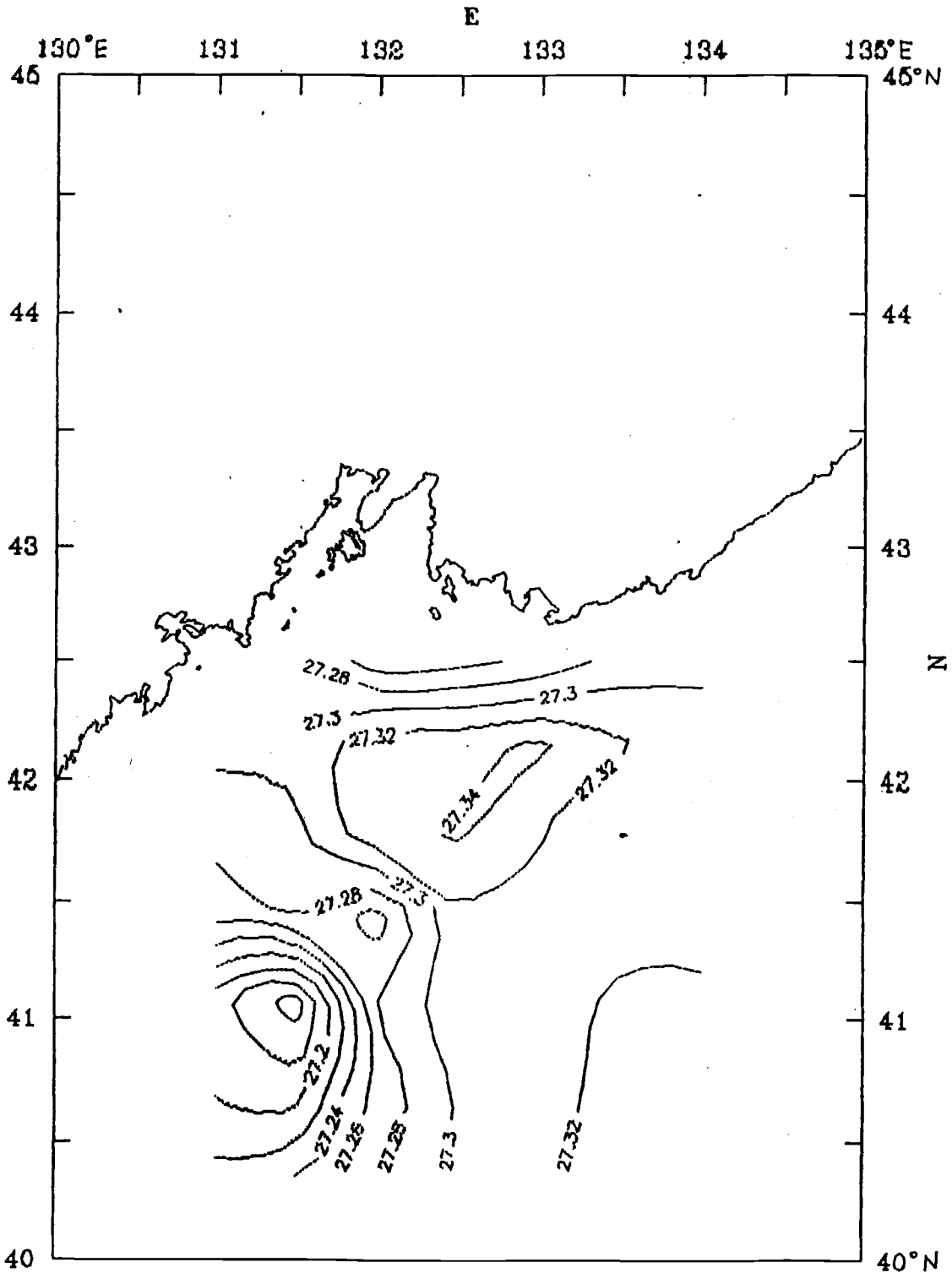

Fig. 1. Distribution of sigma-t at 200 m depth during March 1-8, 1995.

Preliminary Results from a Numerical Circulation Model of the Japan Sea

Christopher N.K. MOOERS and Hee Sook KANG

Ocean Prediction Experimental Laboratory (OPEL), Rosenstiel School of Marine and Atmospheric Science, University of Miami, Miami, FL 33149, U.S.A.

INTRODUCTION

The circulation of the Japan Sea is dominated by the throughflow of the Tsushima Current, which enters through the Korean Straits, branches along the Korean and Japanese coasts, and exits through the Tsugaru and Soya Straits. It is also strongly influenced by atmospheric forcing and river runoff, plus ice formation and tidal circulation, especially in the northern reaches of the Tatarsky Strait. The instantaneous circulation is characterized by intense mesoscale variability; i.e., meandering jets, eddies, and fronts. The upper few hundred meters of the southern half of the basin are much more stratified than the northern half of the basin; the two halves are separated by the subpolar front and jet. The lower few kilometers of the water column are filled with the relatively homogeneous Japan Sea Proper Water, which, however, has fine structure associated with interannual variations in wintertime deep convection.

Major open questions exist concerning the deep convection process, which has at least three candidate source regions: north of the subpolar front off Vladivostok, various shallow sites along the Primorsky Coast (especially Peter the Great Bay), and the Tatarsky Strait in association with ice formation. So far, the physical estimates of deep water formation rates are substantially less than those inferred from geochemical properties. Other open questions include the role of mesoscale variability in the evolution of the general circulation (including deep water formation), the seasonal evolution of the circulation and stratification, the response to Siberian cold air outbreaks and subtropical cyclones, and to seasonal and interannual variability of the inflows. In general, there is presently a strong interest in understanding the circulation of semi-enclosed seas, with the Japan Sea representing a different part of parameter space compared to the Gulf of Mexico/Caribbean Sea and the Okhotsk Sea, for example. Several numerical simulations for the Japan Sea circulation have been undertaken in recent years; for example, Seung and Kim (1993), Kim and Yoon (1994), and Holloway, et al. (1995), with considerable success. However, they have all lacked various elements of realism, and it is desirable to attempt further progress.

Thus, a numerical simulation has been undertaken with an advanced, primitive equation model [Princeton Ocean Model: POM; Blumberg and Mellor (1987)] which can treat realistic bottom topography, atmospheric forcing, free sea surface (for tides and storm surge), and thermohaline processes. The model computes the three-dimensional currents, sea surface height, temperature, salinity, and turbulent exchange variables. POM has been implemented in the Japan Sea (and is called SOJ-POM) with marginal mesoscale eddy-resolution. Thus, it should be capable of treating most (if not all) of the key circulation processes enumerated above. Here, results from the beginning of a long-term campaign are described; namely, some of the properties of the initial spin-up are discussed.

THE JAPAN SEA MODEL

SOJ-POM uses realistic bottom topography from DBDB5 (extending to 20 m at the coastline), a rectangular grid with 10 km resolution in the south and 7.5 km resolution in the north, sigma (terrain-following) coordinates with 15 vertical levels, and Levitus (1982) climatological annual mean temperature and salinity fields. Thus, it has marginal mesoscale eddy-resolution, because the Rossby baroclinic radius of deformation varies from about 17 km in the south to about 8 km in the north. Geostophically-balanced, climatological mean inflow of 2.8 Sv (plus temperature and salinity) through the Korean Straits is specified, and outflows of 2.24 Sv and 0.56 Sv through Tsugaru and Soya Straits, respectively (where a radiation boundary condition is also applied) are designated. For the initial simulation, climatological mean wind stress from Hellerman and Rosenstein (1983) has been applied, and the sea surface temperature and salinity have been clamped to the Levitus climatology. The Mellor-Yamada (1982) level-2½ vertical turbulence closure and Smagorinsky (1963) lateral turbulence closure [with adjustable proportionality constant (HORCON) equal to 0.1] schemes have been utilized. The horizontal integration is on the Arakawa C-grid, vertical time-integration is implicit, and the horizontal time-integration is explicit, split-mode, with a barotropic mode time step of 10 sec. and a baroclinic mode time step of 5 min. The integrations are being carried out on a DEC-Alpha workstation and have been run for 190 days. Early results are also presented from a prognostic 100-day run with a 100-day relaxation of surface temperature and salinity to the Levitus climatology.

INITIAL SPIN-UP OF SOJ-POM

It is of interest to compare the simulation after 190 days of spin-up with the initial condition. Based on the total and eddy kinetic energy (averaged over the volume) versus time (Fig. 1), the model spun-up to statistical equilibrium in about 80 days and undergoes oscillations (due to instabilities) on a timescale of about a month. The surface dynamic height relative to 1,500 m (not shown) from the Levitus climatology (used to initialize SOJ-POM) indicates a broad, weak northeastward surface geostrophic flow from the Korean Coast to the Japanese Coast, which is, of course, consistent with the general circulation; however, the pattern is devoid of the boundary currents and subpolar jet is expected from observations. In contrast, the sea surface height at Day 190 in the prognostic calculation (Fig. 2a) indicates a strong East Korean Warm Current, Nearshore Branch (along Japanese Coast), Middle Branch, and two meandering subpolar jets associated with the bifurcation of the East Korean Warm Current, to be discussed below. There are also several mesoscale eddies or gyres. The surface dynamic height relative to 1,500m (proportional to the approximate baroclinic stream function), computed from the prognostic mass field at Day 190, has an overall pattern and magnitude similar to the sea surface height (Fig. 2b). Compared to a dynamic height difference of about 30 cm across the basin, the difference (barotropic geostrophic) field (Fig. 2c) between sea surface height and surface dynamic height is characterized by anomalies (due to mesoscale eddies and gyres) of typically up to 6 to 8 cm, indicative of the importance of the deep flow and its interaction with bottom topography. The depth-integrated (barotropic) stream function (not shown; similar in pattern to Fig. 2c) is dominated by strong anticyclonic and cyclonic gyres over the deep basin north of 40N. Somewhat weaker cyclonic gyres occurred over basins (Ulleung, Yamato, and southwestern Japan Basins, respectively) off the Korean, Japanese, and southern Primorsky Coasts, plus a mid-basin anticyclonic gyre centered at 39N, 134E over the Yamato Rise and other anticyclonic gyres, generally over rises, are secondary features. The throughflow follows the Japanese Coast. Further details on the basin-scale circulation are given in Mooers and Kang (1995); here other aspects are emphasized: circulation near the inflow and outflow ports, time series and vertical profiles of velocity, etc. at key locations, and a few comparisons of the effects of surface clamping versus 100-day surface relaxation.

The surface currents for in the inflow (Fig. 3) and outflow (Fig. 4) subdomains undergo substantial adjustment from the initial condition (10 day diagnostic run) to 10 days and 190 days of the prognostic run. The inflow is split by Tsushima Island and flows mainly along the Japanese Coast as the Nearshore Branch at Day 10 in the diagnostic run, which is the initial condition for the prognostic run. The East Korean Warm Current and Nearshore Branch developed by Day 10 in the prognostic run. A strong cyclonic meander in the East Korean Warm Current developed just downstream of Tsushima Straits by Day 190 in the prognostic run. For the outflow subdomain, equatorward coastal flow feeds the outflow through both Tsugaru and Soya Straits by Day 10 in the diagnostic run. The equatorward coastal flow intensifies and becomes connected to the offshore flow by Day 10 in the prognostic run. A large anticyclonic meander of the subpolar jet feeds the outflow through Tsugaru Strait by Day 190 in the prognostic run. Obviously, there are strong, complex, and variable cross-isobath flows in the vicinity of the inflow and outflow ports, and it would be useful to understand them.

For several selected levels, time series of currents (Fig. 5) at two grid points (S4 and S5) near CREAMS current meter moorings demonstrate the magnitude and nature of the flow, which varies on a time scale of ca. 1 month. In the upper layer (above 22 m) at S4, the speed is often at least 0.2 ms^{-1}, while in the interior (between 480 and 1,920 m) the speed is generally less than 0.2 ms^{-1}. In contrast, in the upper layer (above 25m) at S5, the speed is generally less than 0.2 ms^{-1}, while in the interior (between 540 and 2,160 m) the speed is often at least 0.2 ms^{-1}. At both S4 and S5 the interior flow is highly (visually) coherent, but the upper layer and deepest level flows are only partially coherent with the interior flow. Thus, there is strong barotropic and shallow baroclinic mesoscale variability, plus variability apparently localized to the surface and bottom layers.

At Day 190, the vertical profiles of velocity (Fig. 6) at S4 and S5 have quite different characteristics. For example, at S4, the zonal velocity is westwards (at about 0.1ms^{-1}) in the upper half of the water column, with a linear shear in the lower half that leads to a reversal to eastward below 2,500 m, and the meridional and vertical velocities are very weak. In contrast, at S5, the zonal velocity decreases from about 0.03ms^{-1} eastward near surface to nearly zero below 500 to 1,700 m, where it increases to about 0.1ms^{-1} near bottom. The meridional velocity is poleward at 0.02 to 0.08ms^{-1} between 200 m below the surface and above the bottom; and the vertical velocity (which is normal to the sigma surfaces) has a downward maximum of 0.2ms^{-1} at 3,000 m (and requires more analysis). At both S4 and S5, the thermocline is largely confined to the upper 400 m and the halocline to the upper 100 m.

A few results at Days 30 and 100 (Figs. 7 and 8, respectively) from a prognostic case in progress with a 100-day relaxation time-scale (*vice* clamping) of the surface thermohaline forcing, illustrate the emerging character of what is expected to be a superior simulation. (This case spun-up to statistical equilibrium in ca. 50 days and at an eddy kinetic energy level about one-half that of the clamped case.) For example, the sea surface height (Figs. 7b and 8b; to be compared with the evolution of the clamped case in Figs. 7a and 8a) has a single subolar jet that separates at 38°N and meanders (gently at Day 30 and vigorously at Day 100) to exit through Tsugaru Straits. There are cyclonic and anticyclonic circulation gyres over the Japan Basin, and there is a cyclonic gyre over the Ulleung (but not the Yamato) Basin. However, comparing Day 100 with Day 30, considerable mesoscale evolution is probably still in progress at mesoscale Day 100.

SUMMARY

Many of the major features of the general circulation of the Japan Sea are revealed in the simulations, and it is clear that flow interaction with bottom topography (JEBAR effect) is an important

factor. However, there are number of improvements to be expected, such as, full separation of the East Korean Warm Current at a lower latitude (ca. 38° to 41°N), as now appears to be emerging in the case of surface relaxation (*vice* clamping).

Improvements are anticipated when the model is run with seasonally-varying wind stress [possibly with the improved climatology provided by Na (1992)] and surface heat and moisture fluxes. It may also be necessary to increase the horizontal resolution, and possibly the vertical resolution and positioning of sigma levels, to account better for the mesoscale variability, especially the smaller (shallow and transient) mesoscale eddies and fronts, and to minimize the effects of spurious horizontal pressure gradients over steep bottom topography.

Another level of improvement can be expected when the model is forced with synoptic wind stress and heat and moisture fluxes, and with river runoff. Then it will be possible to explore the very important wintertime deep convection process, perform energetics calculations for eddy-mean flow interactions, and compare the model output with observations from the CREAMS Program. At that point, the stage will be set for data assimilation (with satellite radar altimetric sea surface heights, etc.), and for development of a nowcast/forecast system.

ACKNOWLEDGMENT

This research has been sponsored by the U.S. Office of Naval Research. The collegiality and friendship of Academician Guri I. Marchuk, Prof. Victor I. Kuzin, Prof. Gennady I. Yurasov, Prof. Masaki Takematsu, and Prof. Kuh Kim (plus other Russian, Japanese, Korean, and American colleagues) were instrumental in motivating this research as the beginning to a long-term collaboration for the International Study of the Circulation of the Japan Sea.

REFERENCES

Blumberg, A.F. and G.L. Mellor. 1987. A description of a three-dimensional coastal ocean circulation model. *In* N.S. Heaps [ed.] Three-Dimensional Coastal Ocean Models, and Coastal Estuarine Sci. 4:1-16. AGU, Washington, D.C.

Hellerman, S. and M. Rosenstein. 1983. Normal monthly windstress over the world ocean with error estimates. J. Phys. Oceanogr. 13:1093-1104.

Holloway, G., T. Sou, and M.. Eby. 1995. Dynamics of circulation of the Japan Sea. J. Mar. Res. 53:539-569.

Kim, C.-H., and J.-H. Yoon. 1994. A numerical study on the seasonal variation of the Tsushima Warm Current along the coast of Japan. Proceedings of the Third CREAMS Workshop, Seoul, Korea, p.73-79.

Levitus, S. 1982. Climatological atlas of the world ocean. NOAA Professional Paper 13, U.S. Dept. of Commerce, NOAA, Rockville, MD.

Mellor, G.L., and T. Yamada. 1982. Development of a turbulence closure model for geophysical fluid problems. Rev. Geophys. Space Phys. 20:851-875.

Mooers, C.N.K., and H.S. Kang. Initial Spin-Up of a Sea of Japan Numerical Circulation Model. AMCA95 Proceedings. (in press)

Na, J.-Y., J.-W. Seo, and S.-K. Han. 1992. Monthly-mean sea surface winds over the adjacent seas of the Korean Peninsula. J. Oceanolog. Soc. Korea. 27:1-10.

Seung, Y.H., and K. Kim. 1993. A Numerical Modelling of the East Sea Circulation. J. Oceanolog. Soc. Korea. 28:292-304.

Smagorinsky, J. 1963. General circulation experiments with the primitive equations, I. The basic experiment. Mon. Weather Rev. 91:99-164.

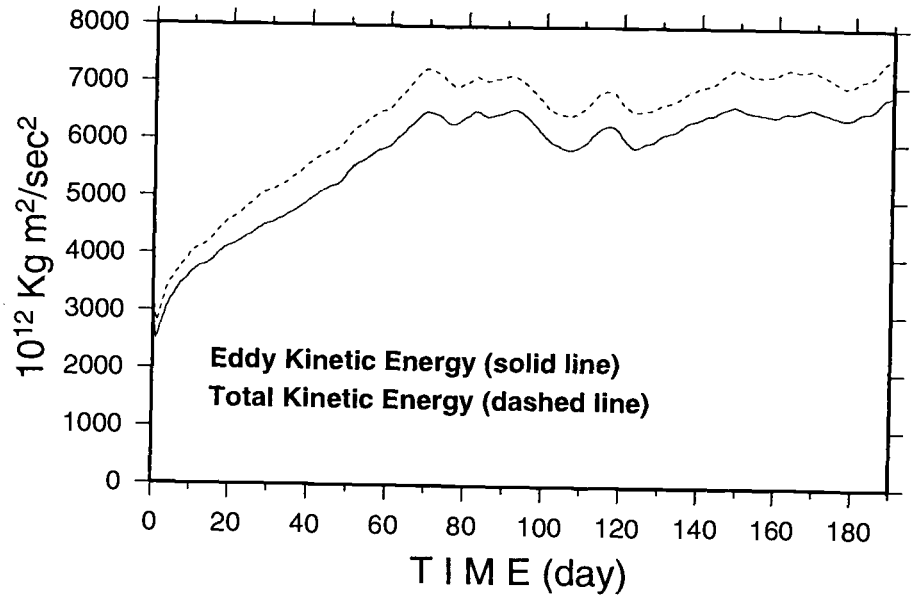

Fig. 1. Volume-integrated total and eddy kinetic energy versus time.

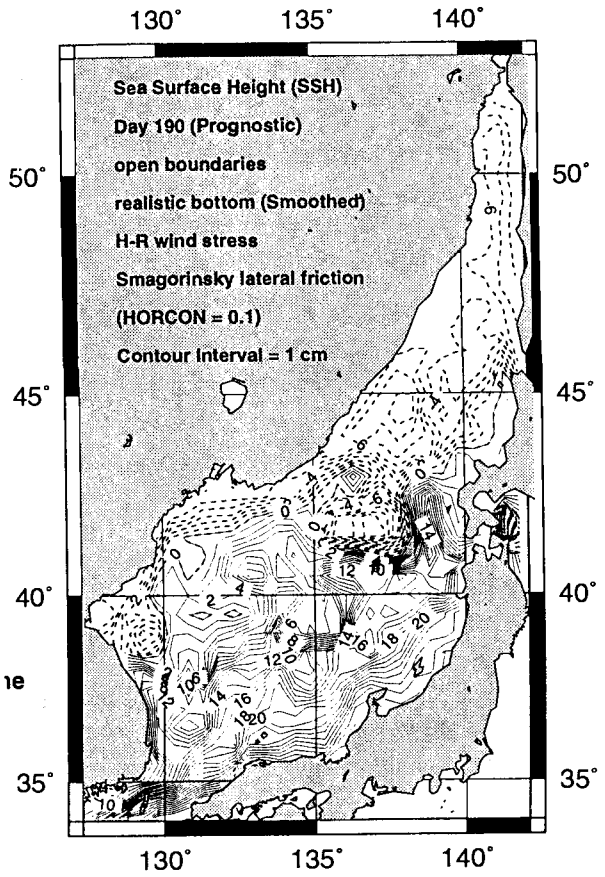

Fig. 2a. Sea Surface - Sea surface height (cm) at Day 190 of prognostic run.

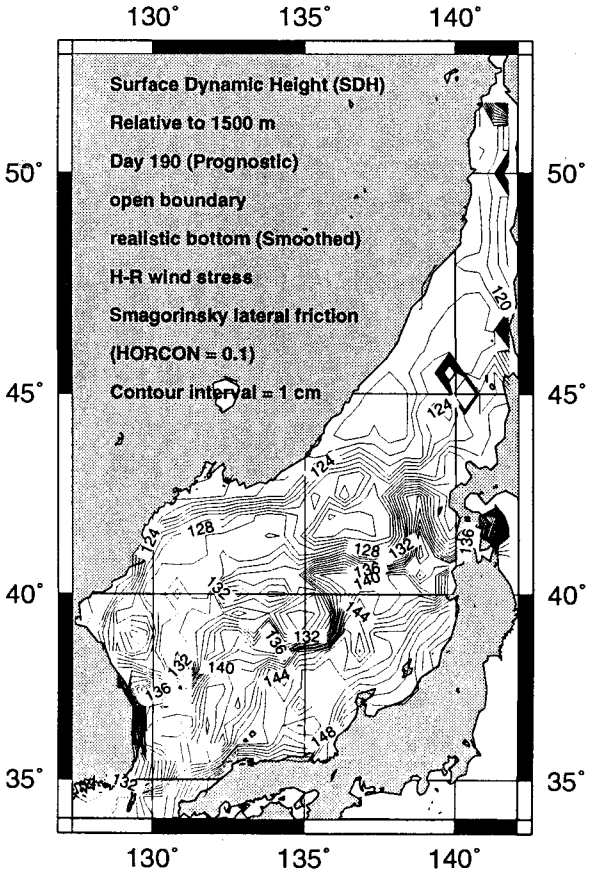

Fig. 2b. Sea Surface - Surface dynamic height (cm) relative to 1500 m at Day 190 based on the prognostic temperature and salinity fields.

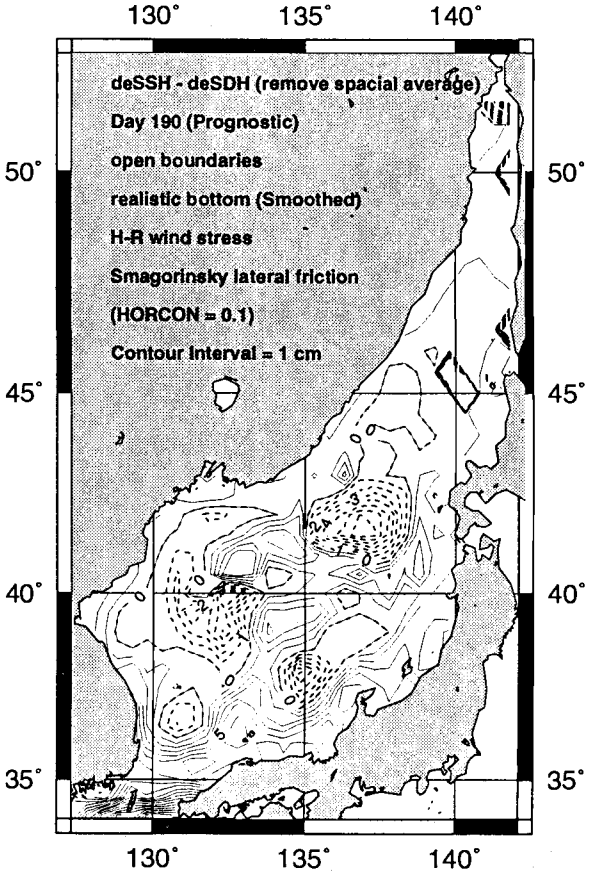

Fig. 2c. Sea Surface - Difference field (cm) (i.e., Fig. 2a-2b).

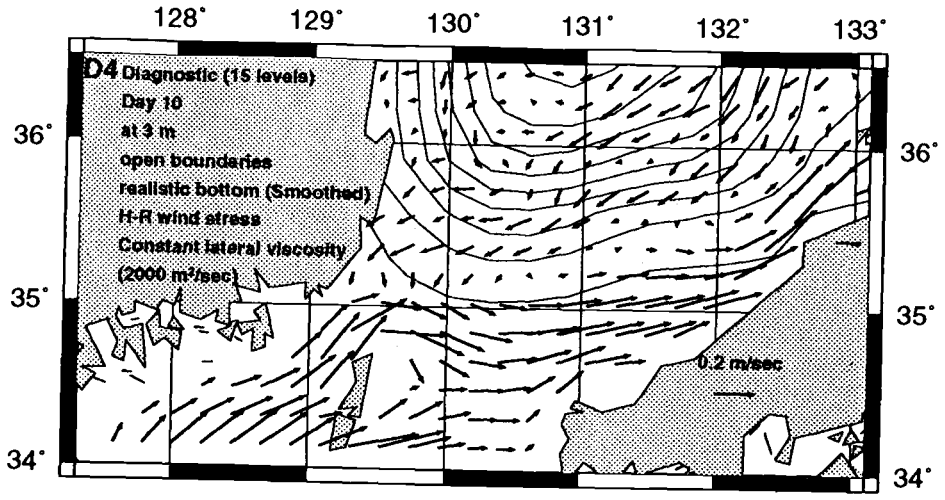

Fig. 3a. Surface currents for inflow subdomain - Day 10 of diagnostic run (initial field for prognostic run).

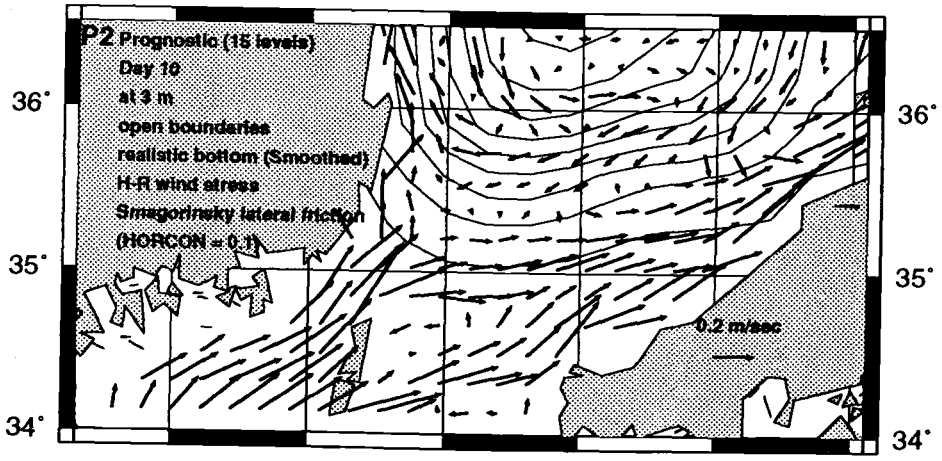

Fig. 3b. Surface currents for inflow subdomain - Day 10 of prognostic run.

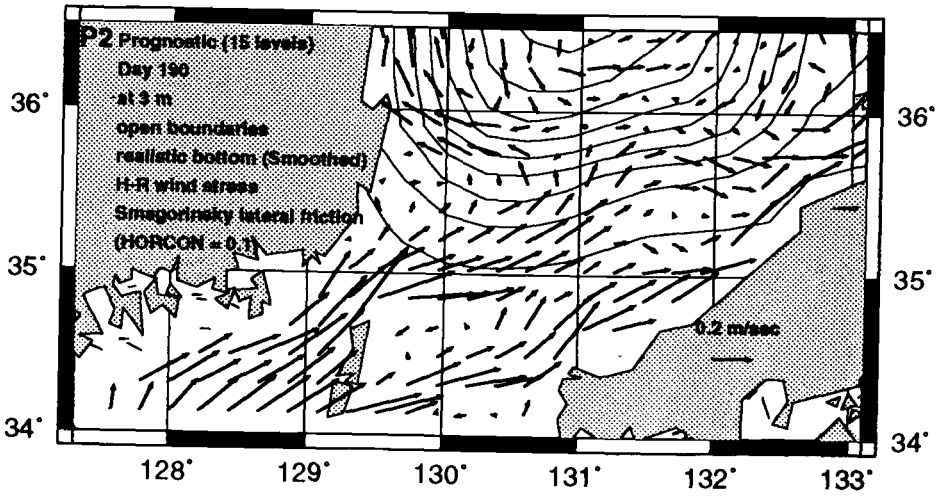

Fig. 3c. Surface currents for inflow subdomain - Day 190 of prognostic run. Contour interval = 200m.

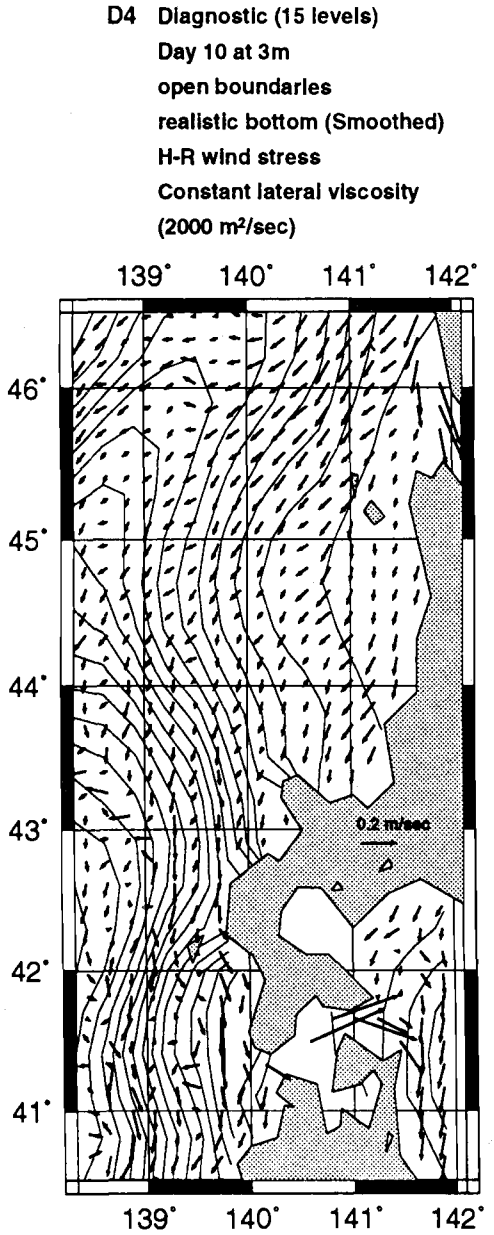

Fig. 4a. Surface currents for outflow subdomain - Day 10 of diagnostic run (initial field for prognostic run).

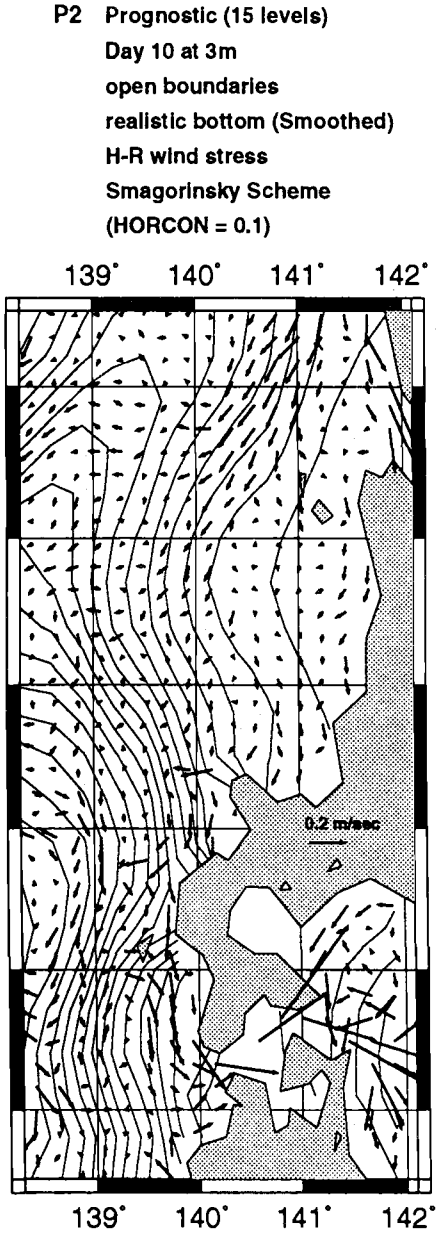

Fig. 4b. Surface currents for outflow subdomain - Day 10 of prognostic run..

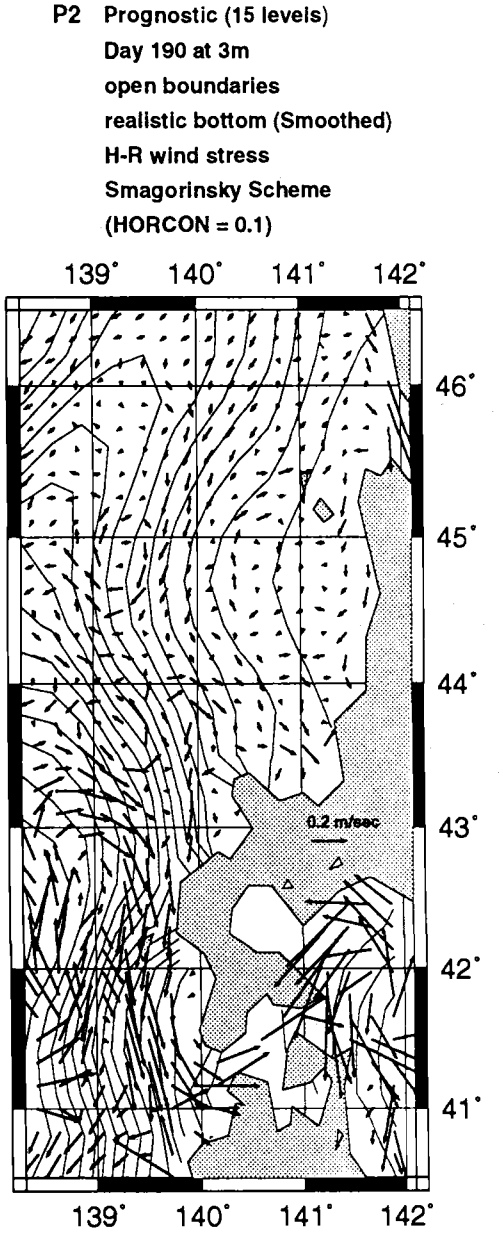

Fig. 4c. Surface currents for outflow subdomain - Day 190 of prognostic run..

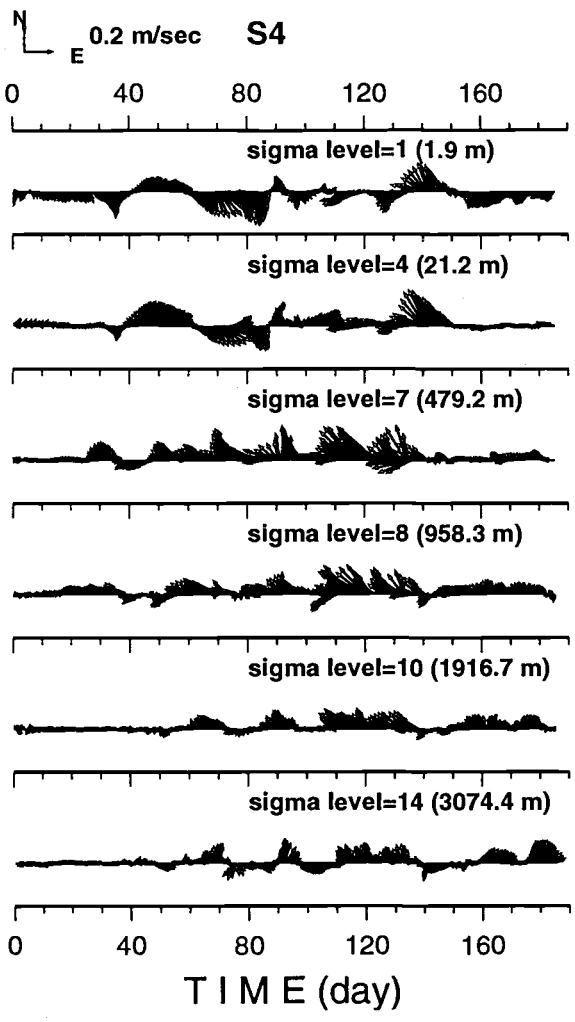

Fig. 5a. Time series of currents at selected levels - S4 (40.7N, 136.2E, water depth 3115 m).

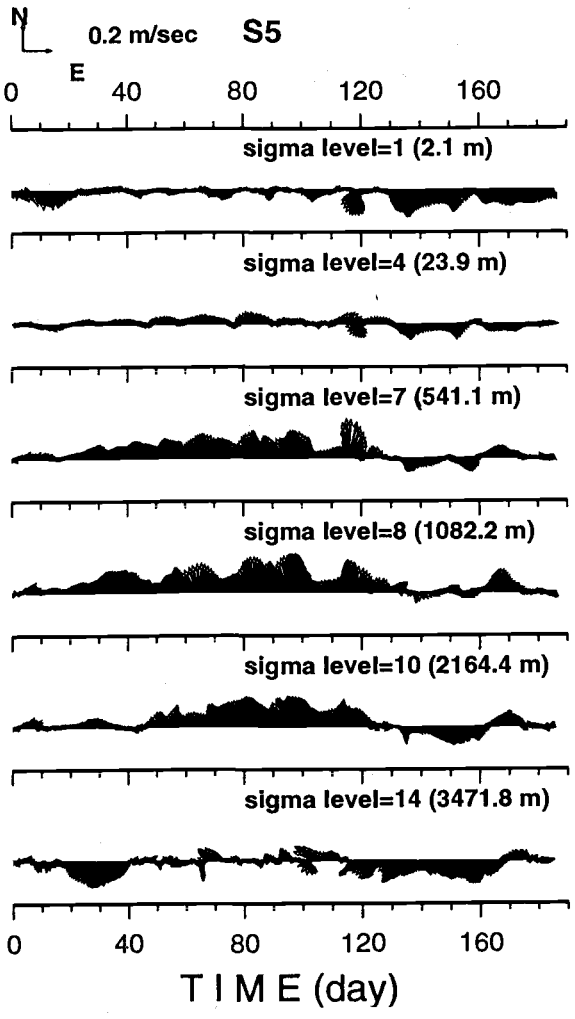

Fig. 5b. Time series of currents at selected levels - S5 (41.5N, 134.4E, water depth 3517 m).

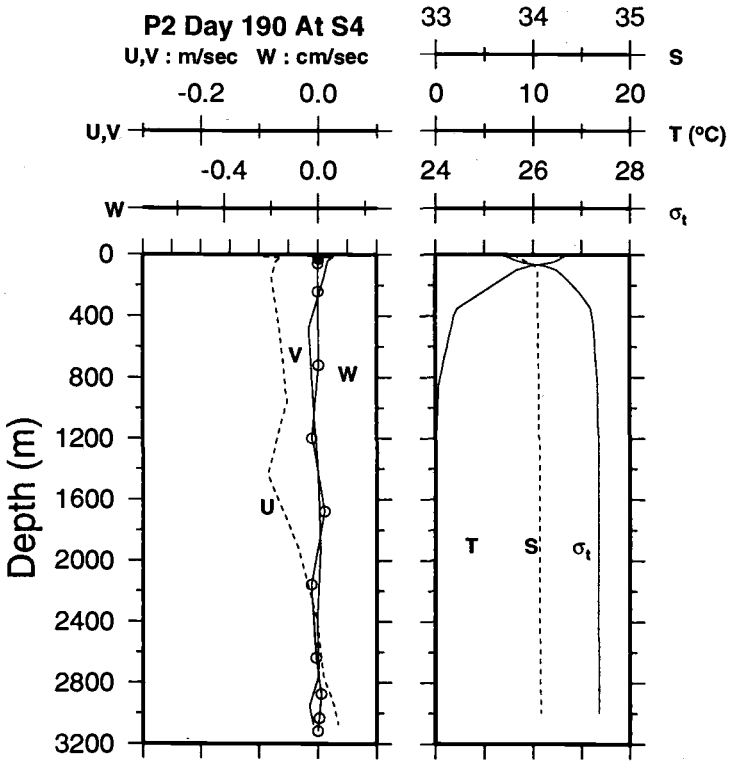

Fig. 6a. Vertical profiles of velocity components and temperature, salinity, and sigma-t at Day 190 - S4 (40.7N, 136.2E, water depth 3115 m).

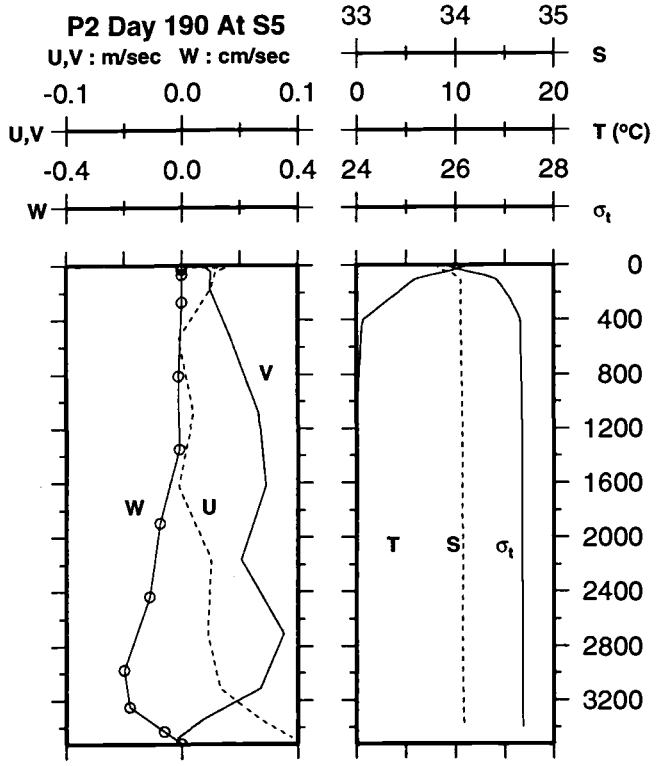

Fig. 6b. Vertical profiles of velocity components and temperature, salinity, and sigma-t at Day 190 - S5 (41.5N, 134.4E, water depth 3517 m).

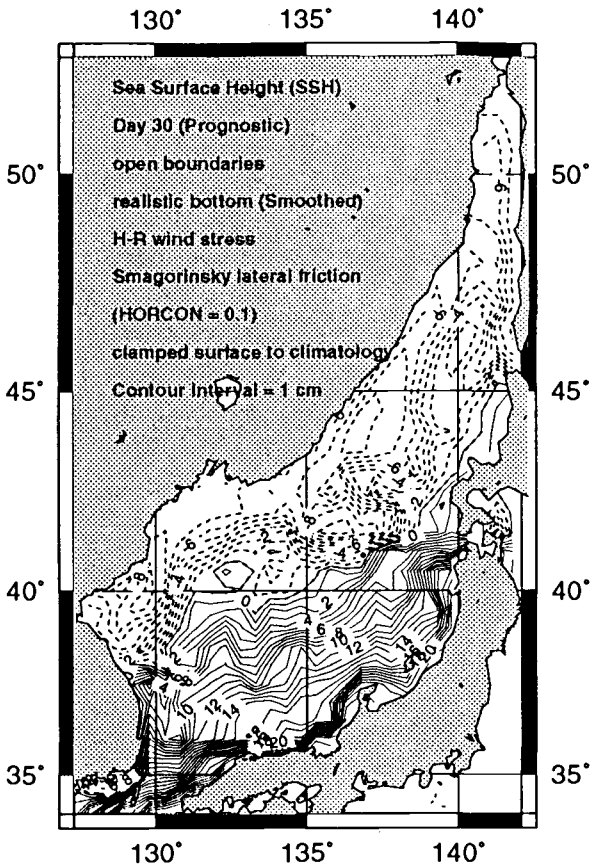

Fig. 7a. Sea Surface - sea surface height (cm) at Day 30 of prognostic run with surface clamping.

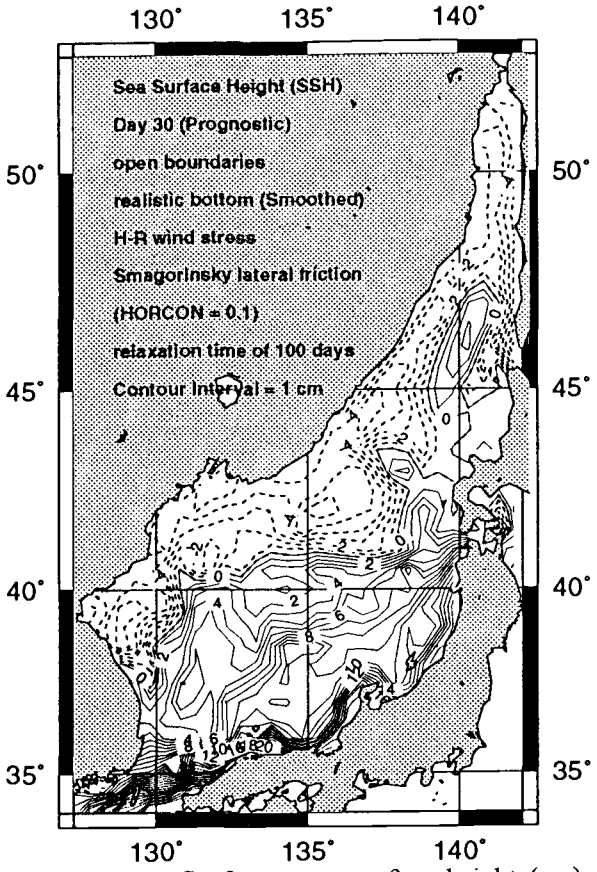

Fig. 7b. Sea Surface - sea surface height (cm) at Day 30 of prognostic run with surface relaxation time of 100 days.

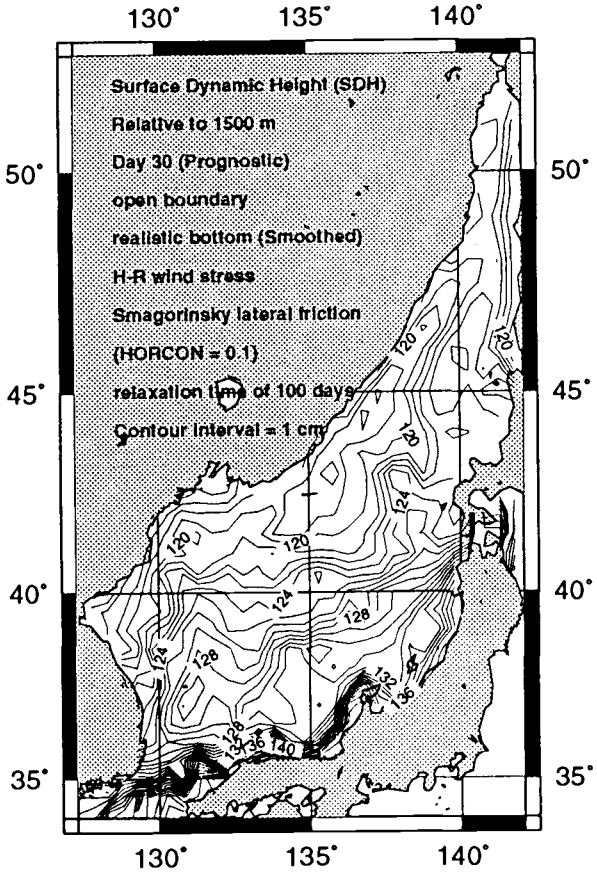

Fig. 7c. Sea Surface - surface dynamic height (cm) relative to 1500 m based on prognostic temperature and salinity fields at Day 30 of prognostic run with surface relaxation time of 100 days.

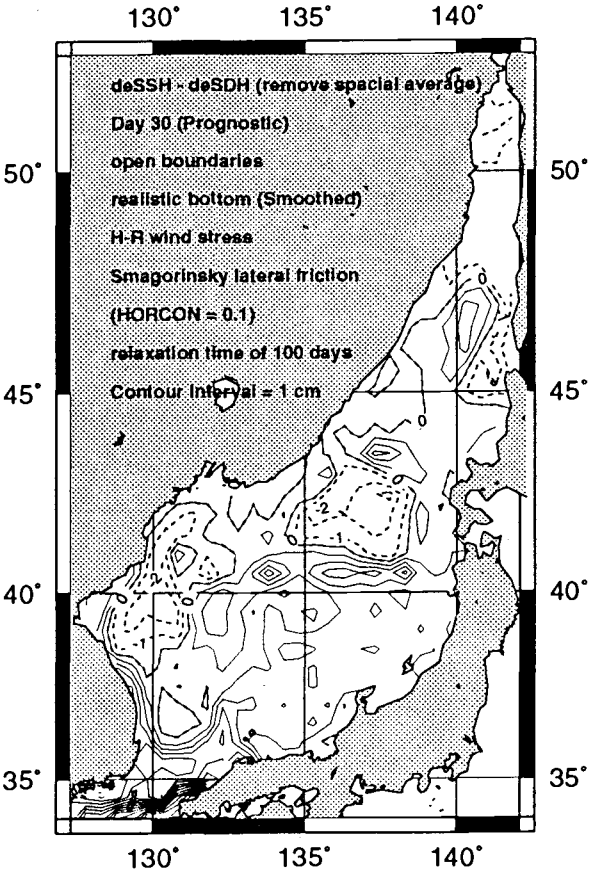

Fig. 7d. Sea Surface - difference field (cm) (i.e., Fig. 7a - 7b) at Day 30 of prognostic run with surface relaxation time of 100 days.

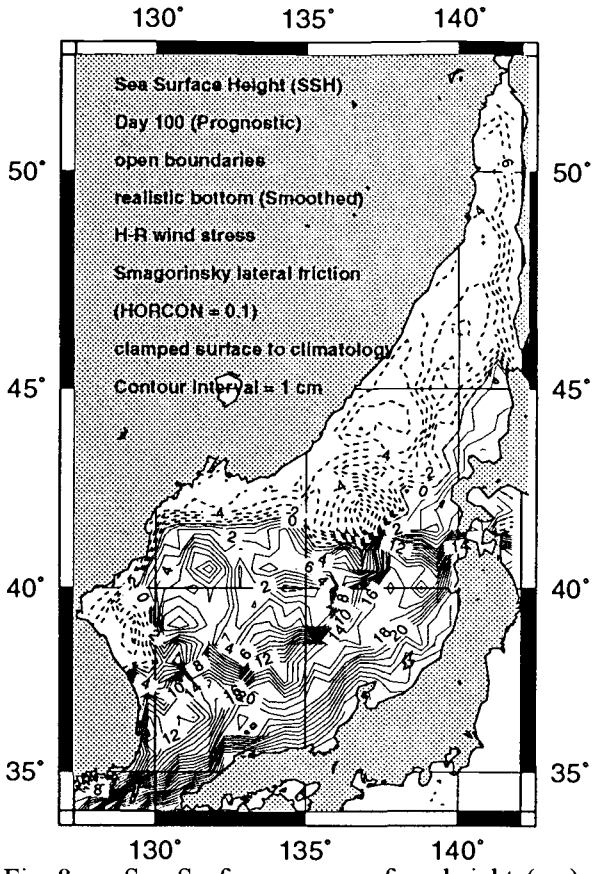

Fig. 8a. Sea Surface - sea surface height (cm) at Day 100 of prognostic run with surface clamping.

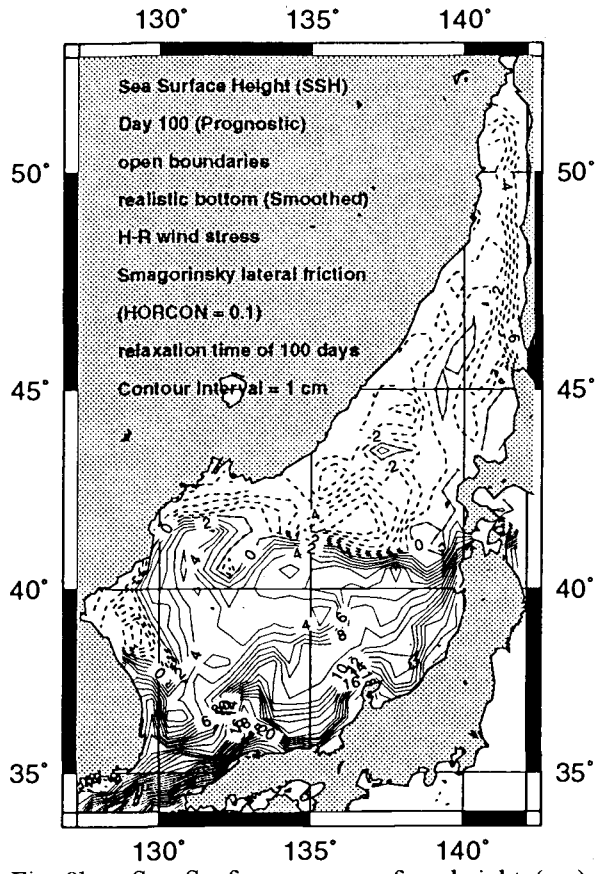

Fig. 8b. Sea Surface - sea surface height (cm) at Day 100 of prognostic run with surface relaxation time of 100 days.

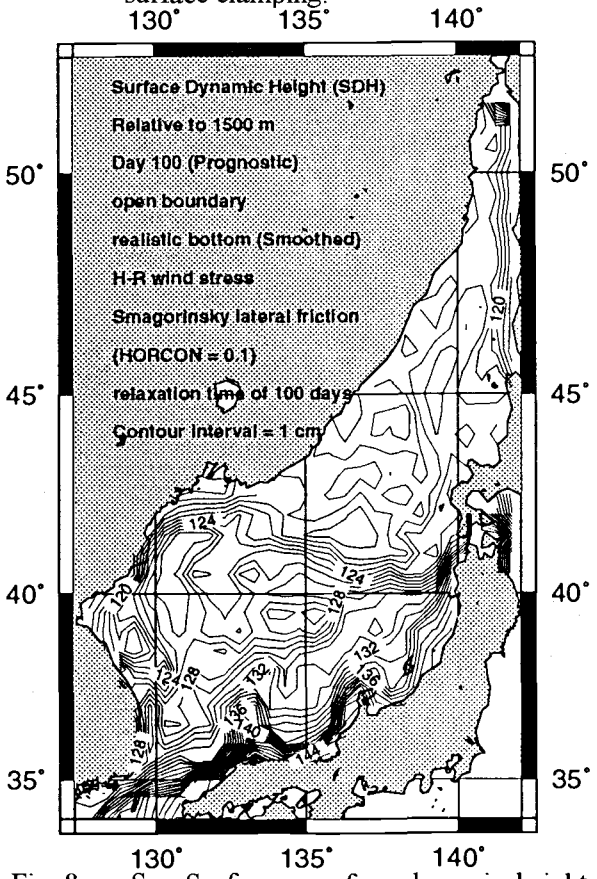

Fig. 8c. Sea Surface - surface dynamic height (cm) relative to 1500 m based on prognostic temperature and salinity fields at Day 100 of prognostic run with surface relaxation time of 100 days.

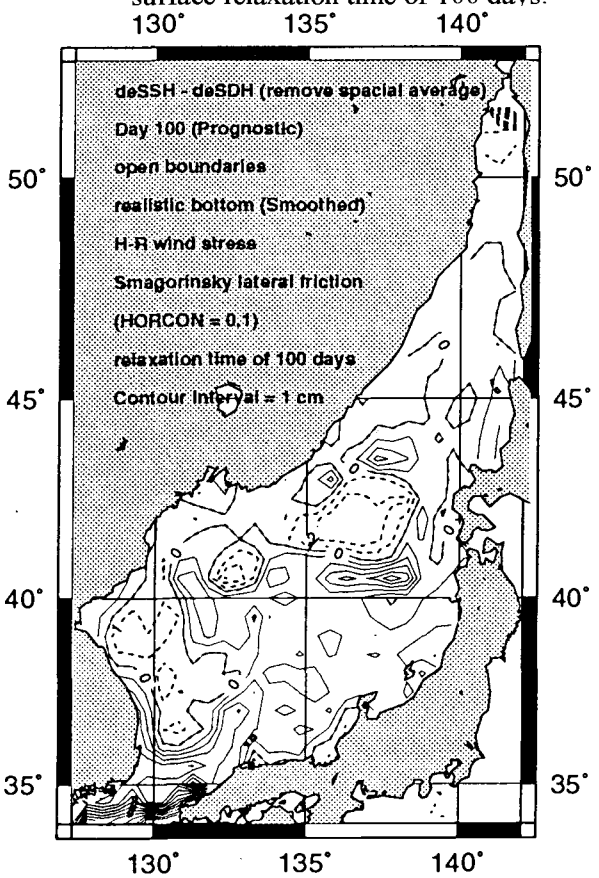

Fig. 8d. Sea Surface - difference field (cm) (i.e., Fig. 7a - 7b) at Day 100 of prognostic run with surface relaxation time of 100 days.

Influence of Ice Production on the Deep Water Formation in the Japan Sea

Lev P. YAKUNIN

Department of Oceanography, Far Eastern State University, Vladivostok, Russia

The main ice-forming areas in the Japan Sea are the Tatarsky Strait and Peter the Great Gulf. More than 90% of ice is produced in winter in the first region and this process occurs the most intensively in February. During that month ice covers 3, 6 and 11% of sea surface, respectively in a warm, temperate, and severe winter. At the same time ice volume changes from 2 to 6 cubic kilometers, with the average of 3 cubic kilometers. Ice is formed to the north off the Strait and, under the influence of wind and streams, moves to the south at an average speed of 11 miles a day. After 15-30 days it reaches the ice edge that is usually situated at 49°N. Further to the south ice starts breaking noticeably.

Assuming that the Tatarsky Strait is divided in two parts by 49°N and taking into account the thickness, concentration, hummock, and the speed of ice drift, we can estimate the amount of ice crossing a selected range:

$$V_i = A*L(h + \Delta h)v \quad \text{and} \quad \Delta h = 0.25T*h \tag{1}$$

where:

- V_i - ice volume, cubic kilometers;
- A - concentration level, decimals;
- L - width of the Strait at 49°N, kilometers;
- h - average ice thickness, kilometers;
- Δh - increase in ice thickness due to hummock, kilometers;
- T - level of hummock, /in 5-level scale/;
- v - speed of ice drift, kilometers per 10 days.

Based on a 26-year (1964-1989) data set we found that the volume of ice moved from north to south beyond 49°N during the "ice lifetime" varies from 12 to 53 cubic kilometers, with the average of 31 cubic kilometers. Martin et al (1972) reported the value of about 25 cubic kilometers a year for the volume of ice formed in 1988-1990, that is comparable with our calculations.

The amount of salt entering the water during the ice formation period can be computed by the simple formula:

$$S_s = \theta_i * V_i \ (S_{sw} - S_i) \tag{2}$$

where:

- S_s - amount of salt going into the water, tons;
- θ_i - density of ice, tons per cubic meter;
- V_i - ice volume, cubic kilometers;
- S_{sw} - salinity ($^0/_{00}$)of the surface-water;
- S_i - salinity ($^0/_{00}$) of ice.

Taking V_i from (1), θ_i = 0.9 tons m^{-3}, S_{sw} =32.5 °/$_{oo}$ and S_i =5 °/$_{oo}$ based on our measurements in the northern part of Tatarsky Strait and Sakhalin Gulf, we evaluated the annual numbers of S_s and the average value equal to 775*10^6 tons.

During the process of ice formation, only about 15% of salt remains in ice whereas the major part goes to increase salinity of the surface water and enables consecutive mixing. As a result, the surface water has T, S - indexes typical for the deep water of the Japan Sea. The volume of deep water formed due to ice production is given by following equation:

$$V_{dw} = \frac{S_s}{\theta_{dw} \cdot S_{dw} - \theta_{sw} \cdot S_{sw}} \qquad (3)$$

where:

V_{dw} - volume of deep water formed, cubic kilometers;
S_s - amount of salt brought into water (calculated by eq.2), tons;
θ_{dw} and θ_{sw} - density of deep and surface water, respectively, tons per cubic meter;
S_{dw} and S_{sw} - salinity of deep water and surface-water, respectively, (°/$_{oo}$).

In accordance with the characteristics of deep (S_{dw} = 34.08 °/$_{oo}$ and T_{dw} = 0.5°C) and surface (S_{sw} =32.5 °/$_{oo}$ and T_{sw} = -1.7°C) waters, the corresponding densities are equal to θ_{dw} = 1.02738 and θ_{sw} = 1.02614 tons per cubic meter (Oceanological Tables, 1975). Our further calculations demonstrated that for the period of observations the volume V_{dw} changes from 185 to 807 cubic kilometers, with the average value of 470 cubic kilometers (Fig. 1).

The amount of ice from other sources in the Japan Sea does not exceed 10% of the square and the volume of ice produced in the Tatarsky Strait. Therefore, in average the volume of deep water originated, because of ice formation, in the entire Japan Sea is under 550 cubic kilometers. This number accounts for less than 0.1% of the Sea volume and cannot significantly effect the hydrological properties of the Sea as a whole. Near the northwestern coast, within the shelf of Peter the Great Gulf and Tatarsky Strait, ice formation seems to have considerable influence on the thermohaline structure of water.

REFERENCES

Martin, S., E. Munoz, and R. Drucker. 1992. The Effect of Severe Storms on the Ice Cover of the Northern Tatarsky Strait. J. Geophys. Res. 97:17,753-17,764.

Oceanological Tables. 1975. Leningrad, Gidrometeoizdat. 477 p. (in Russian)

FIGURES

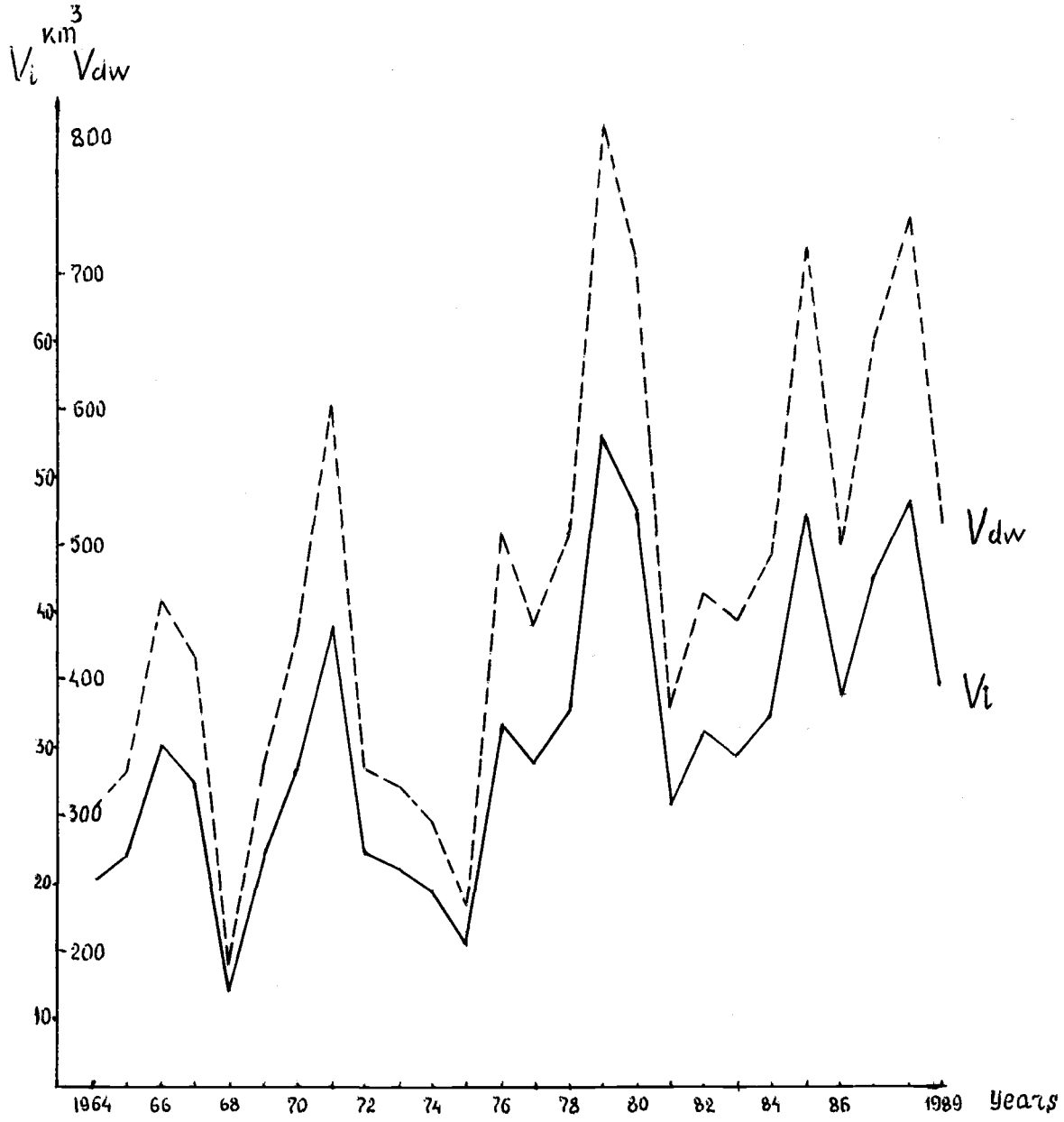

Fig. 1. Volume of ice (V_i) and deep water produced by ice formation (V_{dw}) in the Japan Sea.